Systematic design of reaction systems with prescribed behaviors: Deterministic and stochastic methods

Tomislav Plesa
Somerville College
University of Oxford

A thesis submitted for the degree of
Doctor of Philosophy
Trinity 2018

Abstract

Synthetic biology is a growing interdisciplinary field, with far-reaching applications, which aims to design biochemical systems that behave in a desired manner. With the advancements in nucleic-acid-based technology in general, and strand-displacement DNA computing in particular, a large class of abstract biochemical networks may be physically realized using nucleic acids, which may be integrated into a variety of environments, ranging from test-tubes, cell-sized compartments, to living cells. Mathematical methods for a systematic design of the abstract systems with prescribed behaviors, used as blueprints for the nucleic-acid-based ones, have received less attention, and form the focus of this thesis.

At the (less-detailed) deterministic level, suitable when the abstract reaction networks involve only high-abundance species, and applicable when the nucleic-acid-based physical networks are integrated into test-tubes, the so-called *kinetic transformations* are developed. The transformations map ordinary differential equations with polynomial right-hand sides to reaction-rate equations, allowing one to design biochemical reaction networks with desired deterministic dynamics. At the (more-detailed) stochastic level, suitable when the abstract reaction networks involve some low-abundance species, and applicable when the nucleic-acid-based physical networks are integrated into vesicles or living cells, the so-called *noise approximation algorithm* is developed. The algorithm structurally modifies any given reaction network under mass-action kinetics, in such a way that (i) controllable state-dependent noise is introduced into the stochastic dynamics, while (ii) the deterministic dynamics are preserved.

Combining the developed deterministic and stochastic methods, together with the result that any reaction with more than two reactants may be stochastically approximated by up-to bi-molecular reactions, a deterministic-stochastic hybrid approach of designing reaction networks is put forward. In particular, the kinetic transformations may be used to construct networks with desired deterministic dynamics, and the noise approximation algorithm may then be used to favorably reprogram the intrinsic noise in the stochastic dynamics, while preserving the deterministic skeleton. The capabilities of this approach are demonstrated by designing reaction networks displaying biochemically relevant exotic dynamics, such as (noise-induced) multistability and oscillations, and specific bifurcation structures.

Acknowledgements

I would like to thank my supervisor, Prof. Radek Erban, for the guidance and support during my doctoral studies, and for encouraging my research interests. I would also like to thank Tomáš Vejchodský, Konstantinos Zygalakis and David Anderson for fruitful interactions and collaborations.

The Engineering and Physical Sciences Research Council, which financially supported my doctoral studies through the Systems Biology Doctoral Training Centre, is gratefully acknowledged.

Finally, I would like to thank my family and friends for their support.

Contents

List of Figures

Chapter 1

Introduction

Synthetic biology is an interdisciplinary field of science and engineering that aims to design biochemical systems with prescribed behaviors [1, 2]. At the theoretical level, the synthetic systems may significantly enhance our understanding of biology. At the practical level, they may have broad applications, e.g. in medicine [3, 4, 5, 6, 7], industry [8, 9], and nanotechnology [10, 11]. The systems may also be of interest to space agencies for optimizing extraterrestrial explorations [12]. A proof-of-concept for synthetic biology is a synthetic oscillator called the repressilator, which was implemented in vivo [13]. The experimental advances since the repressilator range from isolated synthetic biochemical networks, to microorganisms containing partially, or even fully, synthetic DNA molecules (synthetic life) [14, 15, 16, 17]. Examples include microorganisms containing a synthetic bistable switch [18], and a cell-density controlling quorum sensor [19], microorganisms producing antimalarial drugs [6, 7], and synthetic systems designed for tumor detection, diagnosis and adaptive drug-response [4, 5].

The construction of biochemical networks in synthetic biology may be broken down into two steps: firstly, an abstract system is constructed, displaying prescribed properties, and taking the form of a chemical reaction network [20, 21, 22]. Secondly, the abstract network is mapped (compiled) to a suitable physical network [23, 24], which may then be integrated into a desired environment (e.g. a test-tube, a vesicle, or a living cell) [25, 26, 27, 28, 29]. The first step generally consists of a number of sub-steps, involving mathematical analyses and computational verifications, depending on the second step, i.e. depending on the nature of the target physical network and its environment.

In the first step of network construction, the goal is to obtain an abstract network with desired dynamics. In this thesis, we consider reaction networks under mass-action kinetics: it is assumed that each reaction fires at the rate proportional to the

product of the concentrations of the underlying reacting species. In this setting, we consider two dynamical models of reaction networks [21, 22]: the deterministic model, and the stochastic model (see Chapter 2 for more details). The deterministic model takes the form of the reaction-rate equations, which are ordinary-differential equations governing the time-evolution of the species concentrations [21, 22]. The stochastic model takes the form of a Markov chain, whose law is governed by the chemical master equation [21, 22, 30], with the underlying sample paths which may be simulated using e.g. the Gillespie stochastic simulation algorithm [31, 32]. The stochastic model is more-detailed, taking into an account the discreteness of the species counts, and the stochastic nature of the dynamics, which is particularly important when reaction networks contain low-abundance species [13, 18, 33, 34, 35, 36, 37], which may occur when the synthetic systems are integrated into vesicles or living cells. On the other hand, the deterministic model is less-detailed, and more appropriate when the species are in high-abundance, and the discreteness and stochasticity are negligible [38], which typically occurs when the synthetic systems are integrated into test-tubes.

In the second step of network construction, the goal is to engineer a physical network whose dynamics match well the dynamics of a given abstract network, over a suitable time-interval. Engineering an appropriate physical network may proceed indirectly, by altering a preexisting physical network, or directly, by engineering a network, which involves a given set of physical species, from scratch. The advantage of the former approach is that a preexisting network may display (partially) desirable dynamical properties. However, such a network may involve DNA and RNA molecules, proteins, and metabolites [2], some of which may have complex biophysical properties. Consequently, the disadvantage is that the structure (and, thus, the dynamics) of such a network cannot generally be modified in an arbitrary manner. In the latter approach, one may choose the physical species, at the expense of having to build a network from scratch. This approach is followed in the field of nucleic-acid-based molecular computing.

For example, in a subfield of DNA computing, physical networks are engineered with chemical species consisting exclusively of DNA molecules, interacting via the toehold-mediated DNA strand-displacement mechanism, which exploits the precision of Watson-Crick basepairing [23]. DNA production is systematic and cost-effective, and due to the fact that DNA biophysics is relatively well-understood, one has more freedom in controlling the structure of the corresponding physical networks. More precisely, an abstract network under mass-action kinetics may be mapped to a DNA-based physical network provided it consists of up to second-order reactions, with rate

coefficients varying over up to six orders of magnitude. The resulting physical network has been proven in [23] to have identical deterministic dynamics as the abstract network (in the asymptotic limit of some of the kinetic parameters), up to a scaling of the dependent variables. In [39], we have shown that the stochastic dynamics are also preserved under the molecular compiler from [23]. Let us note that a molecular compiler capable of dealing with reactions of arbitrarily high order has also been put forward [24]. A proof-of-concept for DNA computing is a synthetic oscillator called the displacillator, which was implemented in vitro [25], demonstrating for the first time that nucleic-acids alone can display oscillatory behaviors. Note that DNA computing, more broadly, may also involve physical DNA-based networks augmented with other types of molecules, such as enzymes [29, 40]. Another emerging approach within nucleic-acid-based molecular computing is based on RNA strand-displacement [41] - a mechanism which is hypothesized to occur naturally within the living cells [42]. While RNAs share many similarities with DNAs, operating via Watson-Crick basepairing, RNAs have a higher propensity to form non-Watson-Crick basepairng, and form an array of tertiary structures, giving them protein-like functionality. In fact, having both the ability to store genetic information, and catalytic activity, RNAs have been put forward as the key molecules on which first living systems were based [43].

The DNA-based reaction networks may involve only high-abundance species, mixed in a test-tube [23]. In such circumstances, it may be sufficient to construct the networks via the (less-detailed) deterministic model. However, recent experimental advancements, involving compartmentalized circuits [27, 28, 29], localized circuits [44, 45] and molecular robots [46, 47], may require reaction network construction via the (more-detailed) stochastic model. For example, in [27, 28, 29], the chemical mixture from a test-tube is split into a large number of cell-size vesicles (allowing for an experimental investigation of biochemistry in cell-like reactors). This corresponds to replacing a given reaction network, involving only high-abundance species, with a large number of topologically equivalent networks which, however, may involve species in a low-abundance, making the (intrinsic) noise an important part of the dynamics. The aim of this thesis is to develop and analyze mathematical methods for systematically designing reaction networks at both the deterministic and stochastic levels. While the main motivation for such constructions arises from (nucleic-acid-based) synthetic biology, where the designed systems may be used as blueprints for designing physical networks, the systems are also useful in systems biology (as caricature models), and numerical analysis (as test problems) [48, 49].

The thesis is structured as follows.

Chapter 2: Background. In this chapter, we introduce the background theory underpinning the thesis, which includes reaction networks and the deterministic and stochastic models describing their space-independent dynamics.

Chapter 3: Deterministic methods. This chapter introduces the so-called *kinetic transformations*, which are suitable (nonlinear) mappings which can transform differential equations, with polynomial right-hand sides, into reaction-rate equations. Combined with the nonlinear dynamics and bifurcation theory, the kinetic transformations allow one to design biochemical reaction networks with desired deterministic dynamics, suitable for (nucleic-acid-based) synthetic biology in test-tubes. The transformations are applied to design reaction networks which display 'exotic dynamics', involving multistability (coexistence of multiple stable attractors), oscillations, and specific bifurcation structures, all of which play important biochemical roles.

Chapter 4: Stochastic methods. In this chapter, we introduce the so-called *noise-approximation algorithm*, which maps an input reaction network to output networks whose stochastic dynamics have an additional controllable state-dependent noise. Importantly, the input and output networks have an identical deterministic model in appropriate limits of some of the parameters introduced by the algorithm. As such, the algorithm allows for a deterministic-stochastic hybrid approach of designing reaction networks: one may first use the kinetic transformations, introduced in Chapter 3, to design reaction networks at the less-detailed deterministic level. The noise-approximation algorithm may then be applied to favorably modify the intrinsic noise in the more-detailed stochastic model, while preserving the desired deterministic skeleton, leading to reaction networks with prescribed stochastic dynamics, suitable for synthetic biology in vesicles and living cells.

Chapter 5: Approximation of high- by bi-molecular reactions. Kinetic transformations and the noise-approximation algorithm may give rise to biochemical networks containing reactions which involve more than two reactants, which may limit their application to synthetic biology. In this chapter, we show that any high-molecular reaction, involving more than two reactants, may be mapped to a system of up-to bi-molecular reactions, involving up-to two reactants, while preserving the underlying stochastic dynamics. In this way, we extend the applicability of the methods introduced in Chapters 3 and 4.

Chapter 6: Discussion. In this chapter, we provide a summary of the findings of this thesis, and suggest possible directions for future work.

While the order of Chapters 3, 4 and 5 forms a logical progression, as described above, the chapters can be read in any order, as they are self-contained, and present results important in and of themselves.

The material presented in this thesis has been adapted from the following manuscripts:

1. Plesa, T., Vejchodský, T., and Erban, R., 2016. Chemical Reaction Systems with a Homoclinic Bifurcation: An Inverse Problem. *Journal of Mathematical Chemistry*, **54**(**10**): 1884–1915.

2. Plesa, T., Vejchodský, T., and Erban, R. Test Models for Statistical Inference: Two-Dimensional Reaction Systems Displaying Limit Cycle Bifurcations and Bistability, 2017. *Stochastic Dynamical Systems, Multiscale Modeling, Asymptotics and Numerical Methods for Computational Cellular Biology*, 2017. Available as https://arxiv.org/abs/1607.07738.

3. Plesa, T., and Zygalakis, K. C., Anderson, D. F., and Erban, R., 2018. Noise control for molecular computing. *Journal of the Royal Society Interface*, **15**(**144**): 20180199.

4. Plesa, T. Stochastic approximation of high-molecular by bi-molecular reactions. In preparation, 2018.

More precisely, Chapter 3 is based on the manuscripts 1. and 2., while Chapters 4 and 5 on the manuscripts 3. and 4., respectively.

Chapter 2

Background: Reaction systems

In Section 2.1, we define reaction networks, which are a suitable *graphical* model for a large class of chemical and biological processes. In Section 2.2, we define reaction systems, by augmenting reaction networks with kinetics (reaction rates). Finally, in Sections 2.3 and 2.4, which form the main part of this chapter, we define deterministic and stochastic *dynamical* models induced by reactions systems, and highlight some relationships between them. The notation and definitions in this chapter are inspired by [22, 50, 20, 21, 51, 52, 30, 53].

Before presenting specific definitions and results regarding reaction networks, let us introduce general notation which is used throughout the thesis.

Definition 2.1. *Set $\mathbb{R}$ is the space of real numbers, $\mathbb{R}_{\geq}$ the space of nonnegative real numbers, and $\mathbb{R}_{>}$ the space of positive real numbers. Similarly, $\mathbb{Z}$ is the space of integer numbers, $\mathbb{Z}_{\geq}$ the space of nonnegative integer numbers, and $\mathbb{Z}_{>}$ the space of positive integer numbers. Euclidean row-vectors are denoted in boldface, $\mathbf{x} = (x_1, \ldots, x_N) \in \mathbb{R}^N = \mathbb{R}^{1\times N}$, while the corresponding column-vector is written as $\mathbf{x}^\top = (x_1, \ldots, x_N)^\top \in \mathbb{R}^{N\times 1}$, where $\cdot^\top$ is the vector transpose operator.* Support *of $\mathbf{x} = (x_1, \ldots, x_N) \in \mathbb{R}^N$ is defined as $supp(\mathbf{x}) = \{i \in \{1, \ldots, N\} | x_i \neq 0\}$. Given a finite set $\mathcal{S}$, we denote its cardinality by $|\mathcal{S}|$.*

2.1 Reaction networks

Definition 2.2. *A* reaction network *is a triple $\{\mathcal{S}, \mathcal{C}, \mathcal{R}\}$, where*

(i) *$\mathcal{S} = \{s_1, s_2, \ldots, s_N\}$ is the set of* species *of the network.*

(ii) *$\mathcal{C}$ is the finite set of* complexes *of the network, which are nonnegative linear combinations of the species, i.e. complex $C \in \mathcal{C}$ reads $\sum_{i=1}^{N} \nu_i s_i$, where $\boldsymbol{\nu} =$*

$(\nu_1, \nu_2 \ldots, \nu_N) \in \mathbb{Z}_{\geq}^N$ *is called the* stoiochiometric vector *of* C*. It is required that* $\bigcup_{C=(\sum_{i=1}^N \nu_i s_i)\in\mathcal{C}} supp(\boldsymbol{\nu}) = \{1, 2, \ldots, N\}$.

(iii) $\mathcal{R} = \{\sum_{i=1}^N \nu_i s_i \to \sum_{i=1}^N \bar{\nu}_i s_i | \sum_{i=1}^N \nu_i s_i, \sum_{i=1}^N \bar{\nu}_i s_i \in \mathcal{C}, \boldsymbol{\nu} \neq \bar{\boldsymbol{\nu}}\}$ *is the finite set of* reactions*, with* $\sum_{i=1}^N \nu_i s_i$ *and* $\sum_{i=1}^N \bar{\nu}_i s_i$ *called the* reactant *and* product complexes*, respectively. The number of distinct reactions is denoted* $|\mathcal{R}| = M$.

Let us note that the condition $\bigcup_{C=(\sum_{i=1}^N \nu_i s_i)\in\mathcal{C}} \text{supp}(\boldsymbol{\nu}) = \{1, 2, \ldots, N\}$, from Definition 2.2, implies that reaction networks do not include redundant species, i.e. species which do not appear in the underlying reactions. Requiring that the stoiochiometric vectors of reactant and product complexes are distinct, $\boldsymbol{\nu} \neq \bar{\boldsymbol{\nu}}$, implies that reaction networks graphically do not contain self-loops.

For simplicity, we denote reaction networks in this thesis by $\mathcal{R}$, with the species and complexes understood from the context. When convenient, we indicate dependence of a reaction network on species of interest: e.g. to indicate dependence on s_i, we write $\mathcal{R}(s_i)$. Furthermore, abusing the notation slightly, we denote the complex $\sum_{i=1}^N \nu_i s_i$ by $\boldsymbol{\nu}$, when convenient. With this convention, reaction $r_j = (C_j \to \bar{C}_j) \in \mathcal{R}$ may be written in the vector form $r_j = (\boldsymbol{\nu}_j \to \bar{\boldsymbol{\nu}}_j) \in \mathcal{R}$. A complex which may appear in reaction networks is the *zero-complex*, $\boldsymbol{\nu} = \mathbf{0}$, which is denoted by $\varnothing$ in the networks. The reaction $\mathbf{0} \to \bar{\boldsymbol{\nu}}$ then represents an inflow of the species, while reaction $\boldsymbol{\nu} \to \mathbf{0}$ represents an outflow of the species [20].

Definition 2.3. *The* order of reaction $r_j = (\boldsymbol{\nu}_j \to \bar{\boldsymbol{\nu}}_j) \in \mathcal{R}$ *is given by* $\boldsymbol{\nu}_j \cdot \mathbf{1} < \infty$*, where* $\mathbf{1} = (1, 1, \ldots, 1) \in \mathbb{Z}^N$*, and* $\cdot$ *is the vector dot product. The* order of reaction network $\mathcal{R}$ *is given by the order of its highest-order reaction.*

While chemical reaction networks from systems biology typically do not include reactions of order three or higher, i.e. reactions between more than three reactants [21], in the nucleic-acid-based synthetic biology it is possible to realize reactions of arbitrary high order in principle [24]. In this thesis, we consider reactions of arbitrary finite order, and also demonstrate in Chapter 5 how such reactions may be approximated by systems of up-to second-order ones. First-order reaction networks display special dynamical properties, which we outline in Section 2.4.1.

Example 2.1. *Consider the following reaction network:*

$$r: \quad s_1 + s_2 \to 2s_1. \tag{2.1}$$

The species, complex and reaction sets are given by $\mathcal{S} = \{s_1, s_2\}$*,* $\mathcal{C} = \{s_1 + s_2, 2s_1\}$*,* $\mathcal{R} = \{s_1 + s_2 \to 2s_1\}$*, respectively. In the vector notation, reaction* (2.1) *may be*

written as $r = ((1,1) \to (2,0))$. *Furthermore,* $N = 2$ *(there are two species),* $M = 1$ *(the reaction network consist of a single reaction), and the network is of second-order.* △

2.2 Reaction kinetics: Continuous and discrete

In this section, we augment each reaction in a reaction network with a rate at which it occurs ('fires').

Definition 2.4. Continuous kinetics. *Let* $\mathcal{R}$ *be a reaction network, and let* $\boldsymbol{\kappa} : \mathbb{R}^N_{\geq} \to \mathbb{R}^M_{\geq}$ *be a continuous function which maps* $\mathbf{x} \in \mathbb{R}^N_{\geq}$ *(called* species concentrations*) into* $\boldsymbol{\kappa}(\mathbf{x}) \in \mathbb{R}^M_{\geq}$ *(called the continuous* reaction rates*). Then,* $\boldsymbol{\kappa}(\mathbf{x})$ *is said to be a* kinetics *for* $\mathcal{R}$ *provided that, for all* $\mathbf{x} \in \mathbb{R}^N_{\geq}$ *and for all* $r_j = (\boldsymbol{\nu}_j \to \bar{\boldsymbol{\nu}}_j) \in \mathcal{R}$, $\kappa_j(\mathbf{x}) > 0$ *if and only if* $\mathrm{supp}(\boldsymbol{\nu}_j) \subseteq \mathrm{supp}(\mathbf{x})$.
Discrete kinetics. *Let* $\boldsymbol{\alpha} : \mathbb{Z}^N_{\geq} \to \mathbb{R}^M_{\geq}$ *be a function which maps* $\mathbf{x} \in \mathbb{Z}^N_{\geq}$ *(called* species copy-numbers*) into* $\boldsymbol{\alpha}(\mathbf{x}) \in \mathbb{R}^M_{\geq}$ *(called the discrete* reaction rates*, or* propensity functions*). Then,* $\boldsymbol{\alpha}(\mathbf{x})$ *is said to be a* kinetics *for* $\mathcal{R}$ *provided that, for all* $\mathbf{x} \in \mathbb{Z}^N_{\geq}$ *and for all* $r_j = (\boldsymbol{\nu}_j \to \bar{\boldsymbol{\nu}}_j) \in \mathcal{R}$, $\alpha_j(\mathbf{x}) > 0$ *if and only if* $\mathrm{supp}(\boldsymbol{\nu}_j) \subseteq \mathrm{supp}(\mathbf{x} - \boldsymbol{\nu}_j + \mathbf{1})$, *where* $\mathbf{1} = (1, 1, \ldots, 1) \in \mathbb{Z}^N$.

An interpretation of Definition 2.4 is that a reaction, to which a continuous kinetics can be associated, can fire provided all the reactant species concentrations are nonzero. On the other hand, a discrete kinetics requires a stronger condition: a reaction can fire provided each reactant species copy-number is, not only nonzero, but sufficiently large (more precisely, if $\nu_{ji} \neq 0$, then reaction r_j fires provided $x_i \geq \nu_{ji}$).

Let us note that, in Definition 2.4, and the reminder of this thesis, we abuse the notation slightly, and use $\mathbf{x} = (x_1, x_2, \ldots, x_N)$ to denote both the concentration and copy-number vectors (state-vectors of the deterministic and stochastic model, respectively, see Section 2.3).

Definition 2.5. Continuous mass-action kinetics. *Kinetics* $\boldsymbol{\kappa}(\mathbf{x})$ *is called continuous* mass-action kinetics *if*

$$\kappa_j(\mathbf{x}) = k_j \mathbf{x}^{\boldsymbol{\nu}_j} \equiv k_j \prod_{i=1}^{N} x_i^{\nu_{ji}}, \quad \mathbf{x} \in \mathbb{R}^N_{\geq}, \tag{2.2}$$

for $r_j = (\boldsymbol{\nu}_j \to \bar{\boldsymbol{\nu}}_j) \in \mathcal{R}$, *where* $k_j \geq 0$ *is the* rate coefficient *of reaction* $r_j \in \mathcal{R}$, *with the convention* $0^0 \equiv 1$.

Discrete mass-action kinetics. *Kinetics* $\boldsymbol{\alpha}(\mathbf{x})$ *is called discrete* mass-action kinetics *if*

$$\alpha_j(\mathbf{x}) = k_j \mathbf{x}^{\underline{\boldsymbol{\nu}_j}} \equiv k_j \prod_{i=1}^{N} x_i^{\underline{\nu_{ji}}}, \quad \mathbf{x} \in \mathbb{Z}_{\geq}^N, \tag{2.3}$$

for $r_j = (\boldsymbol{\nu}_j \to \bar{\boldsymbol{\nu}}_j) \in \mathcal{R}$*, where* $k_j \geq 0$ *is the* rate coefficient *of reaction* $r_j \in \mathcal{R}$*. Here,*

$$x_i^{\underline{\nu_{ji}}} = x_i(x_i - 1)(x_i - 2)\dots(x_i - \nu_{ji} + 1)$$

denotes the ν_{ji}*th factorial power of* x_i*, with the convention* $x_i^{\underline{0}} \equiv 1$ *for all* $x_i \in \mathbb{Z}_{\geq}$*.*

More details on factorial powers are provided in [54], while a review of mass-action kinetics can be found in [55].

Let $V \in \mathbb{R}_{>}$ be the volume of the reactor in which the reaction network is operating. In Definition 2.5, we implicitly assume that reaction network $\mathcal{R}$ is firing in a *unit-volume* reactor, $V = 1$. When the volume of the reactor does not equal to one, we assume the rate coefficients from (2.2) and (2.3) are related via the so-called *classical scaling* [22]. In particular, in this more general case, we replace the rate coefficient k_j, appearing in (2.3), by $k_j V^{(1-\boldsymbol{\nu}_j \cdot \mathbf{1})}$, where k_j is the rate coefficient appearing in (2.2).

Definition 2.6. *A reaction network* $\mathcal{R}$ *augmented with a kinetics is called a* reaction system*. A reaction system with mass-action kinetics is denoted* $\{\mathcal{R}, \mathbf{k}\}$*, where* $\mathbf{k} = (k_1, \dots, k_M) \in \mathbb{R}_{\geq}^M$*, and the underlying reactions are denoted* $r_j = (\boldsymbol{\nu}_j \xrightarrow{k_j} \bar{\boldsymbol{\nu}}_j) \in \mathcal{R}$*.*

Example 2.2. *Consider reaction network*

$$r: \quad 2s_1 + s_2 \xrightarrow{k} s_1 + s_2, \tag{2.4}$$

under mass-action kinetics, firing in a reactor with volume V*. Assuming the abundance of the species is continuous, with the concentration vector* $\mathbf{x} = (x_1, x_2) \in \mathbb{R}_{\geq}^2$*, the reaction fires at the rate* $\kappa(x_1, x_2) = k(x_1, x_2)^{(2,1)} = k x_1^2 x_2$*. On the other hand, assuming the abundance is discrete, with the copy-number vector* $\mathbf{x} = (x_1, x_2) \in \mathbb{Z}_{\geq}^2$*, the reaction fires at the rate* $\alpha(x_1, x_2) = kV^{-2}(x_1, x_2)^{\underline{(2,1)}} = kV^{-2} x_1^{\underline{2}} x_2^{\underline{1}} = kV^{-2} x_1(x_1 - 1)x_2$*.* △

2.3 Dynamical models of reaction systems

In this section, we define the deterministic and stochastic models of reaction systems, while in the next section we highlight relationships between the two models. For ease of notation, we define *reaction vector* of reaction $r_j = (\boldsymbol{\nu}_j \to \bar{\boldsymbol{\nu}}_j) \in \mathcal{R}$ to be given by $\Delta\mathbf{x}_j = (\bar{\boldsymbol{\nu}}_j - \boldsymbol{\nu}_j) \in \mathbb{Z}^N$. The vector $\Delta\mathbf{x}_j$ quantifies the net change in the species counts caused by a single firing of reaction r_j.

2.3.1 The deterministic model: Reaction-rate equations (RREs)

Let us consider reaction networks firing in well-mixed reactors. We now define a suitable model governing the deterministic time-evolution of the (space-independent) species concentration vector $\mathbf{x}(t) = (x_1(t), \ldots, x_N(t)) \in \mathbb{R}^N_{\geq}$, where $t \in \mathbb{R}_{\geq}$ is the time-variable, which we call the deterministic model of reaction systems.

Definition 2.7. *Given a reaction system $\{\mathcal{R}, \boldsymbol{\kappa}\}$, the deterministic model, describing the time-evolution of the species concentration vector $\mathbf{x} = \mathbf{x}(t) \in \mathbb{R}^N_{\geq}$, is given by the autonomous first-order ordinary differential equations (ODEs), called the* reaction-rate equations *(*RREs*):*

$$\frac{\mathrm{d}\mathbf{x}}{\mathrm{d}t} = \boldsymbol{\mathcal{K}}(\mathbf{x};\, \mathcal{R}) = \sum_{j=1}^{M} \kappa_j(\mathbf{x}) \Delta \mathbf{x}_j. \tag{2.5}$$

Here, $\boldsymbol{\mathcal{K}}(\cdot;\, \mathcal{R}) : \mathbb{R}^N_{\geq} \to \mathbb{R}^N$ is the kinetic function*, and $\Delta \mathbf{x}_j = \bar{\boldsymbol{\nu}}_j - \boldsymbol{\nu}_j$ is the reaction vector of $r_j = (\boldsymbol{\nu}_j \to \bar{\boldsymbol{\nu}}_j) \in \mathcal{R}$.*

In this thesis, the species concentrations satisfying equation (2.5) are required to be finite, i.e. $x_i(t) < \infty$, for $i = 1, \ldots, N$, and for $t \geq 0$, except possibly for initial conditions located on a finite number of $(N - l)$-dimensional subspaces of $\mathbb{R}^N_{\geq}$, $l \geq 1$, where infinite-time blow-ups are allowed.

Let us set the left-hand side (LHS) of the RREs from (2.5) to zero, giving the following system of equations

$$\boldsymbol{\mathcal{K}}(\mathbf{x}^*;\, \mathcal{R}) = \mathbf{0}. \tag{2.6}$$

A time-independent solution $\mathbf{x}^*$ is called a *critical point* (equilibrium) of the RREs from (2.5). The critical points are discussed in a greater detail in Chapter 3.

Under mass-action kinetics (2.2), the kinetic function, which we then denote by $\boldsymbol{\mathcal{K}}(\mathbf{x};\, \mathbf{k})$, becomes a *polynomial*, and the ODE from (2.5) reads

$$\frac{\mathrm{d}\mathbf{x}}{\mathrm{d}t} = \boldsymbol{\mathcal{K}}(\mathbf{x};\, \mathbf{k}) = \sum_{j=1}^{M} k_j \mathbf{x}^{\boldsymbol{\nu}_j} \Delta \mathbf{x}_j. \tag{2.7}$$

Example 2.3. *Consider reaction network* (2.4)*, with the concentration vector $\mathbf{x} = (x_1, x_2)$, and $\Delta \mathbf{x} = (1, 1) - (2, 1) = (-1, 1)$. Substitution into* (2.7) *leads to the following system of RREs*

$$\begin{aligned} \frac{\mathrm{d}x_1}{\mathrm{d}t} &= \mathcal{K}_1\,(x_1, x_2;\, k) = -k x_1^2 x_2, \\ \frac{\mathrm{d}x_2}{\mathrm{d}t} &= \mathcal{K}_2\,(x_1, x_2;\, k) = k x_1^2 x_2. \end{aligned} \tag{2.8}$$

△

2.3.2 The stochastic model: Chemical master equation (CME)

Let us now consider reaction networks firing in well-mixed reactors, allowing the species counts to be discrete, and their dynamics stochastic. A suitable stochastic model represents the species copy-number vector $\mathbf{X}(t) = (X_1(t), \ldots, X_N(t)) \in \mathbb{Z}_{\geq}^N$ (with species copy-numbers uniformly distributed in space) as a continuous-time discrete-space Markov chain (CTMC) [56]. Let us now define the stochastic model by specifying the underlying forward Kolmogorov equation [22, 51, 30] underlying the CTMC $\mathbf{X}(t)$.

Definition 2.8. *Given a reaction system $\{\mathcal{R}, \boldsymbol{\alpha}\}$, the stochastic model is given by the partial difference-differential equation, called the* chemical master equation *(*CME*):*

$$\frac{\partial}{\partial t}p(\mathbf{x},t) = \mathcal{L}p(\mathbf{x},t) = \sum_{j=1}^{M}(E_{\mathbf{x}}^{-\Delta\mathbf{x}_j} - 1)\big(\alpha_j(\mathbf{x})p(\mathbf{x},t)\big), \tag{2.9}$$

where $\Delta\mathbf{x}_j = \bar{\boldsymbol{\nu}}_j - \boldsymbol{\nu}_j$ is the reaction vector of $r_j = (\boldsymbol{\nu}_j \to \bar{\boldsymbol{\nu}}_j) \in \mathcal{R}$. Here, $p(\mathbf{x},t)$ is the probability mass function *(*PMF*), i.e. the probability that the copy-number vector $\mathbf{X} = \mathbf{X}(t) \in \mathbb{Z}_{\geq}^N$ at time $t > 0$ is given by $\mathbf{x} \in \mathbb{Z}_{\geq}^N$. The linear operator $\mathcal{L} : \mathcal{D}(\mathcal{L}) \to l^1(\mathbb{Z}_{\geq}^N; \mathbb{R})$ is called the* forward operator*, where $\mathcal{D}(\mathcal{L}) \subseteq l^1(\mathbb{Z}_{\geq}^N; \mathbb{R})$ is a suitable domain of $\mathcal{L}$. The* step operator $E_{\mathbf{x}}^{-\Delta\mathbf{x}} = \prod_{i=1}^N E_{x_i}^{-\Delta x_i}$ *is such that*

$$E_{\mathbf{x}}^{-\Delta\mathbf{x}}p(\mathbf{x},t) = p(\mathbf{x}-\Delta\mathbf{x},t), \quad \forall\Delta\mathbf{x} \in \mathbb{Z}^N, \quad \forall p(\cdot,t) \in l^1(\mathbb{Z}_{\geq}^N; \mathbb{R}), \quad \forall t \geq 0.$$

In Definition 2.8, we denote by $l^1(\mathbb{Z}_{\geq}^N; \mathbb{R})$ the space of sequences whose series is absolutely convergent, defined as

$$l^1(\mathbb{Z}_{\geq}^N; \mathbb{R}) = \{p(\cdot,t) : \mathbb{Z}_{\geq}^N \to \mathbb{R} | \sum_{\mathbf{x}\in\mathbb{Z}_{\geq}^N} |p(\mathbf{x},t)| < \infty\},$$

where $p(\cdot,t) : \mathbb{Z}_{\geq}^N \to \mathbb{R}$ denotes a sequence for each fixed $t \in \mathbb{R}_{\geq}$. In the rest of the thesis, we implicitly assume reaction systems $\{\mathcal{R}, \boldsymbol{\alpha}\}$ are such that $p(\cdot,t) \in l^1(\mathbb{Z}_{\geq}^N; [0,1])$, and $\|p(\cdot,t)\|_1 = \sum_{\mathbf{x}\in\mathbb{Z}_{\geq}^N} p(\mathbf{x},t) = 1$, for every $t \geq 0$, i.e. that $p(\mathbf{x},t)$ is a PMF for each $t \geq 0$. We also assume the following conditions

$$\alpha_j(\mathbf{x}) = 0, \quad p(\mathbf{x},t) = 0, \quad \forall\mathbf{x} \notin \mathbb{Z}_{\geq}^N, \quad \forall t \geq 0, \tag{2.10}$$

which are naturally implied by Definition 2.4.

Let us set the LHS of the CME from (2.9) to zero, giving the following zero-eigenvalue problem (EVP):

$$\mathcal{L}p(\mathbf{x}) = 0, \quad \|p\|_1 = 1. \tag{2.11}$$

Assuming existence and uniqueness, the time-independent solution $p(\mathbf{x})$, satisfying (2.11), is called the *stationary PMF* (equilibrium PMF) of the CME from (2.9). It is the PMF in the long-run, i.e. as time $t \to \infty$, and is often a quantity of interest in the applications. Let us note that a transient PMF, known as a quasi-stationary PMF [53], may also be of interest (see also Example 2.7).

Under mass-action kinetics (2.3), the CME from (2.9) becomes

$$\frac{\partial}{\partial t}p(\mathbf{x},t) = \sum_{j=1}^{M}(E_{\mathbf{x}}^{-\Delta\mathbf{x}_j} - 1)\big(k_j\mathbf{x}^{\underline{\boldsymbol{\nu}_j}}p(\mathbf{x},t)\big). \tag{2.12}$$

In this thesis, we also utilize the adjoint operator of the forward operator $\mathcal{L}$, which is known as the backward operator/generator [22, 51], and which we put in use in Chapters 4 and 5, when applying perturbation theory, and when studying the so-called mean first passage times. To formally derive the adjoint operator, let us consider the Hilbert sequence space

$$l^2(\mathbb{Z}_{\geq}^N;\,\mathbb{R}) = \{p(\cdot,t) : \mathbb{Z}_{\geq}^N \to \mathbb{R} |\, \sum_{\mathbf{x}\in\mathbb{Z}_{\geq}^N} |p(\mathbf{x},t)|^2 < \infty\},$$

with the inner product

$$\langle p, q\rangle = \sum_{\mathbf{x}\in\mathbb{Z}_{\geq}^N} p(\mathbf{x})q(\mathbf{x}). \tag{2.13}$$

In this thesis, we extensively use the l^2 inner-product, involving sums and step operators, in a similar manner the L^2 inner-product, involving integrals and differentials operators, is used for investigating differential equations.

The l^2-adjoint operator corresponding to the forward operator $\mathcal{L}$, which we denote

by $\mathcal{L}^*$ [1], can then be formally obtained as follows

$$\begin{aligned}
\langle \mathcal{L}p, q\rangle &= \sum_{\mathbf{x}=\mathbf{0}}^{+\infty}\left(\sum_{j=1}^{M}(E_{\mathbf{x}}^{-\Delta\mathbf{x}_j}-1)\big(\alpha_j(\mathbf{x})p(\mathbf{x})\big)\right)q(\mathbf{x})\\
&= \sum_{j=1}^{M}\sum_{\mathbf{x}=-\Delta\mathbf{x}_j}^{+\infty}\alpha_j(\mathbf{x})p(\mathbf{x})(E_{\mathbf{x}}^{+\Delta\mathbf{x}_j}-1)q(\mathbf{x})\\
&= \sum_{j=1}^{M}\sum_{\mathbf{x}=(\boldsymbol{\nu}_j-\bar{\boldsymbol{\nu}}_j)}^{+\infty}\alpha_j(\mathbf{x})p(\mathbf{x})(E_{\mathbf{x}}^{+\Delta\mathbf{x}_j}-1)q(\mathbf{x})\\
&= \sum_{\mathbf{x}=0}^{+\infty}p(\mathbf{x})\left(\sum_{j=1}^{M}\alpha_j(\mathbf{x})(E_{\mathbf{x}}^{+\Delta\mathbf{x}_j}-1)q(\mathbf{x})\right)\\
&= \langle p, \mathcal{L}^*q\rangle, \qquad (2.14)
\end{aligned}$$

for all $p, q \in l^2(\mathbb{Z}_{\geq}^N; \mathbb{R})$, where $\sum_{\mathbf{x}=\mathbf{0}}^{+\infty} = \sum_{x_1=0}^{+\infty}\cdots\sum_{x_N=0}^{+\infty}$, and $\mathcal{L}^*$ is given by

$$\mathcal{L}^*q(\mathbf{x}) = \sum_{j=1}^{M}\alpha_j(\mathbf{x})(E_{\mathbf{x}}^{+\Delta\mathbf{x}_j}-1)q(\mathbf{x}). \qquad (2.15)$$

Let us note that we use an index shift when going from the first to second line in (2.14). When going from the third to the fourth line, we use Definition 2.4 and conditions (2.10). More specifically, if $\Delta x_i > 0$, terms with negative arguments, $x_i = (\nu_{ij} - \bar{\nu}_{ij}) < 0$, vanish due to conditions (2.10), and hence the sum indices may be started from zero. On the other hand, if $\Delta x_i < 0$, sums starting at $0 < x_i = (\nu_{ij} - \bar{\nu}_{ij}) \leq \nu_{ij}$ may also be started from zero, since the corresponding terms with $0 \leq x_i < \nu_{ij}$ lead to $\alpha_j(\mathbf{x}) = 0$ by Definition 2.4, and are hence zero.

CME on finite-dimensional state-spaces

We have written (2.9) in a form of a discrete partial-differential equation (with the step operators playing the role of partial derivatives), involving a linear operator between appropriate function spaces [51]. Let us now assume that the state-space is finite-dimensional, so that (2.9) involves a matrix acting on Euclidean vectors. More precisely, we assume that all the species copy-numbers are bounded, $\mathbf{X}(t) \leq \mathbf{C}$, for all $t \geq 0$, where $\mathbf{C} = (C_1, \ldots, C_N) \in \mathbb{Z}_{\geq}^N$, $C_i < \infty$ for $i = 1, \ldots, N$. Furthermore, let us define the corresponding finite-dimensional state-space

$$\Omega_C = \{\mathbf{x} \in \mathbb{Z}_{\geq}^N | x_1 \leq C_1, \ldots, x_N \leq C_N\} \subset \mathbb{Z}_{\geq}^N,$$

[1] It is standard to denote the backward operator by $\mathcal{L}$, while the forward operator by $\mathcal{L}^*$, in the literature (e.g. see [22, 51]). In this thesis, we do the opposite. This is because most of the calculations are performed with the forward operator, and so, to avoid using the star symbol often, we denote the forward operator by $\mathcal{L}$.

and explicitly enumerate all the possible states: $\Omega_C = \{\mathbf{x}_1, \ldots, \mathbf{x}_{N_C}\}$, with $N_C = \prod_{i=1}^{N}(C_i + 1)$. Then, $p(\mathbf{x}, t)$ may be represented as a Euclidean vector

$$\mathbf{p}(t) = (p_1(t), \ldots, p_{N_C}(t)) \in [0,1]^{N_C} \subset \mathbb{R}^{N_C}_{\geq},$$

with $p_i(t) = p(\mathbf{x}_i, t)$, while the forward operator $\mathcal{L}$ may be represented as a matrix $L : \mathbb{R}^{N_C} \to \mathbb{R}^{N_C}$, with elements [57, 58]

$$L_{ik} = \begin{cases} -\sum_{j=1}^{M} \alpha_j(\mathbf{x}_i), & \text{if } i = k, \\ \sum_{j \in \mathcal{J}} \alpha_j(\mathbf{x}_k), & \text{if } i \neq k, \text{where } \mathcal{J} = \{j \in \{1, \ldots, M\} | \Delta\mathbf{x}_j = -(\mathbf{x}_k - \mathbf{x}_i)\}, \end{cases} \tag{2.16}$$

with the convention that sums over empty sets are identically zero, $\sum_{j \in \emptyset} \alpha_j \equiv 0$. System (2.9) then becomes

$$\frac{\mathrm{d}\mathbf{p}^\top}{\mathrm{d}t} = L\mathbf{p}^\top. \tag{2.17}$$

The backward operator $\mathcal{L}^*$, given by (2.15), may be represented as the so-called generator matrix [51, 53]. When the state-space is finite-dimensional, the inner product (2.13) becomes the vector dot product. Hence, equation (2.14) is the definition of matrix transpose, so that the generator matrix is given by $L^\top$, i.e. it is the transpose of the matrix representation of the forward operator.

In this thesis, we use formulation (2.17) to numerically approximate solutions of (2.9). This is achieved by truncating the state-space of the original problem (2.9), and imposing appropriate boundary conditions, i.e. by formulating an appropriate boundary value problem (BVP) for the truncated CME [57, 58].

Example 2.4. *Consider reaction network*

$$\begin{aligned} \mathcal{R}(s, \bar{s}) : \qquad & r_1 : \bar{s} \xrightarrow{k_1} s, \\ & r_2 : s \xrightarrow{k_2} \bar{s}. \end{aligned} \tag{2.18}$$

under mass-action kinetics. Network (2.18) *displays a stoichiometric conservation law:* $X(t) + \bar{X}(t) = C = X(0) + \bar{X}(0)$*, where* $X(t), \bar{X}(t)$ *are the copy-numbers of species* $s, \bar{s}$ *at time* $t \geq 0$*, respectively, while* C *is a time-independent constant, fixed by the initial conditions for the copy-numbers. The conservation law allows us to eliminate* $\bar{X}(t)$ *from dynamical considerations via* $\bar{X}(t) = C - X(t)$*, and implies that the x-state-space, for the species of interest* $X(t)$*, is bounded, i.e.* $X(t) \leq C$ *for all* $t \geq 0$*.*

The propensity function vector is given by $\boldsymbol{\alpha}(x) = (\alpha_1(x), \alpha_2(x)) = (k_1(C - x), k_2 x)$*, while the reaction vectors are* $\Delta x_1 = +1$ *and* $\Delta x_2 = -1$*. Thus, the CME* (2.12) *for network* (2.18) *reads*

$$\begin{aligned}\frac{\partial}{\partial t}p(x,t) &= \Big((E_x^{-1} - 1)k_1(C - x) + (E_x^{+1} - 1)k_2 x\Big)p(x,t) \\ &= k_1(C - x + 1)p(x - 1, t) - \left(k_1(C - x) + k_2 x\right)p(x,t) + k_2(x + 1)p(x + 1, t).\end{aligned} \tag{2.19}$$

Let us assume $C = 3$*, so that* $X(t) \in \{0, 1, 2, 3\}$*, and enumerate the* x*-state-space as follows:* $\Omega_C = \{x_1, x_2, x_3, x_4\}$*, with* $(x_1, x_2, x_3, x_4) = (0, 1, 2, 3)$*. Letting* $p_i(t) = p(x_i, t)$*, the probability vector becomes* $\mathbf{p}(t) = (p_1(t), p_2(t), p_3(t), p_4(t))$*. Constructing the matrix* $L \in \mathbb{R}^{4\times 4}$ *according to* (2.16) *(or directly from* (2.19)*), it follows that equation* (2.19)*, written in a matrix form, reads*

$$\frac{\mathrm{d}}{\mathrm{d}t}\begin{pmatrix} p_1(t) \\ p_2(t) \\ p_3(t) \\ p_4(t) \end{pmatrix} = \begin{pmatrix} -3k_1 & k_2 & 0 & 0 \\ 3k_1 & -(2k_1 + k_2) & 2k_2 & 0 \\ 0 & 2k_1 & -(k_1 + 2k_2) & 3k_2 \\ 0 & 0 & k_1 & -3k_2 \end{pmatrix}\begin{pmatrix} p_1(t) \\ p_2(t) \\ p_3(t) \\ p_4(t) \end{pmatrix}.$$

Assuming $\mathbf{p}(0) = \mathbf{p}_0$*, the solution to the initial value problem (IVP) is readily obtained as* $\mathbf{p}^\top(t) = \exp(tL)\mathbf{p}_0^\top$*.*

In fact, given arbitrary initial conditions, time-dependent solutions of the CME (2.12)*, on both finite- and infinite-dimensional state-spaces, may be* analytically *obtained for a large class of first-order reaction networks, such as network* (2.18) [59]*. For the purposes of this thesis, we are predominantly interested in the stationary PMF (see system* (2.11)*), which may be analytically obtained for a class of higher-order networks as well* [60]*. Setting the LHS of* (2.19) *to zero, it follows that, in the long-run,* $p(x)$ *is the binomial distribution given by*

$$p(x) = \binom{C}{x}\left(\frac{k_1}{k_1 + k_2}\right)^x\left(\frac{k_2}{k_1 + k_2}\right)^{C-x}, \tag{2.20}$$

and is presented in Figure 2.1(a) *for a particular choice of the parameters* k_1, k_2, C*.* △

The Gillespie stochastic simulation algorithm (SSA)

The CME (2.9) specifies how the PMF underlying a reaction system evolves in time. The individual trajectories (sample paths) of the corresponding CTMC may be exactly simulated using the so-called *Gillespie stochastic simulation algorithm* (SSA) [31, 32], given as Algorithm 2.1, which we now briefly describe.

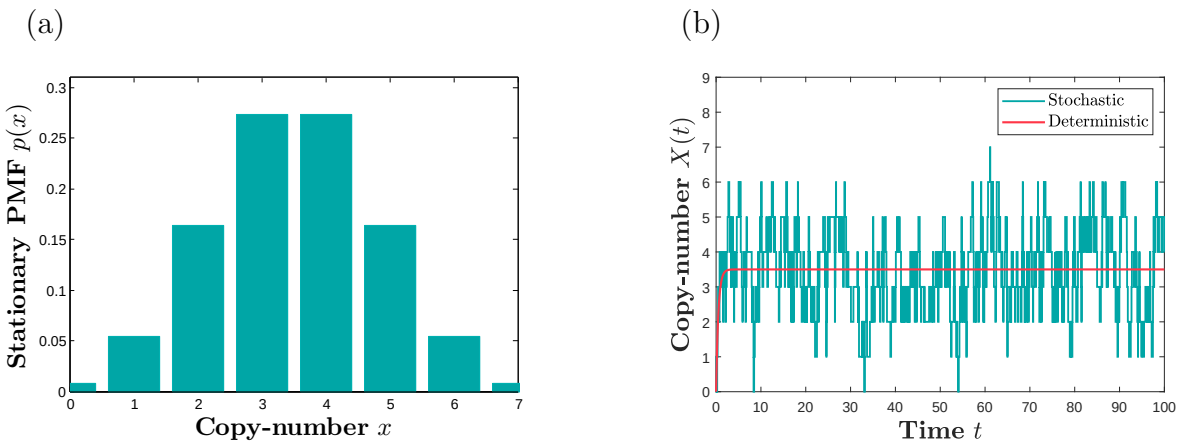

Figure 2.1: *Panel* (a) *displays the stationary probability mass function (PMF) for reaction network* (2.18)*, obtained by solving the chemical master equation (CME)* (2.19)*, with the solution given by* (2.20)*. Panel* (b) *displays in red the solution of the reaction-rate equation (RRE) underlying network* (2.18)*, with the initial condition* $x(0) = 0$*. It also displays in blue a representative sample path, obtained by applying the Gillespie stochastic simulation algorithm (SSA), with the initial condition* $X(0) = 0$*. In both panels, the rate coefficients are fixed to* $\mathbf{k} = (k_1, k_2) = (1, 1)$*, while the conservation constant to* $C = 7$*.*

Let $\mathbf{X}(t)$ be the CTMC underlying a reaction network, and let $\{t_i\}_{i=0}^{\infty}$ be the *event times* (jump times), with $t_{i+1} = t_i + \tau_i$, where $\{\tau_i\}_{i=0}^{\infty}$ are the *interevent times* (interjump times). In other words, $\mathbf{X}(t)$ experiences ith jump at time t_i, while τ_i is the time-interval between the ith and $(i+1)$th jumps, so that $\mathbf{X}(t) = \mathbf{X}(t_i)$ for all $t \in [t_i, t_i + \tau_i)$. The Gillespie SSA simulates the time-evolution of $\mathbf{X}(t)$ by: (i) computing the *time* of the next reaction firing, and (ii) computing *which* reaction fires at that time. The former is a (continuous) exponentially distributed random variable, $\tau \sim \text{Exp}(\alpha(\mathbf{x}))$, while the latter is a discrete random variable with the PMF $\mathbb{P}(m = j) = \alpha_j(\mathbf{x})/\alpha(\mathbf{x})$. Here, $\alpha(\mathbf{x}) = \sum_{j=1}^{M} \alpha_j(\mathbf{x})$ is the *total propensity function*, which is the sum of the propensity functions of the reaction network. Algorithms for generating continuous uniform random variables in the interval $[0, 1]$, denoted $u \sim U([0, 1])$, are available in many software packages. For this reason, it is customary to express the random variables τ and m as functions of u, which may be straightforwardly done (via so-called inverse transform method) [22], and is implemented in Algorithm 2.1 in equations (2.21) and (2.22), respectively. Let us note that another exact SSA is the next reaction method [61], and that there are multiple approximate simulation methods [62, 63]. In this thesis, we utilize Algorithm 2.1.

Example 2.5. *Consider reaction network* (2.18)*. In* Figure 2.1(b)*, we present in red the solution of the underlying RRE, with the initial condition* $x(0) = 0$*. We also*

Input: A chemical reaction network consisting of reactions r_j, $j = 1, \ldots, M$, with propensity functions α_j and reaction vectors $\Delta\mathbf{x}_j$, and initial condition $\mathbf{x}_0 \in \mathbb{Z}^N_{\geq}$. Set $i = 0$, $t_0 = 0$ and $\mathbf{X}(t_0) = \mathbf{x}_0$. Repeat the following steps:

(1) Compute propensity functions $\alpha_j(\mathbf{X}(t_i))$, for all $j = 1, \ldots, M$.

(2) Compute the total propensity function $\alpha(\mathbf{X}(t_i)) = \sum_{j=1}^{M} \alpha_j(\mathbf{X}(t_i))$.

(3) Generate two independent uniform random numbers in the interval $[0, 1]$, $u_i^1, u_i^2 \sim U([0, 1])$.

(4) Set

$$\tau_i = \frac{\ln(1/u_i^1)}{\alpha(\mathbf{X}(t_i))}, \tag{2.21}$$

and $t_{i+1} = t_i + \tau_i$.

(5) Find $m \in [1, \ldots, M]$ such that

$$\frac{\sum_{j=1}^{m-1} \alpha_j(\mathbf{X}(t_i))}{\alpha(\mathbf{X}(t_i))} < u_i^2 \leq \frac{\sum_{j=1}^{m} \alpha_j(\mathbf{X}(t_i))}{\alpha(\mathbf{X}(t_i))}, \tag{2.22}$$

and set $\mathbf{X}(t_{i+1}) = \mathbf{X}(t_i) + \Delta\mathbf{x}_m$.

(6) Set $i \to i + 1$.

Algorithm 2.1: *The Gillespie stochastic simulation algorithm (*SSA*).*

present in blue a single sample path, obtained by applying Algorithm 2.1 *with the same initial condition,* $X(0) = 0$. △

2.4 Relationships between the deterministic and stochastic models

We now briefly outline relationships between the deterministic and stochastic models under under mass-action kinetics, given by (2.7) and (2.12), respectively, which form the central part of this thesis.

To this end, let us obtain an equation governing the time-evolution of expectation of a function $f : \mathbb{Z}^N_{\geq} \to \mathbb{R}$, with $f = f(\mathbf{x})$ depending on the Markov chain $\mathbf{X}(t)$

underlying (2.9). The expectation of $f = f(\mathbf{x})$ is given by

$$\mathbb{E}f(\mathbf{x}) = \sum_{\mathbf{x}\in\mathbb{Z}^N_{\geq}} f(\mathbf{x})p(\mathbf{x},t) = \langle f, p\rangle, \tag{2.23}$$

where $\mathbb{E}f(\mathbf{x}) = (\mathbb{E}f(\mathbf{x}))(t)$, and $p(\mathbf{x},t)$ satisfies the CME (2.9). Using (2.14), one formally obtains

$$\begin{aligned}\frac{\mathrm{d}\mathbb{E}f(\mathbf{x})}{\mathrm{d}t} &= \langle f, \frac{\partial}{\partial t}p\rangle = \langle f, \mathcal{L}p\rangle = \langle \mathcal{L}^*f, p\rangle = \mathbb{E}\mathcal{L}^*f(\mathbf{x}) \\ &= \sum_{j=1}^{M} \mathbb{E}\alpha_j(\mathbf{x})(E_{\mathbf{x}}^{+\Delta\mathbf{x}_j} - 1)f(\mathbf{x}),\end{aligned} \tag{2.24}$$

where we use the fact that $f = f(\mathbf{x})$ does not depend on time explicitly. Setting $f(\mathbf{x}) = x_i$, one obtains the time-evolution equation for the first moment (mean):

$$\frac{\mathrm{d}\mathbb{E}x_i}{\mathrm{d}t} = \sum_{j=1}^{M} \left(\mathbb{E}\alpha_j(\mathbf{x})\right)\Delta x_{ji}, \quad i = 1,\ldots,N. \tag{2.25}$$

2.4.1 First-order reaction networks

Let us consider *first-order* reaction networks $\mathcal{R}$ under mass-action kinetics (see also Definition 2.3). In this case, both $\alpha_j(\mathbf{x})$ and $\kappa_j(\mathbf{x})$, given by (2.2) and (2.3), respectively, are affine functions, and are equal to each other:

$$\alpha_j(\mathbf{x}) = k_j\mathbf{x}^{\underline{\boldsymbol{\nu}_j}} = k_j\mathbf{x}^{\boldsymbol{\nu}_j} = \kappa_j(\mathbf{x}), \quad \mathbf{x}\in\mathbb{R}^N_{\geq}, \quad \forall j\in\{1,\ldots,M\}. \tag{2.26}$$

In (2.26), we extend the domain of discrete kinetics (2.3) from $\mathbb{Z}^N_{\geq}$ to $\mathbb{R}^N_{\geq}$, and use the fact that $x^{\underline{\nu}} = x^{\nu}$, for $x\in\mathbb{R}_{\geq}$, and $\nu\in\{0,1\}$. In other words, for zero- and first-order reactions, factorial power is identical to the usual power operator.

Using (2.26), together with linearity of the expectation operator $\mathbb{E}$, it follows that $\mathbb{E}\alpha_j(\mathbf{x}) = \mathbb{E}\kappa_j(\mathbf{x}) = \kappa_j(\mathbb{E}\mathbf{x})$, so that (2.25), written in a vector form with $\mathbb{E}\mathbf{x} = (\mathbb{E}x_1,\ldots,\mathbb{E}x_N)$, becomes

$$\frac{\mathrm{d}\mathbb{E}\mathbf{x}}{\mathrm{d}t} = \sum_{j=1}^{M} \kappa_j\left(\mathbb{E}\mathbf{x}\right)\Delta\mathbf{x}_j. \tag{2.27}$$

Comparing (2.27) with (2.7), it follows that the RREs for first-order reaction networks under mass-action kinetics describe the time-evolution of the mean copy-numbers of the corresponding stochastic model.

2.4.2 Higher-order reaction networks

For networks involving second- or higher-order reactions, the RREs do not generally describe the time-evolution of the mean of the stochastic model.

Example 2.6. *Consider the following reaction network*

$$\begin{aligned} r_1 &: \quad \bar{s} \xrightarrow{k_1} s, \\ r_2 &: \quad s \xrightarrow{k_2} \bar{s}, \\ r_3 &: \quad s + \bar{s} \xrightarrow{k_3} 2s. \end{aligned} \tag{2.28}$$

The propensity functions of the three reactions are $\alpha_1 = k_1(C - x)$, $\alpha_2 = k_2 x$, $\alpha_3 = k_3 x(C - x)$, *while the reaction vectors are* $\Delta x_1 = 1$, $\Delta x_2 = -1$, $\Delta x_3 = 1$, *and we use the conservation law* $x + \bar{x} = C$.

The RRE induced by network (2.28) *is given by*

$$\frac{\mathrm{d}x}{\mathrm{d}t} = k_1(C - x) - k_2 x + k_3 C x - k_3 x^2, \tag{2.29}$$

while the first-moment equation reads

$$\frac{\mathrm{d}\mathbb{E}x}{\mathrm{d}t} = k_1(C - \mathbb{E}x) - k_2 \mathbb{E}x + k_3 C \mathbb{E}x - k_3 \mathbb{E}x^2. \tag{2.30}$$

As a consequence of the second-order reaction r_3, *and the fact that* $\mathbb{E}x^2 \not\equiv (\mathbb{E}x)^2$ *(since variance of* $X(t)$ *is nonzero), the RRE* (2.29) *and the first-moment equation* (2.30) *are not identical. However, let us note that by embedding reaction* $r_4 : \ s + \bar{s} \xrightarrow{k_3} 2\bar{s}$ *into network* (2.28), *one obtains a second-order network for which the RRE and the first-moment equation are identical.* △

Formally, when the stochastic effects are negligible, setting the variance to zero, $\mathbb{E}(x_i - \mathbb{E}x_i)^2 = 0$, so that $x_i = \mathbb{E}x_i$, it follows that $\mathbb{E}x_i^n = (\mathbb{E}x_i)^n$, for $i = 1, \ldots, N$, and $n \geq 1$, so that the first-moment equations become the RREs when noise is vanishingly small. More precisely, under mass-action kinetics and under mild conditions on the propensity functions, classically-scaled stochastic model converges in probability over finite time-intervals to the deterministic model as the species abundance and reactor volume tend to infinity, with their ratio remaining constant (which is known as the thermodynamic limit) [38]. However, since the convergence is pointwise, and not uniform, in time, the interchange of the long-time and large-volume limits is generally not allowed. As a consequence, the equilibrium solutions of the stochastic and deterministic models may be different in the large-volume limit. Reactions systems displaying

such a disparity have been reported in the literature [64, 65, 66, 67]. In fact, the cause of the disparity in all of the reported reaction systems are noise-induced extinctions of (a subset of) species, which is known as the Keizer paradox [64]. More precisely, for large (but finite) volumes, a typical situation involves the following dynamical behavior [66]. On small time-scales, the PMF of the stochastic model approaches a so-called quasistationary PMF with maxima near the stable critical points of the corresponding deterministic model. On long time-scales, as a result of specific network structure and the presence of intrinsic noise, the PMF accumulates at the boundary of the state-space (corresponding to the extinction events). The average time to the extinctions may be much larger than the time-scale of biological relevance (in fact, for reaction networks reported in [65, 66], the average extinction time was demonstrated to grow exponentially with volume). In such cases, when the extinction is a rare event, the quasistationary PMF is more informative than the long-time PMF and, thus, the deterministic model remains to provide a useful approximation.

Example 2.7. *Consider the following conservative second-order reaction network [66]:*

$$\begin{aligned} \mathcal{R}: \qquad & s + \bar{s} \xrightarrow{k_1} 2s, \\ & 2s \xrightarrow{k_2} s + \bar{s}, \\ & s \xrightarrow{k_3} \bar{s}, \end{aligned} \tag{2.31}$$

firing in a unit-volume reactor. The copy-number of species s, denoted $X(t)$, eventually reaches the left-boundary of the state-space. Once in the absorbing state $x = 0$, no reaction from (2.31) *may fire. Thus, one may conclude that the stationary PMF is given by $p(x) = \delta_{x,0}$, where $\delta_{i,j}$ is the Kronecker-delta function. On the other hand, at the deterministic level, given a nonzero initial condition, the system tends to the stable critical point $x^* = (Ck_1 - k_3)/(k_1 + k_2)$, where C is the conservation constant from $x + \bar{x} = C$. In* Figure 2.2(a)*, we display a representative sample path in blue, while the deterministic solution in red, for $(k_1, k_2, k_3) = (17.5, 10, 10)$ and $C = 10$. One can notice that the stochastic trajectory hits the absorbing boundary at $t \approx 50$, while the deterministic one approaches the stable critical point $x^* = 6$. By increasing the reactor volume, one would observe qualitatively similar behavior. However, quantitatively, the average extinction time increases exponentially with volume [66].*

Instead of considering the stationary PMF, useful information may also be obtained by obtaining the time-independent PMF conditioned on nonextinction, $p(x|x > 0)$, known as a quasistationary PMF, which may be approximated by function $p_>(x)$

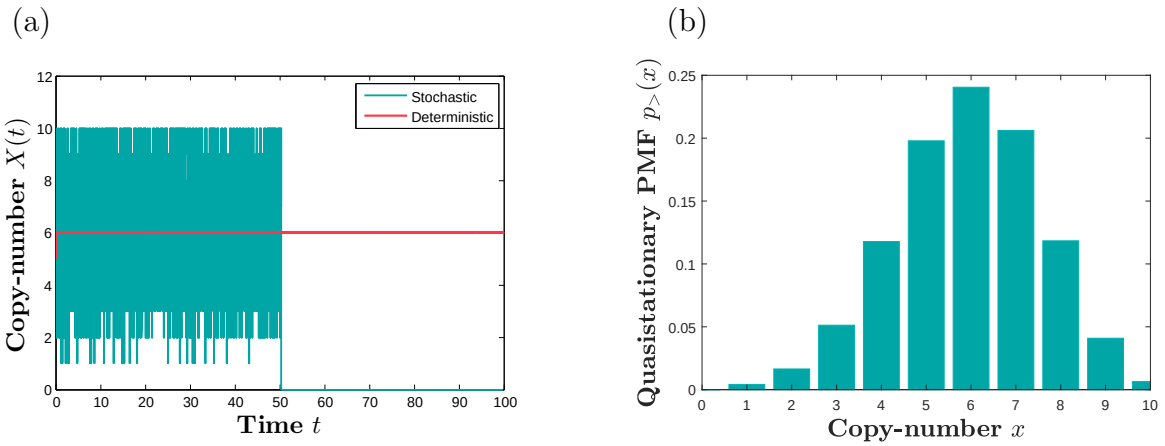

Figure 2.2: *Panel* (a) *displays in red the solution of the deterministic model underlying network* $\mathcal{R}$ *given by* (2.31)*, with the initial condition* $x(0) = 5$*. It also displays in blue a representative sample path, obtained by applying the Gillespie SSA on the underlying stochastic model, with* $X(0) = 5$*. Panel (b) displays the quasistationary probability PMF underlying network* (2.31) *as the blue histogram, obtained by numerically solving system* (2.32)*. In both panels, the rate coefficients are fixed to* $(k_1, k_2, k_3) = (17.5, 10, 10)$*, while the conservation constant to* $C = 10$*.*

(which we also call a quasistationary PMF), satisfying the following zero-EVP [52, 53]

$$\begin{aligned} \mathcal{L}p_>(x) &= 0, \quad x \in [1, C], \\ \alpha_3(1)p_>(1) &= 0, \\ \|p\|_1 &= 1. \end{aligned} \tag{2.32}$$

Here, $\alpha_3(x) = k_3 x$*, and* $\mathcal{L}$*, are the propensity function of the third reaction, and forward operator, underlying* (2.31)*, respectively. The second equation in* (2.32) *imposes a reflective boundary condition at* $x = 1$*, preventing the system from reaching the state* $x = 0$*, implicitly implying* $p_>(0) = 0$*. Taking the same parameter values as in* Figure 2.2(a)*, we show in* Figure 2.2(b) *the quasistationary PMF* $p_>(x)$ *as the blue histogram. It can be noticed that the pre-extinction part of blue sample path from* Figure 2.2(a) *matches well with the blue histrogram from Figure* 2.2(b)*. Furthermore, let us note that the quasistationary PMF peaks at* $x = 6$*, which is the deterministically stable critical point, indicating that, even for low species copy-numbers, the deterministic model may provide useful information.* △

Chapter 3

Deterministic methods: Kinetic transformations

In this chapter, we are interested in the *inverse problem* involving RREs [21, 68]: we are given structural or dynamical properties of reaction systems, and we would then like to construct a particular reaction system which displays the desired properties. A more common problem in applications is the *direct problem*: we are given a reaction system $\{\mathcal{R}, \boldsymbol{\kappa}\}$, and we then analyse the induced deterministic model (2.5). For example, an output of a direct problem might consist of a bifurcation analysis.

The inverse problem may be divided into two steps. The goal in the first step is to design a suitable kinetic function $\boldsymbol{\mathcal{K}}(\mathbf{x}; \mathcal{R})$ (RHS of the RREs), which displays predefined dynamical properties. The goal in the second step is to find a reaction system $\{\mathcal{R}, \boldsymbol{\kappa}\}$ induced by the kinetic function, displaying predefined structural properties. In this thesis, we are more focused on first step. Let us note that the constructions of reaction systems often involve constraints defining 'simplicity' of the system (e.g. see [69]). One can distinguish two overlapping simplicity criteria: dynamical simplicity, related to the RREs (dimension and structure of the RREs or their state-space), and network simplicity (e.g. cardinality, conservability, reversibility, deficiency). How the simplicity constraints are prioritized depends on the application area.

The chapter is organized as follows. In Section 3.1, we provide some definitions regarding structure of ODEs with polynomial RHSs, which are used throughout the chapter. In Section 3.2, we outline an algorithm for constructing reaction networks from a given system of RREs under mass-action kinetics, which is given as Algorithm 3.1. In Section 3.3, we introduce so-called kinetic transformations, which may map ODEs with polynomial RHS into RREs. Finally, in Section 3.4, we summarize relevant dynamical properties of two-dimensional (two-species) RREs with polynomial RHS, and apply the kinetic transformations, along with bifurcation theory, in order to

design two-dimensional reaction systems exhibiting exotic dynamical features, despite involving only two species. More precisely, in Section 3.4.1, we design the homoclinicator, given as network (3.52), which displays a coexisting stable equilibrium and a stable limit cycle (more precisely, nonconcentric mixed bistability), and undergoes a supercritical homoclinic bifurcation, with a phase plane shown in Figure 3.3(b). In Section 3.4.2, we design the bicyclicator, given as network (3.61), which displays two coexisting stable limit cycles (more precisely, nonconcentric bicyclicity), and undergoes two supercritical Hopf bifurcations, with a phase plane shown in Figure 3.4. The results presented in this chapter are based on the published papers [48, 49].

3.1 Kinetic and nonkinetic functions

In Definition 2.7, we have introduced RREs as having kinetic functions on the RHS. In this section, we define so-called nonkinetic functions, and introduce further notation for both kinetic and nonkinetic functions taking the mass-action form.

Definition 3.1. *Let* $\mathbf{f} : \mathbb{R}^N_{\geq} \to \mathbb{R}^N$ *be given componentwise by* $f_i(\mathbf{x}) = \sum_{j=1}^{M} g_{ij}(\mathbf{x})$*, with* $g_{ij}(\mathbf{x}) \in \mathbb{R}$ *for every* $i \in \{1, \ldots, N\}$ *and* $j \in \{1, \ldots, M\}$*. Let us fix index* $i \in \{1, \ldots, N\}$*, and consider the vector* $\mathbf{x} \in \mathbb{R}^N_{\geq}$ *with the* i*th component being zero. If there exists an index* $j \in \{1, \ldots, M\}$ *such that* $g_{ij}(\mathbf{x}) < 0$ *for some* $\mathbf{x} = (x_1, x_2, \ldots, x_{i-1}, 0, x_{i+1}, \ldots, x_N) \in \mathbb{R}^N_{\geq}$*, then* $g_{ij}(\mathbf{x})$ *is called a* cross-negative term*. If* $\mathbf{f}(\mathbf{x})$ *contains a cross-negative term, the function* $\mathbf{f}(\mathbf{x})$ *and the ODE system* $\mathrm{d}\mathbf{x}/\mathrm{d}t = \mathbf{f}(\mathbf{x})$ *are said to be* nonkinetic*; otherwise they are said to be* kinetic*.*

An interpretation of a cross-negative term is that the process corresponding to such a term would consume at least one reactant even when the reactant concentration is zero. Thus, cross-negative terms cannot be represented as reactions to which a kinetics can be associated (see also Definition 2.4).

Kinetic and nonkinetic functions taking the mass-action kinetics form are central to this chapter. The related notation is introduced in the following definition.

Definition 3.2. *Let* $\boldsymbol{\mathcal{P}}(\cdot; \mathbf{k}) : \mathbb{R}^N \to \mathbb{R}^N$*,* $\mathbf{k} \in \mathbb{R}^M$*, be a polynomial function with polynomial degree* $\deg(\boldsymbol{\mathcal{P}}(\mathbf{x}; \mathbf{k})) \leq m$*,* $m \in \mathbb{Z}_{\geq}$*, i.e.* $\mathcal{P}_i(\mathbf{x}; \mathbf{k})$ *is a polynomial in* $\mathbf{x} \in \mathbb{R}^N$ *of degree at most* m *with coefficients* $\mathbf{k} \in \mathbb{R}^M$*, for all* $i \in \{1, \ldots, N\}$*. Then, the set of functions* $\boldsymbol{\mathcal{P}}(\mathbf{x}; \mathbf{k})$ *is denoted by* $\mathbb{P}_m(\mathbb{R}^N; \mathbb{R}^N)$*. If* $\boldsymbol{\mathcal{P}}(\mathbf{x}; \mathbf{k})$ *is a kinetic function, it is denoted by* $\boldsymbol{\mathcal{K}}(\mathbf{x}; \mathbf{k})$*,* $\mathbf{k} \in \mathbb{R}^M_{\geq}$*, and the set of such functions is denoted by* $\mathbb{P}^{\mathcal{K}}_m(\mathbb{R}^N_{\geq}; \mathbb{R}^N)$*. If* $\boldsymbol{\mathcal{P}}(\mathbf{x}; \mathbf{k})$ *is a nonkinetic function, it is denoted by* $\boldsymbol{\mathcal{N}}(\mathbf{x}; \mathbf{k})$*,* $\mathbf{k} \in \mathbb{R}^M$*,*

and the set of such functions with domain $\mathbb{R}^N$ *is denoted by* $\mathbb{P}_m^{\boldsymbol{\mathcal{N}}}(\mathbb{R}^N;\,\mathbb{R}^N)$*, while with domain* $\mathbb{R}^N_{\geq}$ *by* $\mathbb{P}_m^{\boldsymbol{\mathcal{N}}}(\mathbb{R}^N_{\geq};\,\mathbb{R}^N)$*.*

Note that we can view the set $\{\mathcal{R}, \mathbf{k}\}$, corresponding to $\boldsymbol{\mathcal{N}}(\mathbf{x};\,\mathbf{k})$ from Definition 3.2, as containing a well-defined reaction network $\mathcal{R}$ (i.e. for $r = (\boldsymbol{\nu} \to \bar{\boldsymbol{\nu}}) \in \mathcal{R}$, we require $\boldsymbol{\nu}, \bar{\boldsymbol{\nu}} \in \mathbb{Z}_{\geq}$), but an ill-defined kinetics which, while having the mass-action *form*, contains coefficients $\mathbf{k} \in \mathbb{R}^M$, some of which are negative. Thus, coefficients $\mathbf{k} \in \mathbb{R}^M$ corresponding to $\boldsymbol{\mathcal{N}}(\mathbf{x};\,\mathbf{k})$ cannot be interpreted as rate coefficients, as opposed to coefficients $\mathbf{k} \in \mathbb{R}^M_{\geq}$ corresponding to $\boldsymbol{\mathcal{K}}(\mathbf{x};\,\mathbf{k})$ (see also Example 3.1). Note also that

$$\mathbb{P}_m(\mathbb{R}^N_{\geq};\,\mathbb{R}^N) = \mathbb{P}_m^{\boldsymbol{\mathcal{K}}}(\mathbb{R}^N_{\geq};\,\mathbb{R}^N) \cup \mathbb{P}_m^{\boldsymbol{\mathcal{N}}}(\mathbb{R}^N_{\geq};\,\mathbb{R}^N),$$

with $\mathbb{P}_m^{\boldsymbol{\mathcal{K}}}(\mathbb{R}^N_{\geq};\,\mathbb{R}^N) \cap \mathbb{P}_m^{\boldsymbol{\mathcal{N}}}(\mathbb{R}^N_{\geq};\,\mathbb{R}^N) = \emptyset$.

3.1.1 Properties of kinetic functions

From Definitions 2.4 and 3.1, it follows that a kinetic function $\boldsymbol{\mathcal{K}}(\mathbf{x};\,\mathcal{R})$ has a structural property: cross-negative terms are absent. In this section, further properties of $\boldsymbol{\mathcal{K}}(\mathbf{x};\,\mathcal{R})$ are defined: nonnegativity (absence of *cross-negative effect*), and a structural property called $\mathbf{x}$-*factorability*. Kinetic functions always display the former property, but they may not necessarily display the latter.

Definition 3.3. *Let* $\mathbf{f} : \mathbb{R}^N_{\geq} \to \mathbb{R}^N$ *be given componentwise by* $f_i(\mathbf{x}) = \sum_{j=1}^{M} g_{ij}(\mathbf{x})$*, where* $g_{ij}(\mathbf{x}) \in \mathbb{R}$*, for* $\mathbf{x} \in \mathbb{R}^N_{\geq}$*, and* $i \in \{1, \ldots, N\}$*. If* $\forall i \in \{1, \ldots, N\}$*,* $\forall \mathbf{x} \in \mathbb{R}^N_{\geq}$ *with* $x_i = 0$ *it is true that* $f_i(\mathbf{x}) \geq 0$*, then* $\mathbf{f}(\mathbf{x})$ *and* $\mathrm{d}\mathbf{x}/\mathrm{d}t = \mathbf{f}(\mathbf{x})$ *are said to be* nonnegative*, otherwise they are said to be* negative*. If they are negative, then a* cross-negative effect *is said to exists* $\forall \mathbf{x} \in \mathbb{R}^N_{\geq}$ *for which* $\exists i \in \{1, \ldots, N\}$ *such that* $x_i = 0$ *and* $f_i(\mathbf{x}) < 0$*.*

Note that the absence of cross-negative terms implies nonnegativity, but the converse is not necessarily true [21, 70], i.e. an ODE system may have cross-negative terms, without having a cross-negative effect, as we show in Example 3.1.

Cross-negative terms play an important role in mathematical constructions of reaction systems, and in the context of oscillations, multistability and chaos in RREs, as well as in the context of space-dependent reaction systems involving Turing pattern formation [71, 72].

Example 3.1. *Consider the following ODE system with polynomial RHS:*

$$\begin{aligned}\frac{\mathrm{d}x_1}{\mathrm{d}t} &= \mathcal{P}_1(x_1, x_2;\, k) = 1 + x_1^2 + 2kx_2 + x_2^2,\\ \frac{\mathrm{d}x_2}{\mathrm{d}t} &= \mathcal{P}_2(x_1, x_2;\, k) = 1,\end{aligned} \tag{3.1}$$

where $\boldsymbol{\mathcal{P}} = (\mathcal{P}_1, \mathcal{P}_2) \in \mathbb{P}_2(\mathbb{R}^2;\, \mathbb{R}^2)$, $k \in \mathbb{R}$ *and* $\mathbf{x} = (x_1, x_2)$. *Let us set* $\mathbf{x} = (0, x_2)$, *with* $x_2 > 0$. *It follows that the two solutions of* $\mathcal{P}_1(0, x_2;\, k) = 1 + 2kx_2 + x_2^2 = (x_2 - x_2^+)(x_2 - x_2^-) = 0$ *are given by* $x_2^\pm = -k \pm \sqrt{k^2 - 1}$, *and we may draw the following conclusions:*

(i) *If* $k \geq 0$, *then* (3.1) *contains no cross-negative terms, and so it is kinetic:* $\boldsymbol{\mathcal{P}}(\mathbf{x};\, k) \in \mathbb{P}_2^{\mathcal{K}}(\mathbb{R}^2_{\geq};\, \mathbb{R}^2)$.

(ii) *If* $k < 0$, *then* (3.1) *contains exactly one cross-negative term, namely* $2kx_2$, *and so it is nonkinetic:* $\boldsymbol{\mathcal{P}}(\mathbf{x};\, k) \in \mathbb{P}_2^{\mathcal{N}}(\mathbb{R}^2;\, \mathbb{R}^2)$. *Furthermore:*

   (a) *If* $-1 \leq k < 0$, *then* (3.1) *contains no cross-negative effect, and so it is nonnegative. More precisely,* $x_2^\pm$ *are complex if* $-1 < k < 0$, *while they coincide,* $x_2^+ = x_1^-$, *if* $k = -1$, *implying in both cases* $\mathcal{P}_1(0, x_2;\, k) \geq 0$.

   (b) *If* $k < -1$, *then* (3.1) *contains a cross-negative effect for* $\mathbf{x} = (0, x_2)$, *where* $x_2 \in \left(x_2^-, x_2^+\right)$, *and so it is negative.*

ODEs (3.1) *induce a reaction system only in case (i). In particular, let us emphasize that the nonnegative ODE system* (3.1) *with* $\boldsymbol{\mathcal{P}}(\mathbf{x};\, k) \in \mathbb{P}_2^{\mathcal{N}}(\mathbb{R}^2_{\geq};\, \mathbb{R}^2)$ *in part* (ii)(a) *does* not *induce a reaction system (even though, given nonnegative initial conditions, its solutions are nonnegative for all forward times).* △

Definition 3.4. *Let* $\mathbf{f} : \mathbb{R}^N_{\geq} \to \mathbb{R}^N$ *be given componentwise by* $f_i(\mathbf{x}) = \sum_{j=1}^M g_{ij}(\mathbf{x})$, *where* $g_{ij}(\mathbf{x}) \in \mathbb{R}$, *for* $\mathbf{x} \in \mathbb{R}^N_{\geq}$, *and* $i \in \{1, \ldots, N\}$. *Term* $g_{ij}(\mathbf{x})$ *is said to be* x_i-factorable *if* $g_{ij}(\mathbf{x}) = x_i p_{ij}(\mathbf{x})$, *where* $p_{ij}(\mathbf{x})$ *is a polynomial function of* $\mathbf{x}$. *If* $\exists i \in \{1, \ldots, N\}$ *such that* $f_i(\mathbf{x}) = x_i \sum_{j=1}^M p_{ij}(\mathbf{x})$, *then* $\mathbf{f}(\mathbf{x})$ *and ODE system* $\mathrm{d}\mathbf{x}/\mathrm{d}t = \mathbf{f}(\mathbf{x})$ *are said to be* x_i-factorable. *If* $f_i(\mathbf{x})$ *is* x_i*-factorable* $\forall i \in \{1, \ldots, N\}$, *then* $\mathbf{f}(\mathbf{x})$ *and ODE system* $\mathrm{d}\mathbf{x}/\mathrm{d}t = \mathbf{f}(\mathbf{x})$ *are said to be* $\mathbf{x}$-factorable.

Let us note that $\mathbf{x}$-factorable ODE systems are a subset of RREs under mass-action kinetics (see also Section 3.3.2).

Example 3.2. *Consider the reaction network:*

$$\begin{aligned} s_1 &\xrightarrow{k_1} 2s_1, \\ 2s_1 &\xrightarrow{k_2} s_1 + s_2, \\ s_2 &\xrightarrow{k_3} \varnothing. \end{aligned} \tag{3.2}$$

The RREs are given by

$$\begin{aligned} \frac{\mathrm{d}x_1}{\mathrm{d}t} &= x_1(k_1 - k_2 x_1), \\ \frac{\mathrm{d}x_2}{\mathrm{d}t} &= k_2 x_1 - k_4 x_2, \end{aligned} \tag{3.3}$$

and they are x_1-factorable (but not x_2-factorable). △

3.2 Canonical reaction systems

Let us assume we are able to construct RREs (2.5), involving kinetic function $\boldsymbol{\mathcal{K}}(\mathbf{x}; \mathcal{R})$ displaying the desired dynamical properties. Then, one can always find a reaction system induced by the kinetic function [71, 68]. While, for a fixed kinetics, a reaction network induces a kinetic function uniquely by definition (see Definition 2.7), the converse is not true – the inverse mapping of the kinetic function to the reaction systems, with fixed kinetics, is not unique – a fact known as the fundamental dogma of chemical kinetics [73, 74, 75, 71]. For example, in [75], for a fixed kinetic function and a fixed set of complexes ($\mathcal{C}$ fixed), mixed-integer programming is used for numerical computation of different induced mass-action kinetics reaction networks with varying properties. On the other hand, a constructive proof that every kinetic function induces a reaction system is given in [68, 71], where $\mathcal{C}$ is generally not fixed (product complexes may be created), but the construction can be performed analytically, and it uniquely defines the so-called induced canonical reaction system for a given kinetic function under mass-action kinetics. The procedure, in the mass-action kinetics case, is given as Algorithm 3.1.

Let us note that Algorithm 3.1 creates a reaction for each term in each RRE, i.e. if there are N equations, and each RRE has M terms on its RHS, the induced canonical reaction network (3.6) contains $N \times M$ reactions. Furthermore, each reaction in (3.6) leads to a unit-change in precisely one species abundance, i.e. each reaction vector has only one non-zero element, which is equal to -1 or $+1$. (Note that, if a reaction vector contains only zero elements, the corresponding reaction is a self-loop, i.e. of the form $(\boldsymbol{\nu}_j \to \boldsymbol{\nu}_j)$, and so is not included in the canonical reaction network, as

Input: A polynomial function without cross-negative terms (i.e. a mass-action kinetic function)

$$\mathcal{K}_i(\mathbf{x};\, \mathbf{k}_i) = \sum_{j=1}^{M} k_{ij}\mathbf{x}^{\boldsymbol{\nu}_j}, \quad i \in \{1, \ldots, N\}, \tag{3.4}$$

where $\mathbf{x} \in \mathbb{R}^N_{\geq}$, and $k_{ij} \in \mathbb{R}$ for all i, j. Write (3.4) in the *canonical form*

$$\mathcal{K}_i(\mathbf{x};\, \mathbf{k}_i) = \sum_{j=1}^{M} |k_{ij}|\mathbf{x}^{\boldsymbol{\nu}_j}\text{sign}(k_{ij}), \quad i \in \{1, \ldots, N\}, \tag{3.5}$$

where $\text{sign}(\cdot)$ is the sign function. The induced *canonical reaction system* $\{\mathcal{R}^{\mathcal{K}^{-1}}, \boldsymbol{\kappa}^{\mathcal{K}^{-1}}\}$ is then obtained by comparing (3.5) with the RHS of (2.7), as follows:

(1) Assume the zero term in (3.5) is not allowed to induce reactant complexes. The *reactant complexes* are then given by $\{\boldsymbol{\nu}_j\}_{j=1}^{M}$. For each $i \in \{1, \ldots, N\}$ and for each $j \in \{1, \ldots, M\}$, the *reaction vector* is given by $\Delta\mathbf{x}_{(i,j)} = \text{sign}(k_{ij})\mathbf{e}_i$, while the *product complex* by $\bar{\boldsymbol{\nu}}_{(i,j)} = \boldsymbol{\nu}_j + \Delta\mathbf{x}_{(i,j)}$. *The canonical reaction network* is then given by

$$\mathcal{R}^{\mathcal{K}^{-1}} = \{r_j = (\boldsymbol{\nu}_j \to \bar{\boldsymbol{\nu}}_{(i,j)}) | j \in \{1, \ldots, M\}, i \in \{1, \ldots, N\}\}. \tag{3.6}$$

(2) *The canonical kinetics* is given componentwise by

$$\kappa_j^{\mathcal{K}^{-1}}(\mathbf{x}) = |k_{ij}|\mathbf{x}^{\boldsymbol{\nu}_j}, \quad \text{for } r_j = r_j = (\boldsymbol{\nu}_j \to \bar{\boldsymbol{\nu}}_{(i,j)}), \;\; j \in \{1, \ldots, M\}, \;\; i \in \{1, \ldots, N\}. \tag{3.7}$$

Algorithm 3.1: *The algorithm for constructing canonical reaction systems under mass-action kinetics.*

required by Definition 2.2.) Thus, the canonical reaction networks are simple in the sense that they can be constructed from a kinetic function in a straightforward way, but they generally do not contain minimal number of reactions, nor complexes.

Example 3.3. *Let us write RREs underlying network* (2.1) *from* Example 2.1 *in the canonical form* (3.5)*:*

$$\begin{aligned} \frac{\mathrm{d}x_1}{\mathrm{d}t} &= |k|x_1x_2(+1), \\ \frac{\mathrm{d}x_2}{\mathrm{d}t} &= |k|x_1x_2(-1). \end{aligned} \tag{3.8}$$

Applying Algorithm 3.1*, it follows that the induced canonical reaction network is given*

by

$$\begin{aligned} r_1: &\quad s_1 + s_2 \xrightarrow{k} 2s_1 + s_2, \\ r_2: &\quad s_1 + s_2 \xrightarrow{k} s_1. \end{aligned} \tag{3.9}$$

Thus, $\mathcal{S} = \{s_1, s_2\}$, $\mathcal{C} = \{s_1 + s_2, 2s_1 + s_2, s_1\}$, $\mathcal{R}^{\mathcal{K}^{-1}} = \{s_1 + s_2 \to 2s_1 + s_2, s_1 + s_2 \to s_1\}$. *Note that the canonical reaction network* (3.9) *contains more reactions than the original (noncanonical) network* (2.1). △

3.3 Kinetic transformations

When designing ODE systems with desirable dynamical properties, it is much more likely that the RHS turns out to be a nonkinetic function, $\mathcal{N}(x; \mathcal{R})$ (see Definition 3.1) [21]. However, only kinetic functions induce reaction networks, for example via Algorithm 3.1. Furthermore, even if one obtains an ODE system with a kinetic function on the RHS, it may be necessary to modify the function in order to satisfy given constraints, and this may change the kinetic function into a nonkinetic one. For these two reasons, it is beneficial to study mappings that can transform arbitrary functions into kinetic ones. This motivates the following definition, for the case of mass-action kinetics, which relies on the notation introduced in Definition 3.2.

Definition 3.5. *Let* $\boldsymbol{\mathcal{P}}(\mathbf{x}; \mathbf{k}) \in \mathbb{P}_m(\mathbb{R}^N; \mathbb{R}^N)$, $\mathbf{k} \in \mathbb{R}^M$, *i.e.* $\boldsymbol{\mathcal{P}}(\mathbf{x}; \mathbf{k})$ *is a polynomial function. Consider the corresponding ODE system*

$$\frac{\mathrm{d}\mathbf{x}}{\mathrm{d}t} = \boldsymbol{\mathcal{P}}(\mathbf{x}; \mathbf{k}). \tag{3.10}$$

A mapping Ψ *is called a* kinetic transformation *if the following conditions are satisfied:*

(i) $\Psi : \mathbb{P}_m(\mathbb{R}^N; \mathbb{R}^N) \to \mathbb{P}^{\mathcal{K}}_{\bar{m}}(\mathbb{R}^{\bar{N}}_{\geq}; \mathbb{R}^{\bar{N}})$, $\bar{m} \geq m$, $\bar{N} \geq N$, *maps the polynomial function* $\boldsymbol{\mathcal{P}}(\mathbf{x}; \mathbf{k})$ *into a kinetic function* $\boldsymbol{\mathcal{K}}(\bar{\mathbf{x}}; \bar{\mathbf{k}}) \equiv (\Psi\boldsymbol{\mathcal{P}})(\bar{\mathbf{x}}; \bar{\mathbf{k}})$, *with* $\bar{\mathbf{x}} \in \mathbb{R}^{\bar{N}}_{\geq}$ *and* $\bar{\mathbf{k}} \in \mathbb{R}^{\bar{M}}_{>}$.

(ii) *If* Ψ *maps a critical point* $\mathbf{x}^* \in \mathbb{R}^N$ *of* $\boldsymbol{\mathcal{P}}(\mathbf{x}; \mathbf{k})$ *to a nonnegative point* $\bar{\mathbf{x}}^* \in \mathbb{R}^{\bar{N}}_{\geq}$, *then* $\bar{\mathbf{x}}^* \in \mathbb{R}^{\bar{N}}_{\geq}$ *must be a critical point of* $\boldsymbol{\mathcal{K}}(\bar{\mathbf{x}}; \bar{\mathbf{k}})$. *Furthermore, assume that* Ψ *maps the eigenvalue of the Jacobian matrix of* $\boldsymbol{\mathcal{P}}(\mathbf{x}; \mathbf{k})$, $J(\mathbf{x}^*; \mathbf{k})$, *denoted by* λ_n, *to the eigenvalue of Jacobian of* $\boldsymbol{\mathcal{K}}(\bar{\mathbf{x}}; \bar{\mathbf{k}})$, $J_\Psi(\bar{\mathbf{x}}^*; \bar{\mathbf{k}})$, *which is denoted by* $\bar{\lambda}_n$, *for* $n = 1, 2, \ldots, N$. *For each such critical point* $\bar{\mathbf{x}}^* \in \mathbb{R}^{\bar{N}}_{\geq}$, *the following must be true:*

(a) Stability preservation*:* $\mathrm{sign}(\mathrm{Re}(\lambda_n)) = \mathrm{sign}(\mathrm{Re}(\bar{\lambda}_n))$, *for* $n = 1, 2, \ldots, N$,

(b) Orientation preservation*:* $\operatorname{sign}(\operatorname{Im}(\lambda_n)) = \operatorname{sign}(\operatorname{Im}(\bar{\lambda}_n))$*, for* $n = 1, 2, \ldots, N$*,*

(c) Asymptotic stability along the added dimensions*:* $\operatorname{sign}(\operatorname{Re}(\bar{\lambda}_n)) < 0$*, for* $n = N+1, N+2, \ldots, \bar{N}$*,*

where $\operatorname{Re}(\cdot)$ *and* $\operatorname{Im}(\cdot)$ *denote the real and imaginary part of a function, respectively.*

If any of the condition (i)–(ii) *is not true,* Ψ *is called a* nonkinetic transformation.

Requirement (i) from Definition 3.5 is a structural condition, which is restrictive: it is required that kinetic transformations map the input polynomial function into an output kinetic function. On the other hand, requirement (ii) is a dynamical condition, which is mild and readily verifiable: it is required that kinetic transformations preserve desired critical points, that they preserve the sign of the underlying eigenvalues (i.e. they preserve linear stability and orientation of the critical points), and that any additional eigenvalues have negative real parts (i.e. the critical points are asymptotically stable along any added dimensions, so that the dynamics are prevented from escaping the critical points neighbourhood along the added dimensions). For example, requirement (ii) is satisfied by affine transformations (see also Section 3.3.1). Let us note that the output function is defined only in the nonnegative orthant, so that condition (ii) must hold only near the critical points of the input function that are mapped to the nonnegative orthant under kinetic transformations.

One may wish to impose a set of constraints on an output function, such as requiring that a predefined region of interest in the state-space of the input function is mapped to the positive orthant of the corresponding output function. The subset of constraints is now defined that can be formulated purely in terms of the polynomial coefficients.

Definition 3.6. *Let* $\boldsymbol{\mathcal{P}}(\mathbf{x}; \mathbf{k}) \in \mathbb{P}_m(\mathbb{R}^N; \mathbb{R}^N)$*,* $\mathbf{k} \in \mathbb{R}^M$*. Let also* $\boldsymbol{\phi} : \mathbb{R}^M \to \mathbb{R}^J$ *be a continuous function, mapping* $\mathbf{k}$ *into* $\boldsymbol{\phi}(\mathbf{k}) = (\phi_1(\mathbf{k}), \ldots, \phi_J(\mathbf{k}))$*. System* $\phi_1(\mathbf{k}) \geq 0, \phi_2(\mathbf{k}) \geq 0, \ldots, \phi_J(\mathbf{k}) \geq 0$ *is called a* system of constraints.

There are two sets of kinetic transformations. The first, and the preferred, set of possible kinetic transformations are affine transformations, which are discussed in Section 3.3.1. Affine transformations may be used, not only as possible kinetic transformations, but also to satisfy a system of constraints. The second set, necessarily used when affine transformations fail, are nonlinear transformations that replace cross-negative terms with x-factorable terms (see Definition 3.4), without introducing

new cross-negative terms, and two such transformations are discussed in Sections 3.3.2 and 3.3.3. In choosing a nonlinear transformation, one generally chooses between obtaining, on the one hand, lower-dimensional kinetic functions with higher-degree of nonlinearity (i.e. lower $\bar{N}/N$ and higher $\bar{m}/m$ in Definition 3.5(i)) or higher numbers of the nonlinear terms and, on the other hand, higher-dimensional kinetic functions with lower degree of nonlinearity (i.e. higher $\bar{N}/N$ and lower $\bar{m}/m$) or lower numbers of the nonlinear terms.

3.3.1 Affine transformations

Definition 3.7. *Consider substituting* $\bar{\mathbf{x}} = \mathbf{x} + \boldsymbol{\mathcal{T}}$ *in equation* (3.10)*, where* $\boldsymbol{\mathcal{T}} \in \mathbb{R}^N$*, which results in:*

$$\frac{\mathrm{d}\bar{\mathbf{x}}}{\mathrm{d}t} = \boldsymbol{\mathcal{P}}(\bar{\mathbf{x}} - \boldsymbol{\mathcal{T}};\, \bar{\mathbf{k}}) \equiv (\Psi_{\mathcal{T}}\boldsymbol{\mathcal{P}})(\bar{\mathbf{x}};\, \bar{\mathbf{k}}), \tag{3.11}$$

where $\bar{\mathbf{k}}$ *is a vector of the new rate coefficients obtained from* $\mathbf{k}$ *by rewriting the polynomial on the RHS of* (3.11) *into the mass-action form. Then* $\Psi_{\mathcal{T}} : \mathbb{P}_m(\mathbb{R}^N;\, \mathbb{R}^N) \to \mathbb{P}_m(\mathbb{R}^N;\, \mathbb{R}^N)$*, mapping* $\boldsymbol{\mathcal{P}}(\mathbf{x};\, \mathbf{k})$ *to* $(\Psi_{\mathcal{T}}\boldsymbol{\mathcal{P}})(\bar{\mathbf{x}};\, \bar{\mathbf{k}})$*, is called a* translation transformation*.*

Definition 3.8. *Consider applying an arbitrary nonsingular matrix* $A \in \mathbb{R}^{N\times N}$ *on equation* (3.10)*, resulting in:*

$$\frac{\mathrm{d}\bar{\mathbf{x}}}{\mathrm{d}t} = A\,\boldsymbol{\mathcal{P}}(A^{-1}\bar{\mathbf{x}};\, \bar{\mathbf{k}}) \equiv (\Psi_A\boldsymbol{\mathcal{P}})(\bar{\mathbf{x}};\, \bar{\mathbf{k}}), \tag{3.12}$$

where $\bar{\mathbf{x}} = A\mathbf{x}$*, and* $\bar{\mathbf{k}}$ *is a vector of new rate coefficients obtained from* $\mathbf{k}$ *by rewriting the polynomial on the RHS of* (3.12) *into the mass-action form. Then* $\Psi_A : \mathbb{P}_m(\mathbb{R}^N;\, \mathbb{R}^N) \to \mathbb{P}_m(\mathbb{R}^N;\, \mathbb{R}^N)$*, mapping* $\boldsymbol{\mathcal{P}}(\mathbf{x};\, \mathbf{k})$ *to* $(\Psi_A\boldsymbol{\mathcal{P}})(\bar{\mathbf{x}};\, \bar{\mathbf{k}})$*, is called a* centroaffine transformation *(also known as a linear transformation). If* A *is an orthogonal matrix, then* Ψ_A *is called an* orthogonal transformation*.*

A composition of a translation and a centroaffine transformation, $\Psi_{A,\mathcal{T}} = \Psi_A \circ \Psi_{\mathcal{T}}$, i.e. an *affine transformation*, may be used as a possible kinetic transformation (see Definition 3.5). Let us note that condition (ii) in Definition 3.5 is necessarily satisfied for all affine transformations. In fact, affine transformations preserve the dimension and global structure of the state-space, as well as the polynomial degree of the functions being mapped [78]. For these reasons, affine transformations are preferred over the alternative nonlinear transformations, discussed in the next two sections. However, affine transformations do not necessarily satisfy condition (i) in

Definition 3.5, so that they are generally nonkinetic transformations. Despite being generally nonkinetic, affine transformations map rate coefficients $\mathbf{k}$ into new ones $\bar{\mathbf{k}}$ (see equations (3.11) and (3.12)), so that they are suitable for satisfying a given system of constraints imposed on the output function (see Definition 3.6). This motivates the following definition.

Definition 3.9. *Let $\boldsymbol{\mathcal{P}}(\mathbf{x};\,\mathbf{k}) \in \mathbb{P}_m(\mathbb{R}^N;\,\mathbb{R}^N)$. Assume there exists a nonsingular matrix $A \in \mathbb{R}^{N\times N}$, and vector $\boldsymbol{\mathcal{T}} \in \mathbb{R}^N$, such that $(\Psi_A \circ \Psi_{\mathcal{T}}\boldsymbol{\mathcal{P}})(\bar{\mathbf{x}};\,\bar{\mathbf{k}})$ is a kinetic function, and a given system of constraints underlying $\boldsymbol{\phi}(\mathbf{k})$ is satisfied. It is then said that $\boldsymbol{\mathcal{P}}(\mathbf{x};\,\mathbf{k})$, and the corresponding equation* (3.10)*, are* affinely kinetic*, given the constraints. Otherwise, they are said to be* affinely nonkinetic*, given the constraints.*

If no constraints are imposed in Definition 3.6, affinely kinetic functions are called *removably nonkinetic*, while those that are affinely nonkinetic are called *essentially nonkinetic*. Such labels emphasize that, if a function is essentially nonkinetic, a kinetic function that is globally topologically equivalent [79] cannot be obtained, while if a function is removably nonkinetic, a globally topologically equivalent kinetic function can be obtained.

Explicit sufficient conditions for a polynomial function $\boldsymbol{\mathcal{P}}(\mathbf{x};\,\mathbf{k})$ to be affinely kinetic, or nonkinetic, are generally difficult to obtain. Even in the two-dimensional quadratic case, $\boldsymbol{\mathcal{P}}(\mathbf{x};\,\mathbf{k}) \in \mathbb{P}_2(\mathbb{R}^2;\,\mathbb{R}^2)$, such conditions are complicated, and cannot be easily generalized for higher-dimensional systems or systems with higher degree of nonlinearity [78]. In [72], a negative criterion has been put forward, stating that if a given nonkinetic ODE system cannot be transformed into a kinetic one using orthogonal transformations, then the system cannot be transformed into a kinetic one even if the more general centroaffine transformations are used instead.

3.3.2 X-factorable transformations

Definition 3.10. *Consider multipling the RHS of equation* (3.10) *by a diagonal matrix $\mathcal{X}(\mathbf{x}) = \operatorname{diag}(x_1, x_2, \ldots, x_N)$, resulting in*

$$\frac{\mathrm{d}\mathbf{x}}{\mathrm{d}t} = \mathcal{X}(\mathbf{x})\boldsymbol{\mathcal{P}}(\mathbf{x};\,\mathbf{k}) \equiv (\Psi_{\mathcal{X}}\boldsymbol{\mathcal{P}})(\mathbf{x};\,\mathbf{k}). \tag{3.13}$$

$\Psi_{\mathcal{X}} : \mathbb{P}_m(\mathbb{R}^N;\,\mathbb{R}^N) \to \mathbb{P}_{m+1}(\mathbb{R}^N;\,\mathbb{R}^N)$, mapping $\boldsymbol{\mathcal{P}}(\mathbf{x};\,\mathbf{k})$ to $(\Psi_{\mathcal{X}}\boldsymbol{\mathcal{P}})(\mathbf{x};\,\mathbf{k})$ is called an $\mathbf{x}$-factorable transformation*. Let us add a zero-degree term $\varepsilon\mathbf{1}$, with $\varepsilon \geq 0$ and $\mathbf{1} = (1, 1, \ldots, 1) \in \mathbb{R}^N$, to right-hand side of* (3.13)*, leading to*

$$\frac{\mathrm{d}\mathbf{x}}{\mathrm{d}t} = \varepsilon\mathbf{1} + (\Psi_{\mathcal{X}}\boldsymbol{\mathcal{P}})(\mathbf{x};\,\mathbf{k}) \equiv (\Psi_{\mathcal{X}_\varepsilon}\boldsymbol{\mathcal{P}})(\mathbf{x};\,\mathbf{k}). \tag{3.14}$$

$\Psi_{\mathcal{X}_\varepsilon} : \mathbb{P}_m(\mathbb{R}^N; \mathbb{R}^N) \to \mathbb{P}_{m+1}(\mathbb{R}^N; \mathbb{R}^N)$, *mapping* $\boldsymbol{\mathcal{P}}(\mathbf{x}; \mathbf{k})$ *to* $(\Psi_{\mathcal{X}_\varepsilon}\boldsymbol{\mathcal{P}})(\mathbf{x}; \mathbf{k})$, *is called a* perturbed $\mathbf{x}$-factorable transformation *if* $\varepsilon \neq 0$. *If* $\varepsilon = 0$, *we write* $\Psi_{\mathcal{X}} \equiv \Psi_{\mathcal{X}_0}$.

Let us note that, more generally, one may choose matrix $\mathcal{X}$ with some of the diagonal elements being equal to 1:

$$\mathcal{X}_{ii} = \begin{cases} x_i, & \text{if } i \in \mathcal{S}', \mathcal{S}' \neq \emptyset, \mathcal{S}' \subseteq \mathcal{S}, \\ 1, & \text{if } i \in \mathcal{S} \setminus \mathcal{S}'. \end{cases}$$

We then call the corresponding mapping an $(x_i)_{i\in\mathcal{S}'}$-factorable transformation, and denote it by $\Psi_{\mathcal{X}_\varepsilon}^{(x_i)_{i\in\mathcal{S}'}}$. Furthermore, vector $\mathbf{1}$ from (3.14) may be replaced by a vector with some elements being zero, instead of one.

Lemma 3.1. $(\Psi_{\mathcal{X}_\varepsilon}\boldsymbol{\mathcal{P}})(\mathbf{x}; \mathbf{k})$ *from* Defnition 3.10 *is a kinetic function, i.e.* $(\Psi_{\mathcal{X}_\varepsilon}\boldsymbol{\mathcal{P}})(\mathbf{x}; \mathbf{k}) \in \mathbb{P}_{m+1}^{\mathcal{K}}(\mathbb{R}_{\geq}^N; \mathbb{R}^N)$ *for* $\varepsilon \geq 0$.

Proof. $(\Psi_{\mathcal{X}}\boldsymbol{\mathcal{P}})(\mathbf{x}; \mathbf{k})$ is a kinetic function, since it is $\mathbf{x}$-factorable (see Definition 3.4 and also [80]). It follows that $(\Psi_{\mathcal{X}_\varepsilon}\boldsymbol{\mathcal{P}})(\mathbf{x}; \mathbf{k})$ is also a kinetic function, since $\varepsilon\mathbf{1} \geq 0$ for all $\mathbf{x} \in \mathbb{R}_{\geq}^N$. □

The mapping $\Psi_{\mathcal{X}_\varepsilon}$ satisfies condition (i) from Definition 3.5, but not necessarily condition (ii), so that it is generally a nonkinetic transformation. This arises from two overlapping artefacts that $\Psi_{\mathcal{X}_\varepsilon}$ can produce. Firstly, the critical points may change type or stability under $\Psi_{\mathcal{X}_\varepsilon}$. Secondly, the output system $(\Psi_{\mathcal{X}}\boldsymbol{\mathcal{P}})(\mathbf{x}; \mathbf{k})$ has an additional finite number of boundary critical points when compared to the input system $\boldsymbol{\mathcal{P}}(\mathbf{x}; \mathbf{k})$. Let us investigate in a greater detail the artefacts for *two*-dimensional systems induced by $\Psi_{\mathcal{X}}$ (i.e. when $\varepsilon = 0$).

Theorem 3.1. *Let us consider the ODE system* (3.10) *in two dimensions with RHS* $\boldsymbol{\mathcal{P}}(\mathbf{x}; \mathbf{k}) = (\mathcal{P}_1(\mathbf{x}; \mathbf{k}), \mathcal{P}_2(\mathbf{x}; \mathbf{k}))$. *The following statements are true for all the positive critical points* $\mathbf{x}^* \in \mathbb{R}_{>}^2$, *also called* interior critical points, *of the two-dimensional system* (3.10) *under* $\Psi_{\mathcal{X}}^{(x_i)_{i\in\mathcal{S}'}}$, $\mathcal{S}' \subseteq \{1, 2\}$*:*

(i) *All the saddle critical points are unconditionally invariant, i.e. saddle points of* (3.10) *correspond to saddle points of* (3.13).

(ii) *A sufficient condition for stability of a critical point* $\mathbf{x}^*$ *to be invariant is:*

$$\frac{\partial \mathcal{P}_1(\mathbf{x}^*; \mathbf{k})}{\partial x_1} \frac{\partial \mathcal{P}_2(\mathbf{x}^*; \mathbf{k})}{\partial x_2} \geq 0.$$

(iii) *A sufficient condition for a critical point* $\mathbf{x}^*$*, which is a node, to be invariant is:*

$$\frac{\partial \mathcal{P}_1(\mathbf{x}^*;\,\mathbf{k})}{\partial x_2}\frac{\partial \mathcal{P}_2(\mathbf{x}^*;\,\mathbf{k})}{\partial x_1} > 0.$$

Assume that the ODE system (3.10) *does not have critical points on the axes of the state-space. Nevertheless, the two-dimensional system* (3.13) *can have additional critical points on the axes of the state-space, called* boundary critical points*, denoted* $\mathbf{x}_b^* \in \mathbb{R}^2_{\geq}$*. The boundary critical points can be either nodes or saddles, and the following statements are true:*

(iv) *If system* (3.13) *is* $\mathbf{x}$*-factorable, then the origin is a critical point,* $\mathbf{x}_b^* = \mathbf{0}$*, with eigenvalues* $\lambda_i = \mathcal{P}_i(\mathbf{0};\,\mathbf{k}) \neq 0$*,* $i \in \{1,2\}$*, and the corresponding eigenvectors along the state-space axes.*

(v) *For* $x_{b,i}^* = 0$*,* $x_{b,j}^* \neq 0$*,* $\mathbf{x}_b^* \in \mathbb{R}^2_{\geq}$*,* $i,j \in \{1,2\}$*,* $i \neq j$*, a boundary critical point is a node if and only if*

$$\mathcal{P}_i(\mathbf{x}_b^*;\,\mathbf{k})\frac{\partial \mathcal{P}_j(\mathbf{x}^*;\,\mathbf{k})}{\partial x_j} > 0,$$

with the node being stable if $\mathcal{P}_i(\mathbf{x}_b^*;\,\mathbf{k}) < 0$*, and unstable if* $\mathcal{P}_i(\mathbf{x}_b^*;\,\mathbf{k}) > 0$*,* $i,j \in \{1,2\}$*,* $i \neq j$*. Otherwise, the critical point is a saddle.*

Proof. Without loss of generality, we consider two forms of the system (3.13) with $N = 2$:

$$\begin{aligned}\frac{\mathrm{d}x_1}{\mathrm{d}t} &= x_1\mathcal{P}_1(\mathbf{x};\,\mathbf{k}),\\ \frac{\mathrm{d}x_2}{\mathrm{d}t} &= x_2^p\mathcal{P}_2(\mathbf{x};\,\mathbf{k}),\end{aligned} \tag{3.15}$$

where $p \in \{0,1\}$, so that system (3.15) is $\mathbf{x}$-factorable if $p = 1$, and x_1-factorable if $p = 0$. The results derived for an x_1-factorable system hold when the system is x_2-factorable, if the indices are swapped. By writing $\mathcal{P}_i(\mathbf{x};\,\mathbf{k}) = \mathcal{P}_i$, $i \in \{1,2\}$, the Jacobian of (3.15), $J_{\mathcal{X}}$, is for $p \in \{0,1\}$ given by

$$J_{\mathcal{X}}(\mathbf{x}) = \begin{pmatrix} \mathcal{P}_1 + x_1\frac{\partial \mathcal{P}_1}{\partial x_1} & x_1\frac{\partial \mathcal{P}_1}{\partial x_2} \\ x_2^p\frac{\partial \mathcal{P}_2}{\partial x_1} & p\mathcal{P}_2 + x_2^p\frac{\partial \mathcal{P}_2}{\partial x_2} \end{pmatrix}.$$

Interior critical points. Let us consider how critical points of $\boldsymbol{\mathcal{P}}(\mathbf{x};\,\mathbf{k})$ are affected by transformation $\Psi_{\mathcal{X}}^{(x_i)_{i\in\mathcal{S}'}}$. Denoting the Jacobian of two-dimensional system (3.10) by J, and assuming the critical points are not on the axes of the state-space (i.e. $\mathbf{x}^* \in \mathbb{R}^2_{>}$), the Jacobians evaluated at $\mathbf{x}^*$ are given by:

$$J(\mathbf{x}^*) = \begin{pmatrix} \frac{\partial \mathcal{P}_1}{\partial x_1} & \frac{\partial \mathcal{P}_1}{\partial x_2} \\ \frac{\partial \mathcal{P}_2}{\partial x_1} & \frac{\partial \mathcal{P}_2}{\partial x_2} \end{pmatrix}\Bigg|_{\mathbf{x}=\mathbf{x}^*}, \qquad J_{\mathcal{X}}(\mathbf{x}^*) = \begin{pmatrix} x_1\frac{\partial \mathcal{P}_1}{\partial x_1} & x_1\frac{\partial \mathcal{P}_1}{\partial x_2} \\ x_2^p\frac{\partial \mathcal{P}_2}{\partial x_1} & x_2^p\frac{\partial \mathcal{P}_2}{\partial x_2} \end{pmatrix}\Bigg|_{\mathbf{x}=\mathbf{x}^*}.$$

Comparing the trace, determinant and discriminant of $J(\mathbf{x}^*)$ and $J_{\mathcal{X}}(\mathbf{x}^*)$, we deduce (i)–(iii).

Boundary critical points. To prove (iv)–(v), we evaluate $J_{\mathcal{X}}$ at the boundary critical points of the form $\mathbf{x}_b^* = (0, x_{b,2}^*)$ to get

$$J_{\mathcal{X}}(\mathbf{x}_b^*) = \left(\begin{array}{cc} \mathcal{P}_1 & 0 \\ x_2^p \frac{\partial \mathcal{P}_2}{\partial x_1} & p\mathcal{P}_2 + x_2^p \frac{\partial \mathcal{P}_2}{\partial x_2} \end{array} \right) \Big|_{\mathbf{x}=\mathbf{x}_b^*}. \tag{3.16}$$

If $p = 1$, then one of the boundary critical points is $\mathbf{x}_b^* = \mathbf{0}$, and the Jacobian becomes a diagonal matrix, so that condition (iv) holds. If $x_{b,2}^* \neq 0$, then $\mathcal{P}_2(0, x_{b,2}^*; \mathbf{k}) = 0$ in (3.16), and we deduce (v) by computing the trace, determinant and discriminant of $J_{\mathcal{X}}(\mathbf{x}_b^*)$. □

Theorem 3.1 can be used to readily find conditions that an $\mathbf{x}$-factorable transformation, given by $\Psi_{\mathcal{X}} : \mathbb{P}_m(\mathbb{R}^2; \mathbb{R}^2) \to \mathbb{P}_{m+1}(\mathbb{R}^2; \mathbb{R}^2)$, is a kinetic transformation. However, if any of the conditions (ii)–(iii) of Theorem 3.1 fail, or if orientable critical points are considered (foci/centers), or if higher-dimensional state-spaces are considered, then the invariance of such critical points under an $\mathbf{x}$-factorable transformation has to be checked directly by comparing the Jacobian matrices of the input and output systems. If $\Psi_{\mathcal{X}}$ turns out to be nonkinetic, one may consider a composition of an affine transformation and an $\mathbf{x}$-factorable transformation, i.e. $\Psi_{\mathcal{X},A,\mathcal{T}} = \Psi_{\mathcal{X}} \circ \Psi_A \circ \Psi_{\mathcal{T}}$, which also always satisfies (i) from Definition 3.5, and which may be kinetic. Finding an appropriate A and $\boldsymbol{\mathcal{T}}$ to ensure the preservation of the critical points typically means that the region of interest in the state-space has to be positioned at a sufficient distance from the boundary (axes). However, since the introduced boundary critical points may be saddles, this implies that the trajectories in the state-space may be significantly globally changed, regardless of how far away from the axes they are.

A composite transformation $\Psi_{\mathcal{X},A,\mathcal{T}}$ may also be used to control the boundary critical points introduced by $\Psi_{\mathcal{X}}$. The most desirable outcome of controlling the boundary fixed points is to eliminate them, or shift them outside of the nonnegative orthant. This may be particularly important when the stochastic model of reaction networks is considered, in order to avoid the Keizer paradox (see also Example 2.7 from Section 2.4.2). The former can be achieved by ensuring that the nullclines of the ODE system with RHS $(\Psi_A \circ \Psi_{\mathcal{T}} \boldsymbol{\mathcal{P}})(\mathbf{x}; \mathbf{k})$ do not intersect the axes of the state-space. The latter may be achieved by taking $0 < \varepsilon \ll 1$ in (3.14). By taking ε sufficiently small, the interior of the state-space of (3.14) is changed insignificantly. We now investigate this in a greater detail by providing a theorem relating location,

stability and type of the positive critical points of (3.10) and (3.14) in two dimensions (higher-dimensional case is analogous).

Theorem 3.2. *Consider the ODE system* (3.10) *with interior critical points* $\mathbf{x}^* \in \mathbb{R}^2_>$. *Let us assume that* $\mathbf{x}^* \in \mathbb{R}^2_>$ *is a* hyperbolic *critical point, and that the stability and type of* $\mathbf{x}^* \in \mathbb{R}^2_>$ *are invariant under* $\Psi_{\mathcal{X}}$. *It then follows that the positivity, stability and type of the critical point* $\mathbf{x}^* \in \mathbb{R}^2_>$ *are also invariant under* $\Psi_{\mathcal{X}_\varepsilon}$, *for sufficiently small* $\varepsilon > 0$. *Assume* (3.10) *does not have boundary critical points. On the other hand, denote the boundary critical points of the two-dimensional ODE system* (3.13) *by* $\mathbf{x}^*_b \in \mathbb{R}^2_\geq$, $\mathbf{x}^*_b = (x^*_{b,1}, x^*_{b,2})$, $x^*_{b,1}x^*_{b,2} = 0$, *and assume that* $\frac{\partial \mathcal{P}_i(\mathbf{x}^*_b;\mathbf{k})}{\partial x_i} \neq 0$, *if* $x^*_{b,i} \neq 0$, *for all* $i \in \{1,2\}$. *Then, if*

$$\mathcal{P}_i(\mathbf{x}^*_b;\mathbf{k}) > 0, \qquad \textit{if} \quad x^*_{b,i} = 0, \quad \textit{for some } i \in \{1,2\}, \tag{3.17}$$

it follows that the boundary critical point $\mathbf{x}^*_b \in \mathbb{R}^2_\geq$ *of the two-dimensional ODE system* (3.13) *becomes an* exterior critical point $\mathbf{x}^{*\varepsilon} \notin \mathbb{R}^2_\geq$ *of system* (3.14) *for sufficiently small* $\varepsilon > 0$.

Proof. Critical points of (3.14), denoted $\mathbf{x}^{*\varepsilon}$, are solutions of the following regularly perturbed algebraic equation

$$\varepsilon\mathbf{1} + \mathcal{X}(\mathbf{x}^{*\varepsilon})\boldsymbol{\mathcal{P}}(\mathbf{x}^{*\varepsilon};\mathbf{k}) = \mathbf{0}, \quad 0 \leq \varepsilon \ll 1. \tag{3.18}$$

Let us write $\mathbf{x}^{*\varepsilon}$ in the perturbation series

$$\mathbf{x}^{*\varepsilon} = \mathbf{x}^* + \varepsilon\mathbf{x}^{*1} + \mathcal{O}(\varepsilon^2). \tag{3.19}$$

Substituting (3.19) into (3.18), using the Taylor series theorem on $\boldsymbol{\mathcal{P}}(\mathbf{x};\mathbf{k})$, so that $\boldsymbol{\mathcal{P}}(\mathbf{x}^*+\varepsilon\mathbf{x}^{*1}+\mathcal{O}(\varepsilon^2);\mathbf{k}) = \boldsymbol{\mathcal{P}}(\mathbf{x}^*;\mathbf{k})+\varepsilon\nabla\boldsymbol{\mathcal{P}}(\mathbf{x}^*;\mathbf{k})\mathbf{x}^{*1}+\mathcal{O}(\varepsilon^2)$, using $\mathcal{X}(\mathbf{x}^*) = \mathcal{X}(\mathbf{x}^*)+\varepsilon\mathcal{X}(\mathbf{x}^{*1}) + \mathcal{O}(\varepsilon^2)$, and equating terms of equal powers in ε, the following system of polynomial equations is obtained:

$$\begin{aligned} &\mathcal{O}(1) : \mathcal{X}(\mathbf{x}^*)\boldsymbol{\mathcal{P}}(\mathbf{x}^*;\mathbf{k}) = 0, \\ &\mathcal{O}(\varepsilon) : \mathcal{X}(\mathbf{x}^*)\nabla\boldsymbol{\mathcal{P}}(\mathbf{x}^*;\mathbf{k})\mathbf{x}^{*1} + \mathcal{X}(\mathbf{x}^{*1})\boldsymbol{\mathcal{P}}(\mathbf{x}^*;\mathbf{k}) = -\mathbf{1}. \end{aligned} \tag{3.20}$$

Order 1 *equation.* Interior critical points $\mathbf{x}^* \in \mathbb{R}^2_>$ satisfy $\boldsymbol{\mathcal{P}}(\mathbf{x}^*;\mathbf{k}) = \mathbf{0}$, i.e. they are the critical points of (3.13). Since $\boldsymbol{\mathcal{P}}(\mathbf{x};\mathbf{k})$ has no boundary critical points by assumption, critical points $\mathbf{x}^*_b \in \mathbb{R}^2_\geq$ with $x^*_{b,i} = 0$, $x^*_{b,j} \neq 0$ satisfy $\mathcal{P}_i(\mathbf{x}^*_b;\mathbf{k}) \neq 0$, $\mathcal{P}_j(\mathbf{x}^*_b;\mathbf{k}) = 0$, for $i,j \in \{1,2\}$, $i \neq j$.

Order ε equation. Vector $\mathbf{x}^{*1}$, corresponding to an interior critical point $\mathbf{x}^* \in \mathbb{R}^2_>$, satisfies

$$\mathcal{X}(\mathbf{x}^*)\nabla\boldsymbol{\mathcal{P}}(\mathbf{x}^*;\,\mathbf{k})\mathbf{x}^{*1} = -\mathbf{1}, \tag{3.21}$$

which can be solved since $\mathbf{x}^*$ is a hyperbolic critical point (i.e. all of the underlying eigenvalues have nonzero real parts), so that the Jacobian matrix $\nabla\boldsymbol{\mathcal{P}}(\mathbf{x}^*;\,\mathbf{k})$ is invertible. Vector $\mathbf{x}_b^{*1}$, corresponding to a boundary critical point $\mathbf{x}_b^* \in \mathbb{R}^2_\geq$, is given componentwise by

$$x_{b,i}^{*1} = \begin{cases} -(\mathcal{P}_i(\mathbf{x}_b^*;\,\mathbf{k}))^{-1}, & \text{if } x_{b,i}^* = 0, \\ (\frac{\partial\mathcal{P}_i(\mathbf{x}_b^*;\mathbf{k})}{\partial x_i})^{-1}\left((\mathcal{P}_j(\mathbf{x}_b^*;\,\mathbf{k}))^{-1}\frac{\partial\mathcal{P}_i(\mathbf{x}_b^*;\mathbf{k})}{\partial x_j} - (x_{b,i}^*)^{-1}\right), & \text{if } x_{b,i}^* \neq 0, \end{cases} \tag{3.22}$$

with $i, j \in \{1, 2\}$, $i \neq j$. Condition (3.17) then ensures that $x_{b,i}^* < 0$ for $0 < \varepsilon \ll 1$. □

Example 3.4. *Consider the following one-species reaction network*

$$\begin{aligned} s &\xrightarrow{k_1} 2s, \\ 2s &\xrightarrow{k_2} s, \end{aligned} \tag{3.23}$$

whose RRE is x-factorable, and reads

$$\frac{\mathrm{d}x}{\mathrm{d}t} = x(k_1 - k_2 x) \equiv x\mathcal{P}_1(x;\,k_1, k_2). \tag{3.24}$$

The critical points of (3.24) *are $x^* = 0$ (unstable, boundary critical point) and $x^* = k_1/k_2$ (stable, interior critical point). Let us add a zero-degree term $0 < \varepsilon \ll 1$ to the RHS of* (3.24)*, leading to*

$$\frac{\mathrm{d}x}{\mathrm{d}t} = \varepsilon + x\mathcal{P}_1(x;\,k_1, k_2). \tag{3.25}$$

Since $\mathcal{P}_1(0;\,k_1, k_2) = k_1 > 0$, it follows from (3.17) *that the boundary critical point $x = 0$ of* (3.24) *is mapped to a negative critical point of* (3.25)*.*

The ε-dependent term from (3.25) *may be interpreted as a production reaction firing at a slow rate: $\varnothing \xrightarrow{\varepsilon} s$.* △

An alternative transformation, which is always kinetic, and which also does not change the dimension of an ODE system is a suitable time-parametrization transformation [81]. However, while $\Psi_{\mathcal{X}}$ increases the polynomial degree by one, and introduces only a finite number of boundary critical points which are given as solutions of suitable polynomials, the time-parameterization transformation generally increases the nonlinearity degree more than $\Psi_{\mathcal{X}}$, and introduces infinitely many boundary critical points.

3.3.3 Quasistationary transformations

The quasistationary approximation (QSA) is a popular *constructive* method for reducing the dimension of ODE systems by assuming that, at a given time-scale, some of the species reach a quasistationary state, so that they can be described by algebraic, rather than differential, equations [82]. The QSA is based on Tikhonov's theorem [83, 84] that specifies conditions ensuring that the solutions of the reduced system are asymptotically equivalent to the solutions of the original system. The original system is referred to as the *total system*, and it consists of the reduced subsystem, referred to as the *degenerate system*, and the remaining subsystem, called the *adjoined system*, so that the QSA consists of replacing the total system with the degenerate one, by eliminating the adjoined system. On the other hand, Korzukhin's theorem [84] is an *existence* result ensuring that, given any polynomial degenerate system, there exists a corresponding total system that is kinetic.

Thus, Tikhonov's theorem can be seen as a constructive direct asymptotic dimension reduction procedure, while Korzukhin's theorem as an inverse asymptotic dimension expansion existence result. Korzukhin's theorem has an important implication that an application of the QSA can result in a degenerate system that is *structurally* different than the corresponding total system. Violating some of the assumptions of Tikhonov's theorem may lead to dynamical artefacts [81, 85], i.e. the resulting degenerate systems may be, not only structurally different, but also *dynamically* different from the total systems. For example, the artefacts may occur due to the asymptotic parameters in Tikhonov's theorem not being sufficiently small. It has been shown that exotic dynamical phenomena such as multistability and oscillations can exist in a degenerate system, while not existing in the corresponding total system, when model reductions incompatible with Tikhonov's theorem are applied [81, 85].

Using the Tikhonov theorem, we now construct a family of kinetic total systems for an arbitrary nonkinetic polynomial degenerate system.

Definition 3.11. *Consider equation* (3.10)*, and assume that the reaction set is partitioned,* $\mathcal{R} = \mathcal{R}_1 \cup \mathcal{R}_2$*,* $\mathcal{R}_1 \cap \mathcal{R}_2 = \emptyset$*, so that* (3.10)*, together with the initial conditions, can be written componentwise as*

$$\begin{aligned} \frac{\mathrm{d}x_i}{\mathrm{d}t} &= \sum_{j\in\mathcal{R}_1} k_{ij}^1 \mathbf{x}^{\boldsymbol{\nu}_{ij}^1} - \sum_{j\in\mathcal{R}_2} k_{ij}^2 \mathbf{x}^{\boldsymbol{\nu}_{ij}^2}, \qquad \text{for } i \in \mathcal{S} = \{1,\dots,N\}, \\ x_i(t_0) &= x_i^0, \qquad x_i^0 \geq 0, \end{aligned} \tag{3.26}$$

where $\mathbf{x} \in \mathbb{R}^N$*,* $\boldsymbol{\nu}_{ij}^1, \boldsymbol{\nu}_{ij}^2 \in \mathbb{Z}_{\geq}^N$*,* $k_{ij}^1, k_{ij}^2 \in \mathbb{R}_{\geq}$*, and* $\boldsymbol{\nu}_{ij}^1 \neq \boldsymbol{\nu}_{ij}^2$ *for all* $i \in \mathcal{S}$ *and* $j \in \mathcal{R}$*. Assume further that the species set is partitioned,* $\mathcal{S} = \mathcal{S}_1 \cup \mathcal{S}_2$*,* $\mathcal{S}_1 \cap \mathcal{S}_2 = \emptyset$*, with*

$|\mathcal{S}_1| = N_1$, $|\mathcal{S}_2| = N_2$, *so that the RHS of equations for species* s_i *with index* $i \in \mathcal{S}_1$ *are kinetic functions, while those with* $i \in \mathcal{S}_2$ *are nonkinetic. Consider the following total system, consisting of a degenerate system given by*

$$\begin{aligned}
\frac{\mathrm{d}x_i}{\mathrm{d}t} &= \sum_{j\in\mathcal{R}_1} k^1_{ij}\mathbf{x}^{\boldsymbol{\nu}^1_{ij}} - \sum_{j\in\mathcal{R}_2} k^2_{ij}\mathbf{x}^{\boldsymbol{\nu}^2_{ij}}, && \text{for } i \in \mathcal{S}_1,\\
\frac{\mathrm{d}x_i}{\mathrm{d}t} &= \sum_{j\in\mathcal{R}_1} k^1_{ij}\mathbf{x}^{\boldsymbol{\nu}^1_{ij}} - \left(\frac{x_i y_i}{\omega_i}\right)\sum_{j\in\mathcal{R}_2} k^2_{ij}\mathbf{x}^{\boldsymbol{\nu}^2_{ij}}, && \text{for } i \in \mathcal{S}_2, \qquad (3.27)
\end{aligned}$$

which satisfies the initial conditions from (3.26)*, and an adjoined system given by*

$$\begin{aligned}
&\mu\frac{\mathrm{d}y_i}{\mathrm{d}t} = \omega_i - x_i y_i,\\
&y_i(t_0) = y_i^0, \qquad y_i^0 \geq 0, && \text{for } s \in \mathcal{S}_2, \qquad (3.28)
\end{aligned}$$

where $\mu, \omega_i > 0$*, and the initial condition* $y_i^0 \geq 0$ *is arbitrary.* $\Psi_{\mathrm{QS}} : \mathbb{P}_m(\mathbb{R}^N; \mathbb{R}^N) \to \mathbb{P}_{\bar{m}}(\mathbb{R}^{N+N_2}_{\geq}; \mathbb{R}^{N+N_2})$*, mapping the RHS of differential equations in system* (3.26)*, denoted* $\boldsymbol{\mathcal{P}}(\mathbf{x}; \mathbf{k})$*, to the RHS of differential equations of system* (3.27)–(3.28)*, denoted* $(\Psi_{\mathrm{QS}}\boldsymbol{\mathcal{P}})(\mathbf{x}, \mathbf{y}; \bar{\mathbf{k}})$*, is called a* quasistationary transformation*. Here,* $\bar{m} = m + 2$*, and* $\bar{\mathbf{k}}$ *is a vector of the new rate coefficients obtained from* $\mathbf{k}$ *by rewriting the polynomial* $(\Psi_{\mathrm{QS}}\boldsymbol{\mathcal{P}})(\mathbf{x}, \mathbf{y}; \bar{\mathbf{k}})$ *into the mass-action form.*

Theorem 3.3. *Positive solutions of systems* (3.26) *and* (3.27)–(3.28)*, corresponding to* $\boldsymbol{\mathcal{P}}(\mathbf{x}; \mathbf{k})$ *and* $(\Psi_{\mathrm{QS}}\boldsymbol{\mathcal{P}})(\mathbf{x}, \mathbf{y}; \bar{\mathbf{k}})$*, respectively, are* asymptotically equivalent *in the limit* $\mu \to 0$*, and* $\Psi_{\mathrm{QS}}\boldsymbol{\mathcal{P}}$ *is a kinetic function.*

Proof. Equilibria of system (3.28) satisfy $y_i^* = \omega_i(x_i)^{-1}$, where we assume $x_i > 0$ (i.e. we assume the trajectory $x_i(t)$ is contained in the interior of the non-negative orthant for all $t \geq 0$). The equilibria are isolated and, since $x_i > 0\ \forall i \in \mathcal{S}_2$, it follows that they are globally stable. Thus, the conditions of Tikhonov's theorem [84] are satisfied by the total system (3.27)–(3.28). By applying the theorem, i.e. substituting y_i^* into (3.27), one recovers the corresponding degenerate system given by (3.26). Finally, the total system (3.27)–(3.28) is kinetic, which readily follows from Definition 3.1. □

Note that $y_i \gg 1$ when $x_i \ll 1$, i.e. the invariant manifold $y_i = \omega_i(x_i)^{-1}$ takes high y_i-values near the $x_i = 0$ boundary. This may be reduced by taking $\omega_i = \mu$ (which may be straightforwardly justified by using second-order perturbation theory), resulting in the invariant manifold $y_i = \mu(x_i)^{-1}$ becoming 'flatter'.

Corollary 3.1. *The quasistationary transformation* Ψ_{QS}*, introduced in* Definition 3.11*, is a kinetic transformation.*

Example 3.5. *Consider the following polynomial ODEs, introduced in [86] in the context of pattern formation:*

$$\begin{aligned}\frac{\mathrm{d}x_1}{\mathrm{d}t} &= 5x_1 - 6x_2 + 1,\\ \frac{\mathrm{d}x_2}{\mathrm{d}t} &= 6x_1 - 7x_2 + 1.\end{aligned} \tag{3.29}$$

Since the first equation in (3.29) *contains a cross-negative term on its RHS (namely, $-6x_2$), the ODEs cannot be interpreted in terms of a reaction network under mass-action kinetics. To address this issue, we now apply the quasistationary transformation. In particular, we map the cross-negative term to an x_1-factorable one, by multiplying it by x_1y_1, and introducing an appropriate ODE for y_1 from* Definition 3.11 *with $\omega_1 = 1$, for simplicity, obtaining the following RREs*

$$\begin{aligned}\frac{\mathrm{d}x_1}{\mathrm{d}t} &= 5x_1 - 6x_1x_2y_1 + 1,\\ \frac{\mathrm{d}x_2}{\mathrm{d}t} &= 6x_1 - 7x_2 + 1,\\ \frac{\mathrm{d}y_1}{\mathrm{d}t} &= \frac{1}{\mu}(1 - x_1y_1), \quad 0 < \mu \ll 1.\end{aligned} \tag{3.30}$$

The trajectories of the RREs (3.30)*, which remain in the interior of the nonnegative quadrant, are the same as of system* (3.29) *for sufficiently small μ, as exemplified in* Figure 3.1(a)*. On the other hand, trajectories which hit the $x_1 = 0$ boundary of the nonnegative quadrant are modified (they go into the positive y_1-direction, instead of into negative x_1-values), as demonstrated in* Figure 3.1(b)*.*

The canonical reaction network induced by the RREs (3.30) *reads*

$$\begin{aligned}
r_1 &: \quad s_1 \xrightarrow{5} 2s_1, & r_5 &: \quad s_2 \xrightarrow{7} \varnothing,\\
r_2 &: \quad s_1 + s_2 + s_3 \xrightarrow{6} s_2 + s_3, & r_6 &: \quad \varnothing \xrightarrow{1} s_2,\\
r_3 &: \quad \varnothing \xrightarrow{1} s_1, & r_7 &: \quad \varnothing \xrightarrow{1/\mu} s_3,\\
r_4 &: \quad s_1 \xrightarrow{6} s_1 + s_2, & r_8 &: \quad s_1 + s_3 \xrightarrow{1/\mu} s_1,
\end{aligned}$$

where s_1, s_2, and s_3 are the species with concentrations x_1, x_2 and y_1, respectively. △

An alternative transformation, for which condition (i) in Definition 3.5 is also always satisfied, and that also expands the dimension of an ODE system, is an incomplete Carleman embedding [87, 88]. However, condition (ii) in Definition 3.5 is satisfied for the incomplete Carleman embedding only provided initial conditions for the adjoined system are appropriately constrained and, furthermore, the transformation generally results in an adjoined system with a higher nonlinearity degree

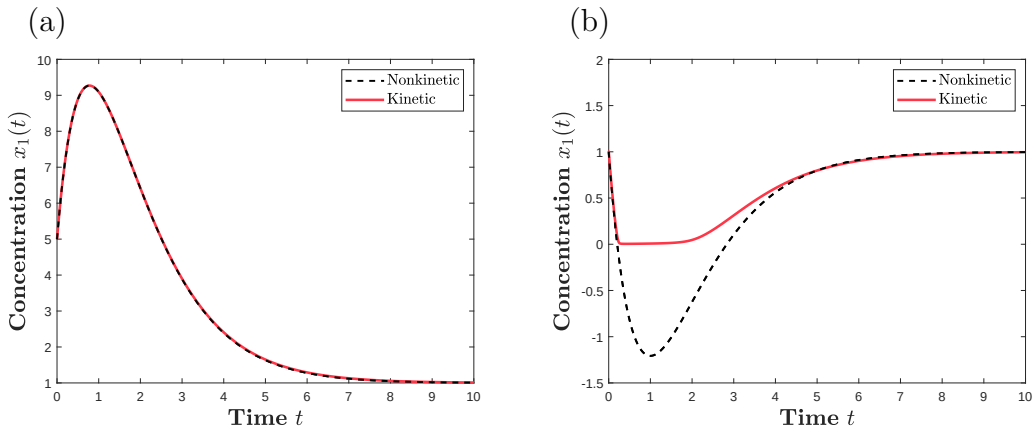

Figure 3.1: *Panel* (a) *displays the positive solution of the nonkinetic ODE system* (3.29) *for the initial condition* $(x_1, x_2) = (5, 2)$ *as the dashed black curve, while of the corresponding kinetic system* (3.30) *with the initial condition* $(x_1, x_2, y_1) = (5, 2, 0)$ *and* $\mu = 10^{-3}$ *as the red curve, showing an almost-perfect match, as predicted by* Theorem 3.3. *Analogously, panel* (b) *displays the solution of* (3.29) *with the initial condition* $(x_1, x_2) = (1, 2)$*, which attains negative values, and the corresponding nonnegative solution of* (3.30) *with the initial condition* $(x_1, x_2, y_1) = (1, 2, 0)$.

when compared to Ψ_{QS}. In contrast, the quasistationary transformation depends on the auxiliary species being governed by sufficiently fast reactions, but not on their initial conditions, which is experimentally more readily implementable using nucleic-acids [23]. Theorem 3.3 can be seen as an asymptotic alternative to the incomplete Carleman embedding, i.e. instead of requiring adjoined variables to satisfy $y_i(t) = x_i^{-1}(t)$, one requires them to satisfy $\lim_{\mu\to 0} y_i(t) = x_i^{-1}(t)$. The theorem can also be seen as an extension of using the QSA to represent reactions of more than two molecules as a limiting case of bimolecular reactions [89] to the case of using the QSA to represent cross-negative terms as a limiting case of kinetic ones.

The quasistationary transformation, which increases the dimension of the state-space, is applicable to polynomial ODE systems of arbitrary dimension, since it is guaranteed to be kinetic by satisfying the straightforward condition $0 < \mu \ll 1$. On the other hand, we have derived a set of conditions ensuring that the **x**-factorable transformations in *two* dimension are kinetic, while in the more general setting this has to be checked on a case-by-case basis. Nevertheless, in this chapter, we utilize more **x**-factorable transformations, because we consider two-dimensional systems, and we wish to preserve the dimension of the state-space to facilitate mathematical analyses.

3.4 Applications: Designing oscillations and multistability

In this section, we outline properties of the two-dimensional ODE system with second-degree polynomial RHSs (also called planar quadratic ODEs) [90, 91], concentrating on multistability, limit cycles and their bifurcations. This is followed by construction of two-dimensional RREs with cubic RHSs, displaying some of the exotic dynamical phenomena.

There are two reasons for focusing on the planar quadratic systems: firstly, the phase plane theory for such systems is well-developed [76, 92, 93], with a variety of concrete examples with interesting phase plane configurations [94, 95, 96]. Secondly, joint application of affine and $\mathbf{x}$-factorable transformations, which increase the polynomial degree of an ODE system by one, allow one to map planar quadratic system to at most cubic planar RREs, which may still be biologically or chemically relevant.

More precisely, let us consider (3.10) in two dimensions, and with quadratic RHSs:

$$\begin{aligned}\frac{\mathrm{d}x_1}{\mathrm{d}t} &= \mathcal{P}_1(x_1, x_2; \mathbf{k}) = k_1 + k_2 x_1 + k_3 x_2 + k_4 x_1^2 + k_5 x_1 x_2 + k_6 x_2^2,\\ \frac{\mathrm{d}x_2}{\mathrm{d}t} &= \mathcal{P}_2(x_1, x_2; \mathbf{k}) = k_7 + k_8 x_1 + k_9 x_2 + k_{10} x_1^2 + k_{11} x_1 x_2 + k_{12} x_2^2,\end{aligned} \tag{3.31}$$

where $\mathbf{k} = (k_1, k_2, \ldots, k_{12}) \in \mathbb{R}^{12}$ is the vector of the corresponding coefficients. We assume that $\mathcal{P}_1$ and $\mathcal{P}_2$ are relatively-prime (their highest-degree common polynomial factor is of zero-degree) and at least one is of second-degree, and allow coefficients $\mathbf{k}$ to be parameter-dependent, $\mathbf{k} = \mathbf{k}(\mathbf{p})$, with $\mathbf{p} \in \mathbb{R}^q$, $q \geq 0$. Let us compare (3.31) with its kinetic (RREs) counterpart

$$\begin{aligned}\frac{\mathrm{d}x_1}{\mathrm{d}t} &= \mathcal{K}_1(x_1, x_2; \mathbf{k}(\mathbf{p})),\\ \frac{\mathrm{d}x_2}{\mathrm{d}t} &= \mathcal{K}_2(x_1, x_2; \mathbf{k}(\mathbf{p})).\end{aligned} \tag{3.32}$$

System (3.32) is obtained from (3.31) by requiring k_1, k_3, k_6, k_7, k_8, $k_{10} \in \mathbb{R}_{\geq}$ (i.e. by precluding existence of the cross-negative terms, see also Definition 3.1). Furthermore, we also demand that the species concentrations $x_1 = x_1(t)$ and $x_2 = x_2(t)$, satisfying (3.32), are uniformly bounded in time for $t \geq 0$ in the nonnegative quadrant $\mathbb{R}^2_{\geq}$, except possibly for initial conditions located on a finite number of one-dimensional subsets of $\mathbb{R}^2_{\geq}$, where infinite-time blow-ups are allowed. This ensures that, for the most part, species concentrations are bounded. Let us note that some of the established results regarding limit cycles and multistability for system (3.31) may not necessarily hold for the more restricted system (3.32).

Bifurcations. Variations of coefficients $\mathbf{k}$ in (3.31) may lead to changes in the topology of the phase plane (e.g. a change may occur in the number of invariant sets or their stability, shape of their region of attraction or their relative position). Variation of $\mathbf{k}(\mathbf{p})$ in (3.32) may be interpreted as a variation of the reaction rate coefficients $\mathbf{k}$ due to changes in the reactor (environment) parameters $\mathbf{p}$, such as the pressure or temperature. If small variations around the parameter value $\mathbf{k}^*$ cause the system to become topologically nonequivalent, the ODE system is said to be *structurally unstable* when $\mathbf{k} = \mathbf{k}^*$, parameter $\mathbf{k}$ is called a *bifurcation parameter*, the value $\mathbf{k}^*$ is called a *bifurcation value*, and it is said that a bifurcation occurs at $\mathbf{k} = \mathbf{k}^*$ [76, 77, 79]. Bifurcations in the RREs have been reported in applications [78, 97, 98, 99, 100, 35, 101, 102]. In this chapter, we focus on bifurcations involving limit cycles and multistability.

Limit cycles. Limit cycles are isolated closed orbits in the phase plane which are not critical points, and they are periodic solutions of (3.31). Limit cycles of (3.32) may correspond to biological clocks, which play an important role in fundamental biological processes, such as the cell cycle, the glycolytic cycle and circadian rhythms [97, 98, 99]. In Appendix A, we show a necessary condition for (3.32) to display a limit cycle is that the induced reaction network must contain at least one autocatalytic reaction of the form $2s_i \to ns_i + ms_j$, with $n \geq 3$, $m \geq 0$, and $i, j \in \{1, 2\}$.

Multistability. System (3.31) is said to display multistability if the total number of the underlying stable critical points and stable limit cycles is greater than one, for a fixed $\mathbf{k}$. Multistability of (3.32) corresponds to biological switches, which may be classified into reversible or irreversible [103, 104, 105]. The former switches play an important role in reversible biological processes (e.g. metabolic pathways dynamics, and reversible differentiation), while the latter in irreversible biological processes (e.g. developmental transitions, and apoptosis). We mathematically classify multistability into *pure multistability*, involving attractors of only the same type (either only stable critical points, or only stable limit cycles), and *mixed multistability*, involving at least one stable critical point, and at least one stable limit cycle. Pure multistability involving only critical points is called *multistationarity* [21], while we call pure multistability involving only limit cycles *multicyclicity*. In Appendix A, we show that (3.31) may display maximally three stable critical points (tristability). However, no tristable quadratic planar RREs (3.32) have been reported in the literature to author's knowledge. Mixed bistability, and bicyclicity, can be further classified into concentric and nonconcentric. Concentric mixed bistability (resp. bicyclicity) occurs when the stable limit cycle encloses the stable critical point (resp. when the first

stable limit cycle encloses the second stable limit cycle), while nonconcentric when this is not the case.

The problem of finding the maximum number and configuration of limit cycles in planar polynomial ODE systems is known as the Hilbert's 16th problem [93], which has not been solved to this date even for the quadratic case. The reported maximum number of stable limit cycles in (3.31) is two, i.e. (3.31) can be *bicyclic*. Furthermore, system (3.31) may also display *mixed tristability*, involving one stable critical point, and two stable limit cycles, in the configuration $(3, 1)$ (three limit cycles enclosing the first critical point, and one limit cycle enclosing the second critical point) [93]. If the solutions of (3.31) are required to be bounded in the whole $\mathbb{R}^2$, system (3.31) was conjectured to have at most two limit cycles [76, 106], and hence have at most one stable limit cycle. It remains an open problem if (3.32) may be bicyclic. Due to the fact that (3.32) is nonnegative, and appropriately bounded in $\mathbb{R}^2_{\geq}$, additional restrictions are imposed on the boundary of $\mathbb{R}^2_{\geq}$, and on the critical points at infinity, complicating constructions of RREs (3.32) displaying multistability involving limit cycles.

Limit cycle bifurcations. Bifurcations of limit cycles of (3.31) can be classified into four categories [76]: (i) (generalized) Hopf bifurcations, where limit cycles are created from a critical point of focus type, (ii) multiple limit cycle bifurcations, where limit cycles are created from a limit cycle of multiplicity greater than one, (iii) separatrix cycle bifurcations, where limit cycles are created from a separatrix cycle, and (iv) bifurcation of limit cycles from a continuous one-parameter family of cycles (e.g. in a neighborhood of a nonlinear center) [76, 92]. Bifurcations (i) and (ii) are examples of local bifurcations, occurring in a neighbourhood of a critical point and a limit cycle, respectively. One the other hand, bifurcations (iii) and (iv) are examples of global bifurcations, occurring near a separatrix cycle and a finite number of cycles in a continuous band, respectively, which are more difficult to analyse compared to the local bifurcations. RREs (3.32) have been shown to display limit cycle bifurcations, such as generalized Hopf, multiple limit cycle, and saddle-node on an invariant cycle bifurcations [78, 101, 102]. However, some of the constructed reaction systems (e.g. displaying a saddle-saddle bifucation) are described by ODEs of the form (3.32), but with solutions which are generally not bounded in $\mathbb{R}^2_{\geq}$, which is particularly problematic when the stochastic model of reaction systems is considered.

As highlighted above, it may be a difficult task to obtain two-dimensional systems with at most quadratic terms, i.e. in the form (3.32), bounded in $\mathbb{R}^2_{\geq}$, which also display multistability involving limit cycles. To make a progress, in what follows

we allow the two-dimensional RREs to contain cubic terms, and we construct two systems in the following two sections, displaying limit cycles, bistability and some of the bifurcations which seem to have not been reported before in two-dimensional RREs.

3.4.1 The homoclinicator

In this section, we apply kinetic transformations, developed in Section 3.3, in order to construct specific two-dimensional reaction systems displaying a separatrix cycle bifurcation (a global bifurcation) giving rise to stable oscillations, known as a supercritical homoclinic bifurcation [76, 79, 109], which has been observed in higher-dimensional biochemical models in applications [100]. The key structure in the phase plane, underlying the bifurcation, is a homoclinic separatrix cycle, from which a limit cycle may bifurcate under suitable perturbations.

Definition 3.12. *Suppose* $\mathbf{x}^*$ *is a saddle critical point of system (3.10). An orbit* $\gamma^*(t)$ *starting at a point* $\mathbf{x}$ *is called* homoclinic *to the saddle* $\mathbf{x}^*$ *if its* α*-limiting and* ω*-limiting sets are both equal to* $\mathbf{x}^*$*. The union of a homoclinic orbit and the corresponding saddle critical point is called a* homoclinic separatrix cycle*.*

An example of a homoclinic separatrix cycle can be seen in Figure 3.2(b), where the homoclinic orbit is shown as the purple loop, while the saddle as the blue dot at the origin.

If a homoclinic orbit to a hyperbolic critical point is present in an ODE system, then the system is structurally unstable [76, 79], i.e. appropriate small perturbations to the equations destroy the homoclinic orbit, and thus qualitatively change the structure of the state-space, so that a bifurcation occurs. The bifurcation may be characterized by two sets of conditions: bifurcation conditions, defining the type of bifurcation, and genericity conditions, ensuring that the system is generic, i.e. can be simplified near the bifurcation to a normal form [79]. In this thesis, we consider two-dimensional systems, for which the bifurcation and genericity conditions for homolicnic bifurcation are completely specified by the Andronov-Leontovich theorem [79, 76], which can be found in Appendix A. In summary, the theorem demands that the sum of the eigenvalues corresponding to the saddle at the bifurcation point, called the saddle quantity, must be nonzero (nondegeneracy condition), and that the so-called Melnikov function corresponding to the homoclinic orbit, at the bifurcation point, must be nonzero (transversality condition). Let us note that in higher-dimensional systems, homoclinic bifurcations may be much more complicated [79, 76].

Construction of reaction systems with prescribed properties is an inverse problem which we will solve by applying kinetic transformations described in Section 3.3. Our goal is to find a mass-action reaction system (see Definition 2.5) such that the induced RREs satisfy assumptions of the Theorem A.2, i.e. they must contain a homoclinic orbit in the nonnegative orthant, and undergo the homoclinic bifurcation in a generic way. The output of this inverse problem will be a canonical reaction network which corresponds to the constructed ODE system. The inverse problem is solved in three steps given in Algorithm 3.2. The first step is solved by using results of Sandstede [109] which leads to a set of polynomial functions satisfying the first three conditions of Theorem A.2. An additional transformation is then performed, based on the Melnikov method, ensuring that the final condition of Andronov-Leontovich theorem is satisfied. In this chapter, nonlinear kinetic transformations are applied on the resulting polynomial function (using Step (2), case (b), in Algorithm 3.2).

Step (1): Construction of polynomial function $\boldsymbol{\mathcal{P}}(\mathbf{x};\, \mathbf{k})$

Definition 3.13. *The plane algebraic curve given by [110]*

$$H(x_1, x_2) = -x_1^2 + x_2^2(1 + x_2) \;\; = \;\; 0, \tag{3.33}$$

is referred to as the alpha curve*. The part of the curve with $x_2 < 0$ is called the* alpha loop*, while the part with $x_2 > 0$ is called the* alpha branches*, with the branch for $x_1 < 0$ being the* negative alpha branch*, and for $x_1 > 0$ being the* positive alpha branch*. Solutions x_1 of equation (3.33) are denoted $x_1^{\pm} = \pm x_2\sqrt{1 + x_2}$.*

The α curve is shown in Figure 3.2(a), with x_1^- plotted as the solid purple curve, and x_1^+ as the dashed green curve. It can be seen that the curve consists of the tear-shaped alpha loop located in region $[-2\sqrt{3}/9, 2\sqrt{3}/9] \times [-1, 0]$, and the positive and negative alpha branches in the first and second quadrant, respectively. As is done in [109], the alpha curve is mapped into a system of polynomial ODEs.

Lemma 3.2. *The two-dimensional polynomial* ODE *system*

$$\begin{aligned} \frac{\mathrm{d}x_1}{\mathrm{d}t} &= \mathcal{P}_1(\mathbf{x};\, a) = ax_1 + x_2 + \frac{3}{2}ax_1x_2 + \frac{3}{2}x_2^2, \\ \frac{\mathrm{d}x_2}{\mathrm{d}t} &= \mathcal{P}_2(\mathbf{x};\, a) = x_1 + ax_2 + ax_2^2, \end{aligned} \tag{3.34}$$

contains the alpha curve (3.33) *as phase plane orbits, with the alpha loop as a homoclinic orbit to the critical point $\mathbf{x}^* = \mathbf{0}$, provided $a^2 < 1$. If $a \in (-1, 0)$, the alpha loop is stable from the inside, and system* (3.34) *has three critical points: a saddle at*

(1) Construction of a polynomial function $\boldsymbol{\mathcal{P}}(\mathbf{x};\, \mathbf{k})$:
Find an ODE system (3.10) which satisfies the assumptions of Theorem A.2.

(2) Construction of a kinetic function $\boldsymbol{\mathcal{K}}(\bar{\mathbf{x}};\, \bar{\mathbf{k}})$:
Find a transformation so that the following conditions are satisfied:

- **(i)** The transformation is kinetic (see Definition 3.5), mapping the polynomial function $\boldsymbol{\mathcal{P}}(\mathbf{x};\, \mathbf{k})$ into a kinetic function $\boldsymbol{\mathcal{K}}(\bar{\mathbf{x}};\, \bar{\mathbf{k}}) \equiv (\Psi\boldsymbol{\mathcal{P}})(\bar{\mathbf{x}};\, \bar{\mathbf{k}})$.
- **(ii)** The system of constraints (see Definition 3.6), ensuring that the homoclinic orbit is in $\mathbb{R}^2_{\geq}$, are satisfied for $\boldsymbol{\mathcal{K}}(\bar{\mathbf{x}};\, \bar{\mathbf{k}})$.

To determine the choice of Ψ, if possible, deduce that $\boldsymbol{\mathcal{P}}(\mathbf{x};\, \mathbf{k})$ is affinely nonkinetic (see Definition 3.9), given the constraints.

- **(a)** If $\boldsymbol{\mathcal{P}}(\mathbf{x};\, \mathbf{k})$ is not affinely nonkinetic, attempt to find an affine transformation $\Psi = \Psi_A$ such that (i)–(ii) are satisfied.
- **(b)** If $\boldsymbol{\mathcal{P}}(\mathbf{x};\, \mathbf{k})$ is affinely nonkinetic, or if determining the opposite is true is computationally complicated, then choose kinetic transformation Ψ satisfying (i)–(ii) as an appropriate composition of Ψ_A, $\Psi_{\mathcal{X}}$ and Ψ_{QS}, where $\Psi_{\mathcal{X}}$ is an $\mathbf{x}$-factorable transformation (see Section 3.3.2) and Ψ_{QS} is a quasi-stationary transformation (see Section 3.3.3).

(3) Construction of a reaction network:
Use Algorithm 3.1 to construct the canonical reaction network $\mathcal{R}^{\mathcal{K}^{-1}}$.

Algorithm 3.2: *A three-step algorithm for constructing reaction systems undergoing a supercritical homoclinic bifurcation.*

the origin, an unstable focus inside the alpha loop, and a stable node on the positive alpha branch.

Proof. Setting $\boldsymbol{\mathcal{P}}(\mathbf{x};\, \mathbf{k}) = (\mathcal{P}_1(\mathbf{x};\, \mathbf{k}), \mathcal{P}_2(\mathbf{x};\, \mathbf{k}))$ in system (3.10) to be a polynomial function of $\mathbf{x} = (x_1, x_2)$ with undetermined coefficients $\mathbf{k}$, and requiring $\boldsymbol{\mathcal{P}} \cdot \nabla H = 0$, one obtains system (3.34), as was done in [109]. As there is only one free parameter, denoted a, we write: $\boldsymbol{\mathcal{P}}(\mathbf{x};\, \mathbf{k}) = \boldsymbol{\mathcal{P}}(\mathbf{x};\, a)$. System (3.34) has three critical points: $\big(0, 0\big)$, $\big(2a/9, -2/3\big)$, and $\big(a^{-1}(1 - a^{-2}),\, -1 + a^{-2}\big)$. Condition $a^2 < 1$ ensures that critical points $\big(2a/9, -2/3\big)$ and $\big(a^{-1}(1 - a^{-2}),\, -1 + a^{-2}\big)$ are not on the alpha loop. The Jacobian $J = \nabla\mathcal{P}(\mathbf{x};\, a)$ is given by

$$J = \begin{pmatrix} a + \frac{3}{2}ax_2 & 1 + \frac{3}{2}ax_1 + 3x_2 \\ 1 & a + 2ax_2 \end{pmatrix}. \tag{3.35}$$

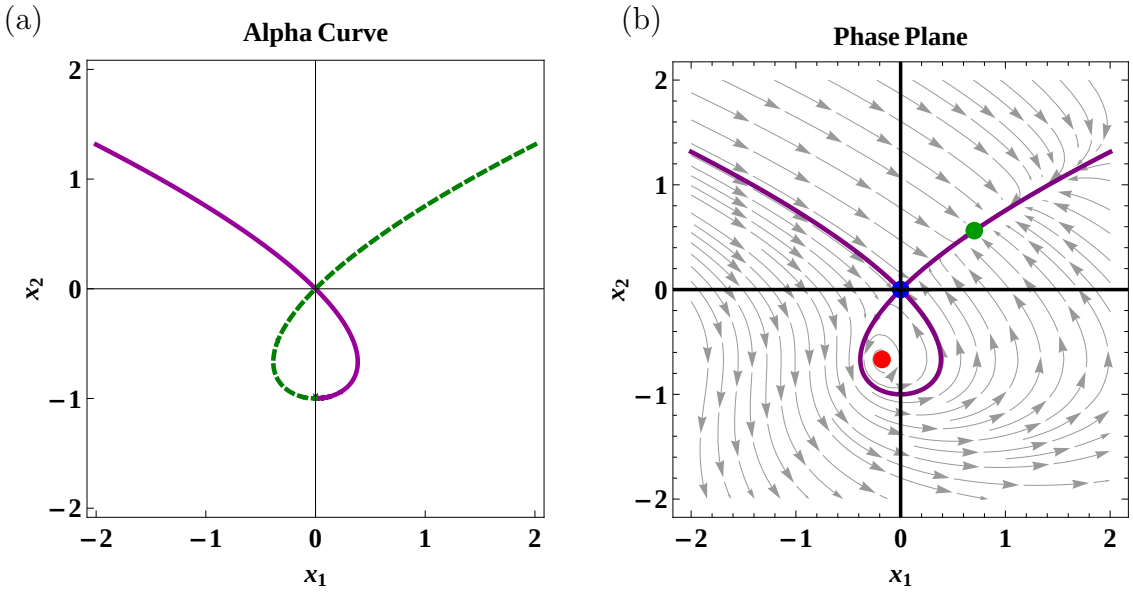

Figure 3.2: (a) *The alpha curve* (3.33)*, with branch* x_1^- *plotted as the solid purple curve, and branch* x_1^+ *as the dashed green curve.* (b) *Phase plane diagram of system* (3.34) *for* $a = -0.8$*, with the stable node, the saddle, and the unstable focus represented as the green, blue and red dots, respectively. The alpha curve is shown in purple, while the vector field as gray arrows.*

Let the determinant and trace of J be denoted by $\delta(J)$ and $\tau(J)$, respectively. Critical point $\big(0,0\big)$ is a saddle, since $\delta(J) = a^2 - 1 < 0$. The saddle quantity from Theorem A.2 is given by $\sigma_0 = 2a$. The alpha loop is stable from the inside provided $\sigma_0 < 0$, implying $a < 0$. It then follows that $\big(2/9a, -2/3\big)$ is an unstable focus, and $\big(a^{-1}(1-a^{-2}),\, -1+a^{-2}\big)$ a stable node. □

A phase plane diagram of system (3.34) is shown in Figure 3.2(b). Note that a part of the positive alpha branch x_1^+ is a heteroclinic orbit connecting the saddle and the node. The Euclidean distance between the saddle and the node is given by $d(a) = \sqrt{a^{-6}(a^2+1)(a^2-1)^2}$, so that $\lim_{a\to 0} d(a) = +\infty$ and $\lim_{a\to -1} d(a) = 0$, i.e. increasing a increases the length of the heteroclinic orbit by sliding the node along x_1^+.

System (3.34) satisfies the first three conditions of Theorem A.2. In order to satisfy the final condition, a set of perturbations must be found that destroy the alpha loop in a generic way, and this is ensured by the Melnikov condition (A.4). The bifurcation parameter controlling the existence of the alpha loop is denoted as $\alpha \in \mathbb{R}$. Note that $\boldsymbol{\mathcal{P}}(\mathbf{x};\, a)$ perturbed by a function of the form $\alpha \nabla H(x_1, x_2) = \alpha(-2x_1, 2x_2 + 3x_2^2)$ satisfies the Melnikov condition [109], but $\mathcal{P}(\mathbf{x};\, a) + \alpha \nabla H(x_1, x_2)$ has three terms

dependent on α. In the following theorem, a simpler set of perturbations is found, introducing only one α-dependent term into (3.34).

Theorem 3.4. *If a perturbation of the form $(\alpha f(x_1), 0)$, where $\alpha \in \mathbb{R}$, is added to the RHS of system* (3.34)*, and if $f(x_1)$ is an odd function, $f(-x_1) = -f(x_1)$, and $f(x_1) \neq 0$, $\forall x_1 \in [-2\sqrt{3}/9, 0)$, then the perturbed system undergoes a supercritical homoclinic bifurcation in a* generic way *as α is varied in the neighbourhood of zero.*

Proof. Consider the perturbed version of system (3.34):

$$\begin{aligned} \frac{\mathrm{d}x_1}{\mathrm{d}t} &= \mathcal{P}_1(\mathbf{x};\, a, \alpha) = ax_1 + x_2 + \frac{3}{2}ax_1x_2 + \frac{3}{2}x_2^2 + \alpha f(x_1), \\ \frac{\mathrm{d}x_2}{\mathrm{d}t} &= \mathcal{P}_2(\mathbf{x};\, a) = x_1 + ax_2 + ax_2^2. \end{aligned} \tag{3.36}$$

Melnikov function (A.4) for system (3.36) is given by

$$M(0) = -\int_{-\infty}^{+\infty} \varphi(t) f(x_1) \mathcal{P}_2(x_1, x_2;\, a)\, \mathrm{d}t.$$

If follows from (3.36) that $\mathrm{d}t = \mathrm{d}x_2/\mathcal{P}_2(x_1, x_2;\, a)$. Thus, we can express $M(0)$ in terms of x_2 as follow:

$$\begin{aligned} M(0) &= -\int_{-\infty}^{0} \varphi(t) f(x_1) \mathcal{P}_2(x_1, x_2;\, a)\, \mathrm{d}t - \int_{0}^{+\infty} \varphi(t) f(x_1) \mathcal{P}_2(x_1, x_2;\, a)\, \mathrm{d}t \\ &= \int_{-1}^{0} \varphi\big(t^+(x_2)\big) f\big(x_2\sqrt{1+x_2}\big)\, \mathrm{d}x_2 - \int_{-1}^{0} \varphi\big(t^-(x_2)\big) f\big(-x_2\sqrt{1+x_2}\big)\, \mathrm{d}x_2, \end{aligned}$$

where $t^+(x_2)$ (resp. $t^-(x_2)$) is the dependence of time t on x_2 along the positive (resp. negative) alpha branch for the trajectory which is at point $(x_1, x_2) = (0, -1)$ at time $t = 0$ (for $\alpha = 0$). Since f is odd and $\varphi(t^\pm) > 0$, we deduce

$$M(0) = \int_{-1}^{0} \Big[\varphi\big(t^+(x_2)\big) + \varphi\big(t^-(x_2)\big)\Big] f\left(x_2\sqrt{1+x_2}\right)\, \mathrm{d}x_2 \quad \neq \quad 0.$$

□

For further simplicity of (3.36), function $f(x_1)$ is set to $f(x_1) = x_1$ in the rest of the chapter.

Step (2): Construction of kinetic function $\boldsymbol{\mathcal{K}}(\bar{\mathbf{x}};\, \bar{\mathbf{k}})$

The RHS of (3.36), $\boldsymbol{\mathcal{P}}(\mathbf{x};\, a, \alpha)$, is a kinetic function. However, the alpha loop, which is the region of interest, is not located in the nonnegative quadrant. In order to position the loop into the $\mathbb{R}^2_{\geq}$, we will apply affine transformations. First, we show that system (3.36) with the homoclinic orbit in nonnegative quadrant is nonkinetic under all translation transformations for $a \in (-1, 0)$, $\alpha \in \mathbb{R}$.

Lemma 3.3. *Function $\boldsymbol{\mathcal{P}}(\mathbf{x};\, a, \alpha)$, given by the* RHS *of* (3.36)*, is nonkinetic under all translation transformations $\Psi_{\mathcal{T}}$, for $a \in (-1, 0)$ and $\alpha \in \mathbb{R}$, given the condition that the homoclinic orbit is mapped into $\mathbb{R}^2_{\geq}$.*

Proof. Let us apply the translation transformation $\Psi_{\mathcal{T}}$ (see Definition 3.7), $\boldsymbol{\mathcal{T}} = (\mathcal{T}_1, \mathcal{T}_2) \in \mathbb{R}^2$, on function $\boldsymbol{\mathcal{P}}(\mathbf{x};\, a, \alpha)$, given by the RHS of (3.36), resulting in:

$$\begin{aligned}(\Psi_{\mathcal{T}}\mathcal{P}_1)(\bar{\mathbf{x}};\, \bar{\mathbf{k}}) &= \bar{k}_1 + \bar{k}_2\bar{x}_1 + \bar{k}_3\bar{x}_2 + \bar{k}_4\bar{x}_1\bar{x}_2 + \bar{k}_5(\bar{x}_2)^2,\\ (\Psi_{\mathcal{T}}\mathcal{P}_2)(\bar{\mathbf{x}};\, \bar{\mathbf{k}}) &= \bar{k}_6 + \bar{k}_7\bar{x}_1 + \bar{k}_8\bar{x}_2 + \bar{k}_9(\bar{x}_2)^2,\end{aligned} \tag{3.37}$$

with $\bar{\mathbf{x}} = \mathbf{x} + \boldsymbol{\mathcal{T}}$, and coefficients $\bar{\mathbf{k}} = \bar{\mathbf{k}}(a, \alpha, \boldsymbol{\mathcal{T}})$ given by

$$\begin{aligned}\bar{k}_1 &= \frac{1}{2}\big(3(\mathcal{T}_2 - \frac{2}{3})(a\mathcal{T}_1 + \mathcal{T}_2) - 2\alpha\mathcal{T}_1\big),\\ \bar{k}_6 &= -\mathcal{T}_1 + a\mathcal{T}_2(\mathcal{T}_2 - 1),\\ \bar{k}_2 &= -\frac{3}{2}a(\mathcal{T}_2 - \frac{2}{3}) + \alpha, \qquad \bar{k}_7 = 1,\\ \bar{k}_3 &= 1 - \frac{3}{2}(a\mathcal{T}_1 + 2\mathcal{T}_2), \qquad \bar{k}_8 = -2a\big(\mathcal{T}_2 - \frac{1}{2}\big),\\ \bar{k}_4 &= \frac{3}{2}a, \qquad \bar{k}_5 = \frac{3}{2}, \qquad \bar{k}_9 = a.\end{aligned} \tag{3.38}$$

Consider the point $\mathbf{x_0} = (0, -1)$, which is on the alpha loop. It is mapped by $\Psi_{\mathcal{T}}$ to the point $\bar{\mathbf{x}}_\mathbf{0} = (\mathcal{T}_1, -1 + \mathcal{T}_2)$. Requiring that the alpha loop is mapped to $\mathbb{R}^2_{\geq}$ implies that the following system of constraints (see Definition 3.6) must be satisfied:

$$\mathcal{T}_1 > 0, \mathcal{T}_2 - 1 \geq 0. \tag{3.39}$$

Using the fact that $a \in (-1, 0)$ and the constraints (3.39), it follows that $\bar{k}_6$ from (3.38) is negative, $\bar{k}_6 < 0$. Thus, $(\Psi_{\mathcal{T}}\boldsymbol{\mathcal{P}})(\bar{\mathbf{x}};\, \bar{\mathbf{k}})$ has a cross-negative term, and the statement of the lemma follows. □

One can also readily prove that $\boldsymbol{\mathcal{P}}(\mathbf{x};\, a, \alpha)$ is nonkinetic under all affine transformations for $|a| \ll 1$, and $|\alpha| \ll 1$. Thus, in the next two sections, we follow Step (2), case (b), in Algorithm 3.2, applying transformations $\Psi_{\mathcal{X}}$ and Ψ_{QS} on the kinetic function $(\Psi_{\mathcal{T}}\boldsymbol{\mathcal{P}})(\bar{\mathbf{x}};\, \bar{\mathbf{k}})$ given by (3.37). We require the following conditions to be satisfied:

$$\begin{aligned}&a \in (-1, 0), \quad |\alpha| \ll 1,\\ &\mathcal{T}_1 - \frac{2\sqrt{3}}{9} > 0, \mathcal{T}_2 - 1 > 0,\end{aligned} \tag{3.40}$$

with the constraints ensuring that the homoclinic orbit is in $\mathbb{R}^2_>$. The reason for requiring $|\alpha| \ll 1$ is that then the following results are more readily derived, and the condition is sufficient for studying system (3.37) near the bifurcation point $\alpha = 0$. A representative phase plane diagram corresponding to the ODE system with RHS (3.37) is shown in Figure 3.3(a), with the critical points, the alpha curve, and the vector field denoted as in Figure 3.2(b), and with the red segments on the axes corresponding to the phase plane regions where the cross-negative effect exists (see Definition 3.3).

X-factorable transformation. Let us apply the perturbed **x**-factorable transformation $\Psi_{\mathcal{X}_\varepsilon}$ on system (3.37). Letting $\Psi_{\mathcal{X}_\varepsilon,\mathcal{T}} \equiv \Psi_{\mathcal{X}_\varepsilon} \circ \Psi_{\mathcal{T}}$, the resulting kinetic function $\boldsymbol{\mathcal{K}}_{\mathcal{X}_\varepsilon,\mathcal{T}}(\bar{\mathbf{x}};\, \bar{\mathbf{k}}) \equiv (\Psi_{\mathcal{X}_\varepsilon,\mathcal{T}}\boldsymbol{\mathcal{P}})(\bar{\mathbf{x}};\, \bar{\mathbf{k}})$ is given componentwise by

$$\begin{aligned}
\mathcal{K}_{1,\mathcal{X}_\varepsilon,\mathcal{T}}(\bar{\mathbf{x}};\, \bar{\mathbf{k}}) &= \varepsilon + \bar{x}_1(\bar{k}_1 + \bar{k}_2\bar{x}_1 + \bar{k}_3\bar{x}_2 + \bar{k}_4\bar{x}_1\bar{x}_2 + \bar{k}_5(\bar{x}_2)^2),\\
\mathcal{K}_{2,\mathcal{X}_\varepsilon,\mathcal{T}}(\bar{\mathbf{x}};\, \bar{\mathbf{k}}) &= \varepsilon + \bar{x}_2(\bar{k}_6 + \bar{k}_7\bar{x}_1 + \bar{k}_8\bar{x}_2 + \bar{k}_9(\bar{x}_2)^2).
\end{aligned} \tag{3.41}$$

Theorem 3.5. *Let us assume that*

$$\begin{aligned}
a \in (-1, 0), \quad |\alpha| \ll 1, \quad 0 \le \varepsilon \ll 1,\\
\frac{2\sqrt{3}}{9} < \mathcal{T}_1 < \infty,\\
\max(1, -a\mathcal{T}_1) < \mathcal{T}_2 < \frac{2}{3} + \frac{8}{3}a^{-2}(3 - a^2)(a + 4\mathcal{T}_1).
\end{aligned} \tag{3.42}$$

It then follows that the ODE systems with RHSs (3.37) *and* (3.41) *have the same number of positive critical points, with the corresponding positive critical points having identical linear stability and orientation, and the homoclinic orbit is in* $\mathbb{R}^2_>$.

Proof. Let us assume $\alpha = 0$.

Interior critical points. It follows from statement (i) of Theorem 3.1 that the saddle critical point of (3.37) is unconditionally preserved under $\Psi_{\mathcal{X}}$. Denoting the node and focus critical points of (3.37) by $\bar{\mathbf{x}}^*_{\mathrm{n}}$ and $\bar{\mathbf{x}}^*_{\mathrm{f}}$, respectively, one finds that the Jacobian is given by:

$$\begin{aligned}
J_{\mathcal{T}}|_{\bar{\mathbf{x}}=\bar{\mathbf{x}}^*_{\mathrm{n}}} &= \begin{pmatrix} a + \frac{3}{2}a^{-1}(1 - a^2) & \frac{1}{2}a^{-2}(3 - a^2) \\ 1 & a^{-1}(2 - a^2) \end{pmatrix} \implies \operatorname{sign}(J_{\mathcal{T}}|_{\bar{\mathbf{x}}=\bar{\mathbf{x}}^*_{\mathrm{n}}}) = \begin{pmatrix} - & + \\ + & - \end{pmatrix},\\
J_{\mathcal{T}}|_{\bar{\mathbf{x}}=\bar{\mathbf{x}}^*_{\mathrm{f}}} &= \begin{pmatrix} 0 & -\frac{1}{3}(3 - a^2) \\ 1 & -\frac{1}{3}a \end{pmatrix} \implies \operatorname{sign}(J_{\mathcal{T}}|_{\bar{\mathbf{x}}=\bar{\mathbf{x}}^*_{\mathrm{f}}}) = \begin{pmatrix} 0 & - \\ + & + \end{pmatrix}.
\end{aligned} \tag{3.43}$$

Conditions (ii) and (iii) of Theorem 3.1 are both unconditionally satisfied for the node, so that it is also perserved under $\Psi_{\mathcal{X}}$. Condition (ii) is also unconditionally satisfied

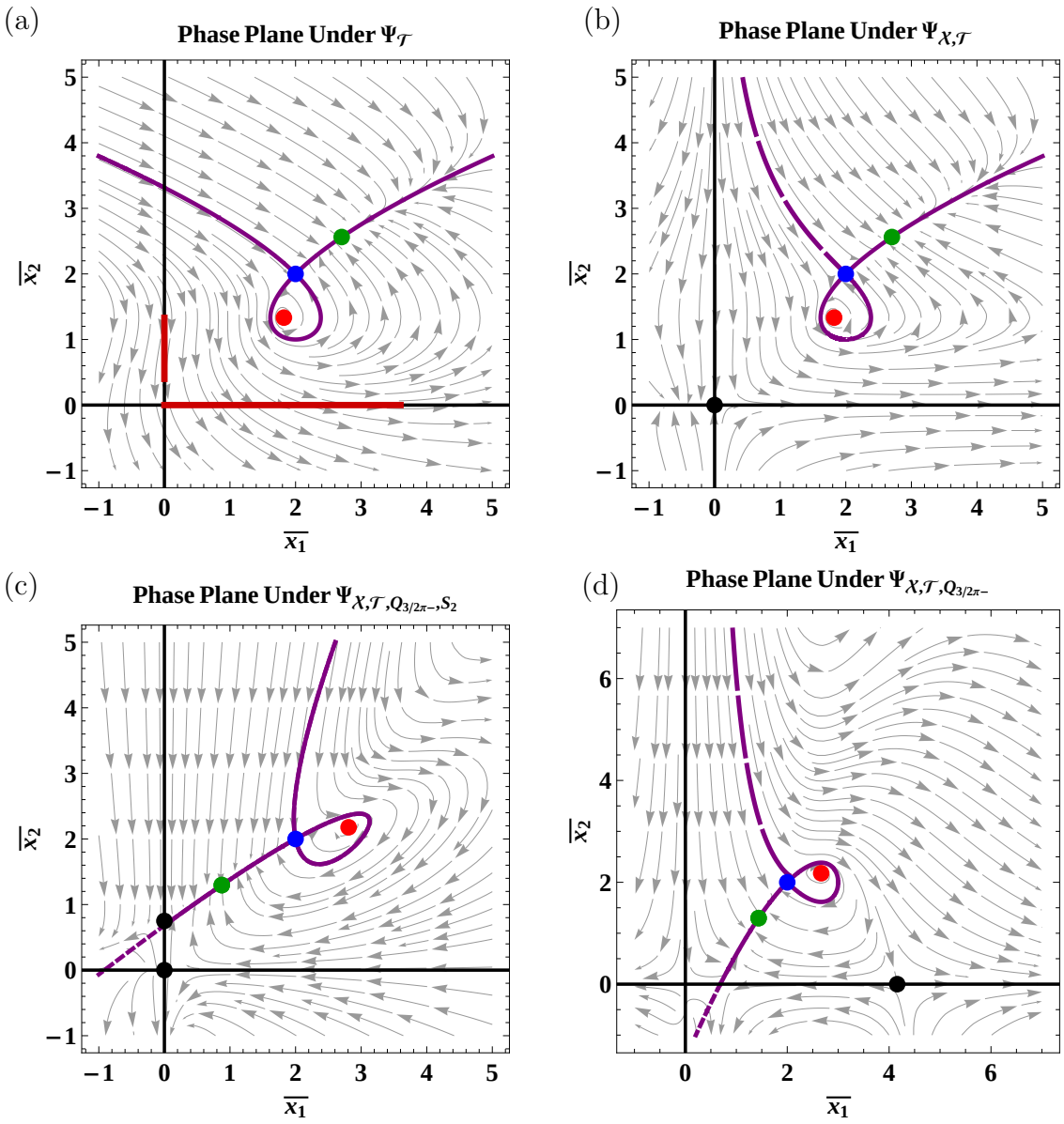

Figure 3.3: *Phase plane diagrams of* (a) *ODE system with RHS* (3.37)*;* (b) *ODE system with RHS* (3.41) *and* $\varepsilon = 0$*;* and (c) *ODE system with RHS* (3.46)*. The stable node, the saddle, and the unstable focus are represented as the green, blue and red dot, respectively. The alpha curve is shown in purple, and the vector field as gray arrows. On each plot it is indicated which kinetic transformation is applied to system* (3.36)*. Red segments of the phase plane axes in* (a) *denote the regions where the cross-negative effect exists. In* (b) *and* (c)*, boundary critical points are represented as the black dots, purple curves with a coarser dashing represent the saddle manifolds that asymptotically approach an axis, while with a finer dashing those that are outside of* $\mathbb{R}^2_{\geq}$*.*
(d) *Phase plane diagram of a system for which* $\mathbf{x}$*-factorable transformation significantly globally influences the phase curves in such a way that a pure translation cannot resolve the artefacts. For more details, see the text. The parameters are fixed to* $a = -0.8$*,* $\alpha = 0$*,* $\mathcal{T}_1 = 2$*,* $\mathcal{T}_2 = 2$*,* $\varepsilon = 0$*.*

for the focus. Furthermore, it is invariant under $\Psi_{\mathcal{X}}$ provided $\operatorname{disc}(J_{\mathcal{X},\mathcal{T}}|_{\bar{\mathbf{x}}=\bar{\mathbf{x}}_{\mathrm{f}}^*}) < 0$, where $\operatorname{disc}(\cdot)$ denotes the discriminant, and $J_{\mathcal{X},\mathcal{T}}$ is the Jacobian of (3.41) with $\varepsilon = 0$. Taking into consideration (3.40), this leads to

$$\mathcal{T}_2 < \frac{2}{3} + \frac{8}{3}a^{-2}(3 - a^2)(a + 4\mathcal{T}_1). \tag{3.44}$$

Boundary critical points. Boundary critical points of (3.41) with $\varepsilon = 0$ are given by $(0, 0)$, $(\mathcal{T}_1 + a^{-1}\mathcal{T}_2, 0)$ and $(0, 1/2(1 \pm \sqrt{1 + 4a^{-1}\mathcal{T}_1}) + \mathcal{T}_2)$. The second critical point can be removed from the nonnegative quadrant by demanding $\mathcal{T}_2 > -a\mathcal{T}_1$, while the pair of the last ones always has a nonzero imaginary part due to (3.40). Statement (iv) of Theorem 3.1 implies that the eigenvalues of the critical point at the origin are given by $\lambda_1 = (\Psi_{\mathcal{T}}\mathcal{P}_1)(\mathbf{0}; \bar{\mathbf{k}}) = \bar{k}_1 = 3/2(\mathcal{T}_2 - 2/3)(a\mathcal{T}_1 + \mathcal{T}_2) > 0$ and $\lambda_2 = (\Psi_{\mathcal{T}}\mathcal{P}_2)(\mathbf{0}; \bar{\mathbf{k}}) = \bar{k}_6 = -\mathcal{T}_1 + a\mathcal{T}_2(\mathcal{T}_2 - 1) < 0$, so that origin is a saddle. Furthermore, since $(\Psi_{\mathcal{T}}\mathcal{P}_1)(\mathbf{0}; \bar{\mathbf{k}}) > 0$, it follows from condition (3.17) from Theorem 3.2 that the saddle at the origin, present in system (3.41) with $\varepsilon = 0$, is mapped outside the nonnegative quadrant when $0 < \varepsilon \ll 1$, while the rest of the positive critical points (all of which are hyperbolic) are preserved.

As α can be chosen arbitrarily close to zero, and as $\boldsymbol{\mathcal{K}}_{\mathcal{X}_\varepsilon,\mathcal{T}}(\bar{\mathbf{x}}; \bar{\mathbf{k}})$ is a continuous function of α, the theorem holds for sufficiently small $|\alpha| \neq 0$, as well. □

A representative phase plane diagram corresponding to the ODE system with RHS (3.41), and $\varepsilon = 0$, is shown in Figure 3.3(b), where the saddle at the origin is shown as the black dot. It can be seen that one of the stable manifolds of the nonboundary saddle, represented as a dashed purple curve, approaches x_2-axis asymptotically, instead of crossing it as in Figure 3.3(a).

The homoclinic orbit of the ODE system with RHS (3.41) is positioned below the node in the phase plane. Suppose the relative position of the stable sets is reversed by, say, applying an orthogonal matrix with the angle fixed to $3\pi/2$, followed by a reflection, denoted $\Psi_{Q_{3\pi/2-}}$, with a representative phase plane shown in Figure 3.3(d). In this case, one can straightforwardly show that the boundary critical point given by $\big(\mathcal{T}_1 + 1/2(1 + \sqrt{1 - 4a^{-1}\mathcal{T}_2}), 0\big)$, shown as the black dot in Figure 3.3(d), cannot be removed from $\mathbb{R}^2_{\geq}$, and is always a saddle. The same conclusions are true for other similar configurations of the stable sets obtained by rotations. This demonstrates that $\mathbf{x}$-factorable transformations can produce boundary artefacts that have a significant *global* influence on the trajectories in the state-space, that cannot be eliminated by simply translating a region of interest sufficiently far away from the axes. In order to

eliminate the particular boundary artefact, a shear transformation may be applied. Consider applying $\Psi_{\mathcal{X},\mathcal{T},\mathcal{Q}_{3\pi/2-},\mathcal{S}_2} = \Psi_{\mathcal{X}} \circ \Psi_{\mathcal{T}} \circ \Psi_{\mathcal{Q}_{3\pi/2-}} \circ \Psi_{\mathcal{S}_2}$ on (3.36), where

$$S_2 = \begin{pmatrix} 1 & 0 \\ -a & 1 \end{pmatrix}, \tag{3.45}$$

and $\mathcal{T}_1 = \mathcal{T}_2 \equiv \mathcal{T} \in \mathbb{R}$, for simplicity, leading to

$$\begin{aligned}
\mathcal{K}_{1,\mathcal{X},\mathcal{T},\mathcal{Q}_{3\pi/2-},\mathcal{S}_2}(\bar{\mathbf{x}};\,\bar{\mathbf{k}}) &= \bar{x}_1(\bar{k}_1 + \bar{k}_2\bar{x}_1 + \bar{k}_3\bar{x}_2 + \bar{k}_4(\bar{x}_1)^2 + \bar{k}_5\bar{x}_1\bar{x}_2 + \bar{k}_6(\bar{x}_2)^2), \\
\mathcal{K}_{2,\mathcal{X},\mathcal{T},\mathcal{Q}_{3\pi/2-},\mathcal{S}_2}(\bar{\mathbf{x}};\,\bar{\mathbf{k}}) &= \bar{x}_2(\bar{k}_7 + \bar{k}_8\bar{x}_1 + \bar{k}_9\bar{x}_2 + \bar{k}_{10}(\bar{x}_1)^2 + \bar{k}_{11}\bar{x}_1\bar{x}_2 + \bar{k}_{12}(\bar{x}_2)^2),
\end{aligned} \tag{3.46}$$

where the coefficients $\bar{\mathbf{k}} = \bar{\mathbf{k}}(a,\alpha,\mathcal{T})$ are given by:

$$\begin{aligned}
&\bar{k}_1 = \frac{1}{2}\mathcal{T}\big(-2 + a(2\alpha + \mathcal{T} + a(2 + 5\mathcal{T}) + 4\mathcal{T}a^2)\big), \\
&\bar{k}_7 = -\frac{1}{2}\mathcal{T}\big(2 + 2\alpha + 3\mathcal{T} + a(4 + 9\mathcal{T} + 6\mathcal{T}a)\big), \\
&\bar{k}_2 = -\frac{1}{2}\mathcal{T}a(2 + 5a), \qquad \bar{k}_8 = 1 + \frac{9}{2}\mathcal{T}(\frac{2}{3} + a), \\
&\bar{k}_3 = 1 - \frac{1}{2}a\big(2\alpha + a(2 + 5\mathcal{T} + 8\mathcal{T}a)\big), \qquad \bar{k}_9 = \alpha + a\big(2 + \frac{9}{2}\mathcal{T} + 6\mathcal{T}a\big), \\
&\bar{k}_4 = \frac{1}{2}a, \;\; \bar{k}_{10} = -\frac{3}{2}, \;\; \bar{k}_5 = \frac{5}{2}a^2, \;\; \bar{k}_{11} = -\frac{9}{2}a, \;\; \bar{k}_6 = 2a^3, \;\; \bar{k}_{12} = -3a^2,
\end{aligned} \tag{3.47}$$

together with $a \in (-1,0)$, $|\alpha| \ll 1$ and $\mathcal{T} > 1$.

Theorem 3.6. *Let us assume that*

$$\begin{aligned}
a \in \left(-1, -\frac{1}{2}\right), \; |\alpha| \ll 1, \\
\max(1, 2a^{-2}(1-a^2)) < \mathcal{T} < 2a^{-1}(1+4a)^{-1}(1-a).
\end{aligned} \tag{3.48}$$

It then follows that the corresponding positive critical points of the ODE systems with RHSs (3.36) *and* (3.46) *have identical linear stability and orientation, the homoclinic orbit is in* $\mathbb{R}^2_>$*, and* (3.46) *has two boundary critical points: a saddle at the origin and a saddle with coordinates* $(0, 1/2\mathcal{T}a^{-1}(1+2a))$.

Proof. Following the same procedure as in the proof of Theorem 3.5, and noting that the saddle, node and focus critical points are given by $\big(\mathcal{T},\mathcal{T}\big)$, $\big(\mathcal{T} - 2a^{-2}(1-a^2), \mathcal{T} + a^{-3}(1-a^2)\big)$, and $\big(\mathcal{T} + 2/9(3+a^2), \mathcal{T} - 2/9a\big)$, respectively, while the five boundary critical points are $(0,0)$, $(\mathcal{T} + 1/2\big(5\mathcal{T}a \pm \sqrt{\mathcal{T}(8a^{-1}(1-a^2) + 9\mathcal{T}a^2)}\big), 0)$, $(0, 1/2\mathcal{T}a^{-1}(1+2a))$, $(0, a^{-1}\big(2/3 + \mathcal{T}(1+a)\big))$, one finds (3.48). □

Note that as $a \to -\frac{1}{2}$, the only boundary critical point in $\mathbb{R}^2_{\geq}$ is a saddle at the origin, and it is connected via a heteroclinic orbit to the node in $\mathbb{R}^2_{>}$. A representative phase plane diagram corresponding to the ODE system with RHS (3.46) is shown in Figure 3.3(c).

Quasistationary transformation. In Lemma 3.3, it was demonstrated that system (3.36) has at least one cross-negative term under translation transformations. It can be readily shown that system (3.36) in fact has minimally two cross-negative terms under translation transformations, $\bar{k}_3 < 0$ and $\bar{k}_6 < 0$, and this is the case when $a \in (-1, 0)$, $\mathcal{T}_1 \in (2\sqrt{3}/9, -\mathcal{T}_2 a), \mathcal{T}_2 > 1$. Let us apply a quasistationary transformation Ψ_{QS} on system (3.37) that eliminates the two cross-negative terms, i.e. two new variables are introduced, $\bar{y}_1, \bar{y}_2 \in \mathbb{R}^2_{>}$ (see also Definition 3.11). System (3.37) is mapped under $\Psi_{\text{QS},\mathcal{T}} \equiv \Psi_{\text{QS}} \circ \Psi_{\mathcal{T}}$ to the following ODE system

$$\begin{aligned}
\frac{\mathrm{d}x_1}{\mathrm{d}t} &= \bar{k}_1 + \bar{k}_2\bar{x}_1 + \bar{k}_3\bar{x}_1\bar{x}_2\bar{y}_1 + \bar{k}_4\bar{x}_1\bar{x}_2 + \bar{k}_5(\bar{x}_2)^2,\\
\frac{\mathrm{d}x_2}{\mathrm{d}t} &= \bar{k}_6\bar{x}_2\bar{y}_2 + \bar{k}_7\bar{x}_1 + \bar{k}_8\bar{x}_2 + \bar{k}_9(\bar{x}_2)^2,\\
\frac{\mathrm{d}y_1}{\mathrm{d}t} &= \mu^{-1}(1 - x_1y_1),\\
\frac{\mathrm{d}y_2}{\mathrm{d}t} &= \mu^{-1}(1 - x_2y_2),
\end{aligned} \tag{3.49}$$

with $0 < \mu \ll 1$.

Note that a composition of **x**-factorable and quasistationary transformations may also be used to make (3.37) kinetic. For example, one may eliminate the cross-negative term $\bar{k}_3$ in (3.37) by using an x_1-factorable transformation $\Psi^{x_1}_{\mathcal{X}}$, and the cross-negative term $\bar{k}_6$ by using an appropriate Ψ_{QS}. An example of RREs obtained by transforming (3.37) using $\Psi_{\text{QS}} \circ \Psi^{x_1}_{\mathcal{X}} \circ \Psi_{\mathcal{T}}$ are given by

$$\begin{aligned}
\frac{\mathrm{d}x_1}{\mathrm{d}t} &= \bar{x}_1(\bar{k}_1 + \bar{k}_2\bar{x}_1 + \bar{k}_3\bar{x}_2 + \bar{k}_4\bar{x}_1\bar{x}_2 + \bar{k}_5(\bar{x}_2)^2),\\
\frac{\mathrm{d}x_2}{\mathrm{d}t} &= \bar{k}_6\bar{x}_2\bar{y}_2 + \bar{k}_7\bar{x}_1 + \bar{k}_8\bar{x}_2 + \bar{k}_9(\bar{x}_2)^2,\\
\frac{\mathrm{d}y_2}{\mathrm{d}t} &= \mu^{-1}(1 - x_2y_2),
\end{aligned} \tag{3.50}$$

with $0 < \mu \ll 1$.

Step (3): Construction of the canonical reaction network $\mathcal{R}^{\mathcal{K}^{-1}}$

Algorithm 3.1 can be used to map the kinetic functions (3.41), (3.46), (3.49), and (3.50) to the associated canonical reaction networks $\mathcal{R}^{\mathcal{K}^{-1}}$. This is illustrated for sys-

tem (3.41) in this section. For clarity, both the RREs and the induced canonical reaction networks are presented.

Writing $\mathbf{x} \equiv \bar{\mathbf{x}}$, the RREs induced by (3.41) are given by

$$\begin{aligned} \frac{\mathrm{d}x_1}{\mathrm{d}t} &= k_1 + x_1(k_2 + k_3 x_1 - k_4 x_2 - k_5 x_1 x_2 + k_6 x_2^2), \\ \frac{\mathrm{d}x_2}{\mathrm{d}t} &= k_7 + x_2(-k_8 + k_9 x_1 + k_{10} x_2 - k_{11} x_2^2), \end{aligned} \tag{3.51}$$

while the induced canonical reaction network reads

$$\begin{aligned} \tilde{\mathcal{R}}: \quad r_1: \quad & \varnothing \xrightarrow{k_1} s_1, & r_7: \quad & \varnothing \xrightarrow{k_7} s_2, \\ r_2: \quad & s_1 \xrightarrow{k_2} 2s_1, & r_8: \quad & s_2 \xrightarrow{k_8} \varnothing, \\ r_3: \quad & 2s_1 \xrightarrow{k_3} 3s_1, & r_9: \quad & s_1 + s_2 \xrightarrow{k_9} s_1 + 2s_2, \\ r_4: \quad & s_1 + s_2 \xrightarrow{k_4} s_2, & r_{10}: \quad & 2s_2 \xrightarrow{k_{10}} 3s_2, \\ r_5: \quad & 2s_1 + s_2 \xrightarrow{k_5} s_1 + s_2, & r_{11}: \quad & 3s_2 \xrightarrow{k_{11}} 2s_2, \\ r_6: \quad & s_1 + 2s_2 \xrightarrow{k_6} 2s_1 + 2s_2, & & \end{aligned} \tag{3.52}$$

where $k_1 = \varepsilon$, $k_j = |\bar{k}_{j-1}|$ for $j \in \{2, \ldots, 6\}$, $k_7 = \varepsilon$, $k_j = |\bar{k}_{j-2}|$ for $j \in \{8, \ldots, 11\}$, with the coefficients $\bar{\mathbf{k}} = (\bar{k}_1, \ldots, \bar{k}_9)$ given by (3.38), and the conditions on the coefficients given by (3.42). Parameter a controls the separation between the stable sets (i.e. the distance between the node and the limit cycle), while α controls the homoclinic bifurcation (and it controls the size of the limit cycle). If ε is taken to be zero, $\varepsilon = 0$, this is equivalent to removing reactions r_1 and r_7 from network (3.52). We call the reaction network (3.52) the *homoclinicator*. A particular choice of the (dimensionless) rate coefficients appearing in (3.52) is given by

$$\begin{aligned} &k_1 = 0.01, \quad k_2 = 0.9, \quad k_3 = 1.55, \quad k_4 = 2.6, \quad k_5 = 1.2, \quad k_6 = 1.5, \\ &k_7 = 0.01, \quad k_8 = 3.6, \quad k_9 = 1, \quad k_{10} = 2.4, \quad k_{11} = 0.8. \end{aligned} \tag{3.53}$$

3.4.2 The bicyclicator

In this section, we apply kinetic transformations in order to construct specific two-dimensional reaction systems displaying two coexisting Hopf bifurcations (local bifurcations) giving rise to bicyclicity (coexistence of two stable limit cycles) - a phenomenon which has been reported in higher-dimensional biochemical models arising in applications [111, 112]. To construct the systems, we use an existing system of the form (3.31), which forms a so-called one-parameter family of uniformly rotated vector fields [76, 113], involving a parameter which rotates the vector field induced

by (3.31) in the phase plane. The rotation form is chosen such that sizes of the two constructed coexisting stable limit cycles are comparable, as opposed to differing by several orders of magnitude (a task that can pose challenges [94]).

To this end, let us consider the following planar quadratic ODE system

$$\begin{aligned}\frac{\mathrm{d}x_1}{\mathrm{d}t} &= \mathcal{P}_1(\mathbf{x}) = \mathcal{Q}_1(\mathbf{x})\\ \frac{\mathrm{d}x_2}{\mathrm{d}t} &= \mathcal{P}_2(\mathbf{x};\, b, \beta) = \beta\mathcal{Q}_1(\mathbf{x}) + \mathcal{Q}_2(\mathbf{x};\, b),\end{aligned} \tag{3.54}$$

where

$$\begin{aligned}\mathcal{Q}_1(\mathbf{x}) &= -x_1x_2,\\ \mathcal{Q}_2(\mathbf{x};\, b) &= b - (b+1)x_1 + \frac{1}{10}x_2 + x_1^2 - \frac{1}{10}x_1x_2 - \frac{1}{2}x_2^2,\end{aligned} \tag{3.55}$$

with $b < -1$ and $\beta \in (-\infty, +\infty)$. System (3.54) is obtained from [78, Equations (2.4)–(2.5)] (see also [114]), by taking $a = 1, b = -1, c = 1/2, d = 1/10$, replacing x_0 with b, reversing the time (replacing t with $-t$) and, instead of embedding [78, Equation (2.5)] into a complete family of rotated vector fields, we embed it into an appropriate semicomplete one.

Lemma 3.4. *Consider system* (3.54)–(3.55)*, with* $b < -1$ *and* $\beta \in (-\infty, +\infty)$*. System* (3.54) *forms a* semicomplete one-parameter family of rotated vector fields *(*mod $\mathcal{P}_1(\mathbf{x}) = 0$*), with the rotation parameter* $\beta \in (-\infty, +\infty)$*, and the following results hold:*

(i) Critical points. *System* (3.54) *has two critical points in the finite part of the phase-plane, given by* $(b, 0)$ *and* $(1, 0)$*, both of which are unstable foci when* $\beta^* < \beta < 0$*, where* $\beta^* = 1/10(1/b - 1)$*.*

(ii) Number and distribution of limit cycles. *System* (3.54) *has two limit cycles in the configuration* $(1, 1)$ *when* $\beta^* < \beta < 0$*. The focus located at* $(b, 0)$ *is surrounded by a negatively-oriented stable limit cycle* L_1*, while the focus at* $(1, 0)$ *by a positively-oriented stable limit cycle* L_2*.*

(iii) Dependence of the limit cycles on the rotation parameter β*. As* β *is monotonically increased in* $(\beta^*, 0)$*, limit cycle* L_1 *monotonically expands, while* L_2 *monotonically contracts.*

Proof. (a) Critical points $(b, 0)$ and $(1, 0)$ of (3.54) are independent of parameter β, and so remain fixed under the variation of β. (b) The vector field angle, defined by

$\tan\theta = \mathcal{P}_2(\mathbf{x};\, b, \beta)/\mathcal{P}_1(\mathbf{x})$, satisfies $\partial\theta/\partial\beta = (\boldsymbol{\mathcal{P}}(\mathbf{x};\, b, \beta) \times \partial\boldsymbol{\mathcal{P}}(\mathbf{x};\, b, \beta)/\partial\beta)/(\mathcal{P}_1^2(\mathbf{x}) + \mathcal{P}_2^2(\mathbf{x};\, b))$ [76, 113], which for (3.54) satisfies $\partial\theta/\partial\beta = \mathcal{P}_1^2(\mathbf{x})/(\mathcal{P}_1^2(\mathbf{x}) + \mathcal{P}_2^2(\mathbf{x};\, b)) > 0$ on regular points, except on the x_1-nullcline $\mathcal{P}_1(\mathbf{x}) = 0$, where $\partial\theta/\partial\beta = 0$. In other words, the vector field angle at regular points increases with increasing β, except on the curve $x_1 x_2 = 0$, where it stays fixed. (c) $\lim_{\beta\to\pm\infty} \tan\theta = \lim_{\beta\to\pm\infty}(\beta + \mathcal{Q}_2(\mathbf{x};\, b)/\mathcal{Q}_1(\mathbf{x})) = \pm\infty$, except on $\mathcal{P}_1(\mathbf{x}) = 0$. In other words, the vector field angle varies through π (and not 2π) radians on its regular points as β varies from $-\infty$ to $+\infty$, except on $x_1 x_2 = 0$, where the angle remains fixed. (a)–(c) imply that that (3.54) forms a semicomplete (and not a complete) one-parameter family of rotated vector fields (mod $\mathcal{P}_1(\mathbf{x}) = 0$) [113].

Critical point $(1, 0)$. Translating the origin to the critical point $(1, 0)$ maps (3.54) to

$$\begin{aligned} \frac{\mathrm{d}x_1}{\mathrm{d}t} &= -x_2 - x_1 x_2 \\ \frac{\mathrm{d}x_2}{\mathrm{d}t} &= (1-b)x_1 - \beta x_2 + x_1^2 - (\frac{1}{10} + \beta)x_1 x_2 - \frac{1}{2}x_2^2. \end{aligned} \tag{3.56}$$

The trace and determinant of the Jacobian matrix underlying (3.56), evaluated at the critical point $(0, 0)$, are given by $\tau = -\beta$ and $\delta = (1 - b) > 0$, respectively, while the discriminant satisfies $\tau^2 - 4\delta = \beta^2 + 4(b - 1) < 0$ for $b < -1$ and $\beta^* < \beta < 0$. It follows that the origin is a weak focus when $\beta = 0$. Setting $x_1 = 0$ in the first equation in (3.54) gives $\mathrm{d}x_1/\mathrm{d}t = -x_2$, so that vector field, in the neighborhood of the origin, rotates counterclockwise, i.e. has a positive orientation. Calculation of the associated Liapunov number σ [76, Section 4.4, Equation (3')] gives $\sigma = 3\pi/20(1 - b)^{-3/2}(1 - 1/2(1 - b)) < 0$ for $b < -1$. Thus, critical point $(1, 0)$ of (3.54) is a positively-oriented stable weak focus of multiplicity one when $\beta = 0$ (in particular, it is not a nonlinear center). It then follows from the theory of one-parameter families of rotated vector fields [113, Theorem H] that $(1, 0)$ generates a unique positively-oriented stable limit cycle L_2 at $\beta = 0$ via a Hopf bifurcation, which monotonically decreases as β monotonically increases in $(\beta^*, 0)$ [76, Figure 1, Section 4.6].

Critical point $(b, 0)$. Similar consideration implies that the Jacobian trace underlying $(b, 0)$ is given by $\tau = 1/10 - (1/10 + \beta)b$, and that critical point $(b, 0)$ of (3.54) is a negatively-oriented stable weak focus of multiplicity one when $\beta = \beta^* = 1/10(1/b - 1) < 0$. Furthermore, $(b, 0)$ generates a unique negatively-oriented stable limit cycle L_1 at $\beta = \beta^*$ via a Hopf bifurcation, which monotonically increases as β monotonically increases in $(\beta^*, 0)$. □

Let us note that we have chosen to rotate the vector field in (3.54), via parameter β, in such a way that the vector field stays fixed on the x_1-nullcline $x_1 = 0$, which is also a trajectory of system (3.54) (so that the two limit cycles cannot cross $x_1 = 0$). If (3.55) is embedded in a one-parameter family of rotated vector fields which do not preserve $x_1 = 0$, then, in addition to the two Hopf (local) bifurcations, a global bifurcation may occur, giving rise to a second limit cycle surrounding L_2 [94]. In this case, sizes of limit cycles L_1 and L_2, and their regions of attraction, may be significantly different (by several orders of magnitude). In order to avoid this, we have used a suitable semicomplete family of rotated vector fields, which preserves the curve $x_1 = 0$, and suppresses the global bifurcation from happening. See also [94] for a discussion on some of the challenges behind limit cycles sizes in quadratic planar systems which display multiple coexisting limit cycles.

Applying the kinetic transformations

In order to map the stable limit cycles of system (3.54) into the nonnegative quadrant, and then map the resulting system to a kinetic one, let us apply $\Psi_{\mathcal{X}_\varepsilon,\mathcal{T}} \equiv \Psi_{\mathcal{X}_\varepsilon} \circ \Psi_{\mathcal{T}}$, with a translation vector $\boldsymbol{\mathcal{T}} = (\mathcal{T}, \mathcal{T}) \in \mathbb{R}^2_>$, which maps (3.54) to the RREs

$$\begin{aligned}
\frac{\mathrm{d}x_1}{\mathrm{d}t} &= k_1 + x_1(-k_2 + k_3 x_1 + k_4 x_2 - k_5 x_1 x_2),\\
\frac{\mathrm{d}x_2}{\mathrm{d}t} &= k_6 + x_2(k_7 - k_8 x_1 + k_9 x_2 + k_{10} x_1^2 - k_{11} x_1 x_2 - k_{12} x_2^2),
\end{aligned} \tag{3.57}$$

with the coefficients $\mathbf{k} = \mathbf{k}(b, \beta, \boldsymbol{\mathcal{T}}, \varepsilon) \in \mathbb{R}^{12}_{\geq}$ given by

$$\begin{aligned}
&k_1 = \varepsilon, \quad k_2 = \mathcal{T}^2, \quad k_3 = \mathcal{T}, \quad k_4 = \mathcal{T}, \quad k_5 = 1,\\
&k_6 = \varepsilon, \quad k_7 = (\frac{2}{5} - \beta)\mathcal{T}^2 + \frac{9}{10}\mathcal{T} + b(1 + \mathcal{T}),\\
&k_8 = (b+1) + (\frac{19}{10} - \beta)\mathcal{T}, \quad k_9 = (\frac{11}{10} + \beta)\mathcal{T} + \frac{1}{10},\\
&k_{10} = 1, \quad k_{11} = \frac{1}{10} + \beta, \quad k_{12} = \frac{1}{2}.
\end{aligned} \tag{3.58}$$

We assume parameters $b, \beta, \mathcal{T}$ are chosen so that $k_7, k_8, k_9, k_{11} \geq 0$ in (3.58). In case some of the coefficients k_7, k_8, k_9, k_{11} are negative, the corresponding sign in (3.57) may simply be reversed, and the coefficients set to their absolute values.

Lemma 3.5. *System* (3.54)*, with* $b < 0$ *and* $\beta \in \mathbb{R}$*, is nonkinetic under all translation transformations* $\Psi_{\mathcal{T}}$*.*

Proof. Let us apply the translation transformation $\Psi_{\mathcal{T}}$ on (3.54), giving

$$\begin{aligned}\frac{\mathrm{d}x_1}{\mathrm{d}t} &= -k_2 + k_3 x_1 + k_4 x_2 - k_5 x_1 x_2,\\ \frac{\mathrm{d}x_2}{\mathrm{d}t} &= k_7 - k_8 x_1 + k_9 x_2 + k_{10} x_1^2 - k_{11} x_1 x_2 - k_{12} x_2^2,\end{aligned} \tag{3.59}$$

with the coefficients given by (3.58). Taking $\mathcal{T} = 0$, we recover system (3.54), the second equation of which contains a cross-negative term $b < 0$, so that the system is nonkinetic. On the other hand, taking $\mathcal{T} \neq 0$, it follows that $k_2 > 0$ in (3.58). Consequently, the first equation in (3.59) contains a cross-negative term $-k_2$, so that (3.59) is nonkinetic. □

Theorem 3.7. *Let us assume that*

$$\beta^* = \frac{1}{10}(\frac{1}{b} - 1) < \beta < 0, \quad b < -1, \quad 0 \leq \varepsilon \ll 1, \quad \mathcal{T} > -\frac{5}{2}b. \tag{3.60}$$

It then follows that the unstable foci in $\mathbb{R}^2$ of the ODE system (3.54) *are mapped to the unstable foci in $\mathbb{R}^2_>$ of system* (3.57)*. Furthermore, for sufficiently small $\varepsilon > 0$, system* (3.57) *has exactly one additional nonnegative critical point: a saddle in the neighborhood of $(\mathcal{T}, 0)$.*

Proof. Interior critical points. In what follows, let us consider (3.57) with $\varepsilon = 0$. Critical point $(1, 0)$ of system (3.54) is mapped to the critical point $(1+\mathcal{T}, \mathcal{T})$ of (3.57). The Jacobian matrix corresponding to (3.57), evaluated at $(1+\mathcal{T}, \mathcal{T})$, is given by the first equation in

$$\begin{aligned}J_{\mathcal{X},\mathcal{T}}(1+\mathcal{T}, \mathcal{T}) &= \begin{pmatrix} 0 & -(1+\mathcal{T}) \\ \mathcal{T}(1-b) & -\beta\mathcal{T} \end{pmatrix},\\ J_{\mathcal{X},\mathcal{T}}(b+\mathcal{T}, \mathcal{T}) &= \begin{pmatrix} 0 & -b(b+\mathcal{T}) \\ -\mathcal{T}(1-b) & \mathcal{T}(\frac{1}{10} - b(\frac{1}{10} + \beta)) \end{pmatrix}.\end{aligned}$$

Since the trace $\tau = -\beta\mathcal{T} > 0$, determinant $\delta = \mathcal{T}(1+\mathcal{T})(1-b) > 0$, and discriminant $\tau^2 - 4\delta < 0$ under the conditions (3.60), it follows that $(1 + \mathcal{T}, \mathcal{T})$ is an unstable focus. Critical point $(b, 0)$ of system (3.54) is mapped to the critical point $(b+\mathcal{T}, \mathcal{T})$ of (3.57), which is in the positive quadrant, since (3.60) implies $\mathcal{T} > -b$. A Jacobian-based analysis implies that, assuming (3.60) is true, the trace and determinant satisfy $\tau, \delta > 0$, and $\tau^2 - 4\delta < 0$ (this condition is fulfilled provided $\mathcal{T}$ is sufficiently large, e.g. $\mathcal{T} > -11/10b$), so that $(b + \mathcal{T}, \mathcal{T})$ is also an unstable focus.

Boundary critical points. The boundary critical points are given by $(0, 0)$, $(\mathcal{T}, 0)$ and $(0, x^*_{2,\pm})$, where

$$\begin{aligned}x^*_{2,\pm} = \frac{1}{10}&(1 + \mathcal{T}(11 + 10\beta)\\ &\pm \sqrt{1 + \mathcal{T}(202 + 201\mathcal{T}) + 200b(1+\mathcal{T}) + 20\mathcal{T}\beta(1 + \mathcal{T}(1 + 5\beta))}).\end{aligned}$$

It follows from condition (iv) in Theorem 3.1 that the eigenvalues of $(0,0)$ are given by $\lambda_1 = -k_2 < 0$ and $\lambda_2 = k_7 > 0$ (under the assumption that $k_7 > 0$), so that $(0,0)$ is a saddle. Using the notation of Theorem 3.2, it follows that $\mathcal{P}_2(0,0) = \lambda_2 > 0$, so that condition (3.17) implies that $(0,0)$ is mapped outside of $\mathbb{R}^2_{\geq}$ when $0 < \varepsilon \ll 1$. On the other hand, $\partial\mathcal{P}_1/\partial x_1(\mathcal{T},0) = \mathcal{T} > 0$ and $\mathcal{P}_2(\mathcal{T},0) = b - 1/10\mathcal{T}(1 + 5\mathcal{T}) < 0$, so that condition (v) from Theorem 3.1 implies that $(\mathcal{T},0)$ is a saddle, and condition (3.17) from Theorem 3.2 that $(\mathcal{T},0)$ is mapped to $\mathbb{R}^2_{>}$ when $0 < \varepsilon \ll 1$. Similar considerations imply that $(0, x^*_{2,\pm})$ are also saddles. Furthermore, $(0, x^*_{2,+})$ is mapped outside $\mathbb{R}^2_{\geq}$ when $0 < \varepsilon \ll 1$, while the condition $\mathcal{T} > -5/2b$ from (3.60) is sufficient for $x^*_{2,-} < 0$, so that $(0, x^*_{2,-}) \notin \mathbb{R}^2_{\geq}$. □

Note that the x_1-nullcline $x_1 = 0$ of system (3.54) is mapped to $x_1 = \mathcal{T}$ under $\Psi_{\mathcal{T}}$. Importantly, $x_1 = \mathcal{T}$ is preserved under $\Psi_{\mathcal{X}}$, i.e. the x_1-nullcline $x_1 = \mathcal{T}$ is a trajectory of system (3.57), when $\varepsilon = 0$. More precisely, it is a stable manifold (separatrix) of the saddle $(\mathcal{T},0)$, separating the two unstable foci (and any limit cycles surrounding them).

Constructing the canonical reaction network

The canonical reaction network induced by (3.57) is given by

$$
\begin{aligned}
r_1 &: \quad \varnothing \xrightarrow{k_1} s_1, & r_6 &: \quad \varnothing \xrightarrow{k_6} s_2,\\
r_2 &: \quad s_1 \xrightarrow{k_2} \varnothing, & r_7 &: \quad s_2 \xrightarrow{k_7} 2s_2,\\
r_3 &: \quad 2s_1 \xrightarrow{k_3} 3s_1, & r_8 &: \quad s_1 + s_2 \xrightarrow{k_8} s_1,\\
r_4 &: \quad s_1 + s_2 \xrightarrow{k_4} 2s_1 + s_2, & r_9 &: \quad 2s_2 \xrightarrow{k_9} 3s_2,\\
r_5 &: \quad 2s_1 + s_2 \xrightarrow{k_5} s_1 + s_2, & r_{10} &: \quad 2s_1 + s_2 \xrightarrow{k_{10}} 2s_1 + 2s_2,\\
& & r_{11} &: \quad s_1 + 2s_2 \xrightarrow{k_{11}} 2s_2,\\
& & r_{12} &: \quad 3s_2 \xrightarrow{k_{12}} 2s_2,
\end{aligned}
\tag{3.61}
$$

with the coefficients given by (3.58), and the conditions on the coefficients given by (3.60). Parameter b controls the separation between the two foci/limit cycles, while β controls the Hopf bifurcations giving rise to the limit cycles (and it controls the sizes of the limit cycles). If ε is taken to be zero, $\varepsilon = 0$, this is equivalent to removing reactions r_1 and r_6 from network (3.61). We call the reaction network (3.61) the *bicyclicator*. A particular choice of the (dimensionless) rate coefficients appearing

in (3.61) is given by

$$\begin{aligned} &k_1 = 0, \quad k_2 = 100, \quad k_3 = 10, \quad k_4 = 10, \quad k_5 = 1, \quad k_6 = 0, \\ &k_7 = 37, \quad k_8 = 19, \quad k_9 = 10.1, \quad k_{10} = 1, \quad k_{11} = 0, \quad k_{12} = 0.5, \end{aligned} \tag{3.62}$$

which is obtained by taking $\varepsilon = 0$, $\mathcal{T} = 10$, $b = -2$ and $\beta = -0.1$ in (3.58). A phase plane diagram for system (3.57) with parameters (3.62) is shown in Figure 3.4, with the stable limit cycles L_1 and L_2 shown in red and purple, respectively, the separatrix $x_1 = \mathcal{T} = 10$ as the dashed black line, and the two unstable foci, $(b + \mathcal{T}, \mathcal{T}) = (8, 10)$ and $(1 + \mathcal{T}, \mathcal{T}) = (11, 10)$, as the blue dots. The distance between the two limit cycles may be increased by decreasing parameter b, while the relative sizes of the limit cycles can be controlled by varying parameter β, as described in Lemma 3.4.

Let us complete this section by emphasizing the similarity in constructing the homoclinicator (3.51) and the bicyclictor (3.57). The homoclinicator was constructed by (i) incorporating the homoclinic orbit (3.33) into polynomial ODEs, resulting in (3.34), (ii) utilizing Melnikov theory to induce the homoclinic bifurcation in (3.34), resulting in (3.36), and (iii) applying appropriate kinetic transformations to map the resulting system to RREs (3.51). Similarly, the bicyclictor (3.57) can be designed from scratch by (i) incorporating the line $x_1 = 0$ into polynomial ODEs, resulting in the vector field (3.55), (ii) utilizing one-parameter family of rotated vector fields to induce two Hopf bifucations, resulting in (3.54), and (iii) applying kinetic transformation to map the resulting system to RREs (3.57).

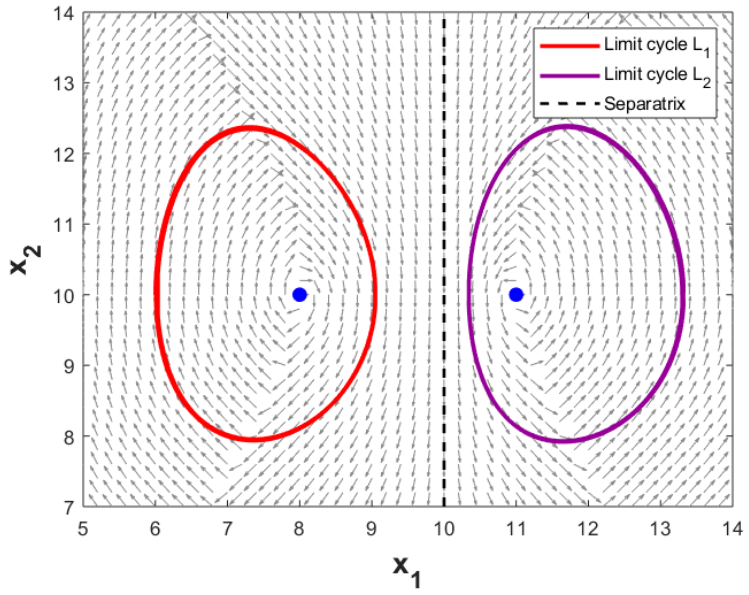

Figure 3.4: *A phase plane diagram of the bicyclicator* (3.57)*, with the stable limit cycles* L_1 *and* L_2 *shown in red and purple, respectively, the separatrix* $x_1 = 10$ *shown as the dashed black line, the two unstable foci as blue dots, and the vector field as grey arrows. The parameters are chosen as specified in* (3.62)*.*

Chapter 4

Stochastic methods: The noise approximation algorithm

In Chapter 3, we have developed the kinetic transformations, allowing one to design reaction networks at the (less-detailed) deterministic level. We have demonstrated that one may construct networks displaying exotic dynamical properties by utilizing kinetic transformations, such as specific bifurcation structures, multistability and oscillations, all of which play important biochemical roles. However, when reaction networks involve species with lower copy-numbers, such as when synthetic systems are interfaced with cell-like reactors [27, 28, 29], the controlled deterministic behavior may be drastically changed in the presence of the intrinsic noise [13, 18, 33, 34, 35, 36, 37]. Hence, new methods are required for designing reaction networks at the (more-detailed) stochastic level.

Constructing networks with predefined stochastic behaviors including, not only predefined probability distributions, but also predefined sample path behaviors, such as noise-induced oscillations, from scratch may be mathematically a very challenging task. The intrinsic noise, underlying the stochastic dynamics, may be controlled in two ways: it may be decreased (e.g. as in [34]), in order to reduce the differences between the stochastic and deterministic dynamics. On the other hand, it may be increased, in a state-dependent manner, in order to favorably change the stochastic dynamics. In the language of molecular computing, the latter approach corresponds to exploiting the proven computational power of the stochastic reaction networks [115], by reprogramming the underlying intrinsic noise. Let us note that exploitations of the noise for enhancing biological functions have been reported in applications [33, 37]. In this chapter, we follow the letter approach, and present the so-called *noise approximation algorithm*, given as Algorithm 4.1, which structurally modifies any given

Input: Let the input reaction network be given by

$$\mathcal{R}(s_1,\ldots,s_N):\ \sum_{i=1}^{N}\nu_{ij}s_i \xrightarrow{k_j}\sum_{i=1}^{N}\bar{\nu}_{ij}s_i,\quad j\in\{1,\ldots,M\}. \tag{4.1}$$

(1) Step: Reaction network $\mathcal{R}$, given by (4.1), is mapped to a *pairwise conservative network* $\mathcal{R}^1$ given by

$$\mathcal{R}^1(s_1,\ldots,s_N,\bar{s}_1,\ldots,\bar{s}_N):\ \sum_{i=1}^{N}\Big(\nu_{ij}s_i+(\Delta x_{ij}\bar{s}_i+I_i^{\Delta x_{ij}})\times 1_{\mathbb{N}}(\Delta x_{ij})\Big)\xrightarrow{k_j}$$
$$\sum_{i=1}^{N}\Big(\bar{\nu}_{ij}s_i-(\Delta x_{ij}\bar{s}_i)\times 1_{\mathbb{N}}(-\Delta x_{ij})+I_i^{\Delta x_{ij}}\times 1_{\mathbb{N}}(\Delta x_{ij})\Big),\quad j\in\{1,\ldots,M\}. \tag{4.2}$$

Here, $\bar{s}_i, I_i^{\Delta x_{ij}}$ are additional species, $\Delta x_{ij}=(\bar{\nu}_{ij}-\nu_{ij})$, and $1_{\mathbb{N}}(\cdot)$ is the indicator function of the natural numbers.

(2) Step: For each species $I_i^{\Delta x_{ij}}$, a *drift-corrector network* is constructed, $\mathcal{R}^2_{\Delta x_{ij}}(\bar{s}_i)=\mathcal{R}^2_{\Delta x_{ij}}(\bar{s}_i;\, I_i^{\Delta x_{ij}},\mu)$, given by

$$\begin{aligned}\mathcal{R}^2_{\Delta x_{ij}}(\bar{s}_i):\quad \varnothing &\xrightarrow{1/\mu} I_i^{\Delta x_{ij}},\\ \Delta x_{ij}\bar{s}_i+I_i^{\Delta x_{ij}} &\xrightarrow{1/\mu}\Delta x_{ij}\bar{s}_i,\quad 0<\mu\ll 1.\end{aligned} \tag{4.3}$$

(3) Step: For each species $\bar{s}_i$, a union of *zero-drift networks* may be constructed. Let $n,\bar{n}\in\mathbb{N}_0$, and $(n+\bar{n})\le C_i$. Network $\mathcal{R}^3_{n,\bar{n}}(s_i,\bar{s}_i)=\mathcal{R}^3_{n,\bar{n}}(s_i,\bar{s}_i;\, k^i_{n,\bar{n}})$, with $n,\bar{n}\neq 0$, is given by

$$\begin{aligned}\mathcal{R}^3_{n,\bar{n}}(s_i,\bar{s}_i):\quad ns_i+\bar{n}\bar{s}_i &\xrightarrow{k^i_{n,\bar{n}}}(n+1)s_i+(\bar{n}-1)\bar{s}_i,\\ ns_i+\bar{n}\bar{s}_i &\xrightarrow{k^i_{n,\bar{n}}}(n-1)s_i+(\bar{n}+1)\bar{s}_i.\end{aligned} \tag{4.4}$$

Network $\mathcal{R}^3_{0,\bar{n}}(s_i,\bar{s}_i)=\mathcal{R}^3_{0,\bar{n}}(s_i,\bar{s}_i;\ B_i,k^i_{0,\bar{n}},\mu_{0,\bar{n}})$, with $\bar{n}\neq 0$, is given by

$$\begin{aligned}\mathcal{R}^3_{0,\bar{n}}(s_i,\bar{s}_i):\quad \bar{n}\bar{s}_i &\xrightarrow{k^i_{0,\bar{n}}}s_i+(\bar{n}-1)\bar{s}_i,\\ C_is_i+B_i &\xrightarrow{k^i_{0,\bar{n}}}(C_i-1)s_i+\bar{s}_i+B_i,\\ \bar{n}\bar{s}_i &\xrightarrow{1/\mu_{0,\bar{n}}}\bar{n}\bar{s}_i+B_i,\\ C_is_i+B_i &\xrightarrow{1/\mu_{0,\bar{n}}}C_is_i,\quad 0<\mu_{0,\bar{n}}\ll 1,\end{aligned} \tag{4.5}$$

where B_i is an additional species. Network $\mathcal{R}^3_{n,0}=\mathcal{R}^3_{0,n}(\bar{s}_i,s_i;\,\bar{B}_i,k^i_{n,0},\mu_{n,0})$.

Output: An output reaction network is given by

$$\mathcal{R}^1\cup\mathcal{R}^2\cup\mathcal{R}^3, \tag{4.6}$$

where $\mathcal{R}^2=\cup_i\cup_{\Delta x_{ij}}\mathcal{R}^2_{\Delta x_{ij}}(\bar{s}_i)$, and $\mathcal{R}^3=\cup_i\cup_{(n,\bar{n})}\mathcal{R}^3_{n,\bar{n}}(s_i,\bar{s}_i)$.

Algorithm 4.1: *The noise approximation algorithm.*

reaction network under mass-action kinetics, in such a way that (i) controllable state-dependent noise is introduced into the stochastic dynamics, while (ii) the deterministic dynamics are preserved. Kinetic transformations and the noise approximation algorithm together allow for a deterministic-stochastic hybrid approach for designing reaction networks. More precisely, one may use the deterministic model to guide the construction, and then apply the algorithm to favorably modify the intrinsic noise in the stochastic model, while preserving the desired deterministic dynamics.

The chapter is organized as follows. In Section 4.1, we introduce Algorithm 4.1 by applying it to the test network (4.7), which at the deterministic level displays a globally attracting equilibrium point. We show that the algorithm can favorably modify the stationary probability distribution underlying (4.7) at arbitrary points in the state-space, without influencing the deterministic dynamics. For example, it is shown that the algorithm may be used to redesign (4.7) to achieve noise-induced multimodality (multistability) (see also Figures 4.2 and 4.4). In Section 4.2, we rigorously establish the properties of Algorithm 4.1, outlined in Section 4.1. In Section 4.3, we apply the algorithm on the homoclinicator, designed in Chapter 3, and given as the reaction network (3.52), which at the deterministic level displays a bistability involving an equilibrium point and a limit cycle. The algorithm is used to redesign (3.52) to control the stochastic switching between the two attractors, and to achieve noise-assisted oscillations (see also Figure 4.3). Finally, in Section 4.4, we provide generalizations of Algorithm 4.1, which further increase its capabilities. The results presented in this chapter are based on the published paper [39].

4.1 Introduction: Application to a test network

Let us consider the production-decay reaction network $\mathcal{R}(s)$, given by

$$\begin{aligned} \mathcal{R}(s): \qquad & \varnothing \xrightarrow{k_1} s, \\ & s \xrightarrow{k_2} \varnothing, \end{aligned} \tag{4.7}$$

with the concentration of the species s, denoted by $x = x(t)$, satisfying the initial-value problem (IVP) for the induced RRE (see also Section 2.3.1), given by

$$\begin{aligned} \frac{\mathrm{d}x}{\mathrm{d}t} &= k_1 - k_2 x, \\ x(0) &= x_0 \geq 0. \end{aligned} \tag{4.8}$$

Let us denote the copy-number of species s from (4.7) at time $t \geq 0$ by $X(t) \in \mathbb{Z}_{\geq}$, where $\mathbb{Z}_{\geq}$ is the set of nonnegative integers (see also Definition 2.1). Under the

stochastic model, $X(t)$ is modelled as a continuous-time discrete-space Markov chain (see also Section 2.3.2). Given $X(t)$, there will be a mean interevent time $1/\alpha(X(t))$ until one of the reactions from (4.7) fires. Here, $\alpha_1(x) = k_1$ and $\alpha_2(x) = k_2 x$ are the propensity functions of the first and second reactions, respectively, while $\alpha(x) = k_1 + k_2 x$ is the total propensity function of network (4.7), i.e. the sum of propensity functions of all the underlying reactions. When the event takes place, the probability that the i-th reaction from (4.7) fires is $\alpha_i(X(t))/\alpha(X(t))$, for $i \in \{1, 2\}$ (see also Section 2.3.2, and the Gillespie SSA, given as Algorithm 2.1).

We now wish to structurally modify network (4.7) in such a way that (i) the deterministic model (4.8) is preserved, while (ii) a control is gained over the interevent time from the stochastic model. We accomplish this by, firstly, imposing a conservation law on the target species s from network (4.7), thereby truncating its state-space, $X(t) \leq C$, where $C \in \mathbb{Z}_{>}$ is a conservation constant. The conservation law is imposed in such a way that the total propensity function of the resulting network, denoted by $\alpha^C : [0, C] \cap \mathbb{Z}_{\geq} \to \mathbb{R}_{\geq}$, is given by $\alpha^C(x) = k_1 + k_2 x$, i.e. it has the same form as the total propensity function of the original network (4.7), but is restricted to the bounded discrete domain $[0, C] \cap \mathbb{Z}_{\geq}$. With the restriction imposed, we furthermore embed appropriate reactions to the conservative network, so that an arbitrary nonnegative function, denoted by $g : [0, C] \cap \mathbb{Z}_{\geq} \to \mathbb{R}_{\geq}$, is added to α^C, i.e. the resulting total propensity function is given by $\alpha(x) = \alpha^C(x) + g(x)$. This implies that the interevent time is controllably decreased for any desired state x, i.e. in a state-dependent manner. Equivalently, the two requirements imply that a controllable state-dependent noise is introduced into the stochastic dynamics. We have designed a three-step algorithm, given as Algorithm 4.1, which achieves such goals for arbitrary reaction networks under mass-action kinetics. Before describing the properties of the algorithm in full generality in Section 4.2, we first describe the algorithm by applying it specifically on the test network (4.7).

4.1.1 State-space truncation and the drift-corrector networks

Firstly, in order to bound the domain of species s, an additional species $\bar{s}$ is introduced into network (4.7), in such a way that s and $\bar{s}$ satisfy a pairwise stoichiometric conservation law, formally written $s + \bar{s} = \text{constant}$. Secondly, to ensure the obtained enlarged network has the same deterministic model as the input network (4.7), despite the added species $\bar{s}$, an auxiliary species I^1 is introduced. More precisely, applying

the first two steps of Algorithm 4.1 leads to the network $\mathcal{R}^1(s,\bar{s}) \cup \mathcal{R}_1^2(\bar{s})$, given by:

$$\begin{aligned} \mathcal{R}^1(s,\bar{s}): \quad & \bar{s} + I^1 \xrightarrow{k_1} s + I^1, \\ & s \xrightarrow{k_2} \bar{s}, \\ \mathcal{R}_1^2(\bar{s}): \quad & \varnothing \xrightarrow{1/\mu} I^1, \\ & \bar{s} + I^1 \xrightarrow{1/\mu} \bar{s}, \end{aligned} \tag{4.9}$$

where the superscripts in subnetworks $\mathcal{R}^1 = \mathcal{R}^1(s,\bar{s})$ and $\mathcal{R}_1^2 = \mathcal{R}_1^2(\bar{s})$ correspond to the first and second steps in Algorithm 4.1, respectively. Reaction network $\mathcal{R}^1$, given in (4.9), is obtained from network $\mathcal{R} = \mathcal{R}(s)$, given by (4.7), in the following way: since the first reaction in $\mathcal{R}$ *increases* the copy-number of s by one, $\bar{s}$ and I^1 are added to the reactants of the reaction, and I^1 is added to the products, leading to the first reaction in $\mathcal{R}^1$. Since the second reaction in $\mathcal{R}$ *decreases* the copy-number of s by one, $\bar{s}$ is added to the products, leading to the second reaction in $\mathcal{R}^1$. This ensures that the desired conservation law, $s + \bar{s} =$ constant, holds. The superscript in I^1 indicates that species I^1 is involved as a catalyst in a reaction of $\mathcal{R}^1$ in which s is *increased by one*. The subscript in $\mathcal{R}_1^2$ is identical to the superscript of I^1, indicating that the network describes production and decay of the species I^1.

Limit $\mu \to 0$

In what follows, we analyze the deterministic and stochastic models of network (4.9) with k_1 and k_2 of order one, $k_1, k_2 = \mathcal{O}(1)$, with respect to the asymptotic parameter $0 < \mu \ll 1$.

Deterministic analysis. At the deterministic level, the IVP for the RREs induced by (4.9) is given by

$$\begin{aligned} \frac{\mathrm{d}\tilde{x}}{\mathrm{d}t} &= k_1(c - \tilde{x})y - k_2\tilde{x}, \\ \frac{\mathrm{d}y}{\mathrm{d}t} &= \frac{1}{\mu}\left(1 - (c - \tilde{x})y\right), \\ \tilde{x}(0) &= \tilde{x}_0 \geq 0, \\ y(0) &= y_0 \geq 0, \end{aligned} \tag{4.10}$$

where $\tilde{x} = \tilde{x}(t) \in [0, c] \cap \mathbb{R}_{\geq}$, and $y = y(t) \in \mathbb{R}_{\geq}$, are the concentrations of species s, and I^1, from (4.9), respectively. We have used the conservation law $\bar{x}(t) = c - \tilde{x}(t)$, where $\bar{x}(t)$ is the concentration of species $\bar{s}$, and $c \in \mathbb{R}_{>}$ is a finite time-independent conservation constant.

Let us now describe relationships between systems (4.8) and (4.10), starting with the weak statement: for $c > k_1/k_2$, and for any $\mu > 0$, the time-independent solutions of (4.8) and (4.10) are the same: the $\tilde{x}$-component of the equilibrium point of (4.10) is identical to the equilibrium point of (4.8). Let us note that both of the equilibria are stable. A generalization of this is given as Lemma 4.1 in Section 4.2. Furthermore, it follows from the Tikhonov theorem [84] that the ODE for y, given by second equation in (4.10), reduces to the algebraic equation $y = (c - \tilde{x})^{-1}$ as $\mu \to 0$. Substituting the algebraic equation into the first equation in (4.10), one obtains

$$\begin{aligned} \frac{\mathrm{d}\tilde{x}}{\mathrm{d}t} &= k_1 - k_2\tilde{x}, \\ \tilde{x}(0) &= \tilde{x}_0, \ \text{ as } \mu \to 0. \end{aligned} \tag{4.11}$$

IVPs (4.8) and (4.11) have the same form, and let us denote their solutions by $x(t; x_0)$ and $\tilde{x}(t; \tilde{x}_0)$, respectively. Then, choosing the conservation constant $c > \max_{t\geq 0} x(t; x_0) < \infty$, ensuring that the concentration of auxiliary species $\bar{s}$ is non-negative, $\bar{x}(t) = c - \tilde{x}(t) \geq 0$, and choosing $\tilde{x}_0 = x_0$, leads to a stronger result: for sufficiently large c, and for $0 < \mu \ll 1$, the time-dependent (outer) solutions of (4.8) and (4.10), with the same initial conditions, are approximately identical (beyond an initial transient). For this reason, we call $\mathcal{R}_1^2$ a *drift-corrector network*, as it ensures networks (4.8) and (4.10) have the same deterministic model (drift). See Theorem 4.1 in Section 4.2 for the corresponding general result.

Let us note that, if we replace the first reaction from (4.9) with $\bar{s} \xrightarrow{k_1} s$, the conservation law $s + \bar{s} =$ constant would still hold (and the state-space of x would be bounded). However, in this case the equilibrium would be given by $\tilde{x} = k_1/(k_1 + k_2)c$, which differs from the equilibrium of (4.8), and the RREs of such a network could not be corrected to the form (4.8). For this reason, we have introduced the drift-corrector species I^1.

Stochastic analysis. At the stochastic level, the CME underlying network $\mathcal{R}^1 \cup \mathcal{R}_1^2$ is given by (see also Section 2.3.2)

$$\frac{\partial}{\partial t}p(x, y, t) = \left(\mathcal{L}^1 + \frac{1}{\mu}\mathcal{L}_1^2\right) p(x, y, t), \tag{4.12}$$

where $x, y \in \mathbb{Z}_{\geq}$ are the copy-numbers of species s, I^1 from (4.9), respectively, with

$$\begin{aligned} \mathcal{L}^1 &= k_1 y(E_x^{-1} - 1)(C - x) + k_2(E_x^{+1} - 1)x, \\ \mathcal{L}_1^2 &= (E_y^{-1} - 1) + (C - x)(E_y^{+1} - 1)y, \end{aligned} \tag{4.13}$$

where $\mathcal{L}^1, \mathcal{L}_1^2$ are the forward operators of subnetworks $\mathcal{R}^1, \mathcal{R}_1^2$, respectively. Let us analyze the CME (4.12) in the limit $\mu \to 0$, by considering the following perturbation series [51]:

$$p(x, y, t) = p_0(x, y, t) + \mu p_1(x, y, t) + \ldots + \mu^i p_i(x, y, t) + \ldots, \quad i \geq 2. \tag{4.14}$$

Substituting (4.14) into (4.12) and equating terms of equal powers in μ, the following system of equations is obtained:

$$\begin{aligned} \mathcal{O}\left(\frac{1}{\mu}\right) &: \ \mathcal{L}_1^2 p_0(x, y, t) = 0, \\ \mathcal{O}(1) &: \ \mathcal{L}_1^2 p_1(x, y, t) = (\frac{\partial}{\partial t} - \mathcal{L}^1) p_0(x, y, t). \end{aligned} \tag{4.15}$$

Order $1/\mu$ *equation.* Let us write $p_0(x, y, t) = p_0(y|x, t)p_0(x, t)$, where $p_0(y|x, t)$ is the PMF of y conditional on x (i.e. with x and t fixed), while $p_0(x, t)$ is the marginal PMF of x at time t. Substituting $p_0(x, y, t) = p_0(y|x, t)p_0(x, t)$ into the first equation in (4.15), with x and t fixed, leads to $\mathcal{L}_1^2 p_0(y|x, t) = 0$. It follows that the zero-order PMF is given by

$$p_0(x, y, t) = \mathcal{P}(y;\, (C - x)^{-1}) p_0(x, t), \tag{4.16}$$

where $\mathcal{P}(y;\, \lambda) = (\lambda)^y / y! \exp(-\lambda)$ is the Poisson distribution with intensity λ. In the degenerate case when $x = C$, operator $\mathcal{L}_1^2$ becomes $\mathcal{L}_1^2 = (E_y^{-1} - 1)$, and in this case we define $\mathcal{P}(y;\, (C - x)^{-1})|_{x=C} \equiv \delta_{y,\infty}$, where $\delta_{i,j}$ denotes the Kronecker-delta function, i.e. the PMF of y is concentrated at infinity. At the network level, the induced fast subnetwork (with x fixed) in this case becomes $\varnothing \xrightarrow{1/\mu} I^1$, i.e. only the first reaction in $\mathcal{R}_1^2$ from (4.9) can fire, since species $\bar{s}$ is not present when the copy-number of species s reaches $x = C$, formally leading to an infinite production of the species I^1.

Order 1 *equation.* The adjoint operator $(\mathcal{L}_1^2)^*$ (see also Section 2.3.2) has a trivial null-space, $\mathcal{N}((\mathcal{L}_1^2)^*) = \{1_y\}$, where $\mathcal{N}(\cdot)$ denotes the null-space of an operator, and 1_y denotes a function independent of y. Consequently, the solvability condition, obtained by summing the second equation in (4.15) over y [51], is given by $\langle 1_y, (\frac{\partial}{\partial t} - \mathcal{L}^1) p_0(x, y, t) \rangle = 0$, with the inner-product $\langle f, g \rangle = \sum_{y=0}^{\infty} f(y)g(y)$. The solvability condition can be simplified as follows

$$\begin{aligned} \frac{\partial}{\partial t} p_0(x, t) = {} & k_1 (E_x^{-1} - 1)(C - x) p_0(x, t) \langle y, \mathcal{P}(y;\, (C - x)^{-1}) \rangle \\ & + k_2 (E_x^{+1} - 1) x p_0(x, t) \langle 1, \mathcal{P}(y;\, (C - x)^{-1}) \rangle. \end{aligned} \tag{4.17}$$

Using the equalities $\langle y, \mathcal{P}(y;\, (C-x)^{-1})\rangle = (C-x)^{-1}$ and $\langle 1, \mathcal{P}(y;\, (C-x)^{-1})\rangle = 1$, equation (4.17) becomes the *effective CME*

$$\frac{\partial}{\partial t} p_0(x,t) = \mathcal{L} p_0(x,t), \tag{4.18}$$

with $\mathcal{L}$ being the forward operator of the input network (4.7):

$$\mathcal{L} = k_1(E_x^{-1} - 1) + k_2(E_x^{+1} - 1)x. \tag{4.19}$$

Let us note that, in the degenerate case $x = C$, the first term in (4.17) becomes $k_1 p_0(C-1,t) - k_1 p_0(C,t)0 \times \infty = k_1 p_0(C-1,t)$. In particular, we define $k_1 p_0(C,t)0 \times \infty \equiv 0$, since, when $x = C$, the first reaction in subnetwork $\mathcal{R}^1$ from (4.9) cannot fire.

It follows from (4.18)–(4.19) that the stochastic models of networks (4.7) and (4.9) also match when the drift-corrector network $\mathcal{R}_1^2$ fires sufficiently fast, $0 < \mu \ll 1$. In Figure 4.1(a), we display the stationary PMF of network (4.9) for a particular choice of parameters, and for two values of the asymptotic parameter μ. More precisely, the PMFs for $\mu = 1$ and $\mu = 10^{-2}$ are shown as the purple curve and blue histrogram, respectively, and the stationary PMF of the input network (4.7) as the black curve (which is a Poissonian with intensity k_1/k_2, $\mathcal{P}(x;\, k_1/k_2)$). One can notice an almost perfect matching at the stochastic level when $\mu = 10^{-2}$. In Figures 4.1(b) and (c), we display representative sample paths for species s and I^1 from (4.9) in blue, while the corresponding deterministic trajectories in red, for $\mu = 10^{-2}$. At the deterministic level, species I^1 quickly reaches the quasistationary manifold $y = (C-x)^{-1}$ in the phase plane, which in the long-run leads to the equilibrium $y^* = (C - x^*)^{-1} = 0.1$, where $C = 15$ and $x^* = 5$. At the stochastic level, $Y(t)$ is a short-lived species, fluctuating at the low copy-numbers, and experiencing short-duration bursts to higher values when $X(t)$ reaches the right-boundary point $x = C = 15$. For example, in Figure 4.1(c), one can notice that species I^1 bursts to $y = 13$ in a small time-interval after $t = 0$, as a consequence of taking the initial condition $X(0) = C = 15$. By decreasing the asymptotic parameter μ, such bursts in y reach increasingly higher values (see also equation (4.16)). However, since the bursts are of short-duration, I^1 spends most of the time at low copy-numbers, and the underlying marginal PMF is concentrated near zero. (Note that the opposite limit, $\mu \to \infty$, which is not of interest in this thesis, gives rise to so-called noise-induced mixing [116].)

Let us note that we have assumed the rate coefficients appearing in subnetwork $\mathcal{R}_1^2(\bar{s})$ from (4.9) are identical for simplicity, and that this assumption may be relaxed. More precisely, if the rate coefficients of the first and second reactions in

$\mathcal{R}_1^2(\bar{s})$ are $1/\mu_1$ and $1/\mu_2$, respectively, then the same conclusions hold, provided the rate coefficient k_1 from subnetwork $\mathcal{R}^1(s,\bar{s})$ is replaced by $(\mu_1/\mu_2)k_1$.

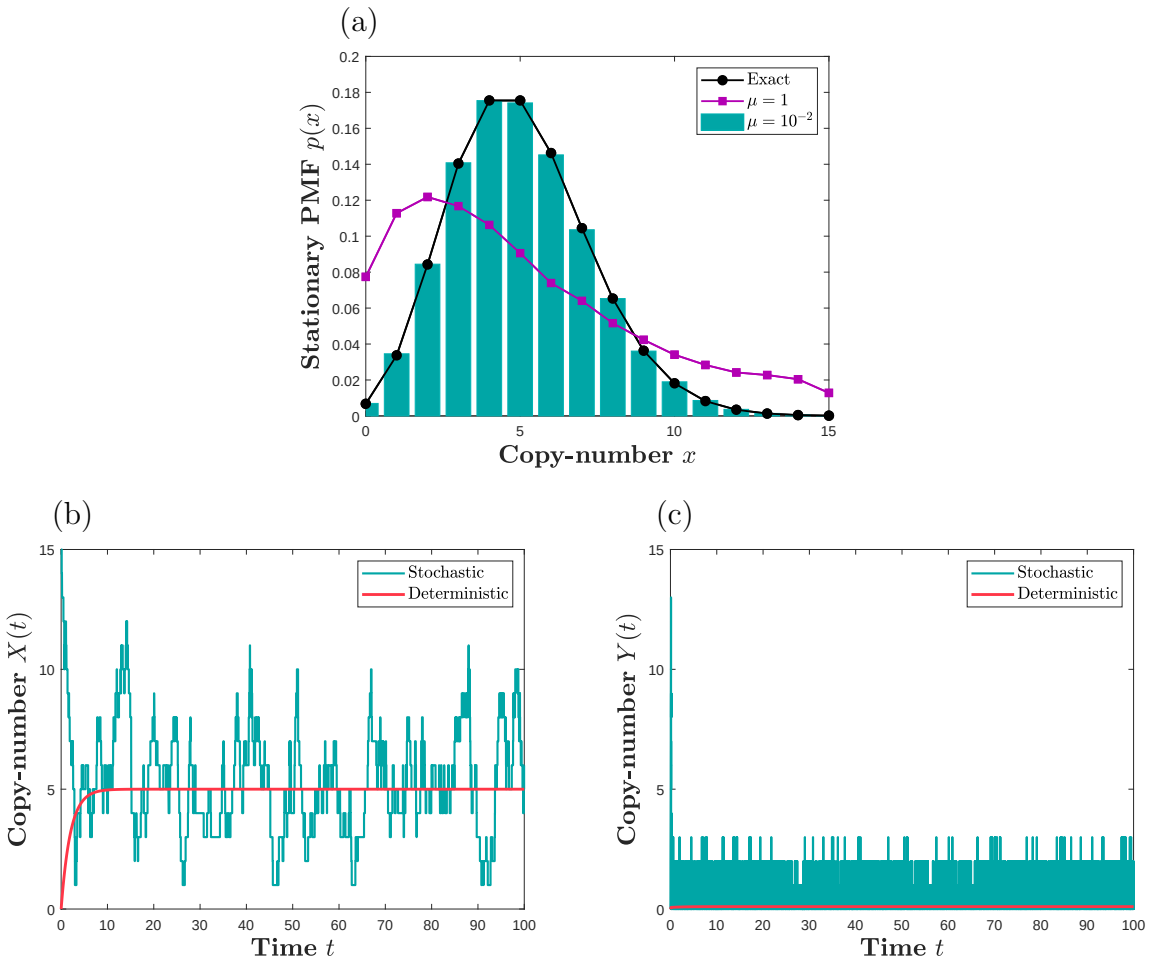

Figure 4.1: *Panel* (a) *displays the stationary PMF of network* $\mathcal{R}^1 \cup \mathcal{R}_1^2$, *given by* (4.9), *for* $\mu = 1$ *and* $\mu = 10^{-2}$ *as the purple curve and the blue histogram, respectively, and the stationary PMF of input network* $\mathcal{R}$, *given by* (4.7), *as the black curve. Panels* (b) *and* (c) *display in blue representative sample paths for species* s *and* I^1 *from* (4.9), *respectively, corresponding to the blue histogram from panel* (a), *and were obtained by applying the Gillespie algorithm. Also shown are the deterministic trajectories in red, obtained by solving the RREs* (4.10). *The dimensionless parameters are fixed to:* $k_1 = 2.5$, $k_2 = 0.5$, $C = 15$, *and* $\mu = 10^{-2}$ *in panels* (b) *and* (c). *The trajectories from* (b) *and* (c) *were initiated at* $(X(0), Y(0)) = (15, 0)$.

4.1.2 Zero-drift network $\mathcal{R}_{1,1}$

Having completed the first two steps of Algorithm 4.1, let us focus on the third (and final) step, in which we introduce arbitrary noise into the stochastic model of

network (4.9), without influencing the underlying deterministic model (4.10). Let us start our consideration by embedding into (4.9) network $\mathcal{R}^3_{1,1} = \mathcal{R}^3_{1,1}(s, \bar{s})$, which is given by

$$\begin{aligned} \mathcal{R}^3_{1,1}(s,\bar{s}): \qquad & s + \bar{s} \xrightarrow{k_{1,1}} 2s, \\ & s + \bar{s} \xrightarrow{k_{1,1}} 2\bar{s}. \end{aligned} \tag{4.20}$$

The subscript in $\mathcal{R}^3_{1,1}$ indicates that the underlying reactions have one molecule of s, and one of $\bar{s}$, as reactants (while the superscript indicates we are performing the third step of Algorithm 4.1). The two reactions in (4.20) preserve the conservation law from (4.9). Furthermore, the first and second reactions produce, and degrade, exactly one molecule of s, respectively, and they fire at the same rate. Consequently, embedding $\mathcal{R}^3_{1,1}$ into (4.9) does not affect the underlying deterministic model (4.10), and we call $\mathcal{R}^3_{1,1}$ a *zero-drift network*. Note that the deterministic dynamics are not preserved if the rate coefficients in (4.20) are different. However, $\mathcal{R}^3_{1,1}$ does affect the underlying stochastic model [117, 118, 119, 21]. To illustrate this, let us consider network $\mathcal{R}^3_{1,1}$ in isolation: the reactions from (4.20) fire when $X(t) \in (0, C)$, but not when $X(t) \in \{0, C\}$, so that $\mathcal{R}^3_{1,1}$ in isolation fires until $X(t)$ takes one of the extreme values $\{0, C\}$. Let us note that a possible biologically-relevant realization of network (4.20), aside from the DNA strand-displacement mechanism, is a dimer version of the bifunctional histidine kinase/phosphatase reported in [120].

The CME underlying network $\mathcal{R}^1 \cup \mathcal{R}^2_1 \cup \mathcal{R}^3_{1,1}$ is given by

$$\frac{\partial}{\partial t} p(x, y, t) = \left(\mathcal{L}^1 + \frac{1}{\mu} \mathcal{L}^2_1 + K_{1,1} \mathcal{L}^3_{1,1} \right) p(x, y, t), \tag{4.21}$$

with operators $\mathcal{L}^1$ and $\mathcal{L}^2_1$ given by (4.13), and $\mathcal{L}^3_{1,1}$, the forward operator of subnetwork (4.20), given by

$$\mathcal{L}^3_{1,1} = (E_x^{-1} + E_x^{+1} - 2)\beta_{1,1}(x). \tag{4.22}$$

Here, $K_{1,1}\beta_{1,1}(x)$ is the propensity function of reactions from the zero-drift network $\mathcal{R}_{1,1}$ with the factors scaled for convenience, so that $\beta_{1,1}(x)$ is normalized, and they are given by

$$K_{1,1} = \left(\frac{C}{2} \right)^2 k_{1,1}, \quad \beta_{1,1}(x) = \left(\frac{C}{2} \right)^{-2} x(C - x). \tag{4.23}$$

Since operator $\mathcal{L}^3_{1,1}$ does not depend on variable y, it follows from (4.18) that, for sufficiently small μ, the CME (4.21) is approximately given by

$$\frac{\partial}{\partial t} p_0(x, t) = \left(\mathcal{L} + K_{1,1} \mathcal{L}^3_{1,1} \right) p_0(x, t), \quad \text{for } 0 < \mu \ll 1. \tag{4.24}$$

Equation (4.24) implies that the effective total propensity function of the network $\mathcal{R}^1 \cup \mathcal{R}^2_1 \cup \mathcal{R}^3_{1,1}$, denoted $\alpha(x)$, satisfies

$$\alpha(x) \approx \alpha^C(x) + 2K_{1,1}\beta_{1,1}(x), \quad \text{for } 0 < \mu \ll 1, \tag{4.25}$$

where $\alpha^C : [0, C] \cap \mathbb{Z}_{\geq} \to \mathbb{R}_{\geq}$ is given by

$$\alpha^C(x) = k_1 + k_2 x, \tag{4.26}$$

and has the form of the total propensity of the input network (4.7). The function $\beta_{1,1}(x)$ is displayed in Figure 4.2(a), where one can notice its parabolic shape, arising from the underlying conservation law $X(t) + \bar{X}(t) = C$, which holds for all $t \geq 0$, where $\bar{X}(t) \in \mathbb{Z}_{\geq}$ is the copy-number of $\bar{s}$ at time $t \geq 0$. Comparing (4.25) and (4.26), it follows that, as $\mu \to 0$, the mean interevent time for network $\mathcal{R}^1 \cup \mathcal{R}^2_1 \cup \mathcal{R}^3_{1,1}$ is lower than for network (4.7), in the regions of the common state-space where $\beta_{1,1}(x) \neq 0$, i.e. for $x \in (0, C)$. Coefficient $K_{1,1}$ controls by how much the interevent time is reduced. Equivalently, $\beta_{1,1}(x)$, and $K_{1,1}$, determine the support, and magnitude, respectively, of the state-dependent intrinsic noise which network (4.20) introduces into the stochastic dynamics of network (4.9). Let us now analyse the long-term solutions of the effective CME (4.24) in the limits $K_{1,1} \to 0$ and $K_{1,1} \to \infty$, i.e. when the zero-drift network (4.20) fires slowly and fast, respectively.

Limit $K_{1,1} \to 0$. Setting the LHS to zero in (4.24), taking $K_{1,1} = 0$, and assuming C is fixed to a sufficiently large value, it follows that the stationary PMF is a Poissonian with parameter k_1/k_2:

$$\lim_{K_{1,1} \to 0} p_0(x) \approx \begin{cases} \frac{1}{x!} \left(\frac{k_1}{k_2}\right)^x \exp\left(-\frac{k_1}{k_2}\right), & \text{if } x \in [0, C], \\ 0, & \text{otherwise.} \end{cases} \tag{4.27}$$

Limit $K_{1,1} \to \infty$. Let us substitute the perturbation series

$$p_0(x) = q_0(x) + \frac{1}{K_{1,1}} q_1(x) + \ldots + \left(\frac{1}{K_{1,1}}\right)^i q_i(x) + \ldots, \quad i \geq 2, \tag{4.28}$$

into (4.24) with the LHS set to zero, and consider the limit $K_{1,1} \to \infty$. Equating terms of equal powers in $1/K_{1,1}$, one obtains:

$$\begin{aligned} \mathcal{O}(K_{1,1}) : \ & \mathcal{L}^3_{1,1} q_0(x) = 0, \\ \mathcal{O}(1) : \ & \mathcal{L}^3_{1,1} q_1(x) = -\mathcal{L} q_0(x). \end{aligned} \tag{4.29}$$

The solution to the first equation in (4.29) is given by

$$q_0(x) = \begin{cases} 1-a, & \text{if } x = 0, \\ a, & \text{if } x = C, \\ 0, & \text{otherwise}, \end{cases} \tag{4.30}$$

where $a \in [0,1]$ is an arbitrary constant.

The null-space of the adjoint operator of $\mathcal{L}^3_{1,1}$, denoted by $(\mathcal{L}^3_{1,1})^*$, is given by $\mathcal{N}((\mathcal{L}^3_{1,1})^*) = \{1_x, x\}$, where 1_x denotes a function independent of x. The solvability condition $0 = \langle 1_x, \mathcal{L}q_0(x)\rangle$, for the second equation in (4.29), is unconditionally satisfied, where $\langle f, g\rangle = \sum_{x=0}^{\infty} f(x)g(x)$. On the other hand, the solvability condition $0 = \langle x, \mathcal{L}q_0(x)\rangle = \langle \mathcal{L}^* x, q_0(x)\rangle = k_1 - k_2 C a$ implies $a = k_1/(Ck_2)$, which, upon substitution into (4.30), implies

$$\lim_{K_{1,1}\to\infty} p_0(x) \approx \begin{cases} 1 - \frac{1}{C}\frac{k_1}{k_2}, & \text{if } x = 0, \\ \frac{1}{C}\frac{k_1}{k_2}, & \text{if } x = C, \\ 0, & \text{otherwise}. \end{cases} \tag{4.31}$$

Let us interpret the approximate results (4.27) and (4.31), and compare them with the numerically obtained counterparts. In Figure 4.2(b), we display numerically obtained stationary x-marginal PMFs for different values of $K_{1,1}$, with the rest of the (dimensionless) parameters fixed to $k_1 = 2.5$, $k_2 = 0.5$, $\mu = 10^{-3}$, and $C = 15$. It can be seen that, for $K_{1,1} = 0$, i.e. when the zero-drift network $\mathcal{R}^3_{1,1}$ does not fire, the PMF matches that of network (4.7), i.e. it is a Poissonian, as predicted by (4.27). Let us note that the matching of the PMFs of networks (4.7) and $\mathcal{R}^1 \cup \mathcal{R}^2_1 \cup \mathcal{R}^3_{1,1}$ relies on choosing sufficiently large rate coefficients $1/\mu$ in the drift-corrector network $\mathcal{R}^2_1$ (see also Figure 4.1). When $K_{1,1} = 5$, the PMF appears closer to a uniform distribution, than does the PMF when $K_{1,1} = 0$. Finally, for the larger value $K_{1,1} = 10^5$, i.e. when zero-drift network $\mathcal{R}^3_{1,1}$ fires much faster than network $\mathcal{R}^1$, the PMF redistributes across the domain, accumulating at the boundary, and becoming bimodal. This is in qualitative agreement with (4.25), and in quantitative agreement with (4.31), which predicts $p(0) \approx 0.7$ and $p(15) \approx 0.3$. In Figure 4.2(c), a representative sample path is shown, obtained by applying the Gillespie algorithm on network $\mathcal{R}^1 \cup \mathcal{R}^2_1 \cup \mathcal{R}^3_{1,1}$, when $K_{1,1} = 10^5$. Also shown is a trajectory obtained by numerically solving the deterministic model (4.10). Consistent with Figure 4.2(b), the sample path switches between the boundary of the state-space, with a bias towards the left boundary point $x = 0$. This is in contrast to the deterministic trajectories, which are globally attracted to the equilibrium $x = 5$.

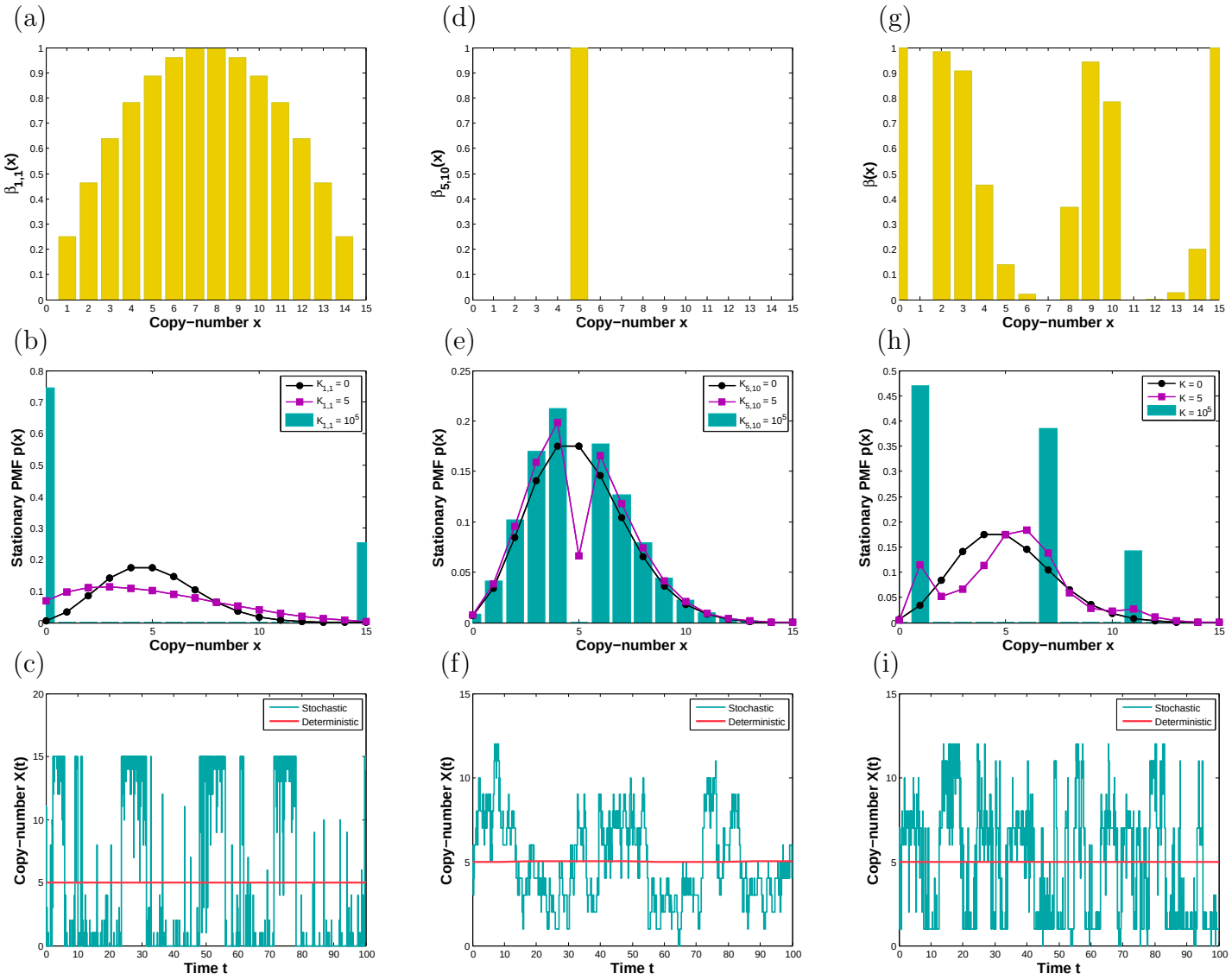

Figure 4.2: *Panels* (a), (d) *and* (g) *display propensity functions* $\beta_{1,1}(x)$, $\beta_{5,10}(x)$ *and* $\beta(x) \equiv \beta_{0,15}(x) + \beta_{2,9}(x) + \beta_{8,5}(x) + \beta_{12,0}(x)$, *respectively. Panels* (b), (e) *and* (h) *display the stationary PMFs of networks* $\mathcal{R}^1 \cup \mathcal{R}^2_1 \cup \mathcal{R}^3_{1,1}$, $\mathcal{R}^1 \cup \mathcal{R}^2_1 \cup \mathcal{R}^2_{5,10}$ *and* $\mathcal{R}^1 \cup \mathcal{R}^2_1 \cup (\mathcal{R}^3_{0,15} \cup \mathcal{R}^3_{2,9} \cup \mathcal{R}^3_{8,5} \cup \mathcal{R}^3_{12,0})$, *respectively, where* $\mathcal{R}^1 \cup \mathcal{R}^2_1$ *is given by* (4.9), *while the rest of the (zero-drift) networks are as given in third step of Algorithm* 4.1. *In* (h), $K \equiv K_{0,15} = K_{2,9} = K_{8,5} = K_{12,0}$. *Panels* (c), (f), *and* (i) *display in blue the sample paths, corresponding to the PMFs shown as the blue histograms in* (b), (e) *and* (h), *respectively, and were obtained by applying the Gillespie algorithm on the underlying networks. Also shown in red are the deterministic trajectories, obtained by numerically solving the corresponding deterministic models. The dimensionless parameters are fixed to:* $k_1 = 2.5$, $k_2 = 0.5$, $\mu = 10^{-3}$, $C = 15$, *and the state-space for species* I^1 *is bounded in* (b), (e) *and* (h) *by* 50. *In* (b) *and* (e), *the two-species stationary CME was numerically solved, while in* (h) *the boundary zero-drift networks are taken in the asymptotic limits* $\mu_{0,15}, \mu_{12,0} \to 0$. *The blue and red trajectories from panel* (i) *were generated with* $(\mu_{0,15})^{-1} M_{0,15} = (\mu_{12,0})^{-1} M_{12,0} = 10^7$. *The trajectories from* (c), (f) *and* (i) *were all initiated at the deterministic equilibrium,* $X(0) = 5$.

4.1.3 General zero-drift networks $\mathcal{R}_{n,\bar{n}}$

The zero-drift network $\mathcal{R}^3_{1,1}(s,\bar{s})$, given by (4.20), involves a single molecule of s and $\bar{s}$ as reactants, and adds the noise at $x \in [1, C-1]$, i.e. in the interior of the state-space. Similar networks may be used to add the noise at any point in the state-space, without influencing the deterministic dynamics. In particular, in (4.4) and (4.5), displayed in Algorithm 4.1, we present general zero-drift networks $\mathcal{R}^3_{n,\bar{n}}(s,\bar{s})$, which involve n molecules of s, and $\bar{n}$ of $\bar{s}$, as reactants, and add the noise at $x \in [n, C-\bar{n}]$, where $n, \bar{n} \in \mathbb{Z}_{\geq}$ and $(n+\bar{n}) \leq C$. Embedding a union of such networks, $\cup_{(n,\bar{n})}\mathcal{R}^3_{n,\bar{n}}(s,\bar{s})$, into (4.9), we arrive at the result similar to (4.25), with $K_{1,1}\beta_{1,1}(x)$ replaced by the linear combination $\sum_{(n,\bar{n})} K_{n,\bar{n}}\beta_{n,\bar{n}}(x)$ - see also Corollary 4.1 in Section 4.2. Before discussing networks (4.4) and (4.5), called the interior and boundary zero-drift networks, respectively, in a greater detail, let us first state their more general properties. The propensity function of reactions underlying $\mathcal{R}^3_{n,\bar{n}}(s,\bar{s})$ is given by $K_{n,\bar{n}}\beta_{n,\bar{n}} : [0, C] \to \mathbb{R}_{\geq}$, with

$$K_{n,\bar{n}} = M_{n,\bar{n}} k_{n,\bar{n}}, \qquad \beta_{n,\bar{n}}(x) = (M_{n,\bar{n}})^{-1} x^{\underline{n}} (C-x)^{\underline{\bar{n}}}, \tag{4.32}$$

where $x^{\underline{n}} = x(x-1)\dots(x-(n-1))$ and $\bar{x}^{\underline{\bar{n}}} = (C-x)^{\underline{\bar{n}}} = (C-x)(C-1-x)\dots(C-(\bar{n}-1)-x)$ (see also Section 2.2). Here, the scaling factor $M_{n,\bar{n}}$ is introduced for convenience, to approximately normalize $\beta_{n,\bar{n}}(x)$, and is given by

$$M_{n,\bar{n}} = \left(\frac{n}{n+\bar{n}}C\right)^{\underline{n}} \left(\frac{\bar{n}}{n+\bar{n}}C\right)^{\underline{\bar{n}}}. \tag{4.33}$$

More specifically, the factor $M_{n,\bar{n}}$ may be obtain as follows. The continuous approximation of the discrete propensity function $\alpha_{n,\bar{n}}(x) = x^{\underline{n}}(C-x)^{\underline{\bar{n}}}$ is given by the rate function $x^n (C-x)^{\bar{n}}$, which is a polynomial with a unique maximum given by $x_m = Cn/(n+\bar{n})$. Substituting x_m into $\alpha_{n,\bar{n}}(x)$, i.e. approximating the maximum of the discrete propensity function with that of the corresponding continuous rate function, leads to $\alpha_{n,\bar{n}}(x_m) = M_{n,\bar{n}}$.

The function $\beta_{n,\bar{n}}(x)$ is nonzero on the interval $[n, C-\bar{n}]$, with the unique maximum approximately at $Cn/(n+\bar{n})$. Stoichiometric coefficients $n, \bar{n}$ control the support of the intrinsic noise, which network $\mathcal{R}^3_{n,\bar{n}}$ introduces into the stochastic dynamics, via the control of support of the propensity function from (4.32). The larger the sum $(n+\bar{n})$ is, with $(n+\bar{n}) \leq C$, the smaller the support of $\beta_{n,\bar{n}}(x)$, and hence one obtains a more precise noise-control. In the special case when $n+\bar{n} = C$, the propensity function (4.32) is nonzero only at a single point in the state-space, $x = n$. We call networks $\mathcal{R}^3_{n,\bar{n}}(s,\bar{s})$, with $n+\bar{n} = C$, *basis zero-drift networks*, and the corresponding

propensity functions *basis propensity functions*. Any nonnegative function, defined on a bounded discrete domain, may be represented by a suitable linear combination of the basis propensity functions (i.e. by a suitable union of the basis zero-drift networks). Put it another way, given arbitrary state-dependent noise, Algorithm 4.1 designs suitable zero-drift networks which approximate (or exactly replicate, if desired) the noise and introduce it into the stochastic dynamics of any given reaction network. Let us note that the basis propensity functions have the form of the Lagrange interpolation polynomial utilized in the approximation theory [121].

The cost of such a precision in noise-control is a larger number of reactants in the underlying zero-drift networks. However, while the higher-molecular reactions introduced by the algorithm are more expensive to synthetize, they do not limit applicability of Algorithm 4.1 to DNA computing. The reason for this is that such reactions may always be broken down into sets of up-to bimolecular reactions, as demonstrated in Chapter 5. Let us stress that the lower the molecular copy-numbers of a given reaction network are, the more important it becomes to control their stochastic behavior, and the *less* costly Algorithm 4.1 becomes (since the zero-drift networks involve less reactants).

Interior zero-drift networks

Zero-drift network $\mathcal{R}^3_{n,\bar{n}}(s,\bar{s})$, involving at least one of each species as reactants, i.e. with $n,\bar{n}\neq 0$, satisfying (4.4), contains two reactions whose propensity function is $K_{n,\bar{n}}\beta_{n,\bar{n}}$, with the factors given in (4.32). It is nonzero only in the interior of the state-space, where it also attains a unique maximum. For this reason, we call such a network an interior zero-drift network.

Let us utilize a basis interior zero-drift network to reduce the probability of finding species s from network (4.9) at the state $x=5$. More precisely, let us embed into network (4.9), with the conservation constant $C=15$, the zero-drift network $\mathcal{R}^3_{5,10}(s,\bar{s})$, satisfying (4.4) with $n=5$ and $\bar{n}=10$. In Figure 4.2(d), we show the propensity function $\beta_{5,10}(x)$, which is nonzero only at $x=5$. In (e), we show the numerically approximated stationary x-marginal PMFs underlying network $\mathcal{R}^1\cup\mathcal{R}^2_1\cup\mathcal{R}^3_{5,10}$ for different values of $K_{5,10}$, with the rest of the parameters as in Figure 4.2(b). One can notice that, under the action of network $\mathcal{R}^3_{5,10}$, the PMF is gradually decreased to nearly zero at $x=5$ (the deterministic equilibrium), and becomes bimodal, with the two noise-induced maxima at $x=4$ and $x=6$. In (f), we show a corresponding representative sample path. Let us note that the mean (first moment) of the PMFs

from Figures 4.2(b) and (e) is approximately given by $x = 5$, independent of the value of $K_{1,1}$ and $K_{5,10}$ (see Lemma 4.2 in Section 4.2).

Boundary zero-drift networks

Since the interior-zero drift networks cannot introduce noise at the boundary of the state-space, we have designed so-called boundary zero-drift networks for this purpose. More specifically, a left-boundary zero-drift network $\mathcal{R}^3_{0,\bar{n}}(s,\bar{s})$, given by (4.5), introduces noise at $x \in [0, C-\bar{n}]$, while a right-boundary zero-drift network $\mathcal{R}^3_{n,0}(s,\bar{s})$, introducing noise at $x \in [n, C]$, takes an analogous form, given by

$$\begin{aligned}
\mathcal{R}^3_{n,0}(s,\bar{s}): \quad ns &\xrightarrow{k_{n,0}} (n-1)s + \bar{s},\\
C\bar{s} + \bar{B} &\xrightarrow{k_{n,0}} s + (C-1)\bar{s} + \bar{B},\\
ns &\xrightarrow{1/\mu_{n,0}} ns + \bar{B},\\
C\bar{s} + \bar{B} &\xrightarrow{1/\mu_{n,0}} C\bar{s}, \quad 0 < \mu_{0,n} \ll 1.
\end{aligned} \tag{4.34}$$

Let us qualitative describe structure of the network (4.5): the first reaction fires when the copy-number of species s satisfies $x \in [0, C-\bar{n}]$, and the reaction generates a drift to the right in the state-space, i.e. it increases x. The second reaction fires when $x = C$, provided there exists at least one molecule of the auxiliary species B, which is a catalyst for the second reaction (i.e. copy-number of B remains unchanged upon firing of the reaction). In this case, the second reaction creates a drift to the left, i.e. it decreases x. Finally, the last two reactions from (4.5), which fire much faster than the first two reactions, describe a production and decay of the auxiliary species B, with the species $s, \bar{s}$ now being catalysts. At the stochastic level, when the last two reactions are fast enough, only the first reaction from (4.5) has an effect on the copy-number of species s. As a consequence, the effective propensity function of network (4.5) is $K_{0,\bar{n}}\beta_{0,\bar{n}}$, satisfying (4.32), which attains its maximum at the left-boundary point $x = 0$, and for this reason we call network (4.5) a left-boundary zero-drift network. On the other hand, at the deterministic level, the right and left drifts introduced by the first and second reactions, respectively, cancel out. Similar considerations apply to the right-boundary zero-drift network (4.34). Put it another way, network (4.5) (respectively, (4.34)) is a zero-drift network only for sufficiently small $\mu_{0,\bar{n}}$ (respectively, $\mu_{n,0}$), allowing the auxiliary species B (respectively, $\bar{B}$) to reach an appropriate quasistationary state. Let us establish this quantitatively by embedding network $\mathcal{R}^3_{0,\bar{n}}$ into (4.9).

At the deterministic level, the RREs for the resulting composite network $\mathcal{R}^1 \cup \mathcal{R}^2_1 \cup \mathcal{R}^3_{0,\bar{n}}$ are given by

$$\begin{aligned}
\frac{\mathrm{d}\tilde{x}}{\mathrm{d}t} &= k_1(c-\tilde{x})y - k_2\tilde{x} - k_{0,\bar{n}}(c-\tilde{x})^{\bar{n}} - k_{0,\bar{n}}\tilde{x}^{\underline{c}}z,\\
\frac{\mathrm{d}y}{\mathrm{d}t} &= \frac{1}{\mu}\left(1-(c-\tilde{x})y\right),\\
\frac{\mathrm{d}z}{\mathrm{d}t} &= \frac{1}{\mu}\left((c-\tilde{x})^{\bar{n}} - \tilde{x}^{\underline{c}}z\right),
\end{aligned} \tag{4.35}$$

where $\tilde{x}$, y and z are the concentrations of species s, I^1 and B, respectively, and we take $\mu_{0,15} = \mu$ for simplicity. For $0 < \mu \ll 1$, the drift-corrector species I^1 reaches the quasistationary state $y = 1/(c-\tilde{x})$, while the boundary species B reaches $z = (C-\tilde{x})^{\bar{n}}/\tilde{x}^{\underline{C}}$, which, upon substitution into the first equation from (4.35), leads to the RRE $\mathrm{d}\tilde{x}/\mathrm{d}t = k_1 - k_2\tilde{x}$. In particular, the last two terms in the first equation from (4.35) cancel out in the limit $\mu \to 0$, justifying that $\mathcal{R}^3_{0,\underline{C}}$ is asymptotically a zero-drift network.

At the stochastic level, the CME for network $\mathcal{R}^1 \cup \mathcal{R}^2_1 \cup \mathcal{R}^3_{0,\bar{n}}$ is given by

$$\frac{\partial}{\partial t}p(x,y,z,t) = \left(\mathcal{L}^1 + k_{0,\bar{n}}\mathcal{L}^3_{0,\bar{n}} + \frac{1}{\mu}(\mathcal{L}^2_1 + \mathcal{L}^B_{0,\bar{n}})\right)p(x,y,z,t), \tag{4.36}$$

where x, y and z are the copy-numbers of species s, I^1 and B. Operators $\mathcal{L}^1$ and $\mathcal{L}^2_1$ are given by (4.13), while $(k_{0,\bar{n}}\mathcal{L}^3_{0,\bar{n}} + 1/\mu\mathcal{L}^B_{0,\bar{n}})$ is the forward operator of network (4.5), with

$$\begin{aligned}
\mathcal{L}^3_{0,\bar{n}} &= (E_x^{-1}-1)(C-x)^{\underline{\bar{n}}} + z(E_x^{+1}-1)x^{\underline{C}},\\
\mathcal{L}^B_{0,\bar{n}} &= (C-x)^{\underline{\bar{n}}}(E_z^{-1}-1) + x^{\underline{C}}(E_z^{+1}-1)z.
\end{aligned} \tag{4.37}$$

More precisely, operator $\mathcal{L}^B_{0,\bar{n}}$ satisfies:

$$\mathcal{L}^B_{0,\bar{n}} = \begin{cases} (C-x)^{\underline{\bar{n}}}(E_z^{-1}-1), & \text{if } x \in [0, C-\bar{n}],\\ x^{\underline{C}}(E_z^{+1}-1)z, & \text{if } x = C,\\ 0, & \text{otherwise,}\end{cases} \tag{4.38}$$

i.e. $\mathcal{L}^B_{0,\bar{n}}$ acts on the dynamics of species z only if $x \in [0, C-\bar{n}] \cup C$.

Substituting the perturbation series

$$p(x,y,z,t) = p_0(x,y,z,t) + \mu p_1(x,y,z,t) + \ldots + \mu^i p_i(x,y,z,t) + \ldots, \quad i \geq 2, \tag{4.39}$$

into (4.36), and equating terms of equal powers in μ, one obtains

$$\begin{aligned}\mathcal{O}\left(\frac{1}{\mu}\right):\ &(\mathcal{L}_1^2+\mathcal{L}_{0,\bar{n}}^B)p_0(x,y,z,t)=0,\\ \mathcal{O}(1):\ &(\mathcal{L}_1^2+\mathcal{L}_{0,\bar{n}}^B)p_1(x,y,z,t)=(\frac{\partial}{\partial t}-\mathcal{L}^1-k_{0,\bar{n}}\mathcal{L}_{0,\bar{n}}^3)p_0(x,y,z,t).\end{aligned}\tag{4.40}$$

Order $1/\mu$ *equation.* It follows from the structure of operators $\mathcal{L}_1^2$ and $\mathcal{L}_{0,\bar{n}}^B$ that we may write $p_0(x,y,z,t)=p_0(y|x,t)p_0(z|x,t)p_0(x,t)$, i.e. the auxiliary species I^1 and B are statistically independent for a fixed x and t (this may also be seen directly from networks $\mathcal{R}_1^2$ and $\mathcal{R}_{0,\bar{n}}^3$, since s is a catalyst for both networks, and since species I^1 and B do not interact directly with each other). As a consequence, the equation reduces to the two equations: $\mathcal{L}_1^2p_0(y|x,t)=0$ and $\mathcal{L}_{0,\bar{n}}^Bp_0(z|x,t)=0$, first of which we have already solved in (4.16). Taking into an account equation (4.38), the z-marginal PMF is given by

$$p_0(z|x,t)=\begin{cases}\delta_{z,\infty}, & \text{if } x\in[0,C-\bar{n}],\\ \delta_{z,0}, & \text{if } x=C.\end{cases}\tag{4.41}$$

Order 1 *equation.* Summing the second equation in (4.29) over y and z, and denoting $\langle f,g\rangle=\sum_{z=0}^{\infty}f(z)g(z)$, one obtains the solvability condition

$$\frac{\partial}{\partial t}p_0(x,t)=\Big(\mathcal{L}+(E_x^{-1}-1)k_{0,\bar{n}}(C-x)^{\underline{\bar{n}}}+(E_x^{+1}-1)k_{0,\bar{n}}x^{\underline{C}}\langle z,p_0(z|x,t)\rangle\Big)p_0(x,t),\tag{4.42}$$

Considering (4.41), it follows that $\langle z,p_0(z|x,t)\rangle=0$ if $x=C$. On the other hand, if $x\in[0,C-\bar{n}]$ then $x^{\underline{C}}\langle z,p_0(z|x,t)\rangle=0\times\infty\equiv 0$, since the last reaction from (4.5), which induces the last term in (4.42), can fire only when $x=C$. Hence, equation (4.42) becomes the effective CME

$$\frac{\partial}{\partial t}p_0(x,t)=\Big(\mathcal{L}+(E_x^{-1}-1)K_{0,\bar{n}}\beta_{0,\bar{n}}(x)\Big)p_0(x,t),\tag{4.43}$$

where $k_{0,\bar{n}}(C-x)^{\underline{\bar{n}}}=K_{0,\bar{n}}\beta_{0,\bar{n}}(x)$, as defined in (4.32)–(4.33). Thus, for $0<\mu\ll 1$, the effect of network (4.5) is to introduce noise at $x\in[0,C-\bar{n}]$ at the stochastic level, while the deterministic dynamics remain unchanged.

Let us note that one may require μ to be very small to ensure validity of the effective CME (4.43). Qualitatively speaking, in the case μ is not sufficiently small, $\delta_{z,0}$ from equation (4.41) is replaced by a more general distribution. As a consequence, in general $x^{\underline{C}}\langle z,p_0(z|x,t)\rangle\neq 0$ when $x=C$, and the effective CME (5.21) has an additional term corresponding to the second reaction from (4.5). For this reason,

we have set the stoichiometric coefficient of s in the second (and fourth) reaction from (4.5) equal to C: in this case, the possibly unwanted noise due to μ not being small enough occurs only at a single point $x = C$. If the stoichiometric coefficient is set to $\nu < C$, then the unwanted noise would be added at a larger region of the state-space, $x \in [\nu, C]$, which would generally be less desirable.

Let us also note that the boundary zero-drift networks (4.5) and (4.34) are not unique. In Appendix B, we present two alternative boundary zero-drift network designs, some of which may have better convergence properties - an investigation we do not pursue in this thesis.

Algorithm 4.1 may be used to achieve noise-induced multimodality. For example, let us synthetize noise such that the stationary PMF of network (4.9) becomes trimodal, and nearly zero everywhere, except at $x \in \{1, 7, 11\}$. Such a task may always be achieved by a suitable combination of the basis zero-drift networks, i.e. those zero-networks that induce noise only at a single point in the state-space. In the present case, one could construct the thirteen basis zero-drift networks which add large enough noise at $x \in [0, 15] \setminus \{1, 7, 11\}$. Here, for simplicity, we achieve the task with only four zero-drift networks. In Figure 4.2(g)–(i), we consider the network $\mathcal{R}^1 \cup \mathcal{R}^2_1 \cup (\mathcal{R}^3_{0,15} \cup \mathcal{R}^3_{2,9} \cup \mathcal{R}^3_{8,5} \cup \mathcal{R}^3_{12,0})$. We denote $\beta(x) \equiv \beta_{0,15}(x) + \beta_{2,9}(x) + \beta_{8,5}(x) + \beta_{12,0}(x)$ and, for simplicity, take $K \equiv K_{0,15} = K_{2,9} = K_{8,5} = K_{12,0}$. The resultant propensity function $\beta(x)$ is shown in (g), while in (h) it can be seen that the PMF becomes trimodal for sufficiently large K, with the noise-induced maxima at $x = \{1, 7, 11\}$. This is consistent with the corresponding representative sample path shown in blue in panel (i), which display tristability. Let us note that, while the stochastic dynamics display multistability in (c), (f) and (i), the corresponding deterministic dynamics, also shown in the plots, remain monostable.

4.2 Properties of Algorithm 4.1

In what follows, we establish properties of Algorithm 4.1 applied to an arbitrary reaction network under mass-action kinetics, firing in a fixed (finite, but arbitrarily large) reactor volume V, which we conveniently suitably absorb into the rate coefficients (see also Section 2.2), by generalizing the results from the previous section. More precisely, we apply Algorithm 4.1 to introduce noise into the input network (4.1) via a single species s_i, without a loss of generality (i.e. introducing noise via multiple species reduces to an iterative application of Algorithm 4.1 to one species at a time).

To this end, we introduce the auxiliary species $\bar{s}_i$ such that s_i and $\bar{s}_i$, whose abundances we denote by x_i and $\bar{x}_i$, respectively, are stoichiometrically pairwise conserved: $x_i + \bar{x}_i = \text{constant}$. For simplicity, we also set the asymptotic parameters appearing in the drift-corrector (given as equation (4.3) in Algorithm 4.1) and boundary zero-drift networks (equations (4.5) and (4.34)) all equal to each other, $\mu_{0,\bar{n}} = \mu_{0,n} = \mu$.

4.2.1 Deterministic Analysis

The RREs induced by the input reaction network (4.1) are given by

$$\begin{aligned} \frac{\mathrm{d}\mathbf{x}}{\mathrm{d}t} &= \sum_{j\in\mathcal{R}_>} \kappa_j(\mathbf{x})\Delta\mathbf{x}_j + \sum_{j\in\mathcal{R}_\leq} \kappa_j(\mathbf{x})\Delta\mathbf{x}_j, \\ \mathbf{x}(0) &= \mathbf{x}_0, \end{aligned} \tag{4.44}$$

where $\mathbf{x} = (x_1, x_2, \ldots, x_N)$ contains the concentrations of the input species $s_1, s_2, \ldots, s_N$, and $\kappa_j(\mathbf{x}) = k_j \mathbf{x}^{\boldsymbol{\nu}_j}$ is the mass-action rate function of the reaction with index j (see also Section 2.2 and 2.3.1). Here, the set of reactions is partitioned according to $\mathcal{R} = \mathcal{R}_> \cup \mathcal{R}_\leq$, $\mathcal{R}_> \cap \mathcal{R}_\leq = \emptyset$, with $\mathcal{R}_>$ being the indices of the set of reactions which increase the copy-number of the target species s_i, while $\mathcal{R}_\leq$ denotes the rest of the reactions (i.e. those where s_i is a catalyst, or those which decrease the copy-number of s_i).

The RREs induced by the output reaction network (4.6) are given by

$$\begin{aligned} \frac{\mathrm{d}\mathbf{x}}{\mathrm{d}t} &= \sum_{j\in\mathcal{R}_>} \kappa_j(\mathbf{x}) y_i^{\Delta x_{ij}} (c_i - x_i)^{\Delta x_{ij}} \Delta\mathbf{x}_j + \sum_{j\in\mathcal{R}_\leq} \kappa_j(\mathbf{x})\Delta\mathbf{x}_j \\ &\quad + k^i_{0,\bar{n}}\Big((c_i - x_i)^{\bar{n}} - x_i^{c_i} z_i\Big)\mathbf{e}_i + k^i_{n,0}\Big(- x_i^n + (c_i - x_i)^{c_i}\bar{z}_i\Big)\mathbf{e}_i, \\ \frac{\mathrm{d}y_i^{\Delta x_{ij}}}{\mathrm{d}t} &= \frac{1}{\mu}\Big(1 - (c_i - x_i)^{\Delta x_{ij}} y_i^{\Delta x_{ij}}\Big), \quad \text{for } \Delta x_{ij} \in \{\Delta x_{ij} | j \in \mathcal{R}_>\}, \\ \frac{\mathrm{d}z_i}{\mathrm{d}t} &= \frac{1}{\mu}\Big((c_i - x_i)^{\bar{n}} - x_i^{c_i} z_i\Big), \\ \frac{\mathrm{d}\bar{z}_i}{\mathrm{d}t} &= \frac{1}{\mu}\Big(x_i^n - (c_i - x_i)^{c_i}\bar{z}_i\Big), \\ \mathbf{x}(0) &= \mathbf{x}_0, \quad \mathbf{y}_i(0) = \mathbf{y}_0, \quad \mathbf{z}_i(0) = \mathbf{z}_0, \end{aligned} \tag{4.45}$$

where $\mathbf{e}_i$ is the ith unit vector, and $c_i \in \mathbb{R}_>$ is the deterministic conservation constant, $\bar{x}_i = c_i - x_i$. Here, $\mathbf{y}_i = (y_i^1, y_i^2, \ldots)$ contains the concentrations of the drift-corrector species $I_i^1, I_i^2, \ldots$, and $\mathbf{z}_i = (z_i, \bar{z}_i)$ of the two boundary species $B_i, \bar{B}_i$. Note that the number of the drift-corrector species (i.e. the dimension of $\mathbf{y}_i$) is equal to $|\{\Delta x_{ij} | j \in \mathcal{R}_>\}|$, i.e. to the number of different positive reaction coefficients Δx_{ij}, with i fixed.

Let us note that we have taken identical initial conditions for $\mathbf{x}$, $\mathbf{x}(0) = \mathbf{x}_0 \in \mathbb{R}^N_{\geq}$, in (4.44) and (4.45).

Setting the LHSs in (4.45) to zero, solving for the equilibria, and comparing them with the equilibria of the input RREs (4.44), one obtains the following result regarding the time-independent solutions of the input and output networks.

Lemma 4.1. *Input and output networks,* (4.1) *and* (4.6)*, with the RREs* (4.44) *and* (4.45)*, respectively, obtained by applying* Algorithm 4.1*, have identical deterministic equilibrium points.*

Put it another way, deterministic equilibria remain fixed under applications of Algorithm 4.1, and no new equilibria are introduced, and this is independent of the value of μ. Let us now state a result regarding time-dependent solutions of the input and output networks, which relies on μ being sufficiently small.

Theorem 4.1. *Assume the RREs for the input and output networks,* (4.1) *and* (4.6)*, respectively, obtained by applying* Algorithm 4.1*, given by* (4.44) *and* (4.45)*, respectively, have identical initial conditions. Assume furthermore that the conservation constant c_i, from $x_i + \bar{x}_i = c_i$, is such that $c_i > max_{t\geq 0} x_i(t) < \infty$, where $x_i(t)$ denotes the ith component of the solution to the input RREs* (4.44)*. Then,* (4.44) *and* (4.45) *have identical solutions in the asymptotic limit $\mu \to 0$.*

Proof. The equilibrium of the adjoined system corresponding to (4.45) is given componentwise by $y_i^{\Delta x_{ij}} = (c_i - x_i)^{-\Delta x_{ij}}$, for $\Delta x_{ij} \in \{\Delta x_{ij} | j \in \mathcal{R}_>\}$, $z_i = (c_i - x_i)^{\bar{n}}/x_i^{c_i}$, and $\bar{z}_i = x_i^n/(c_i - x_i)^{c_i}$. Since the equilibrium is unique and globally stable, Tikhonov's theorem applies [84]. Substituting the equilibrium of the adjoined system into (4.45), one recovers the corresponding degenerate system (4.44). Tikhonov's theorem implies that (4.45) converges to (4.44) as $\mu \to 0$. Requiring $c_i > \max_{t\geq 0} x_i(t)$ ensures that the concentration of the auxiliary species is nonnegative, $\bar{x}_i = c_i - x_i \geq 0$. □

Lemma 4.1 and Theorem 4.1 jointly imply that the equilibria of the input network are fixed under applications of Algorithm 4.1, and that their stability and types are preserved provided $0 < \mu \ll 1$.

4.2.2 Stochastic Analysis

The CME of the input reaction network (4.1) is given by

$$\frac{\partial}{\partial t} p(\mathbf{x}, t) = \mathcal{L} p(\mathbf{x}, t) = \left(\sum_{j \in \mathcal{R}_>} (E_{\mathbf{x}}^{-\Delta \mathbf{x}_j} - 1) \alpha_j(\mathbf{x}) + \sum_{j \in \mathcal{R}_\leq} (E_{\mathbf{x}}^{-\Delta \mathbf{x}_j} - 1) \alpha_j(\mathbf{x}) \right) p(\mathbf{x}, t), \tag{4.46}$$

where $\mathbf{x} = (x_1, x_2, \ldots, x_N)$ contains the copy-numbers of the input species $s_1, s_2, \ldots, s_N$, and $\alpha_j(\mathbf{x}) = k_j \mathbf{x}^{\underline{\boldsymbol{\nu}_j}}$ is the mass-action propensity function of the reaction with index j (see also Section 2.2 and 2.3.2), with the set of reaction partitioned as in (4.44).

The CME of the output reaction network (4.6) is given by

$$\frac{\partial}{\partial t} p(\mathbf{x}, \mathbf{y}_i, \mathbf{z}_i, t) = \left(\mathcal{L}^1 + \frac{1}{\mu}(\mathcal{L}^2 + \mathcal{L}^B) + \mathcal{L}^3 \right) p(\mathbf{x}, \mathbf{y}_i, \mathbf{z}_i, t), \tag{4.47}$$

where $\mathbf{y}_i = (y_i^1, y_i^2, \ldots)$ contains the copy-numbers of the drift-corrector species $I_i^1, I_i^2, \ldots$, and $\mathbf{z}_i = (z_i, \bar{z}_i)$ of the boundary species $B_i, \bar{B}_i$. The operators $\mathcal{L}^1$, $\mathcal{L}^2$, $\mathcal{L}^B$ and $\mathcal{L}^3$ are given by

$$\begin{aligned}
\mathcal{L}^1 &= \sum_{j \in \mathcal{R}_>} y_i^{\Delta x_{ij}} (E_{\mathbf{x}}^{-\Delta \mathbf{x}_j} - 1) \alpha_j(\mathbf{x}) (C_i - x_i)^{\underline{\Delta x_{ij}}} + \sum_{j \in \mathcal{R}_\leq} (E_{\mathbf{x}}^{-\Delta \mathbf{x}_j} - 1) \alpha_j(\mathbf{x}), \\
\mathcal{L}^2 &= \sum_{\{\Delta x_{ij} | j \in \mathcal{R}_>\}} \mathcal{L}^2_{\Delta x_{ij}}, \\
\mathcal{L}^B &= \mathcal{L}^{B_i}_{0,\bar{n}} + \mathcal{L}^{\bar{B}_i}_{n,0}, \\
\mathcal{L}^3 &= k^i_{0,\bar{n}} \mathcal{L}^3_{0,\bar{n}} + \sum_{\substack{(n,\bar{n}) \\ n,\bar{n} \neq 0}} K^i_{n,\bar{n}} \mathcal{L}^3_{n,\bar{n}} + k^i_{n,0} \mathcal{L}^3_{n,0},
\end{aligned} \tag{4.48}$$

where $\mathcal{L}^1$, a drift-corrected version of $\mathcal{L}$, is the forward operator of network (4.2), while $\mathcal{L}^2_{\Delta x_{ij}}$, $(k^i_{0,\bar{n}} \mathcal{L}^3_{0,\bar{n}} + 1/\mu \mathcal{L}^{B_i}_{0,\bar{n}})$, $(k^i_{n,0} \mathcal{L}^3_{n,0} + 1/\mu \mathcal{L}^{\bar{B}_i}_{n,0})$, and $K^i_{n,\bar{n}} \mathcal{L}^3_{n,\bar{n}}$ are the forward operators of the drift-corrector network (4.3), left- and right-boundary zero-drift networks (4.5) and (4.34), and the interior zero-drift network (4.4), respectively, and are given by

$$\begin{aligned}
\mathcal{L}^2_{\Delta x_{ij}} &= (E^{-1}_{y_i^{\Delta x_{ij}}} - 1) + (C_i - x_i)^{\underline{\Delta x_{ij}}} (E^{+1}_{y_i^{\Delta x_{ij}}} - 1) y_i^{\Delta x_{ij}}, \\
\mathcal{L}^3_{0,\bar{n}} &= (E^{-1}_{x_i} - 1)(C_i - x_i)^{\underline{\bar{n}}} + z_i (E^{+1}_{x_i} - 1) x_i^{\underline{C_i}}, \\
\mathcal{L}^{B_i}_{0,\bar{n}} &= (C_i - x_i)^{\underline{\bar{n}}} (E^{-1}_{z_i} - 1) + x_i^{\underline{C_i}} (E^{+1}_{z_i} - 1) z_i, \\
\mathcal{L}^3_{n,0} &= (E^{+1}_{x_i} - 1) x_i^{\underline{n}} + \bar{z}_i (E^{-1}_{x_i} - 1)(C_i - x_i)^{\underline{C_i}}, \\
\mathcal{L}^{\bar{B}_i}_{n,0} &= x_i^{\underline{n}} (E^{-1}_{\bar{z}_i} - 1) + (C_i - x_i)^{\underline{C_i}} (E^{+1}_{\bar{z}_i} - 1) \bar{z}_i, \\
\mathcal{L}^3_{n,\bar{n}} &= (E^{-1}_{x_i} + E^{+1}_{x_i} - 2) \beta_{n,\bar{n}}(x_i),
\end{aligned} \tag{4.49}$$

where $K_{n,\bar{n}}$ and $\beta_{n,\bar{n}}(x)$ are given in (4.32).

Let us consider the following perturbation series

$$p(\mathbf{x}, \mathbf{y}_i, \mathbf{z}_i, t) = p_0(\mathbf{x}, \mathbf{y}_i, \mathbf{z}_i, t) + \mu p_1(\mathbf{x}, \mathbf{y}_i, \mathbf{z}_i, t) + \ldots + \mu^j p_j(\mathbf{x}, \mathbf{y}_i, \mathbf{z}_i, t) + \ldots, \quad j \geq 2. \tag{4.50}$$

Substituting (4.50) into (4.47), and equating terms of equal powers in μ, the following system of equations is obtained:

$$\begin{aligned}\mathcal{O}\left(\frac{1}{\mu}\right):\ &(\mathcal{L}^2+\mathcal{L}^B)p_0(\mathbf{x},\mathbf{y}_i,\mathbf{z}_i,t)=0,\\ \mathcal{O}(1):\ &(\mathcal{L}^2+\mathcal{L}^B)p_1(\mathbf{x},\mathbf{y}_i,\mathbf{z}_i,t)=(\frac{\partial}{\partial t}-\mathcal{L}^1-\mathcal{L}^3)p_0(\mathbf{x},\mathbf{y}_i,\mathbf{z}_i,t).\end{aligned}\tag{4.51}$$

Order $1/\mu$ *equation.* It follows from the structure of the operator $(\mathcal{L}^2+\mathcal{L}^B)$ that

$$p_0(\mathbf{x},\mathbf{y}_i,\mathbf{z}_i,t)=\left(\prod_{\{\Delta x_{ij}|j\in\mathcal{R}_>\}}p_0(y_i^{\Delta x_{ij}}|x_i,t)\right)p_0(z_i|x_i,t)p_0(\bar{z}_i|x_i,t)p_0(\mathbf{x},t),\tag{4.52}$$

i.e. species $\{y_i^{\Delta x_{ij}}\}|_{\{\Delta x_{ij}|j\in\mathcal{R}_>\}}$, z_i and $\bar{z}_i$ are statistically independent for each fixed x_i and time t. Consequently, the first equation from (4.51) reduces to

$$\begin{aligned}\mathcal{L}^2_{\Delta x_{ij}}p_0(y_i^{\Delta x_{ij}}|x_i,t)=0,\quad &\text{for } \Delta x_{ij}\in\{\Delta x_{ij}|j\in\mathcal{R}_>\},\\ \mathcal{L}^{B_i}_{0,\bar{n}}p_0(z_i|x_i,t)=0,&\\ \mathcal{L}^{\bar{B}_i}_{n,0}p_0(\bar{z}_i|x_i,t)=0,&\end{aligned}\tag{4.53}$$

with the solutions given by

$$\begin{aligned}p_0(y_i^{\Delta x_{ij}}|x_i,t)&=\mathcal{P}(y_i^{\Delta x_{ij}};\underline{(C_i-x_i)^{-\Delta x_{ij}}}),\quad \text{for } \Delta x_{ij}\in\{\Delta x_{ij}|j\in\mathcal{R}_>\},\\ p_0(z_i|x_i,t)&=\begin{cases}\delta_{z_i,\infty}, & \text{if } x_i\in[0,C_i-\bar{n}_i],\\ \delta_{z_i,0}, & \text{if } x_i=C_i,\end{cases}\\ p_0(\bar{z}_i|x_i,t)&=\begin{cases}\delta_{\bar{z}_i,0}, & \text{if } x_i=0,\\ \delta_{\bar{z}_i,\infty}, & \text{if } x_i\in[n,C_i].\end{cases}\end{aligned}\tag{4.54}$$

Order 1 *equation.* Summing the second equation from (4.51) over the fast variables $\mathbf{y}_i$, $\mathbf{z}_i$, with $\langle f,g\rangle_{\mathbf{y}_i,\mathbf{z}_i}=\sum_{\mathbf{y}_i}\sum_{\mathbf{z}_i}f(\mathbf{y}_i,\mathbf{z}_i)g(\mathbf{y}_i,\mathbf{z}_i)$, and using (4.52), one obtains the solvability condition

$$\begin{aligned}\frac{\partial}{\partial t}p_0(\mathbf{x},t)=&\langle 1_{\mathbf{y}_i},\mathcal{L}^1\prod_{\{\Delta x_{ij}|j\in\mathcal{R}_>\}}p_0(y_i^{\Delta x_{ij}}|x_i,t)p_0(\mathbf{x},t)\rangle_{\mathbf{y}_i}\\ &+\langle 1_{\mathbf{z}_i},\mathcal{L}^3p_0(z_i|x_i,t)p_0(\bar{z}_i|x_i,t)p_0(\mathbf{x},t)\rangle_{\mathbf{z}_i},\end{aligned}\tag{4.55}$$

where $1_{\mathbf{y}_i}$ and $1_{\mathbf{z}_i}$ are constants in $\mathbf{y}_i$ and $\mathbf{z}_i$, respectively. Using (4.49) and (4.54), one obtains

$$\langle 1_{\mathbf{y}_i},\mathcal{L}^1\prod_{\{\Delta x_{ij}|j\in\mathcal{R}_>\}}p_0(y_i^{\Delta x_{ij}}|x_i,t)p_0(\mathbf{x},t)\rangle_{\mathbf{y}_i}=\mathcal{L}p_0(\mathbf{x},t),$$

where $\mathcal{L}$ is the forward operator of the input network (4.1), given in (4.46), and

$$\langle 1_{\mathbf{z}_i}, \mathcal{L}^3 p_0(z_i|x_i,t)p_0(\bar{z}_i|x_i,t)p_0(\mathbf{x},t)\rangle_{\mathbf{z}_i} = (K^i_{0,\bar{n}}(E^{-1}_{x_i}-1)\beta_{0,\bar{n}}(x_i) + \sum_{\substack{(n,\bar{n})\\ n,\bar{n}\neq 0}} K^i_{n,\bar{n}}\mathcal{L}^3_{n,\bar{n}} + K^i_{n,0}(E^{+1}_{x_i}-1)\beta_{n,0}(x_i))p_0(\mathbf{x},t),$$

which, upon substituting into (4.55), gives the effective CME

$$\frac{\partial}{\partial t}p_0(\mathbf{x},t) = \left(\mathcal{L} + K^i_{0,\bar{n}}(E^{-1}_{x_i}-1)\beta_{0,\bar{n}}(x_i) + \sum_{\substack{(n,\bar{n})\\ n,\bar{n}\neq 0}} K^i_{n,\bar{n}}\mathcal{L}^3_{n,\bar{n}} + K^i_{n,0}(E^{+1}_{x_i}-1)\beta_{n,0}(x_i)\right) p_0(\mathbf{x},t), \tag{4.56}$$

and we reach the following result.

Theorem 4.2. *For any fixed time $t > 0$, the stochastic process $\mathbf{X}(t) = (X_1(t), X_2(t), \ldots, X_N(t))$, satisfying the output CME (4.47), converges weakly to the Markov stochastic process $\mathbf{X}(t) = (X_1(t), X_2(t), \ldots, X_N(t))$, satisfying the CME (4.56), in the limit $\mu \to 0$.*

Proof. We have formally established that the zero-order approximation $p_0(\mathbf{x},t)$, from the perturbation series (4.50), satisfies (4.56). As a part of the general averaging theory, convergence has been established in [51] in the case of finite-dimensional state-space, under suitable boundedness conditions on the first-order corrector p_1 from (4.50). □

The forward operator of the effective CME of the output network (4.6), given by (4.56), is given by the sum of the forward operator of the CME of the input network (4.1), $\mathcal{L}$, and operators induced by the zero-drift networks, and we immediately obtain the following result.

Corollary 4.1. *The effective total propensity function of the output network with the CME (4.47) is given by*

$$\alpha(\mathbf{x}) \approx \alpha^{C_i}(\mathbf{x}) + \left(K^i_{0,\bar{n}}\beta_{0,\bar{n}}(x_i) + 2\sum_{\substack{(n,\bar{n})\\ n,\bar{n}\neq 0}} K^i_{n,\bar{n}}\beta_{n,\bar{n}}(x_i) + K^i_{n,0}\beta_{n,0}(x_i)\right), \quad \text{for } 0 < \mu \ll 1, \tag{4.57}$$

where $\alpha^{C_i}(\mathbf{x}) = \sum_{j\in(\mathcal{R}_>\cup\mathcal{R}_\leq)}\alpha_j(\mathbf{x})$ is the total propensity function of the input reaction network with the CME (4.46), and with x_i defined on the truncated state-space $x_i \in [0, C_i]$.

Let us now investigate the equations governing the time-evolution of the first moments (averages) corresponding to the effective CME (4.56) (see also Section 2.4). Applying the inner-product $\langle x_j, \cdot \rangle_{\mathbf{x}}$ on (4.56), one obtains

$$\frac{\mathrm{d}\mathbb{E}x_i}{\mathrm{d}t} = \langle x_i, \mathcal{L}p_0(\mathbf{x},t)\rangle_{\mathbf{x}} + K^i_{0,\bar{n}}\langle \beta_{0,\bar{n}}(x_i), p_0(x_i,t)\rangle_{x_i} - K^i_{n,0}\langle \beta_{n,0}(x_i), p_0(x_i,t)\rangle_{x_i}, \tag{4.58}$$

$$\frac{\mathrm{d}\mathbb{E}x_j}{\mathrm{d}t} = \langle x_j, \mathcal{L}p_0(\mathbf{x},t)\rangle_{\mathbf{x}}, \quad \text{for } j \neq i. \tag{4.59}$$

One can notice that the RHS of (4.58) has two additional terms when compared to the input reaction networks, with both terms arising from the boundary zero-drift networks. Let us note that, while only the average for the species s_i is modified directly by Algorithm 4.1, the averages for other species, satisfying (4.59), are also modified (indirectly), since they are generally coupled with (4.58). Let us note that the effects of interior zero-drift networks do not appear in (4.58), which leads to the following lemma.

Lemma 4.2. *Assume the input reaction network* (4.1) *is of first-order. Then, assuming boundary zero-drift networks* (4.5) *and* (4.34) *are not embedded into the input network,* Algorithm 4.1 *preserves the first moments of the input network in the limit* $\mu \to 0$.

If the input reaction network is higher-order, then, even if the boundary zero-drift networks are not utilized ($K^i_{0,\bar{n}} = K^i_{n,0} = 0$), the averages are generally altered. This follows from the fact that Algorithm 4.1 modifies the second moments of the input network, and, since for higher-order networks first and second moment equations are coupled, it follows that the first moments are (indirectly) modified as well.

Let us conclude by discussing some of the differences behind the deterministic and stochastic results, involving Algorithm 4.1, established in this section, which stem from the fact that the reaction rates are continuous at the deterministic level, while discrete at the stochastic level. In particular, let us note that the limit $\mu \to 0$ and the thermodynamic limit commute when it comes to the drift-corrector networks (4.3). However, these two limits do not commute when it comes to the boundary zero-drift networks (4.5) and (4.34), i.e. in this case the deterministic and stochastic quasi-stationary approximations differ. In particular, deterministically, boundary zero-drift networks have a zero net effect (see Theorem 4.1), while, stochastically, they produce inward-pointing drifts at the boundary of the state-space (see Theorem 4.2 and equation (4.56)). This stems from the fact that the drift-corrector networks (4.3),

conditional on x_i (i.e. for a fixed x_i), are first-order networks, so that their continuous rate functions have the same form as the underlying discrete propensity functions, leading to the same effective behavior at the deterministic and stochastic levels. On the other hand, boundary zero-drift networks (4.5) and (4.34), for a fixed x_i, are higher-order networks, whose continuous rate functions have a different form than the discrete propensity functions (see also Section 2.2). For example, the rate function of the second reaction from network (4.5) is given by $\kappa_2(x_i, z_i) = k^i_{0,\bar{n}} x_i^{c_i} z_i$, so that, at the deterministic level, the reaction may fire for any $x_i > 0$, provided $z_i \neq 0$. On the other hand, the corresponding propensity function is $\alpha_2(x_i, z_i) = k^i_{0,\bar{n}} x_i^{\underline{c_i}} z_i$, so that, at the stochastic level, the reaction may fire only when $x_i = c_i$. However, when $x_i = c_i$, the fourth reaction from (4.5) fires much faster, leading to $z_i = 0$ in the limit $\mu \to 0$, thus preventing the second reaction from ever firing. Due to this difference, the effects of the first two reactions from (4.5) cancel out at the deterministic level, while at the stochastic level only the first reaction fires.

4.3 Example: The homoclinicator

Let us now apply Algorithm 4.1 in order to control stochastic dynamics of the homoclinicator $\tilde{\mathcal{R}} = \tilde{\mathcal{R}}(s_1, s_2)$, given as the reaction network (3.52), which we have designed in the previous chapter. We denote the copy-numbers of species s_1, and s_2, at time t by $X_1(t)$, and $X_2(t)$, respectively. At the deterministic level, reaction network (3.52) exhibits exotic dynamics: it undergoes a homoclinic bifurcation, and displays a bistability involving a limit cycle and an equilibrium point. Let us now investigate the dynamical behavior of the homoclincator at the stochastic level. In Figure 4.3(c), we show in red numerically approximated x_1-solutions of the underlying RREs (3.51), one initiated in the region of attraction of the equilibrium point, while the other near the limit cycle. For a comparison, we also show in blue a representative sample path generated by applying the Gillespie algorithm on (3.52), for a particular choice of the rate coefficients. It can be seen that the stochastic solution spends significantly more time near the deterministic equilibrium point. To gain a clearer picture, we display in Figures 4.3(a), and (b), the joint, and the x_1-marginal, stationary PMFs, respectively, underlying network (3.52), which have been obtained numerically for the same parameter values as in Figure 4.3(c). In (b), one can notice that the PMF is bimodal, but the left peak, corresponding to the limit cycle, is significantly smaller than the right peak, which corresponds to the stable equilibrium point. As a consequence, the homoclincator behaves effectively in a monostable manner at the stochastic level.

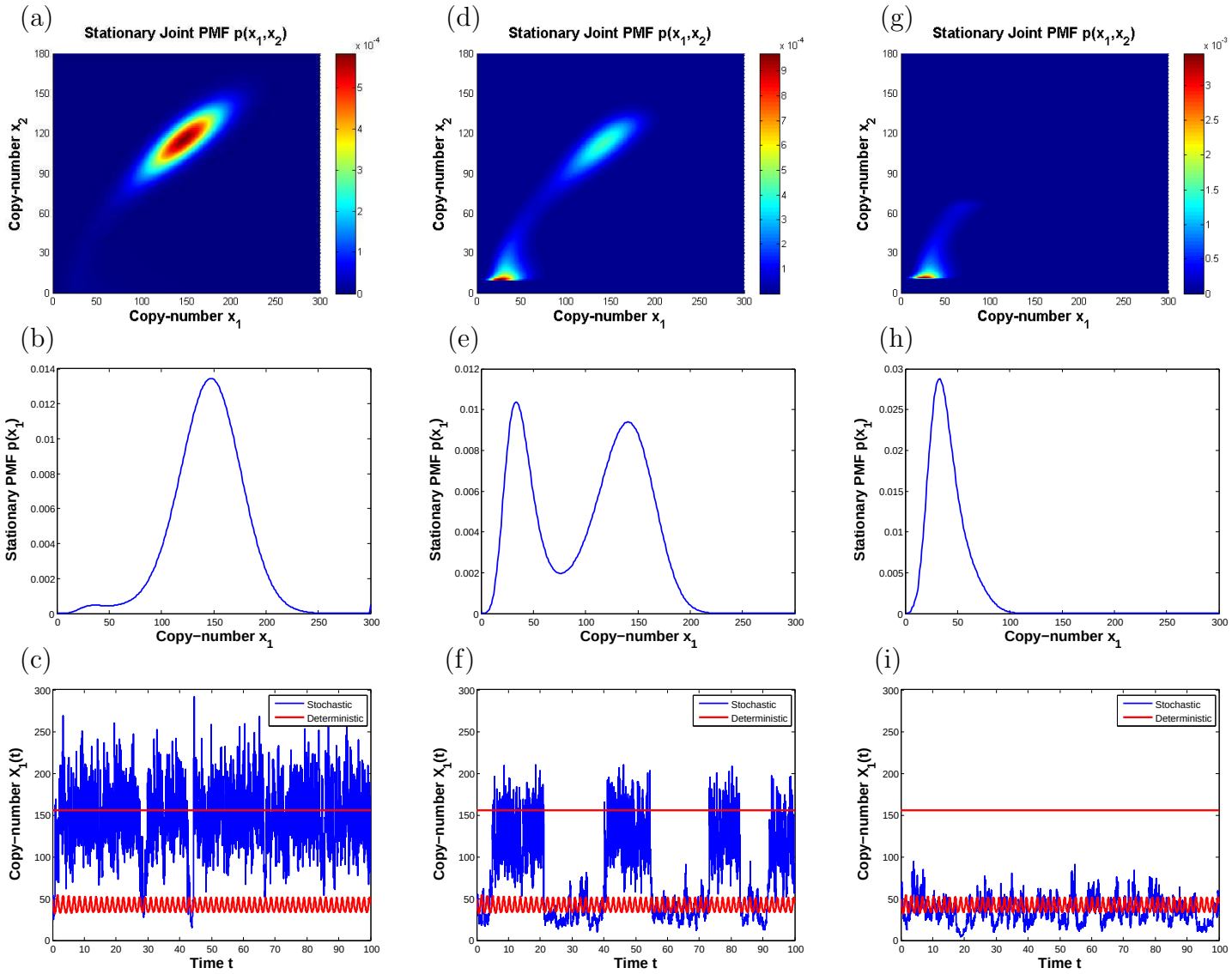

Figure 4.3: *Panel* (a) *displays the joint stationary PMF of network* (3.52)*, while* (d) *and* (g) *display the stationary PMFs of network* (B.3)*, for* $(K_{0,C_2-10}, K_{30,0}) = (10^{18}, 2\times 10^8)$ *and* $(K_{0,C_2-10}, K_{30,0}) = (10^{18}, 10^{18})$*, respectively, with the rest of the parameters being the same. Panels* (b)*,* (e) *and* (h) *display the* x_1*-marginal PMFs corresponding to* (a)*,* (b) *and* (c)*, respectively. Panels* (c)*,* (f) *and* (i) *display in blue the sample paths, corresponding to the PMFs shown in* (b)*,* (e) *and* (h)*, respectively, and were obtained by applying the Gillespie algorithm on the underlying networks. Also shown in red are two deterministic trajectories, one initiated near the equilibrium point, while the other near the limit cycle, obtained by numerically solving the RREs* (3.51)*. The dimensionless parameters are fixed to:* $k_1 = 4$*,* $k_2 = 1.408$*,* $k_3 = 0.0518$*,* $k_4 = 0.164$*,* $k_5 = 3.1\times 10^{-3}$*,* $k_6 = 4.8\times 10^{-3}$*,* $k_7 = 4$*,* $k_8 = 8$*,* $k_9 = 0.16$*,* $k_{10} = 0.104$*,* $k_{11} = 2.1\times 10^{-3}$*. In* (a)–(b)*,* (d)–(e) *and* (g)–(h)*, the stationary CME is numerically solved, with the state-space truncated to* $(x_1, x_2) \in [0, C_1]\times[0, C_2]$*, where* $C_1 = 300$*,* $C_2 = 180$*, and* $\mu, \mu_{0,C_2-10}, \mu_{30,0} \to 0$*. The blue sample paths from panels* (f) *and* (i) *were generated with* $(\mu^{-1}, (\mu_{0,C_2-10})^{-1}M_{0,C_2-10}, (\mu_{30,0})^{-1}M_{30,0}) = (10^3, 10^{20}, 2\times 10^{10})$ *and* $(\mu^{-1}, (\mu_{0,C_2-10})^{-1}M_{0,C_2-10}, (\mu_{30,0})^{-1}M_{30,0}) = (10^3, 10^{20}, 10^{20})$*, respectively. The blue trajectories from* (c)*,* (f) *and* (i) *were all initiated near the deterministic limit cycle.*

We now apply Algorithm 4.1 on network (3.52) to achieve two goals. Firstly, we balance the sizes of the two peaks of the stationary PMF from Figure 4.3(b), thereby forcing the stochastic system to spend comparable amounts of time at the two deterministic attractors. Secondly, we reverse the situation shown in Figure 4.3(b), by making the left PMF peak significantly larger than the right one, thereby forcing the stochastic system to spend most of the time near the limit cycle. We could achieve the goals by introducing species $\bar{s}_1, \bar{s}_2$ into (3.52), and using suitable basis zero-drift networks. We take a simpler approach, by mapping (3.52) to $\tilde{\mathcal{R}}^1(s_1, s_2, \bar{s}_2) \cup \mathcal{R}^2_1(\bar{s}_2) \cup (\mathcal{R}^3_{0,C_2-10}(s_2, \bar{s}_2) \cup \mathcal{R}^3_{30,0}(s_2, \bar{s}_2))$, which is given as equation (B.3) in Appendix B. In particular, we introduce the intrinsic noise using Algorithm 4.1 via only one of species $\bar{s}_1$, $\bar{s}_2$, and exploit the fact that the stochastic dynamics of s_1 and s_2 are coupled (see also Section 4.2, and Section 4.4 for a more general approach). Here, we have chosen $\bar{s}_2$ for convenience, since x_2-state-space may be truncated at a lower value, $C_2 = 180$, than x_1-state-space (see also Figure 4.3 (a)). The x_2-component of the deterministic limit cycle satisfies $x_2 \in (10, 30)$. Correspondingly, we introduce two zero-drift networks: $\mathcal{R}^3_{0,C_2-10}(s_2, \bar{s}_2)$, and $\mathcal{R}^3_{30,0}(s_2, \bar{s}_2)$, which redistribute the PMF from $x_2 \in [0, 10]$, and from $x_2 \in [30, C_2]$, respectively, to the limit cycle region, $x_2 \in (10, 30)$. We fix the scaled rate coefficient K^2_{0,C_2-10} to a large value (so that the PMF is nearly zero for $x_2 \in [0, 10]$), and vary the coefficient $K^2_{30,0}$, which redistributes the PMF from the deterministic equilibrium point to the limit cycle.

In Figures 4.3(d), and (e), we show the joint, and x_1-marginal, stationary PMFs for an intermediate value of $K^2_{30,0}$, when the PMF is partially redistributed from $x_2 \in [30, C_2]$ to $x_2 \in (10, 30)$, so that the two peaks in (e) are of comparable sizes. In Figure 4.3(f), we show a representative sample path, obtained by applying the Gillespie algorithm on network (B.3), together with the deterministic trajectories. One can notice that the stochastic system now spends significantly more time near the limit cycle, when compared to (c). In Figure 4.3(f)–(g), we show analogous plots, but for a sufficiently large value of $K^2_{30,0}$, when the PMF is almost completely redistributed from $x_2 \in [30, C_2]$ to $x_2 \in (10, 30)$. Now, in contrast to Figure 4.3(a)–(c), the PMF becomes unimodal, and concentrated around the limit cycle, with the system displaying noise-assisted oscillations.

Put another way, one may view the dynamics shown in Figures 4.3(a)–(c) as being contaminated by the noise, which disrupts the oscillatory chemical computation. Algorithm 4.1 has been applied to address the disruption by appropriately reprogramming the noise. Such control is of practical relevance, since stochastic switching

between an equilibrium and a limit cycle has already been observed experimentally in a DNA-based network [29].

4.4 Generalizations

We finish this chapter by providing two generalizations of the zero-drift networks (4.4) and (4.5), thereby further increasing the capabilities of Algorithm 4.1. In particular, we introduce multi-step zero-drift networks, which provide further control over how the PMF is reshaped under applications of Algorithm 4.1. More precisely, multi-step zero-drift networks control the range within which the PMF may be propagated in the state-space. We also introduce multi-dimensional zero-drift networks, which provide further control over the support of the noise introduced by Algorithm 4.1, and its direction of action, when multi-species reaction networks are considered. In what follows, we denote the zero-drift networks by $\mathcal{R}^3_{n,\bar{n}}(s_i, \bar{s}_i) = \mathcal{R}_{n,\bar{n}}(s_i)$, for notational simplicity.

4.4.1 Multi-step zero-drift networks

The zero-drift networks from Algorithm 4.1 involve *one-step* reactions: the copy-numbers of the pairwise conserved species s_i and $\bar{s}_i$ experience a unit-change per firing of the zero-drift networks. More generally, *symmetric multi-step* interior zero-drift networks are given by

$$\begin{aligned} \mathcal{R}_{n,\bar{n}}(s_i;\, m): \quad & ns_i + \bar{n}\bar{s}_i \xrightarrow{k^i_{n,\bar{n}}} (n+m)s_i + (\bar{n}-m)\bar{s}_i, \\ & ns_i + \bar{n}\bar{s}_i \xrightarrow{k^i_{n,\bar{n}}} (n-m)s_i + (\bar{n}+m)\bar{s}_i, \end{aligned} \tag{4.60}$$

where $m \in \mathbb{Z}_>$ is required to satisfy $m \leq \min(n, \bar{n})$. Zero-drift network (4.60) changes the copy-numbers of s_i and $\bar{s}_i$ by m per firing. Taking $m = 1$, network (4.60) reduces to the network (4.4). We can further generalize (4.60) as follows:

$$\begin{aligned} \mathcal{R}_{n,\bar{n}}(s_i;\, m_1, m_2): \quad & ns_i + \bar{n}\bar{s}_i \xrightarrow{k^i_{n,\bar{n}}} (n+m_1)s_i + (\bar{n}-m_1)\bar{s}_i, \\ & ns_i + \bar{n}\bar{s}_i \xrightarrow{\frac{m_1}{m_2}k^i_{n,\bar{n}}} (n-m_2)s_i + (\bar{n}+m_2)\bar{s}_i, \end{aligned} \tag{4.61}$$

with $m_1 \leq \bar{n}$ and $m_2 \leq n$. We call (4.61) an *asymmetric multistep-step* zero-drift network if $m_1 \neq m_2$; otherwise, if $m_1 = m_2$, it reduces to the network (4.60). The first, and second, reactions from (4.61) change the copy-numbers of s_i and $\bar{s}_i$ by m_1, and m_2, upon firing, respectively. Let us note that the rate coefficients of the

two reactions from (4.61) are chosen to that the network is a zero-drift network. Asymmetric multi-step boundary zero-drift networks are defined analogously.

The propensity function of the reactions from (4.61) is proportional to $x_i^n(C_i - x_i)^{\bar{n}}$, and the zero-drift network introduces noise at $x_i \in [n, C_i - \bar{n}]$, independent of the value of (m_1, m_2), i.e. the support of the introduced noise is independent of (m_1, m_2). However, the value of (m_1, m_2) determines how the PMF is redistributed: it is propagated from the support of the underlying propensity function, $x_i \in [n, C_i - \bar{n}]$, up to the points $x = (n - m_2)$ and $x = (C_i - \bar{n} + m_1)$. Let us now exemplify this using the test network (4.9).

Example 4.1. *Let us embed the network* (4.61) *with* $(n, \bar{n}) = (5, 10)$ *into the test network* (4.9)*, i.e. let us consider the stochastic behavior of the network* $\mathcal{R}^1(s, \bar{s}) \cup \mathcal{R}_1^2(\bar{s}) \cup \mathcal{R}_{5,10}(s; m_1, m_2)$ *for different values of* (m_1, m_2)*, with the conservation constant* $C = 15$*, and the underlying rate coefficients fixed as in* Figure 4.2*. For* $(m_1, m_2) = (1, 1)$*, the stationary PMF is presented in* Figure 4.2(e)*, where the system jumps from* $x = 5$ *to* $x = 4$ *or* $x = 6$ *upon firing of the zero-drift network. As a consequence, the PMF is redistributed from* $x = 5$ *largely to the first two neighboring points, as discussed in* Section 4.1.3*.*

In Figure (4.4)(a)*, we show as the blue histogram the stationary PMF of the network* $\mathcal{R}^1 \cup \mathcal{R}_1^2 \cup \mathcal{R}_{5,10}(s; m_1, m_2)$ *with* $(m_1, m_2) = (2, 2)$*, while as the black curve the stationary PMF of the input network* $\mathcal{R}(s)$*, given by* (4.7) *(i.e. when the zero-drift network does not fire). One can notice that now the noise-induced maxima are* $x = 3$ *and* $x = 7$*, i.e. the second closest neighbors of* $x = 5$*. One can also notice that the PMF decreases at the closest neighboring points,* $x = 4$ *and* $x = 6$*, as a consequence of the fact that the system now jumps to these states predominantly from one side (as opposed to from both sides, as in the case when the zero-drift network does not fire). In* Figure (4.4)(b)*, we show in blue a sample path corresponding to the blue histogram from* (a)*, together with the underlying deterministic trajectory shown in red. We show analogous plots in* Figure (4.4)(c)–(d)*, where we choose* $(m_1, m_2) = (10, 5)$*, i.e. we chose jumps of the maximum size from* $x = 5$*, leading the system to the boundary of the state-space:* $x = 0$ *or* $x = 15$*. Let us emphasize that in* Figure 4.2(e)*, and* Figures (4.4)(a) *and* (c)*, we introduce the noise at the same point in the state-space,* $x = 5$*, but choose a different size of the* domain of influence *(see next section for more details): it is of minimal (unit-) length in* Figure 4.2(e)*, and maximum length in* Figure (4.4)(c)*.*

Note that one can also embed into test network (4.9) *simultaneously multiple zero-drift networks* $\mathcal{R}_{5,10}(s; m_1, m_2)$*, with different* (m_1, m_2)*. For example, the zero-drift*

networks in $\mathcal{R}^1(s,\bar{s}) \cup \mathcal{R}_1^2(\bar{s}) \cup (\mathcal{R}_{5,10}(s;\,2,2) \cup \mathcal{R}_{5,10}(s;\,10,5))$ *redistribute the PMF from* $x = 5$ *to* $x \in \{0,3,7,15\}$*, and the proportion of the PMF which is propagated to each of the points depends on the ratio of the underlying rate coefficients appearing in the two zero-drift networks,* $K_{5,10}^{2,2}/K_{5,10}^{10,5}$*.* △

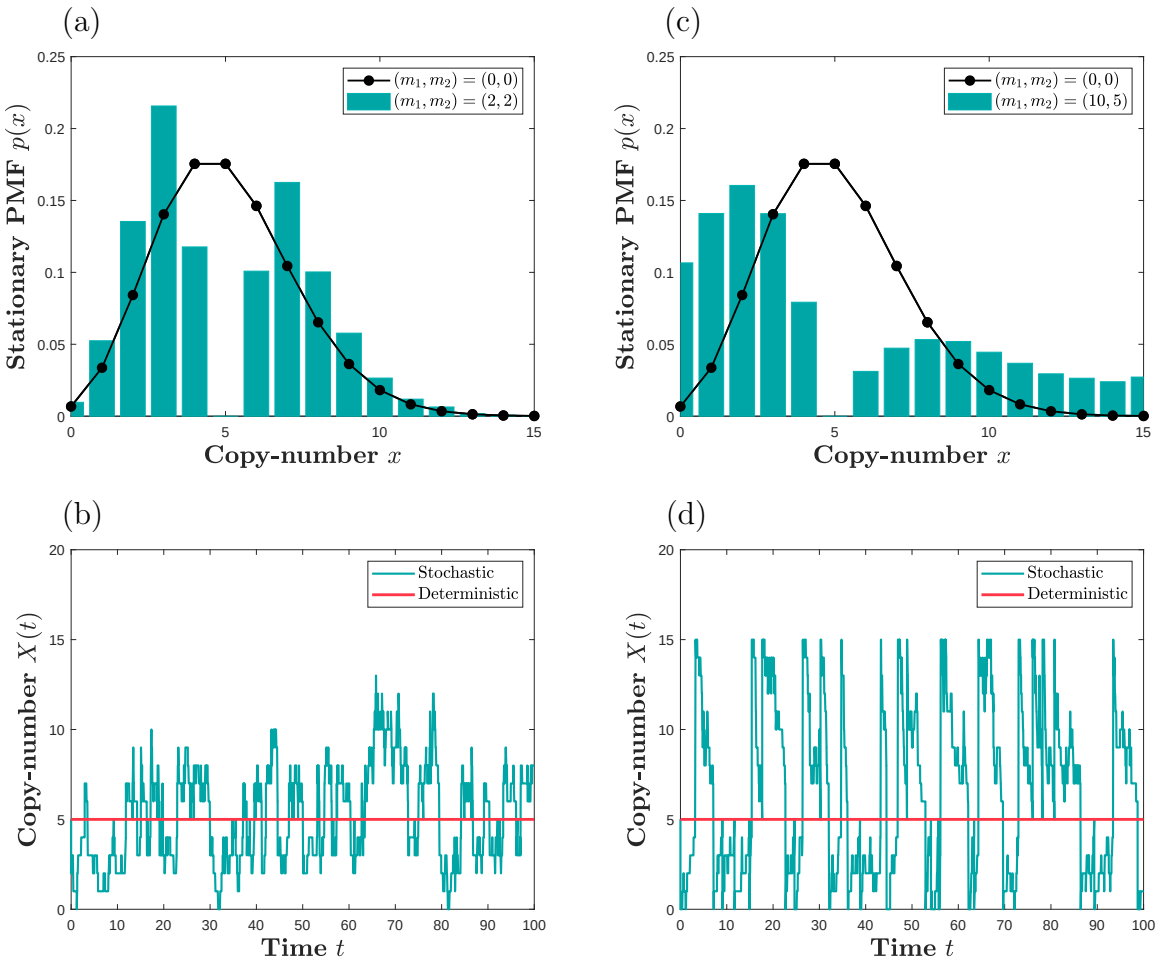

Figure 4.4: *Panels* (a) *and* (c) *display the stationary PMFs of the networks* $\mathcal{R}^1 \cup \mathcal{R}_1^2 \cup \mathcal{R}_{5,10}(s;\,2,2)$ *and* $\mathcal{R}^1 \cup \mathcal{R}_1^2 \cup \mathcal{R}_{5,10}(s;\,10,5)$*, respectively, where* $\mathcal{R}^1 \cup \mathcal{R}_1^2$ *is given by* (4.9)*, while the multi-step zero-drift network* $\mathcal{R}_{5,10}(s;\,m_1,m_2)$ *is given by* (4.61)*. Panels* (b) *and* (d) *display in blue the sample paths, corresponding to the PMFs shown as the blue histograms in* (a) *and* (c)*, respectively, and were obtained by applying the Gillespie algorithm on the underlying networks. Also shown in red are the deterministic trajectories, obtained by numerically solving the corresponding deterministic models. The dimensionless parameters are fixed to:* $k_1 = 2.5$*,* $k_2 = 0.5$*,* $\mu = 10^{-3}$*,* $k_{5,10} = 100$*, and* $C = 15$*. The trajectories from* (b) *and* (d) *were initiated at the deterministic equilibrium,* $X(0) = 5$*.*

4.4.2 Multi-dimensional zero-drift networks

All of the zero-drift networks considered up until now, both the one-step ones from Algorithm 4.1 and the multistep ones, given by (4.61), involve only one pair of the conserved species s_i and $\bar{s}_i$. More precisely, the propensity function of the zero-drift network $\mathcal{R}_{n,\bar{n}}(s_i)$ is proportional to $x_i^{\underline{n}}(C_i - x_i)^{\underline{\bar{n}}}$ (see also equation (4.32)), i.e. it depends only on x_i, the copy-number of s_i, and, for this reason, we say that such a zero-drift network is *one-dimensional*. As a consequence, $\mathcal{R}_{n,\bar{n}}(s_i)$ introduces noise at $x_i \in [n, C_i - \bar{n}]$, independent of the state of the other input species.

We now wish to generalize the one-dimensional to *multi-dimensional* zero-drift networks, suitable when a more precise noise-control is required for multiple-species networks. In particular, we introduce additional degrees of freedom when it comes to the *support* of the noise introduced by the zero-drift networks, and the *direction* of action of the zero-drift networks. To this end, let us introduce the following definition: consider two reactions $r_i : \boldsymbol{\nu}_i \to \bar{\boldsymbol{\nu}}_i$ and $r_j : \boldsymbol{\nu}_j \to \bar{\boldsymbol{\nu}}_j$. We define addition of the two reactions, $r_i + r_j$ (not to be confused with the union of the two reactions), as the new reaction given by $r_i + r_j : \boldsymbol{\nu}_i + \boldsymbol{\nu}_j \to \bar{\boldsymbol{\nu}}_i + \bar{\boldsymbol{\nu}}_j$, i.e. products, and reactants, of the resulting reaction are obtained by adding together products, and reactants, of the summand reactions, respectively. Analogously, we define addition of two reaction networks $\mathcal{R}_i = \{r_{im}\}_{m=1}^M$ and $\mathcal{R}_j = \{r_{jm}\}_{m=1}^M$ as the new reaction network given by $\mathcal{R}_j = \{r_{im} + r_{jm}\}_{m=1}^M$. Note that the result of an addition of two reaction networks depends on the order of the underlying reactions. For this reason, let us denote the zero-drift network containing the same reactions as (4.61), but in the opposite order, by $\mathcal{R}^*_{n_i,\bar{n}_i}(s_i)$. We also define an identity reaction network: $\mathcal{I}_{n_i,\bar{n}_i}(s_i) = \{r_1 = n_i s_i + \bar{n}_i\bar{s}_i \to n_i s_i + \bar{n}_i\bar{s}_i, r_2 = r_1\}$. An N-dimensional interior zero-drift network, introducing noise at $x_i \in [n_i, C_i - \bar{n}_i]$, $i = 1, \ldots, N$, is then given by $\sum_{j=1}^N \mathcal{R}_{n_i,\bar{n}_i}(s_i)$, with the propensity function $\prod_{j=1}^N K^j_{n,\bar{n}}\beta_{n,\bar{n}}(x_j)$ (see also (4.32)–(4.33)). Multi-dimensional boundary zero-drift networks may be defined similarly. Notice that, if any of the factors $\mathcal{R}_{n_i,\bar{n}_i}(s_i)$ from $\sum_{j=1}^N \mathcal{R}_{n_i,\bar{n}_i}(s_i)$ are replaced by $\mathcal{R}^*_{n_i,\bar{n}_i}(s_i)$ or $\mathcal{I}_{n_i,\bar{n}_i}(s_i)$, the propensity function of the resulting zero-drift network remains the same, but the direction of action of the noise changes, proving us with an additional control. Let us now discuss this further by considering a two-dimensional example.

Example 4.2. *Let us consider two pairs of conservative species: s_1, $\bar{s}_1$, and s_2, $\bar{s}_2$, with the conservation laws $x_1 + \bar{x}_1 = 10$, and $x_2 + \bar{x}_2 = 5$. Assume we want to introduce the noise into the stochastic dynamics of the target species s_1 and s_2 at the single point $(x_1, x_2) = (5, 2)$ in the state-space, and let us focus on the one-step zero-drift*

networks. There are four two-dimensional one-step basis zero-drift networks with the support $(x_1, x_2) = (5, 2)$*, given by:* (i) $(\mathcal{R}_{5,5}(s_1) + \mathcal{R}_{2,3}(s_2))$*,* (ii) $(\mathcal{R}_{5,5}(s_1) + \mathcal{R}^*_{2,3}(s_2))$*,* (iii) $(\mathcal{I}_{5,5}(s_1) + \mathcal{R}_{2,3}(s_2))$*, and* (iv) $(\mathcal{R}_{5,5}(s_1) + \mathcal{I}_{2,3}(s_2))$*. More precisely:*

$$\begin{aligned}
\mathcal{R}_{5,5}(s_1) + \mathcal{R}_{2,3}(s_2) : (5s_1 + 5\bar{s}_1) + (2s_2 + 3\bar{s}_2) &\xrightarrow{\kappa} (6s_1 + 4\bar{s}_1) + (3s_2 + 2\bar{s}_2)\,, \\
(5s_1 + 5\bar{s}_1) + (2s_2 + 3\bar{s}_2) &\xrightarrow{\kappa} (4s_1 + 6\bar{s}_1) + (s_2 + 4\bar{s}_2)\,, \\
\mathcal{R}_{5,5}(s_1) + \mathcal{R}^*_{2,3}(s_2) : (5s_1 + 5\bar{s}_1) + (2s_2 + 3\bar{s}_2) &\xrightarrow{\kappa} (6s_1 + 4\bar{s}_1) + (s_2 + 4\bar{s}_2)\,, \\
(5s_1 + 5\bar{s}_1) + (2s_2 + 3\bar{s}_2) &\xrightarrow{\kappa} (4s_1 + 6\bar{s}_1) + (3s_2 + 2\bar{s}_2)\,, \\
\mathcal{I}_{5,5}(s_1) + \mathcal{R}_{2,3}(s_2) : (5s_1 + 5\bar{s}_1) + (2s_2 + 3\bar{s}_2) &\xrightarrow{\kappa} (5s_1 + 5\bar{s}_1) + (3s_2 + 2\bar{s}_2)\,, \\
(5s_1 + 5\bar{s}_1) + (2s_2 + 3\bar{s}_2) &\xrightarrow{\kappa} (5s_1 + 5\bar{s}_1) + (s_2 + 4\bar{s}_2)\,, \\
\mathcal{R}_{5,5}(s_1) + \mathcal{I}_{2,3}(s_2) : (5s_1 + 5\bar{s}_1) + (2s_2 + 3\bar{s}_2) &\xrightarrow{\kappa} (6s_1 + 4\bar{s}_1) + (2s_2 + 3\bar{s}_2)\,, \\
(5s_1 + 5\bar{s}_1) + (2s_2 + 3\bar{s}_2) &\xrightarrow{\kappa} (4s_1 + 6\bar{s}_1) + (2s_2 + 3\bar{s}_2)\,. \qquad (4.62)
\end{aligned}$$

All of the zero-drift networks from (4.62) *have the same propensity function, which is proportional to* $\beta_{5,5}(x_1) \times \beta_{2,3}(x_2)$ *(see also* (4.32)*). We show the support of the propensity function (and, hence, of the noise which networks from* (4.62) *introduce into the stochastic dynamics) in* Figure 4.5(a) *as the yellow dot. However, different networks from* (4.62) *have different directions of action: once in the state* $(x_1, x_2) = (5, 2)$*,* (i) *network* $(\mathcal{R}_{5,5}(s_1,) + \mathcal{R}_{2,3}(s_2))$ *in isolation either simultaneously causes a unit-increase, or a unit-decrease, in the copy-numbers* x_1 *and* x_2*, leading to the points* $(x_1, x_2) = (6, 3)$*, or* $(x_1, x_2) = (4, 1)$*, respectively. Similarly,* (ii) *network* $(\mathcal{R}_{5,5}(s_1) + \mathcal{R}^*_{2,3}(s_2))$ *induces jumps to* $(x_1, x_2) = (6, 1)$ *or* $(x_1, x_2) = (4, 3)$*,* (iii) *network* $(\mathcal{I}_{5,5}(s_1) + \mathcal{R}_{2,3}(s_2))$ *induces jumps to* $(x_1, x_2) = (5, 3)$ *or* $(x_1, x_2) = (5, 1)$*, and* (iv) *network* $(\mathcal{R}_{5,5}(s_1) + \mathcal{I}_{2,3}(s_2))$ *induces jumps to* $(x_1, x_2) = (6, 2)$ *or* $(x_1, x_2) = (4, 2)$*. Put it another way, networks* (i)*,* (ii)*,* (iii) *and* (iv) *induce jumps in the positive diagonal, negative diagonal, vertical and horizontal directions, respectively. All of the states reachable from the state* $(x_1, x_2) = (5, 2)$*, occurring when all of the zero-drift networks from* (4.62) *are included, are shown in* Figure 4.5(a) *as the red dots, which form a square we call the* domain of influence *of the underlying propensity function* $\beta_{5,5}(x_1) \times \beta_{2,3}(x_2)$*.*

Let us note that the two reactions from any of the zero-drift networks from (4.62) *induce jumps to the opposite quadrants of the domain of influence, or to the opposite sides along the axes of the domain of influence, which is a graphical consequence of the fact that the networks do not influence the underlying deterministic model. The axes of the domain of influence for the propensity function* $\beta_{5,5}(x_1) \times \beta_{2,3}(x_2)$ *are shown as the black lines in* Figure 4.5(a)*, which divide the state-space into the four*

quadrants, centered at $(x_1, x_2) = (5, 2)$. *The domain of influence may be desirably extended by replacing the one-step zero-drift networks from* (4.62) *with their suitable multi-step counterparts - an investigation we do not cover in this thesis.*

Let us also note that the noise introduced by e.g. network $(\mathcal{R}^3_{5,5}(s_1, \bar{s}_1) + \mathcal{R}^3_{2,3}(s_2, \bar{s}_2))$ *is different from the noise introduced by the network* $(\mathcal{R}^3_{5,5}(s_1, \bar{s}_1) \cup \mathcal{R}^3_{2,3}(s_2, \bar{s}_2))$, *consisting of the union of the underlying one-dimensional zero-drift networks. In particular, the total propensity function of the latter network is given by* $(2K^1_{(5,5)}\beta_{5,5}(x_1) + 2K^2_{(2,3)}\beta_{2,3}(x_2))$, *and the network introduces the noise at* $(x_1, x_2) \in (\{5\} \times [0, 5]) \cup ([0, 10] \times \{2\})$, *which is shown in* Figure 4.5(b). △

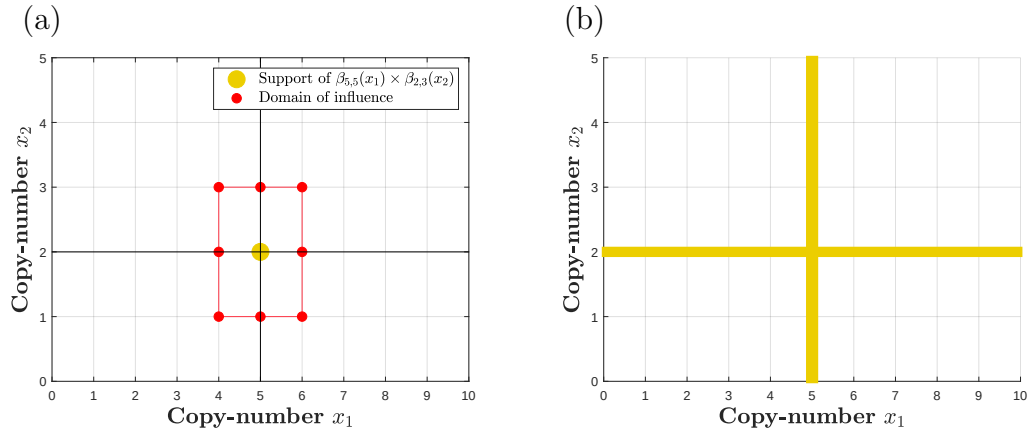

Figure 4.5: *Panel* (a) *displays support and the domain of influence of the two-dimensional interior basis propensity function* $\beta_{5,5}(x_1) \times \beta_{2,3}(x_2)$ *underlying zero-drift networks from* (4.62), *showing that the networks introduce noise at the single point* $(x_1, x_2) = (5, 2)$ *in the state-space. Panel* (b) *displays support of the propensity function* $(2K^1_{(5,5)}\beta_{5,5}(x_1) + 2K^2_{(2,3)}\beta_{2,3}(x_2))$ *corresponding to the zero-drift network* $(\mathcal{R}^3_{5,5}(s_1, \bar{s}_1) \cup \mathcal{R}^3_{2,3}(s_2, \bar{s}_2))$, *demonstrating that the network introduces noise along the two bands* $(x_1, x_2) \in \{5\} \times [0, 5]$ *and* $(x_1, x_2) \in [0, 10] \times \{2\}$. *In both cases, the state-space of the species* s_1 *and* s_2 *is given by* $(x_1, x_2) \in [0, 10] \times [0, 5]$.

Chapter 5

Approximation of high-molecular by bi-molecular reactions

In Chapter 3, we have presented the deterministic methods for designing chemical reaction networks (kinetic transformations, defined in Section 3.3), while in Chapter 4 we have developed the stochastic ones (the noise approximation algorithm, given as Algorithm 4.1). Such procedures may result in higher-order networks, containing reactions involving more than two reactants (see also Definition 2.3 from Chapter 2). While it is in principle possible to map such higher-order (higher-molecular) abstract reaction networks into physical, nucleic-acid based ones, using e.g. the molecular compiler from [24], it is of both theoretical and practical interest to approximate such networks by second-order (bi-molecular) ones, and use e.g. the molecular compiler from [23], which preserves the stochastic dynamics [39].

An algorithm for approximating reaction networks of arbitrarily high-order by second-order ones at the *deterministic level* has been used for decades, e.g. see [80, 122, 123, 124]. The algorithm has been rigorously established in the deterministic setting in [89, Section 3] for general third- and fourth-order reactions using perturbation theory. Its performance depends upon an asymptotic parameter (appearing as a rate coefficient of some of the underlying chemical reactions), but not on the initial conditions of the chemical species involved, making it suitable for nucleic-acid-based synthetic biology [23, 27, 28, 29]. Another, more elaborate, procedure, not based on an existence of an asymptotic parameter, but which depends on the initial conditions of some of the species, has been presented in [125, 126]. Since the initial conditions are more challenging to control than the rate coefficients in the experimental set-ups put forward in [27, 28, 29], in such situations the procedure from [125, 126] is less suitable.

Less attention has been paid to the validity of such approximations at the *stochastic level*: it has been shown in [127], using a projection operator method, that the specific third-order reaction, given by $3s \xrightarrow{k} 2s$, may be stochastically approximated by a second-order network using the algorithm from [89, Section 3], and this has also been qualitatively described in [128]. However, the question of whether the general deterministic results from [89, Section 3] extend into the stochastic setting remains unanswered. In particular, validity of perturbation results at the deterministic level does not generally guarantee validity at the stochastic level [129, 130, 131], as we now exemplify.

Example 5.1. *Let us consider the third-order reaction*

$$3s \xrightarrow{k} 2s, \tag{5.1}$$

and the second-order network given by

$$\begin{aligned} s + Q &\xrightarrow{k} Q, \\ 2s &\xrightarrow{1/\varepsilon} 2s + Q, \\ Q &\xrightarrow{1/\varepsilon} \varnothing. \end{aligned} \tag{5.2}$$

At the deterministic level, one may readily show, using Tikhonov's theorem [84]*, that the effective* RRE*, in the limit $\varepsilon \to 0$, for network* (5.2) *is given by*

$$\frac{\mathrm{d}x}{\mathrm{d}t} = -kx^3, \quad \textit{for } 0 < \varepsilon \ll 1,$$

where $x \in \mathbb{R}_{\geq}$ denotes the concentration of species s. Hence, the third-order reaction (5.1) *may be approximated by the second-order network* (5.2) *with $0 < \varepsilon \ll 1$ at the deterministic level.*

On the other hand, at the stochastic level, the effective CME *underlying network* (5.2) *is given by*

$$\frac{\partial}{\partial t}p(x,t) = (E_x^{+1} - 1)kx^2(x-1)p(x,t), \quad \textit{for } 0 < \varepsilon \ll 1,$$

where $x \in \mathbb{Z}_{\geq}$ is the copy-number of species s, and $p(x,t)$ its marginal PMF*. The effective propensity function, $\alpha_{\mathit{eff}}(x) = kx^2(x-1)$, does not correspond to a reaction under discrete mass-action kinetics (see also* Section 2.2*). Furthermore, network* (5.2) *may fire at the stochastic level when $x = 2$, which is not the case with* (5.1)*, whose propensity function is $\alpha(x) = kx(x-1)(x-2)$. Hence, second-order network* (5.2)

is not a good approximation of the third-order reaction (5.1) *at the stochastic level, when low copy-numbers of* s *are considered.*

Note that if we replace (5.1) *with* $s_1 + s_2 + s_3 \xrightarrow{k} \varnothing$*, then appropriate second-order networks of the form* (5.2) *provide good approximations at both deterministic and stochastic levels, as in this case falling factorials (see* Section 2.2 *in* Chapter 2*) do not appear in the underlying propensity functions.* △

In this chapter, we apply singular perturbation theory, known in the context of chemical reaction networks as stochastic quasi-stationary approximations (QSAs) [132, 133], in order to show that networks of arbitrarily high-order may be approximated by second-order ones at the stochastic level using the algorithm from [89, Section 3]. The chapter is organized as follows. In Section 5.1, we start by showing that any third-order reaction, involving identical reactants, may be approximated stochastically by a family of second-order networks, stated as Lemma 5.1. In Section 5.1.1, we apply the lemma on the third-order test network (5.25), which displays both deterministic and stochastic bistabilities for the chosen rate coefficients, and we demonstrate that an approximating second-order network displays the same stationary PMF and switching pattern between the two PMF modes as the original third-order network in an asymptotic limit (see also Figures 5.1 and 5.2). In Section 5.2, we show that reaction networks of arbitrarily high order may be stochastically approximated by a family of second-order networks, by generalizing Lemma 5.1 to Theorem 5.1. We also establish a weak-convergence result in Theorem 5.2 for a particular family of approximating second-order networks. Furthermore, it is shown in Lemma 5.2 that Theorem 5.1 may be applied iteratively when multiple higher-order reactions are considered. The results are also applied in Section 5.2.1 on the seventh-order test network (5.51), obtained from an application of the noise approximation algorithm, given as Algorithm 4.1 in Chapter 4, which displays noise-induced trimodality (a purely stochastic phenomenon). It is shown that the stationary PMF of the approximating second-order network converges to the PMF of (5.51) (see also Figure 5.3).

5.1 Special case: Third-order homoreactions

Let us start our analysis by considering an arbitrary third-order *homoreaction*, i.e. a reaction involving three reactant molecules of *the same species*, which is given by

$$\mathcal{R}_0 : \quad 3s_1 \xrightarrow{k} \sum_{l=1}^{N} \bar{\nu}_l s_l, \tag{5.3}$$

where $\bar{\nu}_l \in \mathbb{Z}_{\geq}$ for $l \in \{1, 2, \ldots, N\}$. Let us also consider the following second-order network

$$\mathcal{R}_\varepsilon = \mathcal{R}_1^\varepsilon \cup \mathcal{R}_2, \tag{5.4}$$

with the subnetworks

$$\begin{aligned} \mathcal{R}_1^\varepsilon : \quad & 2s_1 \underset{1/\varepsilon}{\overset{\kappa_1}{\rightleftharpoons}} Q_1, \\ \mathcal{R}_2 : \quad & s_1 + Q_1 \xrightarrow{\kappa_2} \tilde{\nu}_1 s_1 + \sum_{l=2}^{M} \bar{\nu}_l s_l + \bar{\gamma}_1 Q_1, \end{aligned} \tag{5.5}$$

where $\tilde{\nu}_1, \bar{\gamma}_1 \in \mathbb{Z}_{\geq}$, and $\kappa_1, \kappa_2 = \mathcal{O}(1)$ with respect to $0 < \varepsilon \ll 1$. Here, for convenience, we denote two irreversible reactions $(\boldsymbol{\nu} \to \bar{\boldsymbol{\nu}}) \in \mathcal{R}$, called the forward reaction, and $(\bar{\boldsymbol{\nu}} \to \boldsymbol{\nu}) \in \mathcal{R}$, called the backward reaction, jointly as the single reversible reaction $(\boldsymbol{\nu} \rightleftharpoons \bar{\boldsymbol{\nu}}) \in \mathcal{R}$. For mathematical convenience, we also define the fast subnetwork

$$\mathcal{R}_0^\varepsilon : \quad Q_1 \xrightarrow{1/\varepsilon} 2s_1. \tag{5.6}$$

In what follows, we use perturbation theory to formally show that, under appropriate conditions, stochastic dynamics of the third-order input network (5.3) and the second-order output network (5.4)–(5.5) are approximately the same in a weak sense. Before doing so, we set up the notation and equations.

Let $\mathbf{x} = (x_1, x_2, \ldots, x_N) \in \mathbb{Z}_{\geq}^N$ be the vector of copy-numbers of the species $s_1, s_2, \ldots, s_N$, and $y_1 \in \mathbb{Z}_{\geq}$ the copy-number of the auxiliary species Q_1, appearing in the network (5.4)–(5.5). The forward operator of the fast subnetwork $\mathcal{R}_0^\varepsilon$ is given by $\mathcal{L}_0 = 1/\varepsilon(E_{x_1}^{-2} E_{y_1}^{+1} - 1)y_1$. The backward operator satisfies $\mathcal{L}_0^*(x_1 + 2y_1) = 0$, i.e. the fast process has one conservation law: $x_1 + 2y_1 = \bar{x}_1$, where $\bar{x}_1$ is a time-independent constant for the process induced by $\mathcal{L}_0$. Therefore, we may simplify the operator $\mathcal{L}_0$ by introducing a new vector $\bar{\mathbf{x}} = (\bar{x}_1, x_2, \ldots, x_N) \in \mathbb{Z}_{\geq}^N$, with the first coordinate given by

$$\bar{x}_1 = x_1 + 2y_1, \tag{5.7}$$

i.e. we may reduce the number of fast variables from two, (x_1, y_1), to only one, (y_1), by replacing x_1 with the auxiliary slow variable $\bar{x}_1$ via $x_1 = \bar{x}_1 - 2y_1$. The CME corresponding to the network (5.4)–(5.5), on the slow time-scale $\tau = \mathcal{O}(1)$ defined by

$t = \tau/\varepsilon$ (the time is rescaled in order to capture nontrivial dynamics, as explained in what follows), and expressed in terms of the new coordinates $\bar{\mathbf{x}}$, reads

$$\frac{\partial}{\partial \tau} p_\varepsilon(\bar{\mathbf{x}}, y_1, \tau) = \left(\frac{1}{\varepsilon^2} \mathcal{L}_0 + \frac{1}{\varepsilon} \mathcal{L}_1 \right) p_\varepsilon(\bar{\mathbf{x}}, y_1, \tau), \tag{5.8}$$

with operators $\mathcal{L}_0$, and $\mathcal{L}_1$, being induced by the fast subnetwork $\mathcal{R}_0^1$, and the remaining (slow) subnetwork $\mathcal{R}_\varepsilon \setminus \mathcal{R}_0^\varepsilon$, respectively, and given by

$$\begin{aligned} \mathcal{L}_0 &= \left(E_{y_1}^{+1} - 1 \right) y_1, \\ \mathcal{L}_1 &= \left(E_{y_1}^{-1} - 1 \right) \alpha_1(\bar{x}_1, y_1) + \left(E_{\bar{\mathbf{x}}}^{-\Delta \bar{\mathbf{x}}} E_{y_1}^{-\Delta y_1} - 1 \right) y_1 \alpha_2(\bar{x}_1, y_1). \end{aligned} \tag{5.9}$$

Functions $\alpha_1(\bar{x}_1, y_1)$, and $y_1 \alpha_2(\bar{x}_1, y_1)$, are the propensity functions of the reactions from $\mathcal{R}_\varepsilon \setminus \mathcal{R}_0^\varepsilon$, expressed in terms of (5.7), and are given by

$$\begin{aligned} \alpha_1(\bar{x}_1, y_1) &= \kappa_1 x_1 (x_1 - 1) = \kappa_1 (\bar{x}_1 - 2y_1)(\bar{x}_1 - 2y_1 - 1), \\ \alpha_2(\bar{x}_1, y_1) &= \kappa_2 x_1 = \kappa_2 (\bar{x}_1 - 2y_1). \end{aligned} \tag{5.10}$$

The jump vector $\Delta \bar{\mathbf{x}}$ is given by $\Delta \bar{\mathbf{x}} = (\Delta \bar{x}_1, \bar{\nu}_2, \ldots, \bar{\nu}_N)$, where $\Delta \bar{x}_1$ may be obtained by formally applying the difference operator Δ on (5.7), and reads

$$\Delta \bar{x}_1 = \Delta x_1 + 2(\Delta y_1) = (\tilde{\nu}_1 - 1) + 2(\bar{\gamma}_1 - 1). \tag{5.11}$$

Let us note that, while $\bar{x}_1$ is a constant during firing of the network $\mathcal{R}_1^\varepsilon$ (i.e. it is a conservation constant for operator $\mathcal{L}_0$), it generally changes as a function of time during firing of the network $\mathcal{R}_2$ (i.e. it is a variable for the operator $\mathcal{L}_1$).

Perturbation analysis

Let us write the solution of (5.8) as the perturbation series

$$p_\varepsilon(\bar{\mathbf{x}}, y_1, \tau) = p_0(\bar{\mathbf{x}}, y_1, \tau) + \varepsilon p_1(\bar{\mathbf{x}}, y_1, \tau) + \varepsilon^2 p_2(\bar{\mathbf{x}}, y_1, \tau) + \ldots. \tag{5.12}$$

Note that we expect the perturbation series to converge to a PMF as $\varepsilon \to 0$ and, consequently, we require the *zero-order approximation* $p_0(\bar{\mathbf{x}}, y_1, \tau)$ to be a PMF (i.e. it must be nonnegative and normalized). Substituting (5.12) into (5.8), and equating terms of equal powers in ε, the following system of three equations is obtained:

$$\begin{aligned} \mathcal{O}\left(1/\varepsilon^2\right): &\ \mathcal{L}_0 p_0(\bar{\mathbf{x}}, y_1, \tau) = 0, \\ \mathcal{O}\left(1/\varepsilon\right): &\ \mathcal{L}_0 p_1(\bar{\mathbf{x}}, y_1, \tau) = -\mathcal{L}_1 p_0(\bar{\mathbf{x}}, y_1, \tau), \\ \mathcal{O}(1): &\ \mathcal{L}_0 p_2(\bar{\mathbf{x}}, y_1, \tau) = \frac{\partial}{\partial \tau} p_0(\bar{\mathbf{x}}, y_1, \tau) - \mathcal{L}_1 p_1(\bar{\mathbf{x}}, y_1, \tau). \end{aligned} \tag{5.13}$$

The first equation in (5.13) is homogeneous, and forms a zero-eigenvalue problem (EVP), while the remaining two are inhomogeneous and form boundary-value problems (BVPs).

Order $1/\varepsilon^2$ equation. It follows from the structure of $\mathcal{L}_0$ that we may write $p_0(\bar{\mathbf{x}}, y_1, \tau) = p_0(y_1)p_0(\bar{\mathbf{x}}, \tau)$, so that the first equation from (5.13) reduces to $\mathcal{L}_0 p_0(y_1) = 0$ (here, we also assume $p_0(\bar{\mathbf{x}}, \tau) > 0$ for any $\bar{\mathbf{x}} \in \mathbb{Z}_{\geq}^N$ and any $\tau > 0$, so that we may divide out the nonzero factor $p_0(\bar{\mathbf{x}}, \tau)$). Operator $\mathcal{L}_0$ has a one-dimensional null-space, $\mathcal{N}(\mathcal{L}_0) = \{1_{y_1}\delta_{y_1,0}\}$, where 1_{y_1} is a function independent of y_1, and $\delta_{i,j}$ is the Kronecker-delta function, non-zero only at $i = j$, where it is equal to one. We seek an element of this one-dimensional space which is normalized (so that it is a PMF), resulting in

$$p_0(\bar{\mathbf{x}}, y_1, \tau) = p_0(\bar{\mathbf{x}}, \tau)\delta_{y_1,0}, \qquad \sum_{\bar{\mathbf{x}}} p_0(\bar{\mathbf{x}}, \tau) = 1, \quad \text{for } \tau \geq 0. \tag{5.14}$$

In other words, under the infinitely fast reaction $Q_1 \xrightarrow{1/\varepsilon} 2s_1$, the y_1-marginal PMF is concentrated at zero, making Q_1 a short-lived species.

Order $1/\varepsilon$ equation. Using (5.14), the RHS of the second equation from (5.13) becomes

$$\mathcal{L}_1 p_0(\bar{\mathbf{x}}, y_1, \tau) = p_0(\bar{\mathbf{x}}, \tau)\left(E_{y_1}^{-1} - 1\right)\alpha_1(\bar{x}_1, y_1)\delta_{y_1,0}. \tag{5.15}$$

The second equation from (5.13) has either no solutions or infinitely many solutions, since $\mathcal{L}_0^* = y_1\left(E_{y_1}^{-1} - 1\right)$ has a non-trivial null-space, given by $\mathcal{N}(\mathcal{L}_0^*) = \{1_{y_1}\}$. In order to achieve the latter, the Fredholm alternative theorem [51] implies that the RHS of the equation has to be orthogonal to the null-space of the backward operator $\mathcal{L}_0^*$. Using (5.15), the solvability condition becomes $0 = \langle 1_{y_1}, \mathcal{L}_1 p_0(\bar{\mathbf{x}}, y_1, \tau)\rangle = \langle (E_{y_1}^{+1} - 1)1_{y_1}, \alpha_1(\bar{x}_1, y_1)p_0(\bar{\mathbf{x}}, y_1, \tau)\rangle$, which is unconditionally satisfied since $(E_{y_1}^{+1} - 1)1_{y_1} = 0$, where $\langle f, g\rangle = \sum_{y_1=0}^{\infty} f(y_1)g(y_1)$. Note that if the time had not been rescaled according to $t = \tau/\varepsilon$ in (5.8), the second equation from (5.13) would read $\mathcal{L}_0 p_1(\bar{\mathbf{x}}, y_1, t) = (\frac{\partial}{\partial t} - \mathcal{L}_1)p_0(\bar{\mathbf{x}}, y_1, t)$, and the solvability condition would give a trivial effective CME, $\frac{\partial}{\partial t}p_0(\bar{\mathbf{x}}, t) = 0$. For this reason, we have rescaled the time to a longer scale - a procedure which is used when a solvability condition at the highest-order equation in the perturbation hierarchy gives a zero time-derivative.

Let us write the solution of the second equation in (5.13) in the separable form given by

$$p_1(\bar{\mathbf{x}}, y_1, \tau) = p_0(\bar{\mathbf{x}}, \tau)p_1(y_1; \bar{\mathbf{x}}). \tag{5.16}$$

We write function $p_1(\bar{\mathbf{x}}, y_1, \tau)$ in the form (5.16), i.e. with the y_1-independent factor $p_0(\bar{\mathbf{x}}, \tau)$, which also appears in the zero-order approximation (5.14), so that the effective CME we obtain at $\mathcal{O}(1)$ depends only on the common factor $p_0(\bar{\mathbf{x}}, \tau)$. It is possible to write $p_1(\bar{\mathbf{x}}, y_1, \tau)$ in the separable form (5.16) because the operator $\mathcal{L}_0$ acts only on y_1 variable, and because of equality (5.15). Note that the factor $p_1(y_1; \bar{\mathbf{x}})$ generally cannot be interpreted as a (conditional) PMF (e.g. it may be negative), and hence we write $p_1 = p_1(y_1; \bar{\mathbf{x}})$ instead of $p_1 = p_1(y_1|\bar{\mathbf{x}})$. Substituting (5.16) into the second equation in (5.13), and using the operator equality $(E_{y_1}^{-1} - 1) = -(E_{y_1}^{+1} - 1)E_{y_1}^{-1}$, one obtains

$$p_0(\bar{\mathbf{x}}, \tau)(E_{y_1}^{+1} - 1)\left(y_1 p_1(y_1; \bar{\mathbf{x}}) - E_{y_1}^{-1}\alpha_1(\bar{x}, y_1)\delta_{y_1,0}\right) = 0,$$

which, assuming positivity of $p_0(\bar{\mathbf{x}}, \tau)$, becomes

$$(E_{y_1}^{+1} - 1)\left(y_1 p_1(y_1; \bar{\mathbf{x}}) - E_{y_1}^{-1}\alpha_1(\bar{x}, y_1)\delta_{y_1,0}\right) = 0,$$

implying that the solutions $p_1(y_1; \bar{\mathbf{x}})$ satisfy

$$y_1 p_1(y_1; \bar{\mathbf{x}}) = E_{y_1}^{-1}\alpha_1(\bar{x}_1, y_1)\delta_{y_1,0}. \tag{5.17}$$

Order 1 *equation.* The solvability condition for the third equation from (5.13) is given by

$$0 = \left\langle 1, \frac{\partial}{\partial \tau} p_0(\bar{\mathbf{x}}, y_1, \tau) \right\rangle - \langle 1, \mathcal{L}_1 p_1(\bar{\mathbf{x}}, y_1, \tau)\rangle, \tag{5.18}$$

where we have divided out the common factor 1_{y_1}. Equation (5.14) implies that the first term from (5.18) reads $\langle 1, \partial/\partial\tau p_0(\bar{\mathbf{x}}, y_1, \tau)\rangle = \partial/\partial\tau p_0(\bar{\mathbf{x}}, \tau)$. Using (5.9), and the fact that $\langle 1, (E_{y_1}^{-1} - 1)\alpha_1(\bar{x}_1, y_1)p_1(\bar{\mathbf{x}}, y_1, \tau)\rangle = \langle (E_{y_1}^{+1} - 1)1, \alpha_1(\bar{x}_1, y_1)p_1(\bar{\mathbf{x}}, y_1, \tau)\rangle = 0$, the second term from (5.18) is given by

$$\begin{aligned}
\langle 1, \mathcal{L}_1 p_1(\bar{\mathbf{x}}, y_1, \tau)\rangle &= \langle 1, (E_{\bar{\mathbf{x}}}^{-\Delta\bar{\mathbf{x}}} E_{y_1}^{-\Delta y_1} - 1) y_1 \alpha_2(\bar{x}_1, y_1) p_1(\bar{\mathbf{x}}, y_1, \tau)\rangle \\
&= \langle E_{y_1}^{+\Delta y_1} 1, E_{\bar{\mathbf{x}}}^{-\Delta\bar{\mathbf{x}}} y_1 \alpha_2(\bar{x}_1, y_1) p_1(\bar{\mathbf{x}}, y_1, \tau)\rangle \\
&\quad - \langle 1, y_1 \alpha_2(\bar{x}_1, y_1) p_1(\bar{\mathbf{x}}, y_1, \tau)\rangle \\
&= \langle 1, (E_{\bar{\mathbf{x}}}^{-\Delta\bar{\mathbf{x}}} - 1) y_1 \alpha_2(\bar{x}_1, y_1) p_1(\bar{\mathbf{x}}, y_1, \tau)\rangle \\
&= (E_{\bar{\mathbf{x}}}^{-\Delta\bar{\mathbf{x}}} - 1) p_0(\bar{\mathbf{x}}, \tau)\langle 1, \alpha_2(\bar{x}_1, y_1)\left(y_1 p_1(y_1; \bar{\mathbf{x}})\right)\rangle,
\end{aligned} \tag{5.19}$$

where we use (5.16) to obtain the last line. Using (5.17), equation (5.19) becomes

$$\begin{aligned}
\langle 1, \mathcal{L}_1 p_1(\bar{\mathbf{x}}, y_1, \tau)\rangle &= (E_{\bar{\mathbf{x}}}^{-\Delta\bar{\mathbf{x}}} - 1) p_0(\bar{\mathbf{x}}, \tau)\langle 1, \alpha_2(\bar{x}_1, y_1) E_{y_1}^{-1}\alpha_1(\bar{x}_1, y_1)\delta_{y_1,0}\rangle, \\
&= (E_{\bar{\mathbf{x}}}^{-\Delta\bar{\mathbf{x}}} - 1) p_0(\bar{\mathbf{x}}, \tau)\langle \alpha_2(\bar{x}_1, y_1), E_{y_1}^{-1}\alpha_1(\bar{x}_1, y_1)\delta_{y_1,0}\rangle \\
&= (E_{\bar{\mathbf{x}}}^{-\Delta\bar{\mathbf{x}}} - 1) p_0(\bar{\mathbf{x}}, \tau)\langle E_{y_1}^{+1}\alpha_2(\bar{x}_1, y_1), \alpha_1(\bar{x}_1, y_1)\delta_{y_1,0}\rangle \\
&= (E_{\bar{\mathbf{x}}}^{-\Delta\bar{\mathbf{x}}} - 1)\alpha_1(\bar{x}_1, 0)\alpha_2(\bar{x}_1, 1) p_0(\bar{\mathbf{x}}, \tau),
\end{aligned} \tag{5.20}$$

which, upon substitution into (5.18), using (5.10), and changing the time back to the original scale, $\tau = \varepsilon t$, gives the *effective* CME

$$\frac{\partial}{\partial t} p_0(\bar{\mathbf{x}}, t) = \left(E_{\bar{\mathbf{x}}}^{-\Delta\bar{\mathbf{x}}} - 1\right) \varepsilon \kappa_1 \kappa_2 \bar{x}_1 (\bar{x}_1 - 1)(\bar{x}_1 - 2) p_0(\bar{\mathbf{x}}, t). \tag{5.21}$$

The presence of the factor ε on the RHS of the effective CME (5.21) stems from the fact that non-trivial dynamics (i.e. an effective CME with a non-zero RHS) occur at $t = \mathcal{O}(1/\varepsilon)$. Put it another way, the most common firing pattern of the network $\mathcal{R}_\varepsilon$, given by (5.4)–(5.5), consists of a firing of the reaction $2s_1 \xrightarrow{\kappa_1} Q_1$, which produces the short-lived species Q_1, followed by the fast reaction $Q_1 \xrightarrow{1/\varepsilon} 2s_1$, which quickly converts Q_1 back to $2s_1$, which leads to a trivial dynamics of s_1. However, after long enough time, another firing pattern is also occasionally observed: after Q_1 is produced from $2s_1$, instead of being quickly converted back to $2s_1$, it participates in the target slow reaction $s_1 + Q_1 \xrightarrow{\kappa_2} \tilde{\nu}_1 s_1 + \sum_{l=2}^{M} \bar{\nu}_l s_l + \bar{\gamma}_1 Q_1$, which gives rise to non-trivial dynamics of s_1.

Validity of the effective CME

Let us now compare the CME of the input network (5.3) with that of the output network (5.4)–(5.5) when $0 < \varepsilon \ll 1$, given by (5.21). Before doing so, note that (5.21) is expressed in terms of the variable $\bar{x}_1$, defined in (5.7), and not the original copy-number x_1. Denoting by $Y_1(t)$ the time-dependent copy-number of Q_1, and assuming convergence of the perturbation series (5.12) (see also Theorem 5.2 in Section 5.2), it follows from (5.14) that $Y_1(t)$ converges to zero. As a consequence, equation (5.7) implies that $\bar{X}_1(t)$ converges to $X_1(t)$ as $\varepsilon \to 0$, so that we may replace $\bar{x}_1$ by x_1 in (5.21), ensuring that the effective CME describes copy-number of the species s_1.

Stoichiometric and kinetic conditions. While the effective propensity function, $\alpha_{\text{eff}}(x) \equiv \varepsilon \kappa_1 \kappa_2 x_1^3$, appearing in (5.21), has the same form as the propensity function of the input network (5.3), $\alpha(x) \equiv k x_1^3$, the two underlying chemical reactions generally have different reaction vectors and rate coefficients. In order for the effective CME (5.21) of the network (5.4)–(5.5) to match the CME of network (5.3), we must hence require two conditions. Firstly, we require that the effective reaction vector element $\Delta\bar{x}_1$, given by (5.11), is equal to the original one, $\Delta x_1 = \bar{\nu}_1 - 3$. This imposes the *stoichiometric condition* on $\tilde{\nu}_1$ and $\bar{\gamma}_1$:

$$\tilde{\nu}_1 = \bar{\nu}_1 - 2\bar{\gamma}_1. \tag{5.22}$$

Note that if we take $\bar{\gamma}_1 = 0$ in (5.22), then $\tilde{\nu}_1 = \bar{\nu}_1$. Secondly, we require that the effective propensity function is equal to the original one. This imposes the *kinetic condition*:

$$\varepsilon\kappa_1\kappa_2 = k, \quad \text{with } \varepsilon\kappa_1, \varepsilon\kappa_2 \ll 1, \ \text{ for } 0 < \varepsilon \ll 1. \tag{5.23}$$

Let us now summarize the established results.

Lemma 5.1. *Consider the third-order input network $\mathcal{R}_0$, given by* (5.3)*, and the second-order output network $\mathcal{R}_\varepsilon$, given by* (5.4)–(5.5)*. The* **x***-marginal zero-order* PMF *of the output network $\mathcal{R}_\varepsilon$, with $0 < \varepsilon \ll 1$, satisfies the effective* CME (5.21)*. Furthermore, assume the stoichiometric and kinetic conditions* (5.22) *and* (5.23) *are satisfied, respectively. Then, the effective* CME (5.21) *of the output network $\mathcal{R}_\varepsilon$ is identical to the* CME *of the input network $\mathcal{R}_0$.*

Convergence. Lemma 5.1 provides conditions under which the effective CME of the output network matches the CME of the input network. This has been obtained by means of formal asymptotics, under the assumption that the rate coefficients $\kappa_1, \kappa_2 = \mathcal{O}(1)$ with respect to $0 < \varepsilon \ll 1$. However, Lemma 5.1, on its own, does not establish convergence of the perturbation series (5.12) as $\varepsilon \to 0$. In order to establish convergence results, one may choose the coefficients κ_1, κ_2 according to (5.23), expand the PMF of the output network into an appropriate perturbation series, and then study a convergence.

For example, by choosing $\kappa_1 = \tilde{\kappa}_1\varepsilon^{-1/2}$ and $\kappa_2 = \tilde{\kappa}_2\varepsilon^{-1/2}$, with $\tilde{\kappa}_1\tilde{\kappa}_2 = k$, one obtains

$$\|p_\varepsilon(\mathbf{x}, y_1, t) - p_0(\mathbf{x}, y_1, t)\|_1 = \mathcal{O}(\varepsilon^{\frac{1}{2}}), \quad \text{as } \varepsilon \to 0, \tag{5.24}$$

for any finite-time interval, see Theorem 5.2 (with $n = 3$) in Section 5.2. Different scaling of κ_1 and κ_2 generally leads to a different order of convergence. For example, one can readily show that choosing $\kappa_1 = \mathcal{O}(\varepsilon^{-1/3})$ and $\kappa_2 = \mathcal{O}(\varepsilon^{-2/3})$ leads to a slower convergence: $\|p_\varepsilon(\mathbf{x}, y_1, t) - p_0(\mathbf{x}, y_1, t)\|_1 = \mathcal{O}(\varepsilon^{\frac{1}{3}})$, for sufficiently small ε.

Lemma 5.1 and equation (5.24) imply that the generators of the input and output networks match when $0 < \varepsilon \ll 1$. Consequently, the statistics of the common species from the two networks are close for each fixed *finite-time* interval. In the next section, we numerically investigate how well the *long-time* statistics of the input and output networks match for a particular test model.

5.1.1 Example: The Schlögl system

Let us consider the one-species third-order input reaction network, known as the Schlögl system [108], given by

$$\begin{aligned} \mathcal{R}_0: \quad & \varnothing \underset{k_2}{\overset{k_1}{\rightleftharpoons}} X, \\ & 2X \underset{k_4}{\overset{k_3}{\rightleftharpoons}} 3X. \end{aligned} \tag{5.25}$$

For particular choices of the rate coefficients, system (5.25) is deterministically bistationary (displays two coexisting stable equilibria), and stochastically bimodal [35, 108], and, in what follows, we consider such a choice of the dimensionless rate coefficients: $(k_1, k_2, k_3, k_4) = (1125, 37.5, 0.36, 10^{-3})$. Let us approximate the input network (5.25) with a second-order output network by applying Lemma 5.1 on the third-order reaction $3s \xrightarrow{k_4} 2s$, leading to the output network

$$\begin{aligned} \mathcal{R}_\varepsilon: \quad & \varnothing \underset{k_2}{\overset{k_1}{\rightleftharpoons}} s, \\ & 2s \xrightarrow{k_3} 3s, \\ & 2s \underset{1/\varepsilon}{\overset{\kappa_1}{\rightleftharpoons}} Q, \\ & s + Q \xrightarrow{\kappa_2} \tilde{\nu} s + \bar{\gamma} Q. \end{aligned} \tag{5.26}$$

Using the notation from (5.5), $\mathcal{R}_1^\varepsilon : 2s \underset{1/\varepsilon}{\overset{\kappa_1}{\rightleftharpoons}} Q$, and $\mathcal{R}_2 : s + Q \xrightarrow{\kappa_2} \tilde{\nu} s + \bar{\gamma} Q$. Let us impose the stoichiometric and kinetic conditions on the network (5.26), as specified in Lemma 5.1. In particular, the stoichiometric condition, given by (5.22), implies $\tilde{\nu} = 2 - 2\bar{\gamma}$, and there are two options: (i) taking $\bar{\gamma} = 0$ implies $\tilde{\nu} = 2$, (ii) taking $\bar{\gamma} = 1$ implies $\tilde{\nu} = 0$, i.e. increasing the stoichiometric coefficient $\bar{\gamma}$ by one, decreases $\tilde{\nu}$ by two, and this can be done as long as $\tilde{\nu} \geq 0$, which is a consequence of the conservation law for the fast process defined by (5.7). On the other hand, the kinetic condition, given by (5.23), implies $\varepsilon \kappa_1 \kappa_2 = k_4$. In what follows, we consider (5.26) with $(\tilde{\nu}, \bar{\gamma}) = (0, 1)$, and $\kappa_1 = \kappa_2 = \varepsilon^{-1/2}\sqrt{k_4}$, and denote copy-numbers of the species s and Q by x and y, respectively.

Stationary PMF. Let us compare the stationary PMFs of the input network (5.25), denoted by $p_0 = p_0(x)$, with the x-marginal stationary PMF of the output network (5.26), denoted by $p_{\varepsilon,x} = p_{\varepsilon,x}(x)$, which capture the long-time behavior of the systems, and are thus of practical importance. In Figure 5.1(a), we display the stationary PMF $p_{\varepsilon,x}(x)$ for various values of the asymptotic parameter ε. In particular, we show the input (target) PMF $p_0(x)$ as the black curve, while the output PMF

$p_{\varepsilon,x}(x)$ for $\varepsilon = 10^{-3}$ and $\varepsilon = 10^{-6}$ as the dashed purple curve and the blue histogram, respectively. When $\varepsilon = 10^{-3}$, the output PMF is bimodal, but the PMF is inaccurately distributed. Such a mismatch arises from the fact that the asymptotic parameter is not sufficiently small: $1/\varepsilon$ should be larger than the largest rate coefficient appearing in the input network (5.25) (which is $k_3 = \mathcal{O}(10^3)$). On the other hand, when $\varepsilon = 10^{-6}$, i.e. when $1/\varepsilon$ is three orders of magnitude higher than k_3, the matching between the input and output networks is excellent. In Figure 5.1(b), we show the y-marginal PMF for the output network when $\varepsilon = 10^{-6}$, and one can notice that it is concentrated around $y = 0$. In Figures 5.1(c)–(d), we show representative sample paths corresponding to the histograms from (a)–(b), respectively, where one can notice a stochastic switching phenomenon for the species s.

To gain more quantitative information, let us measure the distance (error) between the input and output PMFs as a function of the asymptotic parameter ε by using the l^1-norm:

$$\|p_{\varepsilon,x} - p_0\|_1 = \sum_x |p_{\varepsilon,x}(x) - p_0(x)|. \tag{5.27}$$

In Figure 5.2(a), we display a log-log plot of $\|p_{\varepsilon,x} - p_0\|_1$, as a function of the asymptotic parameter ε, as the black dots interpolated with the black lines, which was obtained by numerically solving the underlying stationary CMEs. We also show as the dashed blue line a log-log plot of the reference line $\|p_{\varepsilon,x} - p_0\|_1 = \sqrt{\varepsilon}$. One can notice an excellent match in the slopes of the two curves, in accordance with equation (5.24). In Figure 5.2(b), we plot the stationary y-marginal PMF evaluated at zero, $p_{\varepsilon,y}(0)$, which converges to 1 as $\varepsilon \to 0$, in agreement with (5.14) and (5.24).

Mean first passage time. PMFs provide the probability that the underlying sample paths are at particular states. For multimodal PMFs, another quantity of practical importance is the mean switching time, i.e. the average time it takes the sample paths, starting near one of the PMF maximum, to reach another PMF maximum for the first time. Such information is not provided in Figure 5.1, as PMFs do not uniquely capture time-parametrization of the underlying sample paths, i.e. sample paths with different switching times may give rise to identical PMFs.

In order to compare the switching times of the input and output networks (5.25) and (5.26), respectively, as a function of the asymptotic parameter ε, let us note that the three deterministic equilibria of the input network (5.25) are approximately given by $(x^*_{s,1}, x^*_u, x^*_{s,2}) \approx (53, 105, 202)$, where $x_{s,1}$ and $x_{s,2}$ are stable, while x_u is the unstable equilibrium. The mean switching time from the lower to the higher PMF modes may be measured by the average time it takes $X(t)$, starting in a neighborhood

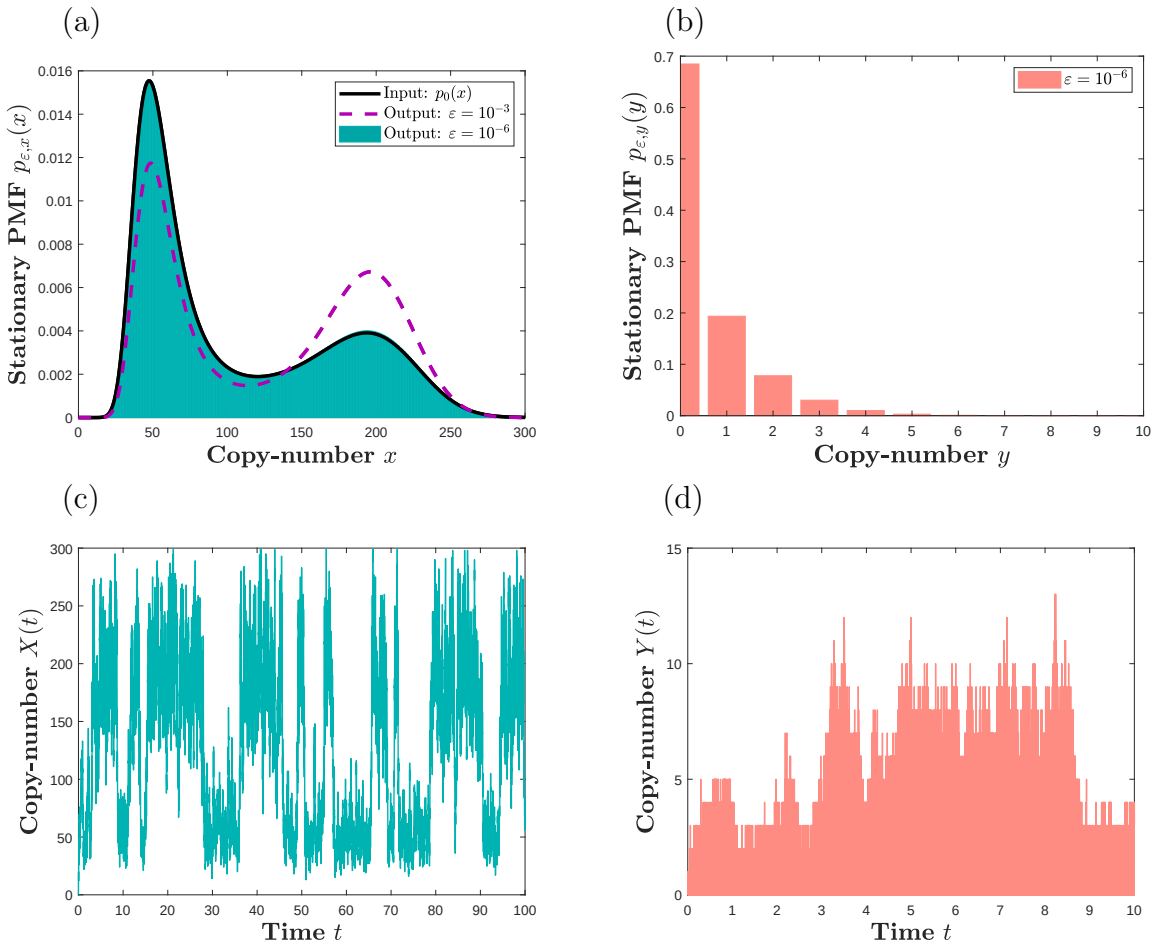

Figure 5.1: *Panel* (a) *displays the stationary* PMF *of the input network* (5.25) *as the black curve, and the* x*-marginal* PMF *for the output network* (5.26) *for different values of the asymptotic parameter* ε*. Panel* (c) *shows a representative sample path corresponding to the blue histogram from* (a)*, which displays bistability and stochastic switching. Panels* (b)*, and* (d)*, display the* y*-marginal* PMF *for* (5.26)*, which is concentrated near* $y = 0$*, and an underlying representative sample path, respectively. The parameters are fixed to:* $(k_1, k_2, k_3, k_4) = (1125, 37.5, 0.36, 10^{-3})$*,* $(\tilde{\nu}, \bar{\gamma}) = (0, 1)$*, and* $\kappa_1 = \kappa_2 = \varepsilon^{-1/2}\sqrt{k_4}$*.*

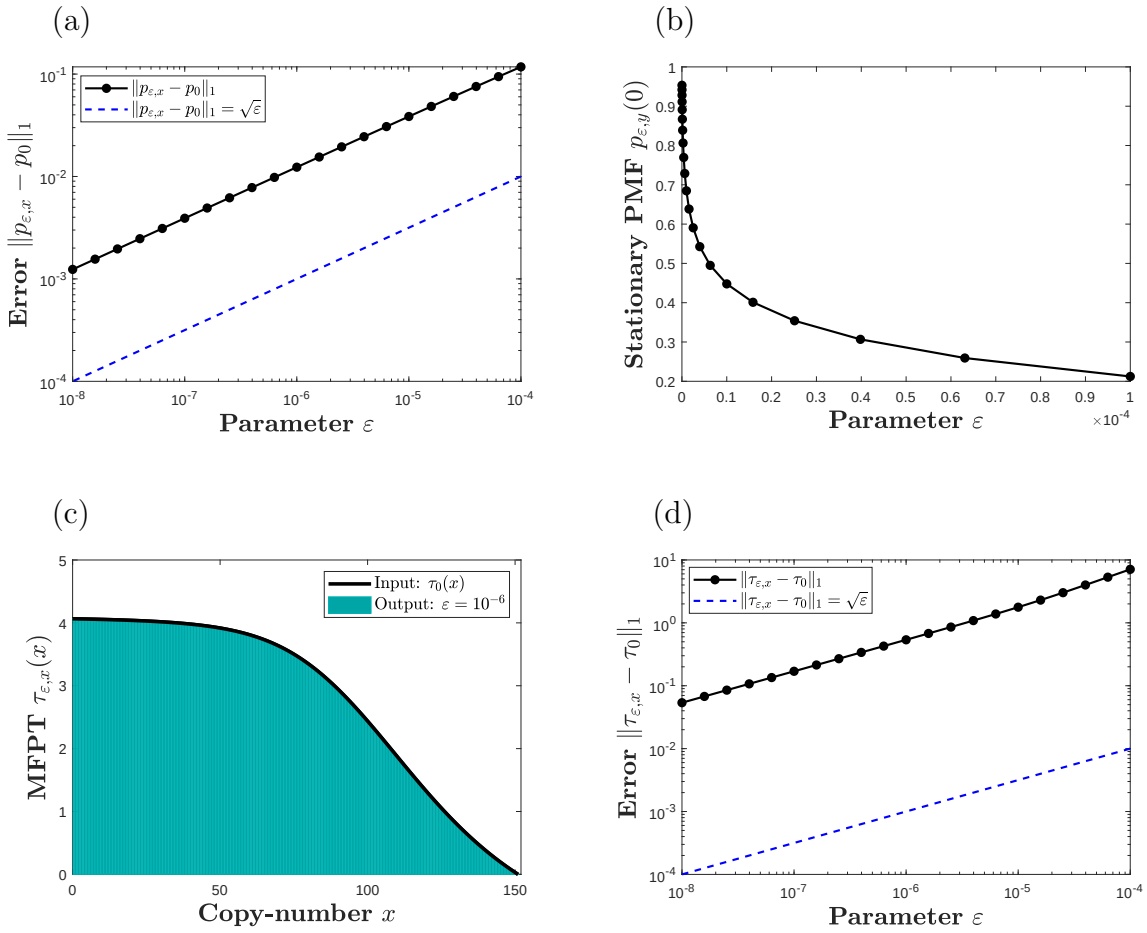

Figure 5.2: *Panel* (a) *displays a log-log plot of the* l^1*-distance between the* PMF*s of the input and output networks, given by* (5.25) *and* (5.26)*, respectively, given as equation* (5.27)*, as a function of the asymptotic parameter* ε*, as the black dots interpolated with the black lines. Also shown as the dashed blue line is the reference line* $y = \sqrt{\varepsilon}$*. Panel* (b) *shows the* y*-marginal* PMF *of the auxiliary species* Q *from the output network* (5.26)*, evaluated at* $y = 0$*, as a function of* ε*. Panel* (c) *shows the* MFPT *for the input network* (5.25) *as the black curve, while for the output network* (5.26) *as the blue histogram when* $\varepsilon = 10^{-6}$*. Similar to panel* (a)*, panel* (d) *displays a log-log plot of the* l^1*-distance between mean first passage times (*MFPT*s) of the input and output networks, obtained by solving equations* (5.28)–(5.29)*, as described in the main text. The parameters are fixed as in* Figure 5.1.

of $x^*_{s,1}$, to reach $R \approx (x^*_u + x^*_{s,2})/2$ for the first time [35]. This can be formulated for the input network (5.25) as the BVP [52]

$$\begin{aligned} \mathcal{L}^*\tau_0(x) &= -1, \quad x \in [0, R-1], \\ \tau_0(R) &= 0, \end{aligned} \tag{5.28}$$

where $\tau_0(x)$ is the mean first passage time (MFPT), given that the initial condition is fixed to x, and $\mathcal{L}^*$ is the backward operator of (5.25). The second line in (5.28) is the absorbing boundary condition, expressing the fact that the MFPT, with the starting point $x = R$, is zero. Numerically solving the BVP (5.28) with $R = 150$ produces the black curve shown in Figure 5.2(c). Analogous to (5.28), the BVP for the MFPT of the output network (5.26), denoted $\tau_\varepsilon(x, y)$, reads:

$$\begin{aligned} \mathcal{L}^*_\varepsilon\tau_\varepsilon(x, y) &= -1, \quad (x, y) \in [0, R_x - 1] \times [0, R_y], \\ \tau_\varepsilon(R_x, y) &= 0, \quad y \in [0, R_y], \end{aligned} \tag{5.29}$$

where $\mathcal{L}^*_\varepsilon$ is the backward operator of (5.26). We take $R_x = R = 150$, and truncate the y-state-space by taking $R_y = 100$. In what follows, we compare the one-variable quantity $\tau_0(x)$ with the two-variable quantity $\tau_\varepsilon(x, y)$. Since $Y(t)$ spends most of the time at $y = 0$, i.e. since $p_y(y) \approx \delta_{y,0}$ for $0 < \varepsilon \ll 1$, we compare $\tau_0(x)$ with $\tau_{\varepsilon,x}(x) \equiv \tau_\varepsilon(x, 0)$ (i.e. we set the initial condition for y at $y = 0$), and measure the error using the l^1-norm, $\|\tau_{\varepsilon,x} - \tau_0\|_1$. The error is shown Figure 5.2(d), and, similar to Figure 5.2(a), one can notice a $\sqrt{\varepsilon}$-convergence to zero. In Figure 5.2(c), we show $\tau_{\varepsilon,x}(x)$ for $\varepsilon = 10^{-6}$ as the blue histogram, which is in an excellent agreement with $\tau_0(x)$ shown in black.

5.2 General case: nth-order reactions

Let us now consider an arbitrary nth-order reaction with m distinct reactants, $\mathcal{R}_0 = \mathcal{R}_0(s_1, s_2, \ldots, s_M)$, given by

$$\mathcal{R}_0 : \quad \sum_{l=1}^{m} \nu_l s_l \xrightarrow{k} \sum_{l=1}^{N} \bar{\nu}_l s_l, \tag{5.30}$$

where $\sum_{l=1}^{m} \nu_l = n$, $n \geq 3$, $m \leq n$, $N \geq m$, and the stoichiometric coefficients $\nu_l, \bar{\nu}_l \in \mathbb{Z}_{\geq}$ for each l. For convenience, it is assumed that the reactant species are ordered according to increasing stoichiometric coefficients, $\nu_l \leq \nu_r$ if $l < r$, for

$l, r \in \{1, 2, \ldots, m\}$. Let us also consider the second-order reaction network $\mathcal{R}_\varepsilon = \mathcal{R}_\varepsilon(s_1, s_2, \ldots, s_M; Q_1, Q_2, \ldots, Q_{n-2})$, given by

$$\mathcal{R}_\varepsilon = \begin{cases} \mathcal{R}_1^\varepsilon(s_1, s_1) \cup \cup_{i=2}^{c_1-2} \mathcal{R}_i^\varepsilon(s_1) \cup \mathcal{R}_{n-1}(s_1), & \text{if } m = 1, \\ \mathcal{R}_1^\varepsilon(s_1, s_2) \cup \cup_{i=2}^{c_1} \mathcal{R}_i^\varepsilon(s_1) \cup \cup_{l=2}^{m-1} \cup_{i=\sum_{j=1}^{l-1} c_j + \delta_{l,2}}^{\sum_{j=1}^{l} c_j - 1} \mathcal{R}_i^\varepsilon(s_l) & \\ \cup \cup_{i=\sum_{j=1}^{m-1} c_j + \delta_{m,2}}^{n-2} \mathcal{R}_i^\varepsilon(s_m) \cup \mathcal{R}_{n-1}(s_m), & \text{if } m \geq 2, \end{cases} \tag{5.31}$$

with the convention that $\cup_{l=a}^{b} \mathcal{R}(l) = \emptyset$, if $a < b$, where $\mathcal{R}(l)$ is an arbitrary set indexed by l, and $\emptyset$ is the empty set. The subnetworks from (5.31) are given by

$$\begin{aligned} \mathcal{R}_1^\varepsilon(s_l, s_r): &\quad s_l + s_r \underset{1/\varepsilon}{\overset{\kappa_1}{\rightleftharpoons}} Q_1, \\ \mathcal{R}_i^\varepsilon(s_l): &\quad s_l + Q_{i-1} \underset{1/\varepsilon}{\overset{\kappa_i}{\rightleftharpoons}} Q_i, \quad i \in [2, n-2] \cap \mathbb{Z}, \\ \mathcal{R}_{n-1}(s_r): &\quad s_r + Q_{n-2} \xrightarrow{\kappa_{n-1}} \sum_{l=1}^{m} \tilde{\nu}_l s_l + \sum_{l=m+1}^{N} \bar{\nu}_l s_l + \bar{\gamma}_{n-2} Q_{n-2}, \end{aligned} \tag{5.32}$$

with $\tilde{\nu}_l, \bar{\gamma}_{n-2} \in \mathbb{Z}_\geq$ for each l. Network (5.31)–(5.32) contains $(n-2)$ auxiliary species Q_i, $i = 1, \ldots, n-2$, and consists of $(2n-3)$ reactions: $(n-2)$ faster first-order, and $(n-1)$ slower second-order ones.

We denote the copy-numbers of species $s_1, s_2, \ldots, s_N$ by $\mathbf{x} = (x_1, x_2, \ldots, x_N) \in \mathbb{Z}_\geq^N$, while the copy-numbers of $Q_1, Q_2, \ldots, Q_{n-2}$ by $\mathbf{y} = (y_1, y_2, \ldots, y_{n-2}) \in \mathbb{Z}_\geq^{n-2}$. In what follows, a generalization of Lemma 5.1 is provided, and we consider the perturbation series (C.8) from Appendix C, where $p_\varepsilon(\mathbf{x}, \mathbf{y}, t)$ is the PMF of the output network (5.31)–(5.32), while $p_0(\mathbf{x}, \mathbf{y}, t)$ its zero-order approximation. The $\mathbf{x}$-marginal zero-order PMF is given by $p_0(\mathbf{x}, t) = \sum_{\mathbf{y}} p_0(\mathbf{x}, \mathbf{y}, t)$.

Theorem 5.1. *Consider the nth-order input network $\mathcal{R}_0$, given by* (5.30)*, and the second-order output network $\mathcal{R}_\varepsilon$, given by* (5.31)–(5.32)*. The* $\mathbf{x}$*-marginal zero-order* PMF *of the output network $\mathcal{R}_\varepsilon$, with $0 < \varepsilon \ll 1$, satisfies the effective* CME (C.27)*. Let us assume that the parameters $\tilde{\nu}_l, \bar{\gamma}_{n-2}$, from the output network $\mathcal{R}_\varepsilon$, satisfy the stoichiometric conditions*

$$\tilde{\nu}_l = \bar{\nu}_l - (\nu_l - \delta_{l,m})\bar{\gamma}_{n-2}, \quad l = 1, 2, \ldots, m, \tag{5.33}$$

and that the coefficients κ_i, $i \in \{1, 2, \ldots, n-1\}$, satisfy the kinetic condition:

$$\varepsilon^{n-2} \prod_{i=1}^{n-1} \kappa_i = k, \quad \varepsilon\kappa_i \ll 1, \quad i = 1, 2, \ldots, n-1, \quad \textit{for } 0 < \varepsilon \ll 1. \tag{5.34}$$

Then, the effective CME *of the output network* (5.31)–(5.32) *is identical to the* CME *of the input network* (5.30)*.*

Proof. See Appendix C. □

Let us also state a readily obtainable convergence result, for a special choice of the rate coefficients κ_i, satisfying (5.34).

Theorem 5.2. *Consider the output network* (5.31)–(5.32)*, satisfying the condition* (5.34)*, with the following choice of the rate coefficients:*

$$\kappa_i = \tilde{\kappa}_i \varepsilon^{-\left(\frac{n-2}{n-1}\right)}, \quad \prod_{i=1}^{n-1} \tilde{\kappa}_i = k, \quad \tilde{\kappa}_i = \mathcal{O}(1), \quad i \in \{1, 2, \ldots, n-1\}. \tag{5.35}$$

Then, the PMF *of the output network converges to its zero-order approximation for any finite-time interval, $p_\varepsilon \to p_0$ as $\varepsilon \to 0$, with*

$$\|p_\varepsilon(\mathbf{x}, \mathbf{y}, t) - p_0(\mathbf{x}, \mathbf{y}, t)\|_1 \leq c(T) \varepsilon^{\frac{1}{n-1}}, \quad \text{for } 0 \leq t \leq T, \quad \text{as } \varepsilon \to 0, \tag{5.36}$$

where $c(T)$ is constant independent of ε.

Proof. See Appendix C. □

Note that the order of convergence predicted by equation (5.36), given by $1/(n-1)$, decreases as the order of the input network (5.30) increases. Generally, note also that the convergence order depends on the kinetic condition (5.34), i.e. it depends on how the rate coefficients κ_i are chosen, but is independent of the stoichiometric conditions (5.33).

The family of output networks (5.31)–(5.32), parametrized by the stoichiometric coefficients $\tilde{\nu}_l, \bar{\gamma}_{n-2}$, is not a unique approximation of the input network (5.30) with a second-order network, i.e. the ordering of the reactants and reactions in (5.31)–(5.32) is not unique.

Example 5.2. *Consider the input third-order reaction*

$$\mathcal{R}: \quad s_1 + 2s_2 \xrightarrow{k} \varnothing. \tag{5.37}$$

Under the conditions of Theorem 5.1*, reaction* (5.37) *may be approximated according to* (5.31)–(5.32) *with an output network $\mathcal{R}_\varepsilon = \mathcal{R}_1^\varepsilon(s_1, s_2) \cup \mathcal{R}_2(s_2)$, with subnetworks*

$$\begin{aligned} \mathcal{R}_1^\varepsilon(s_1, s_2): \quad & s_1 + s_2 \underset{1/\varepsilon}{\overset{\kappa_1}{\rightleftharpoons}} Q_1, \\ \mathcal{R}_2(s_2): \quad & s_2 + Q_1 \xrightarrow{\kappa_2} \varnothing, \end{aligned} \tag{5.38}$$

i.e. the forward reaction from $\mathcal{R}_1^\varepsilon$ *is a heteroreaction, involving the distinct reactants* s_1 *and* s_2*. However, the second-order output network* $\mathcal{R}_1^\varepsilon(s_2, s_2) \cup \mathcal{R}_2(s_1)$*, given by*

$$\begin{aligned} \mathcal{R}_1^\varepsilon(s_2, s_2): &\quad 2s_2 \underset{1/\varepsilon}{\overset{\kappa_1}{\rightleftharpoons}} Q_1, \\ \mathcal{R}_2(s_1): &\quad s_1 + Q_1 \xrightarrow{\kappa_2} \varnothing, \end{aligned} \tag{5.39}$$

for which the forward reaction from $\mathcal{R}_1^\varepsilon$ *is a homoreaction, also approximates the input reaction* (5.37) *under the conditions of* Theorem 5.1*, as is readily proved analogously as in* Appendix C. △

In order to facilitate the proof of Theorem 5.1, we have followed the convention of ordering the reactants in the input reaction (5.30) according to increasing stoichiometric coefficients, and we have also fixed the ordering of reactants and reactions in the output networks (5.31)–(5.32). For example, if the input reaction is $2s_1 + s_2 \xrightarrow{k} \varnothing$, we would re-label the species to obtain $s_1 + 2s_2 \xrightarrow{k} \varnothing$. In what follows, we are no longer concerned with proving Theorem 5.1 and, to gain a greater flexibility, we allow arbitrary orderings, and use both of the designs (5.38) and (5.39), depending on convenience.

Let us now interpret conditions (5.33) and (5.34) from Theorem 5.1. The kinetic condition (5.34) simply states that the product of the rate coefficients of all of the $(n-1)$ forward (slower) reactions reactions from the output network (5.32), $\kappa_1\kappa_2 \ldots \kappa_{n-1}$, divided by the product of all of the $(n-2)$ backward (faster) reactions, $(1/\varepsilon)^{n-2}$, must be equal to the rate coefficient of the input reaction (5.30). Furthermore, asymptotic conditions $\varepsilon\kappa_i \ll 1$ state that we require the forward reactions to be slower than the backward ones, ensuring validity of the perturbation analysis from Appendix C. The stoichiometric condition (5.33) also has an intuitive interpretation, as we now exemplify.

Example 5.3. *Consider the input fourth-order reaction*

$$\mathcal{R}: \quad 2s_1 + 2s_2 \xrightarrow{k} 4s_1 + 4s_2, \tag{5.40}$$

where, using the notation of Theorem 5.1*,* $\nu_1 = \nu_2 = 2$ *and* $\bar{\nu}_1 = \bar{\nu}_2 = 4$*. A suitable family of output networks is given by* $\mathcal{R}_\varepsilon = \mathcal{R}_1^\varepsilon(s_1, s_2) \cup \mathcal{R}_2^\varepsilon(s_1) \cup \mathcal{R}_3(s_2)$*, with*

$$\begin{aligned} \mathcal{R}_1^\varepsilon(s_1, s_2): &\quad s_1 + s_2 \underset{1/\varepsilon}{\overset{\kappa_1}{\rightleftharpoons}} Q_1, \\ \mathcal{R}_2^\varepsilon(s_2): &\quad s_1 + Q_1 \underset{1/\varepsilon}{\overset{\kappa_2}{\rightleftharpoons}} Q_2, \\ \mathcal{R}_2(s_2): &\quad s_2 + Q_2 \xrightarrow{\kappa_3} \tilde{\nu}_1 s_1 + \tilde{\nu}_2 s_2 + \bar{\gamma}_2 Q_2. \end{aligned} \tag{5.41}$$

If $\bar{\gamma}_2 = 0$*, then* (5.33) *implies that* $\tilde{\nu}_1 = \tilde{\nu}_2 = 4$*, i.e. that* $\mathcal{R}_2(s_2)$ *from* (5.41) *has the same products as the input network* (5.40)*,*

$$\mathcal{R}_2(s_2): \quad s_2 + Q_2 \xrightarrow{\kappa_3} 4s_1 + 4s_2. \tag{5.42}$$

When $0 < \varepsilon \ll 1$*, intuitively speaking, at the network level, we formally have* $Q_1 = s_1 + s_2$ *and* $Q_2 = s_1 + Q_1 = 2s_1 + s_2$*. With this notation, condition* (5.33) *states that we may add the complex* $\varnothing = (Q_2 - 2s_1 - s_2)$ *to the products of* $\mathcal{R}_2(s_2)$ *from* (5.41) *as many times as desired, as long as the resulting complex is nonnegative (so that reaction* $\mathcal{R}_2(s_2)$ *retains a chemical interpretation). By adding the product complex* $\varnothing = (Q_2 - 2s_1 - s_2)$ *once to* (5.42)*, one obtains*

$$\mathcal{R}_2(s_2): \quad s_2 + Q_2 \xrightarrow{\kappa_3} 2s_1 + 3s_2 + Q_2, \tag{5.43}$$

while by adding it twice, one gets

$$\mathcal{R}_2(s_2): \quad s_2 + Q_2 \xrightarrow{\kappa_3} 2s_2 + 2Q_2. \tag{5.44}$$

All of the three members (5.42)–(5.44) *of the family of output networks* (5.41) *are valid. However, note that by adding the product complex* $\varnothing = (Q_2 - 2s_1 - s_2)$ *three times to* (5.42) *leads to*

$$\mathcal{R}_2(s_2): \quad s_2 + Q_2 \xrightarrow{\kappa_3} -2s_1 + s_2 + 3Q_2, \tag{5.45}$$

for which the product complex is not nonnegative: the reaction is non-chemical, and hence not a valid approximation of the input network (5.40). △

Multi-input networks

Theorem 5.1 provides conditions under which a *single* input higher-order reaction (5.30) may be approximated by a second-order network (5.31)–(5.32). A generalization to the case of input networks containing *multiple* higher-order reactions is straightforward: Theorem 5.1 may be applied iteratively to each desired (higher-order) input reaction, one at a time, while the other input reactions, which one does not wish to approximate, are copied directly from the input to the output network without any modifications.

Lemma 5.2. *Assume* $\mathcal{R}_0$ *is an input network containing multiple reactions. Let* $\mathcal{R}_\varepsilon$ *be an output network, obtained by replacing each desired input reaction with a suitable reaction chain of the form* (5.32)*, with each chain containing distinct auxiliary species* Q_i*. If the conditions* (5.33)–(5.34) *are satisfied for each chain in the output network, then the effective* CME *of the output and input networks are identical.*

Proof. In what follows, we prove Lemma 5.2 for an input network involving two arbitrary homoreactions. A generalization to input networks containing arbitrarily many reactions, both homoreactions and heteroreactions, follows readily.

Consider an input reaction network, involving two homoreactions, given by

$$\begin{aligned} \mathcal{R}_0: \quad r: \quad & ns_1 \xrightarrow{k} \sum_{l=1}^{N} \bar{\nu}_l s_l, \\ \bar{r}: \quad & ms_1 \xrightarrow{\bar{k}} \sum_{l=1}^{N} \bar{\eta}_l s_l, \end{aligned} \tag{5.46}$$

with $n, m \geq 3$. Consider also the second-order output network $\mathcal{R}_\varepsilon \cup \bar{\mathcal{R}}_\varepsilon$, with

$$\begin{aligned} \mathcal{R}_\varepsilon: \quad & 2s_1 \underset{1/\varepsilon}{\overset{\kappa_1}{\rightleftharpoons}} Q_1, \quad \{s_1 + Q_{i-1} \underset{1/\varepsilon}{\overset{\kappa_i}{\rightleftharpoons}} Q_i\}_{i=2}^{n-2}, \quad s_1 + Q_{n-2} \xrightarrow{\kappa_{n-1}} \tilde{\nu}_1 s_1 + \sum_{l=2}^{N} \bar{\nu}_l s_l + \bar{\gamma}_{n-2} Q_{n-2}, \\ \bar{\mathcal{R}}_\varepsilon: \quad & 2s_1 \underset{1/\varepsilon}{\overset{\bar{\kappa}_1}{\rightleftharpoons}} \bar{Q}_1, \quad \{s_1 + \bar{Q}_{i-1} \underset{1/\varepsilon}{\overset{\bar{\kappa}_i}{\rightleftharpoons}} \bar{Q}_i\}_{i=2}^{m-2}, \quad s_1 + \bar{Q}_{m-2} \xrightarrow{\bar{\kappa}_{m-1}} \tilde{\eta}_1 s_1 + \sum_{l=2}^{N} \bar{\eta}_l s_l + \bar{\delta}_{m-2} Q_{m-2}, \end{aligned} \tag{5.47}$$

where the chains $\mathcal{R}_\varepsilon$, and $\bar{\mathcal{R}}_\varepsilon$, approximate the input reactions r, and $\bar{r}$, respectively. Here, $\{Q_i\}_{i=1}^{n-2}$ and $\{\bar{Q}_i\}_{i=1}^{m-2}$ are distinct auxiliary species. Let us also define the fast subnetwork $\mathcal{R}_0^\varepsilon \cup \bar{\mathcal{R}}_0^\varepsilon$, given by

$$\begin{aligned} \mathcal{R}_0^\varepsilon: \quad & Q_1 \xrightarrow{\frac{1}{\varepsilon}} 2s_1, \quad \{Q_i \xrightarrow{\frac{1}{\varepsilon}} s_1 + Q_{i-1}\}_{i=2}^{n-2}, \\ \bar{\mathcal{R}}_0^\varepsilon: \quad & \bar{Q}_1 \xrightarrow{\frac{1}{\varepsilon}} 2s_1, \quad \{\bar{Q}_i \xrightarrow{\frac{1}{\varepsilon}} s_1 + \bar{Q}_{i-1}\}_{i=2}^{m-2}. \end{aligned} \tag{5.48}$$

The proof of Theorem 5.1, given in Appendix C.1, in the case of a single input homoreaction, relies on the coordinate transformation (C.1), which reduces the forward operator of the fast subnetwork (C.3) to the desired form (C.5). Analogously, by defining the new coordinates by

$$\bar{x}_1 = \begin{cases} x_1 + \sum_{i=1}^{n-2}(i+1)y_i + \sum_{i=1}^{m-2}(i+1)\bar{y}_i, & \text{if } l = 1, \\ x_l, & \text{if } l \neq 1, \end{cases} \tag{5.49}$$

where y_i and $\bar{y}_i$ are the copy-numbers of the auxiliary species Q_i and $\bar{Q}_i$, respectively, one can readily show that the fast subnetwork (5.48) reduces to the desired form

$$\begin{aligned} \mathcal{R}_0^\varepsilon: \quad & Q_{n-2} \xrightarrow{\frac{1}{\varepsilon}} Q_{n-3} \xrightarrow{\frac{1}{\varepsilon}} \ldots \xrightarrow{\frac{1}{\varepsilon}} Q_1 \xrightarrow{\frac{1}{\varepsilon}} \varnothing, \\ \bar{\mathcal{R}}_0^\varepsilon: \quad & \bar{Q}_{m-2} \xrightarrow{\frac{1}{\varepsilon}} \bar{Q}_{m-3} \xrightarrow{\frac{1}{\varepsilon}} \ldots \xrightarrow{\frac{1}{\varepsilon}} \bar{Q}_1 \xrightarrow{\frac{1}{\varepsilon}} \varnothing. \end{aligned} \tag{5.50}$$

The rest of the proof of Lemma 5.2 closely follows Appendix C.1. □

If some of the input reactions involve common reactant subcomplexes, then some of the intermediate species Q_i may be re-used to simultaneously approximate such reactions. Put it another way, reactions with common subcomplexes may be approximated by multiple chains of reactions of the form (5.32), which all branch out from a suitable common subchain. This may be proved analogously as Lemma 5.2. Such re-using of intermediates may greatly reduce the number of auxiliary species and reactions in the output networks, making the output networks less costly from the synthetic biology point of view, as we now exemplify.

5.2.1 Example: Noise-induced trimodality

Consider the seventh-order input reaction network $\mathcal{R} \cup \mathcal{R}_{2,5} \cup \mathcal{R}_{4,2}$, given by

$$\begin{aligned}
\mathcal{R}(s,\bar{s}): \quad & \bar{s} \underset{k_2}{\overset{k_1}{\rightleftharpoons}} s, \\
\mathcal{R}_{2,5}(s,\bar{s}): \quad & 2s+5\bar{s} \xrightarrow{k_{2,5}} 3s+4\bar{s}, \\
& 2s+5\bar{s} \xrightarrow{k_{2,5}} s+6\bar{s}, \\
\mathcal{R}_{4,2}(s,\bar{s}): \quad & 4s+2\bar{s} \xrightarrow{k_{4,2}} 5s+\bar{s}, \\
& 4s+2\bar{s} \xrightarrow{k_{4,2}} 3s+3\bar{s}, \qquad (5.51)
\end{aligned}$$

which has been obtained by applying the noise approximation algorithm, given as Algorithm 4.1 in Chapter 4, on the network $\bar{s} \underset{k_2}{\overset{k_1}{\rightleftharpoons}} s$ (since this network is already pairwise conserved, the second step in Algorithm 4.1 is skipped). In what follows, we fix the dimensionless parameters to $k_1 = k_2 = k_{2,5} = k_{4,2} = 1$, and $c = 7$, where c is the conservation constant, i.e. we take $x + \bar{x} = c = 7$, where x and $\bar{x}$ denote the copy-numbers of species s and $\bar{s}$, respectively. The one-step zero-drift networks $\mathcal{R}_{2,5}$ and $\mathcal{R}_{4,2}$ introduce the noise at $x = 2$ and $x \in \{4, 5\}$, respectively. In Figure 5.3, we show the stationary PMF underlying (5.51) as the black dots, which are interpolated with the solid black lines for visual clarity. One can notice that the network displays noise-induced trimodality, which is not observed at the deterministic level, where network (5.51) is monostable, displaying a globally stable equilibrium $x^* = k_1/(k_1 + k_2)c = 3.5$. We now apply Theorem 5.1 on the network (5.51) in order to reduce its order to two, thereby justifying that Algorithm 4.1 may be useful for molecular computing, where one typically experimentally implements second-order reactions [23].

Applying Theorem 5.1 to independently reduce the order of each of the four reactions underlying $\mathcal{R}_{2,5} \cup \mathcal{R}_{4,2}$ requires 18 auxiliary species and 40 reactions in total, i.e.

10 independent auxiliary species for the network $\mathcal{R}_{2,5}$ (5 species for each of the underlying reactions) and, similarly, 8 species for $\mathcal{R}_{4,2}$. However, 5 auxiliary species are in fact sufficient to reduce the order of network $\mathcal{R}_{2,5}$, since each of the two underlying reactions involve the same reactants, so that we may re-use the auxiliary species. Similar reasoning implies that we require only 4 auxiliary species to approximate the network $\mathcal{R}_{4,2}$. Hence, 9 auxiliary species are sufficient to approximate $\mathcal{R}_{2,5} \cup \mathcal{R}_{4,2}$ by a second-order network. Furthermore, all of the reactions from $\mathcal{R}_{2,5} \cup \mathcal{R}_{4,2}$ involve a common reactant subcomplex $(2s+2\bar{s})$, i.e. they involve at least 2 molecules of s, and 2 of $\bar{s}$, which we may further exploit to reduce the number of the auxiliary species. In particular, since $(2s + 2\bar{s})$ may be converted into an auxiliary species in three steps, we may re-use 3 species in both networks $\mathcal{R}_{2,5}$ and $\mathcal{R}_{4,2}$, hence requiring in total $9 - 3 = 6$ auxiliary species. More precisely, subnetwork $\mathcal{R}_{2,5}$ may be approximated by

$$
\begin{aligned}
\mathcal{R}_1^\varepsilon(s): &\qquad 2s \underset{1/\varepsilon}{\overset{\kappa_1}{\rightleftharpoons}} Q_1,\\
\mathcal{R}_2^\varepsilon(\bar{s}): &\qquad \bar{s} + Q_1 \underset{1/\varepsilon}{\overset{\kappa_2}{\rightleftharpoons}} Q_2,\\
\mathcal{R}_3^\varepsilon(\bar{s}): &\qquad \bar{s} + Q_2 \underset{1/\varepsilon}{\overset{\kappa_3}{\rightleftharpoons}} Q_3,\\
\mathcal{R}_4^\varepsilon(\bar{s}): &\qquad \bar{s} + Q_3 \underset{1/\varepsilon}{\overset{\kappa_4}{\rightleftharpoons}} Q_4,\\
\mathcal{R}_5^\varepsilon(\bar{s}): &\qquad \bar{s} + Q_4 \underset{1/\varepsilon}{\overset{\kappa_5}{\rightleftharpoons}} Q_5,\\
\mathcal{R}_6(s,\bar{s}): &\qquad \bar{s} + Q_5 \overset{\kappa_6}{\longrightarrow} 3s + 4\bar{s},\\
&\qquad \bar{s} + Q_5 \overset{\kappa_6}{\longrightarrow} s + 6\bar{s},
\end{aligned}
\tag{5.52}
$$

and we may re-use the species $Q_3 = 2s + 2\bar{s}$ from (5.52) to make the approximation of the subnetwork $\mathcal{R}_{4,2}$ more efficient, as follows:

$$
\begin{aligned}
\bar{\mathcal{R}}_4^\varepsilon(s): &\qquad s + Q_3 \underset{1/\varepsilon}{\overset{\bar{\kappa}_4}{\rightleftharpoons}} \bar{Q}_4,\\
\bar{\mathcal{R}}_5(s,\bar{s}): &\qquad s + \bar{Q}_4 \overset{\bar{\kappa}_5}{\longrightarrow} 5s + \bar{s},\\
&\qquad s + \bar{Q}_4 \overset{\bar{\kappa}_5}{\longrightarrow} 3s + 3\bar{s}.
\end{aligned}
\tag{5.53}
$$

In summary, we have approximated the seventh-order input reaction network $\mathcal{R} \cup \mathcal{R}_{2,5} \cup \mathcal{R}_{4,2}$, given by (5.51), involving 2 species and 6 reactions, with the second-order output network $\mathcal{R}_\varepsilon \equiv \mathcal{R} \cup (\cup_{i=1}^5 \mathcal{R}_i^\varepsilon \cup \bar{\mathcal{R}}_4^\varepsilon) \cup \mathcal{R}_6 \cup \bar{\mathcal{R}}_5$, involving 8 species and 18 reactions. The subnetwork $\mathcal{R}_{2,5}$ from (5.51) is approximated by $\cup_{i=1}^5 \mathcal{R}_i^\varepsilon \cup \mathcal{R}_6$, while $\mathcal{R}_{4,2}$ by $\cup_{i=1}^3 \mathcal{R}_i^\varepsilon \cup \bar{\mathcal{R}}_4^\varepsilon \cup \bar{\mathcal{R}}_5$. Let us note that additional freedom in stoichiometry of the

networks $\mathcal{R}_6$ and $\bar{\mathcal{R}}_5$ may be achieved by utilizing suitable multi-step counterparts of the zero-drift networks $\mathcal{R}_{2,5}$ and $\mathcal{R}_{4,2}$ (see Section 4.4.1).

The kinetic condition

Having met the stoichimetric conditions (5.33), it remains to also satisfy the kinetic condition (5.34). In particular, the rate coefficients from (5.52)–(5.53) must satisfy:

$$\begin{aligned} &\varepsilon^5\kappa_1\kappa_2\kappa_3\kappa_4\kappa_5\kappa_6 = k_{2,5}, \\ &\varepsilon^4\kappa_1\kappa_2\kappa_3\bar{\kappa}_4\bar{\kappa}_5 = k_{4,2}, \quad \varepsilon\kappa_i, \varepsilon\bar{\kappa}_4, \varepsilon\bar{\kappa}_5 \ll 1, \ \text{ for } i \in \{1,2,\ldots,6\}. \end{aligned} \tag{5.54}$$

Let us first focus on the first equation from (5.54). A particular choice of the rate coefficients may be obtained by taking $\kappa_1 = \kappa_2 = \ldots = \kappa_6$, giving $\kappa_i = \varepsilon^{-5/6}(k_{2,5})^{1/6}$, $i \in \{1,2,\ldots,6\}$. Such a simple choice of the rate coefficients, while valid, may be less desirable, as we now explain.

The perturbation analysis employed in this chapter relies on scaling the rate coefficients of reactions. A more detailed analysis would consider the whole propensity functions of the reactions. While we do not pursue such an analysis in this thesis, let us make a remark. The output subnetwork (5.52) consists of an ordered chain of reactions: in order for the subnetwork $\mathcal{R}_6$ from (5.52) to fire, and mimic the action of $\mathcal{R}_{2,5}$ from (5.51), one first requires that the forward reactions in the subnetworks $\{\mathcal{R}_i^\varepsilon\}_{i=1}^5$ fire. The forward reaction from $\mathcal{R}_1^\varepsilon$, forming the start of the chain, involves the complex $2s$ as the reactant, with the propensity function $\alpha_1(x) = \kappa_1 x(x-1)$. On the other hand, the forward reactions from $\{\mathcal{R}_i^\varepsilon\}_{i=2}^6$ involve the short-lived low-copy-number intermediates $\{Q_i\}_{i=1}^5$ as reactants, with the propensity functions $\{\alpha_i(\bar{x},y) = \kappa_i\bar{x}y_{i-1}\}_{i=2}^6$. If the induced stochastic dynamics predominantly take place near the $\bar{x}$-axis and sufficiently far from the origin (i.e. for lower copy-numbers $\{y_i\}_{i=1}^5$, and higher copy-numbers $\bar{x}$), then one may observe that $\alpha_i(\bar{x},y)/\kappa_i \ll \alpha_1(x)/\kappa_1$, $i = 2,3,\ldots,6$. In such settings, in order to speed up the slower reactions $\{\mathcal{R}_i^\varepsilon\}_{i=2}^6$, a more efficient choice of the rate coefficients involves larger values of $\{\kappa_i\}_{i=2}^6$, and, consequently, due to the constraint (5.34), smaller values of κ_1. However, this should be balanced with the fact that, by taking a smaller κ_1, the chain of reactions (5.52) is triggered less often.

Going back to the first equation from (5.54), let us then choose the rate coefficients as follows

$$\begin{aligned} &\kappa_1 = \varepsilon^{-\frac{5}{6}}(k_{2,5})^{\frac{1}{6}}\varepsilon^{5\alpha}, \\ &\kappa_i = \varepsilon^{-\frac{5}{6}}(k_{2,5})^{\frac{1}{6}}\varepsilon^{-\alpha}, \ \ i \in \{2,3,\ldots,6\}, \ \ 0 \leq \alpha < 1/6, \end{aligned} \tag{5.55}$$

where the condition $0 \leq \alpha < 1/6$ ensures that $\varepsilon\kappa_i \ll 1$, as $\varepsilon \to 0$, for $i \in \{2, 3, \ldots, 6\}$. Having chosen κ_i, $i \in \{1, 2, \ldots, 6\}$, we set for simplicity $\bar{\kappa}_4 = \bar{\kappa}_5$ in the second equation from (5.54), obtaining:

$$\bar{\kappa}_i = \varepsilon^{-2}(\kappa_1\kappa_2\kappa_3)^{-\frac{1}{2}}(k_{4,2})^{\frac{1}{2}}, \quad i = 4, 5. \tag{5.56}$$

Fixing $\alpha = 1/10$, in Figure 5.3 we display the stationary x-marginal PMF of the output network $\mathcal{R}_\varepsilon$ for $\varepsilon = 10^{-3}$, and $\varepsilon = 10^{-6}$, as the purple squares, interpolated with the purple dashed lines, and the blue histogram, respectively. Similar to Figures 5.1(a), when $\varepsilon = 10^{-3}$, the output PMF is qualitatively accurate, capturing the multimodality, but is quantitatively inaccurately distributed. On the other hand, when $\varepsilon = 10^{-6}$, one can notice a good matching with the stationary PMF of the input network (5.51), denoted by $p_0(x)$ and shown as the black dots.

Let us note that we take the initial conditions for all of the auxiliary species $Q_i, \bar{Q}_4$, $i \in \{1, 2, \ldots, 5\}$, to be equal to zero, for the following reason. While the stoichiometric conservation law $x + \bar{x} = c = 7$ is valid for the input network, it no longer holds for the output network. However, provided the auxiliary species are initially not present in the system, the subconservation law $x + \bar{x} \leq 7$ is valid for the output network. This ensures that the x-state-space of the input and output networks is identical, $x \in [0, 7]$, and hence that the Algorithm 4.1 is correctly implemented, i.e. that the networks (5.52) and (5.53) accurately mimic the action of the zero-drift networks $\mathcal{R}_{2,5}$ and $\mathcal{R}_{4,2}$ from (5.51), respectively.

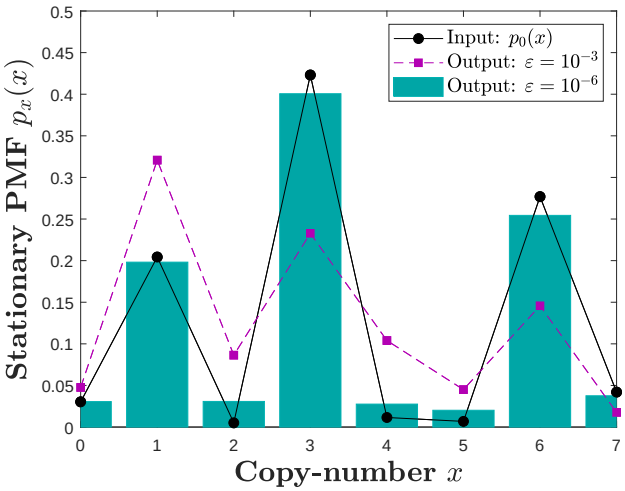

Figure 5.3: *The stationary* PMF *of the input network* $\mathcal{R} \cup \mathcal{R}_{2,5} \cup \mathcal{R}_{4,2}$*, given by* (5.51)*, is shown as the black curve, while the* x*-marginal* PMF *of the output network* $\mathcal{R}_\varepsilon = \mathcal{R} \cup (\cup_{i=1}^{5} \mathcal{R}_i^\varepsilon \cup \bar{\mathcal{R}}_4^\varepsilon) \cup \mathcal{R}_6 \cup \bar{\mathcal{R}}_5$*, with the subnetworks given by* (5.52)–(5.53)*, is shown as the dashed purple curve when the asymptotic parameter is fixed to* $\varepsilon = 10^{-3}$*, and as the blue histogram when* $\varepsilon = 10^{-6}$*. The stationary* PMF*s have been obtained by applying the Gillespie algorithm on the underlying reaction networks. The rest of the dimensionless parameters are fixed to:* $k_1 = k_2 = k_{2,5} = k_{4,2} = 1$*,* κ_i*,* $i \in \{1, 2, \ldots, 6\}$*, and* $\bar{\kappa}_1, \bar{\kappa}_2$ *are chosen according to* (5.55) *and* (5.56)*, respectively, with* $\alpha = 1/10$*. The conservation constant for the input network is fixed to* $c = 7$*, and the initial conditions for all of the auxiliary species from the output network,* $Q_i, \bar{Q}_4$*,* $i \in \{1, 2, \ldots, 5\}$*, are fixed to* 0*.*

Chapter 6

Discussion

In this final chapter, we summarize the results reached in the thesis, and suggest some possible future directions.

6.1 Summary

Chapter 3. In Sections 3.1–3.3, a framework for constructing reaction systems with prescribed deterministic dynamics has been formulated as an inverse problem. As a part of the framework, kinetic transformations have been defined in Section 3.3, enabling one to map an arbitrary polynomial ODE system with a set of constraints, possibly containing the cross-negative terms, into reaction-rate equations. Augmented with the results from [125], such transformations can be applied to a large class of non-polynomial systems as well. In particular, we have presented the x-factorable transformations [80] in Section 3.3.2, which do not change the dimensions of the ODE systems being transformed, but which introduce a higher number of nonlinear terms. We have more closely analyzed properties of such mappings in the two-dimensional case. In Section 3.3.3, we have developed a novel kinetic transformation, called the quasistationary transformation, which increases the dimensions of the systems being transformed, but generally introduces a lower number of nonlinear terms.

In Section 3.4, we have applied the framework in order to construct lower-dimensional reaction systems displaying exotic dynamical features. More precisely, in Section 3.4.1, following Algorithm 3.2, we have designed the two-species network (3.52), which displays a coexisting stable equilibrium and stable limit cycle, and undergoes a homoclinic bifurcation, with a phase plane presented in Figure 3.3(b). In Section 3.4.2, we have designed the two-species network (3.61), which displays two coexisting stable limit cycles, with a phase plane presented in Figure 3.4.

Chapter 4. In this chapter, we have developed the noise-approximation algorithm, given as Algorithm 4.1, and established its properties. The algorithm maps an input chemical reaction network to output networks, all under mass-action kinetics, by introducing appropriate additional species and reactions, such that the output networks satisfy the following two properties. Firstly, the output networks have the same deterministic model as the input network, in appropriate limits of some of the parameters (rate coefficients) introduced by the algorithm. Secondly, controllable state-dependent noise is introduced into the stochastic model of the output networks. In Section 4.2, we have shown that the asymptotic conditions for the algorithm parameters are necessary for preservation of the time-dependent deterministic solutions. However, the time-independent deterministic solutions (the deterministic equilibrium points), which capture important features of the deterministic dynamics, remain fixed under the applications of the algorithm, even if the asymptotic conditions are not satisfied. In Section 4.4, we have provided generalizations of Algorithm 4.1, which further increase its capabilities.

In Section 4.1, the algorithm has been applied to a one-species test problem given by (4.7), and it was shown that the underlying probability distribution and sample paths may be favorably modified at arbitrary points in the state-space, as demonstrated in Figure 4.2. For example, in Figure 4.2(b), the noise is added to the whole interior of the state-space, while in (e) only at a single point, in both cases resulting in noise-induce bimodality. On the other hand, in Figure 4.2(h), by adding the noise to specific points in the state-space, the network is redesigned to display noise-induced trimodality. As shown in Figures 4.2(c), (f), (i), the blue stochastic trajectories display multistability, while the red deterministic ones remain fixed and display monostability. In Section 4.3, the algorithm has been applied to a more challenging problem, taking the form of the bistable two-species system given by (3.52), involving a stable equilibrium and limit cycle, and designed in Chapter 3. At the stochastic level, the system is significantly more likely to be found near the equilibrium point, as demonstrated in Figures 4.3(a)–(c). We have used the algorithm to map the network (3.52) to (B.3), so that the stochastic system spends comparable amounts of time near the two attractors, as demonstrated in Figures 4.3(d)–(f). The network has also been redesigned to display noise-assisted oscillations, which is shown in Figures 4.3(g)–(i).

Chapter 5. Motivated by the fact that the deterministic and stochastic methods developed in Chapters 3–4 may give rise to higher-order (higher-molecular) reactions, involving three or more reactants, we have shown in this chapter that such reactions

may be mapped to up-to second-order (bi-molecular) reaction networks, while the underlying stochastic dynamics are preserved. This has been first established and exemplified for specific third-order reactions in Section 5.1. We have then generalized the theoretical results to arbitrary higher-order reactions in Section 5.2. The general framework has then been applied on the seventh-order test network (5.51), designed using the previously developed noise-approximation algorithm.

6.2 Future work

Ergodic noise-control. The operation of the noise-approximation algorithm, given as Algorithm 4.1, depends upon pairwise conserved species. Consequently, its performance depends (weakly) on the initial conditions of some of the underlying species (i.e. the output networks, produced by the algorithm, are nonergodic). This problem also extends when the procedure from Chapter 5 is applied (see Section 5.2.1). Since the initial conditions may be experimentally challenging to control in small nucleic-acid-based circuits [27, 28, 29], the applicability of the algorithm may be limited. In a future publication, we will show that, by introducing appropriate catalytic reactions, it is possible to map Algorithm 4.1 to an ergodic form, thus eliminating dependence of the output networks on the initial conditions.

Probability distribution design and mixing. The deterministic-stochastic hybrid approach, put forward in this thesis, enables one to design stochastic reaction networks with controlled sample paths and probability distributions, partially inherited from the deterministic skeleton. However, in general, the framework does not allow one to (i) design arbitrary probability distributions, nor does it allow one to (ii) mix (combine) multiple reaction networks, each with their own probability distribution, in a controlled way. By combining the framework presented in this thesis, and the noise-approximation algorithm in particular, with the so-called *noise-induced mixing* - a design principle utilized by gene regulatory networks, which we have investigated in [116], it will be shown that both of the outlined tasks can be achieved.

Applications. The deterministic-stochastic hybrid framework may be applied to a multitude of problems in systems and synthetic biology, facilitating investigations and control of intrinsic noise in biochemical processes. For example, the noise-approximation algorithm may be utilized as a molecular filter for variance-reduction [134], by favorably redistributing the probability distributions of various molecular computing modules, thus increasing their efficiency.

Experimental implementations. Finally, future work also includes collaborations with experimentalists, with the goal of implementing some of the DNA-based networks, which are obtained by utilizing the methodology from this thesis. In particular, as a proof-of-concept of the noise-approximation algorithm, we put forward a reaction network containing the zero-drift network (4.20), and displaying the kind of dynamics as shown in blue in Figure 4.2(c) (see also [39] for more details). An experimental challenge in this setting is reaching sufficiently low molecular copy-numbers in order for the intrinsic noise to become significant [27, 28, 29]. Further work involves utilizing an ergodic version of Algorithm 4.1 to implement more general zero-drift networks, and, hence, more intricate noise-driven biochemical dynamics.

Appendix A

Supplementary material for Chapter 3

A.1 Oscillations and multistability in two-dimensional RREs

Let us present a necessary condition for the existence of a limit cycle in (3.32).

Theorem A.1. *Consider the two-dimensional ODE system with a quadratic polynomial RHSs, given by* (3.31)*. If* $k_4 \leq 0$ *and* $k_{12} \leq 0$*, and if system* (3.31) *is* nonnegative*, then the system has no limit cycles fully contained in the positive quadrant.*

Proof. Let us consider $\boldsymbol{\mathcal{P}} = \boldsymbol{\mathcal{P}}(\mathbf{x}; \mathbf{k})$ in the simply connected region $\mathbb{R}^2_>$, and apply the Dulac criterion [76], with the Dulac function $B = B(x_1, x_2) = (x_1 x_2)^{-1}$, so that

$$\begin{aligned}\nabla \cdot (B\boldsymbol{\mathcal{P}}) &= \frac{\partial}{\partial x_1}\big(B\mathcal{P}_1\big) + \frac{\partial}{\partial x_2}\big(B\mathcal{P}_2\big) \\ &= -\left(\frac{k_1}{x_1^2 x_2} + \frac{k_3}{x_1^2} + \frac{k_6 x_2}{x_1^2}\right) + \frac{k_4}{x_2} - \left(\frac{k_7}{x_1 x_2^2} + \frac{k_8}{x_2^2} + \frac{k_{10} x_1}{x_2^2}\right) + \frac{k_{12}}{x_1} \\ &= -(x_1 x_2)^{-2}\left(x_2\left(\mathcal{P}_1(0, x_2) - k_4 x_1^2\right) + x_1\left(\mathcal{P}_2(x_1, 0) - k_{12} x_2^2\right)\right). \qquad \text{(A.1)}\end{aligned}$$

Let us assume $k_4 \leq 0$ and $k_{12} \leq 0$, and that system (3.31) is nonnegative (i.e. that $\mathcal{P}_1(0, x_2) \geq 0$ and $\mathcal{P}_2(x_1, 0) \geq 0$). It then follows from (A.1) that $\nabla \cdot (B\boldsymbol{\mathcal{P}}) \leq 0$, i.e. the divergence of $(B\boldsymbol{\mathcal{P}})$ does not change sign in $\mathbb{R}^2_>$. Thus, limit cycles fully contained in $\mathbb{R}^2_>$ do not exist. (If $\nabla \cdot \boldsymbol{\mathcal{P}} \equiv 0$ identically, then limit cycles cannot exist [76].) $\square$

Let us note that result similar to Theorem A.1 has been derived in [107], where it was shown that the absence of cross-negative terms in $\boldsymbol{\mathcal{P}}(\mathbf{x}; \mathbf{k}) \in \mathbb{P}_2(\mathbb{R}^2; \mathbb{R}^2)$, with $k_4 \leq 0$ and $k_{12} \leq 0$, implies the absence of positive limit cycles, i.e. one requires the more restrictive condition $\boldsymbol{\mathcal{P}}(\mathbf{x}; \mathbf{k}) \in \mathbb{P}_2^{\mathcal{K}}(\mathbb{R}^2_{\geq}; \mathbb{R}^2)$. Theorem A.1 shows that,

in fact, absence of the cross-negative effect in $\boldsymbol{\mathcal{P}}(\mathbf{x};\,\mathbf{k}) \in \mathbb{P}_2(\mathbb{R}^2;\,\mathbb{R}^2)$, with $k_4 \leq 0$ and $k_{12} \leq 0$, implies the absence of positive limit cycles, i.e. one requires the less restrictive condition $\boldsymbol{\mathcal{P}}(\mathbf{x};\,\mathbf{k}) \in \mathbb{P}_2(\mathbb{R}^2_{\geq};\,\mathbb{R}^2) = \mathbb{P}_2^{\mathcal{K}}(\mathbb{R}^2_{\geq};\,\mathbb{R}^2) \cup \mathbb{P}_2^{\mathcal{N}}(\mathbb{R}^2_{\geq};\,\mathbb{R}^2)$.

Since RREs (3.32) are a subset of nonnegative polynomial ODEs, Theorem A.1 applies, and gives a necessary condition for the existence of a positive limit cycle in (3.32): $k_4 > 0$ or $k_{12} > 0$.

Let us now prove that (3.31) can have at most three coexisting stable critical points, i.e. (3.31) can be at most *tristationary*.

Lemma A.1. *The maximum number of coexisting stable critical points in two-dimensional relatively-prime second-degree polynomial ODE systems* (3.31)*, with fixed coefficients* $\mathbf{k}$*, is three.*

Proof. Let us assume system (3.31) has four, the maximum number, of real finite critical points. Then, using an appropriate centroaffine (linear) transformation, system (3.31) can be mapped to [90, 91]

$$\begin{aligned}\frac{\mathrm{d}x_1}{\mathrm{d}t} &= a_1x_1(x_1-1) + b_1x_2(x_2-1) + c_1x_1x_2,\\ \frac{\mathrm{d}x_2}{\mathrm{d}t} &= a_2x_1(x_1-1) + b_2x_2(x_2-1) + c_2x_1x_2,\end{aligned} \tag{A.2}$$

which is topologically equivalent to (3.31), with the critical points located at $A = (0,0)$, $B = (1,0)$, $C = (0,1)$ and $D = (\alpha,\beta)$, with $\alpha \neq 0$, $\beta \neq 0$, $\alpha+\beta \neq 1$, and the coefficients c_1, c_2 given by

$$\begin{aligned}c_1 &= -\frac{\alpha-1}{\beta}a_1 - \frac{\beta-1}{\alpha}b_1,\\ c_2 &= -\frac{\alpha-1}{\beta}a_2 - \frac{\beta-1}{\alpha}b_2.\end{aligned}$$

The trace and determinant of the Jacobian matrix of (A.2), denoted τ and δ, respectively, evaluated at the four critical points, A, B, C, D, are given by:

$$\begin{aligned}\tau_A &= -(a_1+b_2), & \delta_A &= a_1b_2 - a_2b_1,\\ \tau_B &= a_1 - a_2\frac{(\alpha-1)}{\beta} - b_2\frac{(\alpha+\beta-1)}{\alpha}, & \delta_B &= -\frac{\alpha+\beta-1}{\alpha}\delta_A,\\ \tau_C &= b_2 - a_1\frac{(\alpha+\beta-1)}{\beta} - b_1\frac{(\beta-1)}{\alpha}, & \delta_C &= -\frac{\alpha+\beta-1}{\beta}\delta_A,\\ \tau_D &= \alpha a_1 + \beta b_2 - a_2\frac{\alpha(\alpha-1)}{\beta} - b_1\frac{\beta(\beta-1)}{\alpha}, & \delta_D &= (\alpha+\beta-1)\delta_A.\end{aligned} \tag{A.3}$$

System (A.2) may have three stable critical points if and only if the quadrilateral $ABCD$, formed by the critical points, is nonconvex, and the only saddle critical point is the one located at the interior vertex of the quadrilateral [90, 91]. This is the case when $\alpha > 0$, $\beta > 0$, $\alpha + \beta < 1$, and $\delta_A > 0$, in which case A, B, and C are nonsaddle critical points, while D is a saddle. Imposing also the conditions $\tau_A < 0$, $\tau_B < 0$, $\tau_C < 0$, ensuring that A, B, and C are stable, a solution of the resulting system of algebraic inequalities is given by $a_1 = 1$, $b_1 = -1$, $a_2 = 1$, $0 < \alpha < 1/2\left((1+2\beta) - \sqrt{1+8\beta^2}\right)$, $-1 < b_2 < \alpha(-\alpha+\beta+1)/(\beta(\alpha+\beta-1))$. □

Let us note that if (A.2) are RREs, then they cannot have three stable critical points. More precisely, requiring $b_1 \geq 0$, $a_2 \geq 0$, and $d_A > 0$ and $\tau_A < 0$ in (A.3), implies $a_1 > 0$ and $b_2 > 0$, which further implies $\tau_B > 0$, so that B is unstable. Tristationary RREs (3.32) do not appear to exist in the literature. On the other hand, bistationary RRE (3.32) do exist (in fact, even one-dimensional cubic RRE may be bistationary, e.g. the Schlögl model [108]).

A.2 Andronov-Leontovich theorem

Theorem A.2. ***Andronov-Leontovich theorem.*** *Consider system* (3.10) *with* $\boldsymbol{\mathcal{P}}(\mathbf{x};\mathbf{k},\alpha) \in \mathbb{P}_m(\mathbb{R}^2;\mathbb{R}^2)$, $m \in \mathbb{Z}_{\geq}$, *where* $\alpha \in \mathbb{R}$ *is a bifurcation parameter. Let* $\lambda_1(\alpha)$ *and* $\lambda_2(\alpha)$ *be eigenvalues of the Jacobian corresponding to the two-dimensional system* (3.10), $J = \nabla\boldsymbol{\mathcal{P}}(\mathbf{x};\mathbf{k},\alpha)$, *and suppose that at* $\alpha = 0$, *the following* homoclinic bifurcation conditions (i)–(ii) *are satisfied, and that* (3.10) *is* generic, *i.e. the following* homoclinic genericity conditions (iii)–(iv) *are satisfied:*

(i) *System has saddle critical point* $\mathbf{x}^* = 0$ *with eigenvalues* $\lambda_1(0) < 0 < \lambda_2(0)$.

(ii) *System has a homoclinic orbit* $\gamma^*(t)$ *to the saddle critical point* $\mathbf{x}^*$.

(iii) Nondegeneracity condition: $\sigma_0 = \nabla\cdot\boldsymbol{\mathcal{P}}(\mathbf{x}^*;\mathbf{k},0) = \lambda_1(0)+\lambda_2(0) \neq 0$, *where* $\sigma_0 \in \mathbb{R}$ *is called the* saddle quantity. *In other words, the separatrix cycle* $\gamma^* \cup \{\mathbf{x}^*\}$ *is* simple.

(iv) Transversality condition: Melnikov function, $M(\alpha)$, *evaluated at* $\alpha = 0$ *satisfies:*

$$M(0) = \int_{-\infty}^{+\infty} \varphi(t)\left(\boldsymbol{\mathcal{P}}(\gamma^*(t);\mathbf{k},0) \times \left.\frac{\partial\boldsymbol{\mathcal{P}}(\gamma^*(t);\mathbf{k},\alpha)}{\partial\alpha}\right|_{\alpha=0}\right)\mathrm{d}t \neq 0, \quad \text{(A.4)}$$

where $\varphi(t) = \exp\left(-\int_0^t(\nabla\cdot\boldsymbol{\mathcal{P}}(\gamma^*(t);\mathbf{k},0)d\tau\right)$.

Then, for all sufficiently small $|\alpha|$, a unique hyperbolic limit cycle bifurcates in a neighborhood of the homoclinic separatrix cycle $\gamma^* \cup \{\mathbf{x}^*\}$. If $\sigma_0 < 0$, the homoclinic bifurcation is supercritical*, giving rise to a unique* stable *limit cycle, while if $\sigma_0 > 0$, the homoclinic bifurcation is* subcritical*, giving rise to a unique* unstable *limit cycle.*

Appendix B

Supplementary material for Chapter 4

B.1 Alternative boundary zero-drift networks

An alternative network to the left-boundary zero-drift network (4.5) is given by

$$\begin{aligned}
\bar{n}\bar{s} &\xrightarrow{k_{0,\bar{n}}} s + (\bar{n}-1)\bar{s},\\
\nu s + B_1 + B_2 &\xrightarrow{k_{0,\bar{n}}} (\nu-1)s + \bar{s} + B_1 + B_2,\\
\varnothing &\xrightarrow{1/\mu_{0,\bar{n}}} B_1,\\
\nu s + B_1 &\xrightarrow{1/\mu_{0,\bar{n}}} \nu s,\\
\bar{n}\bar{s} &\xrightarrow{1/\mu_{0,\bar{n}}} \bar{n}\bar{s} + B_2,\\
B_2 &\xrightarrow{1/\mu_{0,\bar{n}}} \varnothing, \quad 0 < \mu_{0,\bar{n}} \ll 1,
\end{aligned} \tag{B.1}$$

where $0 < \nu \leq C$. Analogous to network (4.5), network (B.1) is a zero-drift network in the limit $\mu_{0,\bar{n}} \to 0$, and it introduces noise at $x \in [0, C-\bar{n}]$. Furthermore, it also preserves the deterministic equilibria, independent of the choice of the asymptotic parameter $\mu_{0,\bar{n}}$. Roughly speaking, the boundary species B from (4.5) is split into two boundary species B_1 and B_2 in (B.1). Analogous network may be constructed to introduce noise at the right-boundary, $x \in [n, C]$.

Another alternative to (4.5) is given by

$$\begin{aligned}
\bar{s} + B &\xrightarrow{k_{0,n}} s + B,\\
(C-n)\bar{s} &\xrightarrow{1} (C-n)\bar{s} + B,\\
(n+1)s + B &\xrightarrow{1/\mu_{0,n}} (n+1)s, \quad 0 < \mu_{0,n} \ll 1.
\end{aligned} \tag{B.2}$$

Network (B.2) is a zero-drift network in the limit $\mu_{0,n} \to 0$, and introduces noise at $x \in [0, n]$. However, when (B.2) is embedded into an input network, the equilibria

are not fixed: they remain preserved only in the limit $\mu_{0,n} \to 0$, which may require a very small $\mu_{0,n}$ for convergence. The structure of the network is as follows: when $x \leq n$ (equivalently, $\bar{x} \geq (C-n)$), the second reaction from (B.2) starts producing the boundary species B, which may then be used by the first reaction to generate a drift to the right, i.e. to increase copy-number of species s. Once $x \geq (n+1)$, the final reaction from (B.2) rapidly destroys the boundary species B, thus 'switching-off' the first reaction. Analogous network may be constructed to introduce noise at the right-boundary, $x \in [n, C]$.

B.2 An application of Algorithm 4.1 on network (3.52)

Network $\tilde{\mathcal{R}}^1(s_1, s_2, \bar{s}_2) \cup \mathcal{R}_1^2(\bar{s}_2) \cup (\mathcal{R}_{0,C_2-10}^3(s_2, \bar{s}_2) \cup \mathcal{R}_{30,0}^3(s_2, \bar{s}_2))$, obtained by an application of Algorithm 4.1 on network $\tilde{\mathcal{R}}$, given by (3.52), reads

$$
\begin{aligned}
\tilde{\mathcal{R}}^1(s_1, s_2, \bar{s}_2): \quad & \varnothing \xrightarrow{k_1} s_1, \\
& s_1 \xrightarrow{k_2} 2s_1, \\
& 2s_1 \xrightarrow{k_3} 3s_1, \\
& s_1 + s_2 \xrightarrow{k_4} s_2, \\
& 2s_1 + s_2 \xrightarrow{k_5} s_1 + s_2, \\
& s_1 + 2s_2 \xrightarrow{k_6} 2s_1 + 2s_2, \\
& \bar{s}_2 + I_2^1 \xrightarrow{k_7} s_2 + I_2^1, \\
& s_2 \xrightarrow{k_8} \bar{s}_2, \\
& s_1 + s_2 + \bar{s}_2 + I_2^1 \xrightarrow{k_9} s_1 + 2s_2 + I_2^1, \\
& 2s_2 + \bar{s}_2 + I_2^1 \xrightarrow{k_{10}} 3s_2 + I_2^1, \\
& 3s_2 \xrightarrow{k_{11}} 2s_2 + \bar{s}_2, \\
\mathcal{R}_1^2(\bar{s}_2): \quad & \varnothing \xrightarrow{1/\mu} I_2^1, \\
& \bar{s}_2 + I_2^1 \xrightarrow{1/\mu} \bar{s}_2,
\end{aligned}
$$

$$
\begin{aligned}
\mathcal{R}^3_{0,C_2-10}(s_2,\bar{s}_2): \qquad & (C_2-10)\bar{s}_2 \xrightarrow{k^2_{0,C_2-10}} s_2+(C_2-11)\bar{s}_2,\\
& C_2s_2+B_2 \xrightarrow{k^2_{0,C_2-10}} (C_2-1)s_2+\bar{s}_2+B_2,\\
& (C_2-10)\bar{s}_2 \xrightarrow{1/\mu_{0,C_2-10}} (C_2-10)\bar{s}_2+B_2,\\
& C_2s_2+B_2 \xrightarrow{1/\mu_{0,C_2-10}} C_2s_2,\\
\mathcal{R}^3_{30,0}(s_2,\bar{s}_2): \qquad & 30s_2 \xrightarrow{k^2_{30,0}} 29s_2+\bar{s}_2,\\
& C_2\bar{s}_2+\bar{B}_2 \xrightarrow{k^2_{30,0}} s_2+(C_2-1)\bar{s}_2+\bar{B}_2,\\
& 30s_2 \xrightarrow{1/\mu_{30,0}} 30s_2+\bar{B}_2,\\
& C_2\bar{s}_2+\bar{B}_2 \xrightarrow{1/\mu_{30,0}} C_2\bar{s}_2. \qquad \text{(B.3)}
\end{aligned}
$$

Appendix C

Supplementary material for Chapter 5

C.1 Proof of Theorem 5.1

Let $\mathbf{x} = (x_1, \ldots, x_m, x_{m+1}, \ldots, x_N) \in \mathbb{Z}_{\geq}^N$ be the vector of copy-numbers of the species $s_1, \ldots, s_N$, and $\mathbf{y} = (y_1, \ldots, y_{n-2}) \in \mathbb{Z}_{\geq}^{n-2}$ the copy-number vector of the auxiliary species $Q_1, \ldots, Q_{n-2}$ from the output network (5.31)–(5.32). Let us introduce new variables $\bar{\mathbf{x}} = (\bar{x}_1, \ldots, \bar{x}_m, x_{m+1}, \ldots, x_N) \in \mathbb{Z}_{\geq}^N$ as follows: if there is only one distinct reactant species in the input network (5.30), $m = 1$, then

$$\bar{x}_l = \begin{cases} x_1 + \sum_{i=1}^{n-2}(i+1)y_i, & \text{if } l = 1, \\ x_l, & \text{if } l \neq 1. \end{cases} \tag{C.1}$$

On the other hand, if $m \geq 2$, then

$$\bar{x}_l = \begin{cases} x_1 + \sum_{i=1}^{\nu_1} i y_i + \sum_{i=\nu_1+1}^{n-2} \nu_1 y_i, & \text{if } l = 1, \\ x_2 + \sum_{i=1}^{\nu_1} y_i + \sum_{i=\nu_1+1}^{\nu_1+\nu_2-1}(i - \nu_1 + 1)y_i + \sum_{i=\nu_1+\nu_2}^{n-2} \nu_2 y_i, & \text{if } l = 2, \text{ and } m \neq 2, \\ x_l + \sum_{i=\sum_{j=1}^{l-1}\nu_j}^{\sum_{j=1}^{l}\nu_j - 1}(i - \sum_{j=1}^{l-1}\nu_j + 1)y_i + \sum_{i=\sum_{j=1}^{l}\nu_j}^{n-2} \nu_l y_i, & \text{if } l = 3, \ldots, m-1, \\ x_m + \delta_{m,2}\sum_{i=1}^{\nu_1} y_i + \sum_{i=\sum_{j=1}^{m-1}\nu_j + \delta_{m,2}}^{n-2}(i - \sum_{j=1}^{m-1}\nu_j + 1)y_i, & \text{if } l = m. \end{cases} \tag{C.2}$$

In what follows, for mathematical convenience, we define the fast network

$$\begin{aligned} \mathcal{R}_0^{\varepsilon}: \quad & Q_1 \xrightarrow{\frac{1}{\varepsilon}} s_l + s_r, \\ & Q_i \xrightarrow{\frac{1}{\varepsilon}} s_l + Q_{i-1}, \quad i \in [2, n-2] \cap \mathbb{Z}. \end{aligned} \tag{C.3}$$

The CME corresponding to (5.31)–(5.32), rescaled in time according to $t = \tau/\varepsilon^{n-2}$, and expressed in terms of the new variables $\bar{\mathbf{x}}$, is given by

$$\frac{\partial}{\partial t} p_\varepsilon(\bar{\mathbf{x}}, \mathbf{y}, \tau) = \left(\frac{1}{\varepsilon^{n-1}} \mathcal{L}_0 + \frac{1}{\varepsilon^{n-2}} \mathcal{L}_1 \right) p_\varepsilon(\bar{\mathbf{x}}, \mathbf{y}, \tau), \tag{C.4}$$

where $\mathcal{L}_0$ is the forward operator of network $\mathcal{R}_0^1$ in the new coordinates, given by

$$\mathcal{L}_0 = \sum_{i=1}^{n-2} \mathcal{L}_0^i, \qquad \mathcal{L}_0^i = \left(E_{y_{i-1}}^{-1} E_{y_i}^{+1} - 1 \right) y_i, \;\; i = 1, \ldots, n-2, \tag{C.5}$$

while $\mathcal{L}_1$ is the forward operator of the slow subnetwork $\mathcal{R}_\varepsilon \setminus \mathcal{R}_0^\varepsilon$, and reads

$$\begin{aligned} \mathcal{L}_1 &= \sum_{i=1}^{n-1} \mathcal{L}_1^i, \qquad \mathcal{L}_1^i = \left(E_{y_{i-1}}^{+1} E_{y_i}^{-1} - 1 \right) y_{i-1} \alpha_i(\bar{\mathbf{x}}, \mathbf{y}), \quad i = 1, \ldots, n-2, \\ \mathcal{L}_1^{n-1} &= \left(E_{\bar{\mathbf{x}}}^{-\Delta \bar{\mathbf{x}}} E_{y_{n-2}}^{-\Delta y_{n-2}} - 1 \right) y_{n-2} \alpha_{n-1}(\bar{\mathbf{x}}, \mathbf{y}). \end{aligned} \tag{C.6}$$

Here, we take the convention that $y_0 \equiv 1$, and that the operators $E_{y_0}^{\pm 1}$ are identity operators, denoted $E_{y_0}^{\pm 1} \equiv 1$. Function $y_{i-1}\alpha_i(\bar{\mathbf{x}}, \mathbf{y})$, $i = 1, \ldots, n-1$, is the propensity function of the forward reaction in the subnetwork $\mathcal{R}_i^\varepsilon$, $i = 1, \ldots, n-2$, and $\mathcal{R}_{n-1}$, from (5.32), expressed in terms of the new variables (C.1)–(C.2). Let us note that $\mathcal{L}_1^{n-1}$ is the only operator which acts on the variable $\bar{\mathbf{x}}$, while the rest of the operators act only on $\mathbf{y}$.

It follows from (5.32) that $\Delta y_{n-2} = \bar{\gamma}_{n-2} - 1$. On the other hand, jump size vector $\Delta \bar{\mathbf{x}}$ is obtained by formally applying the difference operator Δ on (C.2). Since $\Delta y_i = 0$ for $i \neq (n-2)$, one readily obtains

$$\begin{aligned} \Delta \bar{x}_l &= \Delta x_l + (\nu_l - \delta_{l,m}) \Delta y_{n-2} \\ &= (\tilde{\nu}_l - \delta_{l,m}) + (\nu_l - \delta_{l,m})(\bar{\gamma}_{n-2} - 1), \quad l \in \{1, 2, \ldots, m\}. \end{aligned} \tag{C.7}$$

Let us write the solution of (C.4) as the perturbation series

$$p_\varepsilon(\bar{\mathbf{x}}, \mathbf{y}, \tau) = \sum_{i=0}^{n-1} \varepsilon^i p_i(\bar{\mathbf{x}}, \mathbf{y}, \tau) + \ldots. \tag{C.8}$$

Substituting (C.8) into (C.4), and equating terms of equal powers in ε, the following system of n equations is obtained:

$$\begin{aligned} \mathcal{O}\left(\frac{1}{\varepsilon^{n-i}} \right) &: \; \mathcal{L}_0 p_{i-1}(\bar{\mathbf{x}}, \mathbf{y}, \tau) = -\mathcal{L}_1 p_{i-2}(\bar{\mathbf{x}}, \mathbf{y}, \tau), \quad i = 1, \ldots, n-1, \\ \mathcal{O}(1) &: \; \mathcal{L}_0 p_{n-1}(\bar{\mathbf{x}}, \mathbf{y}, \tau) = \frac{\partial}{\partial \tau} p_0(\bar{\mathbf{x}}, \mathbf{y}, \tau) - \mathcal{L}_1 p_{n-2}(\bar{\mathbf{x}}, \mathbf{y}, \tau), \end{aligned} \tag{C.9}$$

with the convention that $p_{-1}(\bar{\mathbf{x}}, \mathbf{y}, \tau) \equiv 0$.

Order $1/\varepsilon^{n-1}$ equation. Operator $\mathcal{L}_0$, given in (C.5), acts only on the variable $\mathbf{y}$, and each summand $\mathcal{L}_0^i$ is multiplied on the right by a factor y_i. It follows that $p_0(\bar{\mathbf{x}}, \mathbf{y}, \tau) = p_0(\mathbf{y}, \tau) p_0(\bar{\mathbf{x}}, \tau)$, so that the equation becomes $\mathcal{L}_0 p_0(\mathbf{y}, \tau) = 0$. Operator

$\mathcal{L}_0$ has a one-dimensional null-space, $\mathcal{N}(\mathcal{L}_0) = \{1_{\mathbf{y}} \prod_{i=1}^{n-2} \delta_{y_i,0}\}$, where $1_{\mathbf{y}}$ is a function independent of $\mathbf{y}$. A normalized element of the null-space is given by

$$p_0(\bar{\mathbf{x}}, \mathbf{y}, \tau) = p_0(\bar{\mathbf{x}}, \tau) \prod_{i=1}^{n-2} \delta_{y_i,0}, \qquad \sum_{\bar{\mathbf{x}}} p_0(\bar{\mathbf{x}}, \tau) = 1, \ \text{ for } \tau \geq 0. \tag{C.10}$$

Order $1/\varepsilon^{n-2}$ equation. Since each summand $\mathcal{L}_1^i$, $i = 2, \ldots, n-1$, from (C.6) is multiplied on the right by a nonconstant factor y_{i-1}, equation (C.10) implies

$$\mathcal{L}_1 p_0(\bar{\mathbf{x}}, \mathbf{y}, \tau) = p_0(\bar{\mathbf{x}}, \tau) \prod_{i=2}^{n-2} \delta_{y_i,0} \mathcal{L}_1^1 \delta_{y_1,0}. \tag{C.11}$$

The null-space of the backward operator is given by $\mathcal{N}(\mathcal{L}_0^*) = \{1_{\mathbf{y}}\}$, and the solvability condition is $0 = \langle 1_{\mathbf{y}}, \mathcal{L}_1 p_0(\bar{\mathbf{x}}, \mathbf{y}, \tau)\rangle = \langle (\mathcal{L}_1^1)^* 1_{\mathbf{y}}, p_0(\bar{\mathbf{x}}, \tau) \prod_{i=1}^{n-2} \delta_{y_i,0}\rangle$, where $(\mathcal{L}_1^1)^* = \alpha_1(\bar{\mathbf{x}}, \mathbf{y})(E_{y_1}^{+1} - 1)$ and $\langle f, g\rangle = \sum_{\mathbf{y}} f(\mathbf{y}) g(\mathbf{y})$. Since $(\mathcal{L}_1^1)^* 1_{\mathbf{y}} = 0$, the solvability condition is unconditionally satisfied.

Let us write the solution of the $\mathcal{O}(1/\varepsilon^{n-2})$ equation from (C.9) in the separable form

$$p_1(\bar{\mathbf{x}}, \mathbf{y}, \tau) = p_0(\bar{\mathbf{x}}, \tau) p_1(y_1;\, \bar{\mathbf{x}}) \prod_{i=2}^{n-2} \delta_{y_i,0}. \tag{C.12}$$

Substituting (C.12) into the $\mathcal{O}(1/\varepsilon^{n-2})$ equation, using (C.11) and

$$\mathcal{L}_0 p_1(\bar{\mathbf{x}}, \mathbf{y}, \tau) = p_0(\bar{\mathbf{x}}, \tau) \prod_{i=2}^{n-2} \delta_{y_i,0} \mathcal{L}_0^1 p_1(y_1;\, \bar{\mathbf{x}}),$$

and the operator equality $(E_{y_1}^{-1} - 1) = -(E_{y_1}^{+1} - 1) E_{y_1}^{-1}$, one obtains

$$\prod_{i=2}^{n-2} \delta_{y_i,0} (E_{y_1}^{+1} - 1) \left(y_1 p_1(y_1;\, \bar{\mathbf{x}}) - E_{y_1}^{-1} \alpha_1(\bar{\mathbf{x}}, \mathbf{y}) \delta_{y_1,0} \right) = 0. \tag{C.13}$$

Equation (C.13) is identically satisfied if $(y_2, y_3, \ldots, y_{n-2}) \neq \mathbf{0}_{n-3}$, where $\mathbf{0}_n$ is the zero element of $\mathbb{Z}_{\geq}^n$. On the other hand, if $(y_2, y_3, \ldots, y_{n-2}) = \mathbf{0}_{n-3}$, it follows that the solutions satisfy

$$y_1 p_1(y_1;\, \bar{\mathbf{x}}) = E_{y_1}^{-1} \alpha_1 \left(\bar{\mathbf{x}}, (y_1, \mathbf{0}_{n-3}) \right) \delta_{y_1,0}. \tag{C.14}$$

Order $1/\varepsilon^{n-3}$ equation. It follows from (C.6) and (C.12) that

$$\mathcal{L}_1 p_1(\bar{\mathbf{x}}, \mathbf{y}, \tau) = p_0(\bar{\mathbf{x}}, t) \prod_{i=3}^{n-2} \delta_{y_i,0} \left(\mathcal{L}_1^1 + \mathcal{L}_1^2 \right) p_1(y_1;\, \bar{\mathbf{x}}) \delta_{y_2,0}, \tag{C.15}$$

and the solvability condition $0 = \langle 1_{\mathbf{y}}, \mathcal{L}_1 p_1(\bar{\mathbf{x}}, \mathbf{y}, \tau)\rangle$ is unconditionally satisfied, since $(\mathcal{L}_1^1 + \mathcal{L}_1^2)^* 1_{\mathbf{y}} = 0$.

Let us write the solution of the $\mathcal{O}(1/\varepsilon^{n-3})$ equation from (C.9) in the separable form

$$p_2(\bar{\mathbf{x}}, \mathbf{y}, \tau) = p_0(\bar{\mathbf{x}}, \tau) p_2(y_1, y_2; \bar{\mathbf{x}}) \prod_{i=3}^{n-2} \delta_{y_i,0}. \tag{C.16}$$

Substituting (C.16) into the $\mathcal{O}(1/\varepsilon^{n-3})$ equation, using (C.15) and

$$\mathcal{L}_0 p_2(\bar{\mathbf{x}}, \mathbf{y}, \tau) = p_0(\bar{\mathbf{x}}, \tau) \prod_{i=3}^{n-2} \delta_{y_i,0} \left(\mathcal{L}_0^1 + \mathcal{L}_0^2\right) p_2(y_1, y_2; \bar{\mathbf{x}}),$$

and the operator equalities $(E_{y_1}^{-1} - 1) = -(E_{y_1}^{+1} - 1)E_{y_1}^{-1}$, $(E_{y_1}^{+1}E_{y_2}^{-1} - 1) = -(E_{y_1}^{-1}E_{y_2}^{+1} - 1)E_{y_1}^{+1}E_{y_2}^{-1}$, one obtains

$$\begin{aligned} 0 = &\prod_{i=3}^{n-2} \delta_{y_i,0}(E_{y_1}^{+1} - 1) \left[y_1 p_2(y_1, y_2; \bar{\mathbf{x}}) - E_{y_1}^{-1}\alpha_1(\bar{\mathbf{x}}, \mathbf{y})\delta_{y_2,0} p_1(y_1; \bar{\mathbf{x}})\right] \\ &+ \prod_{i=3}^{n-2} \delta_{y_i,0}(E_{y_1}^{-1}E_{y_2}^{+1} - 1) \left[y_2 p_2(y_1, y_2; \bar{\mathbf{x}}) - E_{y_1}^{+1}E_{y_2}^{-1}\alpha_2(\bar{\mathbf{x}}, \mathbf{y})\delta_{y_2,0} y_1 p_1(y_1; \bar{\mathbf{x}})\right]. \end{aligned} \tag{C.17}$$

Equation (C.17) is identically satisfied if $(y_3, y_4, \ldots, y_{n-2}) \neq \mathbf{0}_{n-4}$. On the other hand, if $(y_3, y_4, \ldots, y_{n-2}) = \mathbf{0}_{n-4}$, the solutions satisfy

$$y_1 p_2(y_1, y_2; \bar{\mathbf{x}}) = E_{y_1}^{-1}\alpha_1\left(\bar{\mathbf{x}}, (y_1, y_2, \mathbf{0}_{n-4})\right) \delta_{y_2,0} p_1(y_1; \bar{\mathbf{x}}), \tag{C.18}$$

and

$$\begin{aligned} y_2 p_2(y_1, y_2; \bar{\mathbf{x}}) &= E_{y_1}^{+1}E_{y_2}^{-1}\alpha_2\left(\bar{\mathbf{x}}, (y_1, y_2, \mathbf{0}_{n-4})\right) \delta_{y_2,0}\left(y_1 p_1(y_1; \bar{\mathbf{x}})\right) \\ &= E_{y_1}^{+1}E_{y_2}^{-1}\alpha_2\left(\bar{\mathbf{x}}, (y_1, y_2, \mathbf{0}_{n-4})\right) \delta_{y_2,0}\left(E_{y_1}^{-1}\alpha_1\left(\bar{\mathbf{x}}, (y_1, \mathbf{0}_{n-3})\right) \delta_{y_1,0}\right) \\ &= \delta_{y_1,0}\alpha_1\left(\bar{\mathbf{x}}, (y_1, \mathbf{0}_{n-3})\right) E_{y_1}^{+1}E_{y_2}^{-1}\alpha_2\left(\bar{\mathbf{x}}, (y_1, y_2, \mathbf{0}_{n-4})\right) \delta_{y_2,0}, \end{aligned} \tag{C.19}$$

where we have used (C.14) when going from the first to the second line in (C.19).

Order $1/\varepsilon^{n-i}$ equation, $i = 3, 4, \ldots, n-1$. One can inductively proceed to the higher-order equations from (C.9), with solutions of the $\mathcal{O}(1/\varepsilon^{n-i})$ equation written in the separable form

$$p_{i-1}(\bar{\mathbf{x}}, \mathbf{z}, t) = p_0(\bar{\mathbf{x}}, t) p_{i-1}(z_1, \ldots, z_{i-1}; \bar{\mathbf{x}}) \prod_{j=i}^{n-2} \delta_{z_j,0}, \quad i = 1, \ldots, n-1, \tag{C.20}$$

with the convention that $\prod_{i=a}^{b} f(i) = 1$ if $a > b$, where $f(i)$ is an arbitrary function of i, and $p_0(z_0;\, \bar{\mathbf{x}}) \equiv 1$ (see also equations (C.10), (C.12) and (C.16)). It can be readily shown that the results (C.14) and (C.19) generalize to

$$y_i p_i(y_1, \ldots, y_i;\, \bar{\mathbf{x}}) = \left(\prod_{j=1}^{i-1} \delta_{y_j,0} E_{y_{j-1}}^{+1} \alpha_j \left(\bar{\mathbf{x}}, (y_1, \ldots, y_j, \mathbf{0}_{n-2-j}) \right) \right) \times E_{y_{i-1}}^{+1} E_{y_i}^{-1} \alpha_i(\bar{\mathbf{x}}, (y_1, \ldots, y_i, \mathbf{0}_{n-2-i})) \delta_{y_i,0}, \quad i = 1, \ldots, n-2. \tag{C.21}$$

As is shortly shown, the effective CME, at the order one, depends on p_{n-2} only via the product $y_{n-2}p_{n-2}$ satisfying (C.21); see equation (C.23).

Order 1 *equation.* The solvability condition is given by $0 = \langle 1, \partial/\partial\tau p_0(\bar{\mathbf{x}}, \mathbf{y}, \tau)\rangle - \langle 1, \mathcal{L}_1 p_{n-2}(\bar{\mathbf{x}}, \mathbf{y}, \tau)\rangle$. Equation (C.10) implies $\langle 1, \partial/\partial\tau p_0(\bar{\mathbf{x}}, \mathbf{y}, \tau)\rangle = \frac{\partial}{\partial\tau} p_0(\bar{\mathbf{x}}, \tau)$. On the other hand, using (C.6), and the fact that $(\sum_{i=1}^{n-2} \mathcal{L}_1^i)^* 1 = 0$, imply that $\langle 1, \mathcal{L}_1 p_{n-2}(\bar{\mathbf{x}}, \mathbf{y}, \tau)\rangle = \langle 1, \mathcal{L}_1^{n-1} p_{n-2}(\bar{\mathbf{x}}, \mathbf{y}, \tau)\rangle$, so that the solvability condition becomes

$$\frac{\partial}{\partial\tau} p_0(\bar{\mathbf{x}}, \tau) = \langle 1, \mathcal{L}_1^{n-1} p_{n-2}(\bar{\mathbf{x}}, \mathbf{y}, \tau)\rangle. \tag{C.22}$$

Let us simplify the RHS from (C.22):

$$\begin{aligned}
\langle 1, \mathcal{L}_1^{n-1} p_{n-2}(\bar{\mathbf{x}}, \mathbf{y}, \tau)\rangle &= \langle 1, \left(E_{\bar{\mathbf{x}}}^{-\Delta\bar{\mathbf{x}}} E_{y_{n-2}}^{-\Delta y_{n-2}} - 1 \right) \alpha_{n-1}(\bar{\mathbf{x}}, \mathbf{y}) y_{n-2} p_{n-2}(\bar{\mathbf{x}}, \mathbf{y}, \tau)\rangle \\
&= \langle E_{y_{n-2}}^{+\Delta y_{n-2}} 1, E_{\bar{\mathbf{x}}}^{-\Delta\bar{\mathbf{x}}} \alpha_{n-1}(\bar{\mathbf{x}}, \mathbf{y}) y_{n-2} p_{n-2}(\bar{\mathbf{x}}, \mathbf{y}, \tau)\rangle \\
&\quad - \langle 1, \alpha_{n-1}(\bar{\mathbf{x}}, \mathbf{y}) y_{n-2} p_{n-2}(\bar{\mathbf{x}}, \mathbf{y}, \tau)\rangle \\
&= \langle 1, \left(E_{\bar{\mathbf{x}}}^{-\Delta\bar{\mathbf{x}}} - 1 \right) \alpha_{n-1}(\bar{\mathbf{x}}, \mathbf{y}) y_{n-2} p_{n-2}(\bar{\mathbf{x}}, \mathbf{y}, \tau)\rangle \\
&= \left(E_{\bar{\mathbf{x}}}^{-\Delta\bar{\mathbf{x}}} - 1 \right) p_0(\bar{\mathbf{x}}, \tau) \langle 1, \alpha_{n-1}(\bar{\mathbf{x}}, \mathbf{y}) y_{n-2} p_{n-2}(\mathbf{y};\, \bar{\mathbf{x}})\rangle
\end{aligned} \tag{C.23}$$

where, when going to the last line, we use $p_{n-2}(\bar{\mathbf{x}}, \mathbf{y}, \tau) = p_0(\bar{\mathbf{x}}, \tau) p_{n-2}(\mathbf{y};\, \bar{\mathbf{x}})$. Hence, the effective CME depends on the p_{n-2} only via the product $y_{n-2}p_{n-2}$. Using (C.21)

with $i = n-2$, one obtains

$$\begin{aligned}\langle 1, \alpha_{n-1}(\bar{\mathbf{x}}, \mathbf{y}) y_{n-2} p_{n-2}(\mathbf{y};\, \bar{\mathbf{x}})\rangle &= \langle \alpha_{n-1}(\bar{\mathbf{x}}, \mathbf{y}) \left(\prod_{j=1}^{n-3} \delta_{y_j,0} E^{+1}_{y_{j-1}} \alpha_j \left(\bar{\mathbf{x}}, (y_1, \ldots, y_j, \mathbf{0}_{n-2-j})\right)\right), \\ &\quad E^{+1}_{y_{n-3}} E^{-1}_{y_{n-2}} \alpha_{n-2}(\bar{\mathbf{x}}, \mathbf{y}) \delta_{y_{n-2},0}\rangle \\ &= \langle E^{+1}_{y_{n-2}} \alpha_{n-1}(\bar{\mathbf{x}}, \mathbf{y}) \left(\prod_{j=1}^{n-3} \delta_{y_j,0} E^{+1}_{y_{j-1}} \alpha_j \left(\bar{\mathbf{x}}, (y_1, \ldots, y_j, \mathbf{0}_{n-2-j})\right)\right), \\ &\quad E^{+1}_{y_{n-3}} \alpha_{n-2}(\bar{\mathbf{x}}, \mathbf{y}) \delta_{y_{n-2},0}\rangle \\ &= \langle 1, \left(\prod_{j=1}^{n-2} \delta_{y_j,0} \right) \left(\prod_{j=1}^{n-3} E^{+1}_{y_{j-1}} \alpha_j \left(\bar{\mathbf{x}}, (y_1, \ldots, y_j, \mathbf{0}_{n-2-j})\right)\right) \\ &\quad \left(E^{+1}_{y_{n-3}} \alpha_{n-2}(\bar{\mathbf{x}}, \mathbf{y})\right) \left(E^{+1}_{y_{n-2}} \alpha_{n-1}(\bar{\mathbf{x}}, \mathbf{y})\right)\rangle \\ &= \prod_{j=1}^{n-1} \alpha_j \left(\bar{\mathbf{x}}, (\mathbf{0}_{j-2}, 1, \mathbf{0}_{n-(j+1)})\right), \end{aligned} \tag{C.24}$$

with the convention that $\alpha_1(\bar{\mathbf{x}}, (\mathbf{0}_{-1}, 1, \mathbf{0}_{n-2})) \equiv \alpha_1(\bar{\mathbf{x}}, \mathbf{0}_{n-2})$, $\alpha_2(\bar{\mathbf{x}}, (\mathbf{0}_0, 1, \mathbf{0}_{n-3})) \equiv \alpha_2(\bar{\mathbf{x}}, (1, \mathbf{0}_{n-3}))$, and $\alpha_{n-1}(\bar{\mathbf{x}}, (\mathbf{0}_{n-3}, 1, \mathbf{0}_0)) \equiv \alpha_{n-1}(\bar{\mathbf{x}}, (\mathbf{0}_{n-3}, 1))$. In words, propensity function α_j is evaluated at $y_{j-1} = 1$, and $y_i = 0$ for $i \neq (j-1)$ in (C.24).

Now, if $m = 1$, using (C.1), it follows that $\alpha_1(x_1, \mathbf{0}_{n-2}) = \kappa_1 \bar{x}_1(\bar{x}_1 - 1)$, and $\alpha_j\left(\bar{x}_1, (\mathbf{0}_{j-2}, 1, \mathbf{0}_{n-(j+1)})\right) = \kappa_j(\bar{x}_1 - j)$, $j = 2, \ldots, n-1$. Hence, in this case,

$$\prod_{j=1}^{n-1} \alpha_j \left(\bar{\mathbf{x}}, (\mathbf{0}_{j-2}, 1, \mathbf{0}_{n-(j+1)})\right) = \left(\prod_{j=1}^{n-1} \kappa_j \right) \bar{x}_1^{\underline{n}}, \quad \text{if } m = 1. \tag{C.25}$$

Similarly, in the case $m \geq 2$, using (C.2), one obtains

$$\prod_{j=1}^{n-1} \alpha_j \left(\bar{\mathbf{x}}, (\mathbf{0}_{j-2}, 1, \mathbf{0}_{n-(j+1)})\right) = \left(\prod_{j=1}^{n-1} \kappa_j \right) \prod_{l=1}^{m} \bar{x}_l^{\underline{\nu_l}}, \quad \text{if } m \geq 2. \tag{C.26}$$

Substituting (C.23)–(C.26) into (C.22), and changing the time back to the original scale, $\tau = \varepsilon^{n-2} t$, one obtains the effective CME

$$\frac{\partial}{\partial t} p_0(\bar{\mathbf{x}}, t) = \left(E^{-\Delta \bar{\mathbf{x}}}_{\bar{\mathbf{x}}} - 1\right) \left(\varepsilon^{n-2} \prod_{j=1}^{n-1} \kappa_j \right) \prod_{l=1}^{m} \bar{x}_l^{\underline{\nu_l}} p_0(\bar{\mathbf{x}}, t). \tag{C.27}$$

In order for the effective CME (C.27) to match the CME of the input network (5.30), we firstly require that the stoichiometric vectors of the input and output networks are the same: $\Delta \bar{x}_l = (\bar{\nu}_l - \nu_l)$, which, using (C.7), gives the stoichiometric conditions (5.33). And, secondly, we require that the effective propensity function is equal

to the propensity function of the input network, $\alpha_{\text{eff}}(\mathbf{x}) = \varepsilon^{n-2}\prod_{j=1}^{n-1}\kappa_j\prod_{l=1}^{m}x_l^{\nu_l} = \alpha(\mathbf{x}) = k\prod_{l=1}^{m}x_l^{\nu_l}$, which results in the kinetic condition (5.34).

Assuming convergence of the perturbation series (C.8), it follows from (C.10) that the time-dependent copy-number vector $\mathbf{Y}(t) \in \mathbb{Z}_{\geq}^{n-2}$ converges weakly (in distribution) to $\mathbf{0} \in \mathbb{Z}_{\geq}^{n-2}$ (a deterministic variable), and hence it also converges to zero in probability. It then follows from (C.1)–(C.2) that $\bar{\mathbf{X}}(t)$ converges to $\mathbf{X}(t)$ in probability as $\varepsilon \to 0$, and so we may replace $\bar{\mathbf{x}}$ by $\mathbf{x}$ in (C.27), ensuring that the effective CME tracks copy-numbers of the species $s_1, \ldots, s_N$.

C.2 Proof of Theorem 5.2

Consider the the output network (5.31)–(5.32), satisfying the kinetic condition (5.34) with the rate coefficients satisfying (5.35), whose CME is given by

$$\frac{\partial}{\partial t}p_\varepsilon(\bar{\mathbf{x}},\mathbf{y},t) = \left(\frac{1}{\varepsilon}\mathcal{L}_0 + \frac{1}{\varepsilon^{\frac{n-2}{n-1}}}\mathcal{L}_1\right)p_\varepsilon(\bar{\mathbf{x}},\mathbf{y},t). \tag{C.28}$$

Here, the operators $\mathcal{L}_0$ and $\mathcal{L}_1$ have the form (C.5)–(C.6), and involve rate coefficients which are $\mathcal{O}(1)$ with respect to ε. In what follows, we assume the state-space for (C.28) is bounded.

Let us write the solution $p_\varepsilon(\bar{\mathbf{x}},\mathbf{y},t)$ in the following form:

$$p_\varepsilon(\bar{\mathbf{x}},\mathbf{y},t) = \sum_{i=0}^{n-1}\varepsilon^{\frac{i}{n-1}}p_i(\bar{\mathbf{x}},\mathbf{y},t) + r_n(\bar{\mathbf{x}},\mathbf{y},t), \tag{C.29}$$

with $p_i(\bar{\mathbf{x}},\mathbf{y},t)$, $i = 1,2,\ldots,n-1$, satisfying (C.9). As shown in Section C.1, there are infinitely many solutions $p_i(\bar{\mathbf{x}},\mathbf{y},t)$ for each fixed i (see equations (C.20)–(C.21)), and we now chose those that are bounded, with bounded time-derivatives. Substituting (C.29) into (C.28), using (C.9), and writing $p_i(t) = p_i(\bar{\mathbf{x}},\mathbf{y},t)$, $r_n(t) = r_n(\bar{\mathbf{x}},\mathbf{y},t)$ and $\mathcal{L}_\varepsilon \equiv (\varepsilon^{-1}\mathcal{L}_0 + \varepsilon^{-(n-2)/(n-1)}\mathcal{L}_1)$, one obtains an equation governing the time-evolution of the error function $r_n(t)$:

$$\frac{\partial}{\partial t}r_n(t) = \left(\frac{1}{\varepsilon}\mathcal{L}_0 + \frac{1}{\varepsilon^{\frac{n-2}{n-1}}}\mathcal{L}_1\right)r_n(t) + \varepsilon^{\frac{1}{n-1}}\left(\mathcal{L}_1 p_{n-1}(t) - \frac{\partial}{\partial t}p_1(t)\right) + \sum_{i=2}^{n-1}\varepsilon^{\frac{i}{n-1}}\frac{\partial}{\partial t}p_i(t). \tag{C.30}$$

The solution of the non-homogenous linear ODE (C.30) may be written as

$$\begin{aligned} r_n(t) = e^{\mathcal{L}_\varepsilon t}r_n(0) &+ \varepsilon^{\frac{1}{n-1}}\int_0^t e^{\mathcal{L}_\varepsilon(t-s)}\left(\mathcal{L}_1 p_{n-1}(s) - \frac{\partial}{\partial s}p_1(s)\right)\mathrm{d}s \\ &+ \sum_{i=2}^{n-1}\varepsilon^{\frac{i}{n-1}}\int_0^t e^{\mathcal{L}_\varepsilon(t-s)}\frac{\partial}{\partial s}p_i(s)\mathrm{d}s, \end{aligned} \tag{C.31}$$

where $r(t)$ and $p_i(t)$ are interpreted here as column vectors on the bounded state-space, and $e^{\mathcal{L}_\varepsilon t}$ is a matrix exponential. Let us assume $p_\varepsilon(0) = p_0(0)$, so that (C.29) implies an initial condition for the error function:

$$r_n(0) = -\sum_{i=1}^{n-1} \varepsilon^{\frac{i}{n-1}} p_i(0). \tag{C.32}$$

Let $\|\cdot\|_1$ denote the l^1-norm over the bounded state-spaces of $\bar{\mathbf{x}}$ and $\mathbf{y}$, as well as the induced matrix-operator norm. Applying the l^1-norm on (C.31), using the triangle inequality, and the fact that $\|e^{\mathcal{L}_\varepsilon t}\|_1 = 1$ [51], one obtains

$$\begin{aligned}\|r_n(t)\|_1 \leq \varepsilon^{\frac{1}{n-1}} \left(\|p_1(0)\|_1 + t \sup_{0\leq s\leq t} \|\mathcal{L}_1 p_{n-1}(s) - \frac{\partial}{\partial s} p_1(s)\|_1 \right) \\ + \sum_{i=2}^{n-1} \varepsilon^{\frac{i}{n-1}} \left(\|p_i(0)\|_1 + t \sup_{0\leq s\leq t} \|\frac{\partial}{\partial s} p_i(s)\|_1 \right).\end{aligned} \tag{C.33}$$

Hence, since $p_i(t)$ are chosen to be bounded, with bounded time-derivatives, for each fixed $t > 0$, the error function $r_n(t) \to 0$ as $\varepsilon \to 0$ for any fixed $t > 0$. It then follows from (C.29) that $p_\varepsilon \to p_0$ as $\varepsilon \to 0$. Since $p_0(\bar{\mathbf{x}}, \mathbf{y}, t) = p_0(\bar{\mathbf{x}}, t) \prod_{i=1}^{n-2} \delta_{y_i,0}$ (see equation (C.10)), it follows that the auxiliary species converge to zero, $\mathbf{Z}(t) \to \mathbf{0}$, and equations (C.1)–(C.2) imply $\bar{\mathbf{X}}(t) \to \mathbf{X}(t)$. For sufficiently small ε, the error is asymptotically given by $\|r_n(t)\|_1 = \mathcal{O}(\varepsilon^{\frac{1}{n-1}})$, so that (C.29) implies (5.36).

Bibliography

[1] Endy, D., 2005. Foundations for engineering biology *Nature*, **484**: 449–453.

[2] Andrianantoandro, E., Basu, S., Karig, D. K., Weiss, R., 2006. Synthetic biology: new engineering rules for an emerging discipline. *Molecular Systems Biology*, **2**: 2006.0028.

[3] Abil Z., Xiong X., Zhao H., 2015. Synthetic biology for therapeutic applications. *Molecular Pharmaceutics*, **12**(**2**): 322–331.

[4] Anderson, J. C., Clarke, E. J., Arkin, A. P., Voigt, C. A., 2006. Environmentally controlled invasion of cancer cells by engineered bacteria. *Journal of Molecular Biology*, **355**(**4**): 619–627.

[5] Benenson, Y., Gil, B., Ben-Dor, U., Adar, R., Shapiro, E., 2004. Autonomous molecular computer for logical control of gene expression. *Nature*, **429**: 423–429.

[6] Ro, D., Paradise, E. M., Ouellet, M., Fisher, K. J., Newman, K. L., Ndungu, J. M., et al., 2006. Production of the antimalarial drug precursor artemisinic acid in engineered yeast. *Nature*, **440**: 940–943.

[7] Westfall, P. J., Pitera, D. J., Lenihan, J. R., Eng, D., Woolard, F. X., Regentin, R., et al., 2012. Production of amorphadiene in yeast, and its conversion to dihydroartemisinic acid, precursor to the antimalarial agent artemisinin. *Proc. Natl Acad. Sci. USA*, **109**: E111–E118.

[8] Widmaier, D. M., Tullman-Ercek, D., Mirsky, E. A., Hill, R., Govindarajan, S., Minshull, J., et al., 2009. Engineering the salmonella type III secretion system to export spider silk monomers. *Molecular Systems Biology*, **355**(**309**).

[9] Sedlak, M., Ho, W. Y., 2004. Production of ethanol from cellulosic biomass hydrolysates using genetically engineered saccharomyces yeast capable of cofermenting glucose and xylose. *Applied Biochemistry and Biotechnology*, **114**(**1**): 403–416.

[10] Ball, P., 2005. Synthetic biology for nanotechnology. *Nanotechnology*, **16**: R1–R8.

[11] Jungmann, R., Renner, S., Simmel, F.C., 2008. From DNA nanotechnology to synthetic biology. *Applied Biochemistry and Biotechnology*, **2**(**2**): 99–109.

[12] Menezes, A. A., Cumbers, J., Hogan, J. A., Arkin, A. P., 2015. Towards synthetic biological approaches to resource utilization on space missions. *Journal of The Royal Society Interface*, **12**(**102**): 20140715.

[13] Elowitz, M. B., Leibler, S., 2000. A synthetic oscillatory network of transcriptional regulators. *Nature*, **403**: 335–338.

[14] Deamer, D., 2005. A giant step towards artificial life? *Trends in Biotechnology*, **23**(**7**): 336–338.

[15] Glass, J. I., Assad-Garcia, N., Alperovich, N., Yooseph, S., Lewis, M. R., Maruf, M., et al., 2006. Essential genes of a minimal bacterium. *Proceedings of the National Academy of Sciences*, **103**(**2**): 425–430.

[16] Gibson, D. G., Benders, G. A., Andrews-Pfannkoch, C., Denisova, E. A., Baden-Tillson, H., Zaveri, J., et al., 2008. Complete chemical synthesis, assembly, and cloning of a Mycoplasma genitalium genome. *Sciences STKE*, **319**(**5867**): 1215–1220.

[17] Gibson, D. G., 2010. Creation of a bacterial cell controlled by a chemically synthesized genome. *Science*, **329**(**5987**): 52–56.

[18] Gardner, T. S., Cantor, C. R., Collins, J. J., 2000. Construction of a genetic toggle switch in Escherichia coli. *Nature*, **403**: 339–342.

[19] You, L., Cox, Ill R. S., Weiss, R., Arnold, F. H., 2004. Programmed population control by cell-cell communication and regulated killing. *Nature*, **428**: 868–871.

[20] Feinberg, M. *Lectures on chemical reaction networks*. Delivered at the Mathematics Research Center, University of Wisconsin, 1979.

[21] Érdi, P., Tóth, J. *Mathematical models of chemical reactions. Theory and applications of deterministic and stochastic Models*. Manchester University Press, Princeton University Press, 1989.

[22] Anderson, D. F., Kurtz, T. G. *Stochastic analysis of biochemical systems*. Springer, 2015.

[23] Soloveichik, D., Seeling, G., Winfree E., 2010. DNA as a universal substrate for chemical kinetics. *Proceedings of the National Academy of Sciences*, **107**(**12**): 5393–5398.

[24] Cardelli L., 2013. Two-domain DNA strand displacement *Math. Struc. in Comp. Science*, **23**: 247–271.

[25] Srinivas, N., Parkin, J., Seeling, G., Winfree, E., Soloveichik D., 2017. Enzyme-free nucleic acid dynamical systems. *Science*, **358**: eaal2052.

[26] Chen, Y. J., Dalchau, N., Srinivas, N., Phillips, A., Cardelli, L., Soloveichik, D., Seelig, G., 2013. Programmable chemical controllers made from DNA. *Nature Nanotechnology*, **8**: 755–762.

[27] Hasatani, K., Leocmach, M., Genot, A. J., Estévez-Torres, A., Fujii, T., Rondelez, Y., 2013. High-throughput and long-term observation of compartmentalized biochemical oscillators. *ChemComm*, **49**: 8090–8092.

[28] Weitz, M., Kim, J., Kapsner, K., Winfree, E., Franco, E., Simmel, F. C., 2014. Diversity in the dynamical behaviour of a compartmentalized programmable biochemical oscillator. *Nature Chemistry*, **6**: 295–302.

[29] Genot, A. J., Baccouche, A., Sieskind, R., Aubert-Kato, N., Bredeche, N., Bartolo, J. F., et al., 2016. High-resolution mapping of bifurcations in nonlinear biochemical circuits. *Nature Chemistry*, 10.1038/nchem.2544.

[30] Van Kampen, N. G. *Stochastic processes in physics and chemistry*. Elsevier, 2007.

[31] Gillespie, D. T., 1976. A general method for numerically simulating the stochastic time evolution of coupled chemical reactions. *Journal of Computational Physics*, **22**: 403–434.

[32] Gillespie, D. T., 1977. Exact stochastic simulation of coupled chemical reactions. *Journal of Physical Chemistry*, **81**(25): 2340–2361.

[33] Vilar, J. M. G., Kueh, H. Y., Barkai, N., Leibler S., 2002. Mechanisms of noise-resistance in genetic oscillators. *Proceedings of the National Academy of Sciences*, **99**(**9**): 5988–5992.

[34] Dublanche, Y., Michalodimitrakis, K., Kummerer, N., Foglierini, M., Serrano L., 2006. Noise in transcription negative feedback loops: simulation and experimental analysis. *Molecular Systems Biology*, **2**(**41**): E1–E12.

[35] Erban, R., Chapman, S. J., Kevrekidis, I. and Vejchodsky, T., 2009. Analysis of a stochastic chemical system close to a SNIPER bifurcation of its mean-field model. *SIAM Journal on Applied Mathematics*, **70**(**3**): 984–1016.

[36] Yates, C., Erban, R., Escudero, C., Couzin, I., Buhl, J., Kevrekidis, I., et al., 2009. Inherent noise can facilitate coherence in collective swarm motion. *Proceedings of the National Academy of Sciences*, **106**(**14**): 5464–5469.

[37] Duncan, A., Liao, S., Vejchodsḱy, T., Erban, R., Grima, R., 2015. Noise-Induced Multistability in Chemical Systems: Discrete vs Continuum Modelling. *Physical Review E*, **91**: 042111.

[38] Kurtz, T. G., 1972. The relationship between stochastic and deterministic models for chemical reactions. *Journal of Chemical Physics*, **57**: 2976–2978.

[39] Plesa, T., and Zygalakis, K. C., Anderson, D. F., and Erban, R., 2018. Noise control for molecular computing. *Journal of the Royal Society Interface*, **15**(**144**): 20180199.

[40] Fujii, T., Rondelez, Y., 2013. Predator-prey molecular ecosystems. *ACS Nano*, **7**: 27–34.

[41] Šulc, P., Ouldridge, T. E., Romano, F., Doye, J. P. K., Louis, A. A., 2015. Modelling toehold-mediated RNA strand displacement. *Biophysical Journal*, **108**: 1238–1247.

[42] Homann, M., Nedbal, W., and Sczakiel, G., 1996. Dissociation of long-chain duplex RNA can occur via strand displacement in vitro: biological implications. *Nucleic Acids Research*, **24**: 4395–4400.

[43] Gilbert, W., 1986. Origin of life: the RNA world. *Nature*, **319**: 618.

[44] Teichmann, M., Kopperger, E., Simmel, F. C., 2014. Robustness of localized DNA strand displacement cascades. *ACS Nano*, **8**: 8487–8496.

[45] Chatterjee, G., Dalchau, N., Muscat, R. A., Phillips, A., Seelig G., 2017. A spatially localized architecture for fast and modular DNA computing. *Nature nanotechnology*, **12**: 920–927.

[46] Wickham, S. F. J., Bath, J., Katsuda, Y., Endo, M., Hidaka, K., Sugiyama, H., Turberfield, A. J., 2012. A DNA-based molecular motor that can navigate a network of tracks. *Nature nanotechnology*, **7**: 169–173.

[47] Thubagere, A. J., Li, W., Johnson, R. F., Chen, Z., Doroudi, S., Lee, Y. L., Izatt, G., Wittman, S., Srinivas, N., Woods, D., Winfree, E., Qian, L., 2017. A cargo-sorting DNA robot. *Science*, **357**: eaan6558.

[48] Plesa, T., Vejchodský, T., and Erban, R., 2016. Chemical Reaction Systems with a Homoclinic Bifurcation: An Inverse Problem. *Journal of Mathematical Chemistry*, **54**(**10**): 1884–1915.

[49] Plesa, T., Vejchodský, T., and Erban, R. Test Models for Statistical Inference: Two-Dimensional Reaction Systems Displaying Limit Cycle Bifurcations and Bistability, 2017. *Stochastic Dynamical Systems, Multiscale Modeling, Asymptotics and Numerical Methods for Computational Cellular Biology*, 2017. Available as https://arxiv.org/abs/1607.07738.

[50] Erban, R., Chapman, S. J., Maini, P. *A practical guide to stochastic simulations of reaction-diffusion processes*, 2007. Available as http://arxiv.org/abs/0704.1908.

[51] Pavliotis, G. A., Stuart, A. M. *Multiscale methods: Averaging and homogenization*. Springer, New York, 2008.

[52] Gardiner, C. *Handbook of stochastic methods for physics, chemistry, and the natural sciences*. Springer series in synergetics, Springer, New York, 2004.

[53] Allen, L. J. S. *An introduction to stochastic processes with applications to biology*. Second edition, Chapman and Hall/CRC, 2010.

[54] Spiegel, M. R.. *Schaum's outline of calculus of finite differences and difference equations*. McGraw-Hill Education, 1971.

[55] Voit, E. O., Martens, H. A., Omholt, S. W., 2015. 150 years of the mass action law. *PLOS Computational Biology*, **11**(**1**).

[56] Gillespie, D. T., 1992. A rigorous derivation of the chemical master equation. *Physica A: Statistical Mechanics and its Applications*, **188**(1): 404–425.

[57] Munsky, B., Khammash, M., 2006. The finite state projection algorithm for the solution of the chemical master equation. *Journal of Chemical Physics*, **124**, 044104.

[58] Udrescu, T. *Numerical methods for the chemical master equation*. PhD Thesis. The Karlsruhe Institute of Technology, Germany, 2012.

[59] Jahnke, T., Huisinga, W., 2007. Solving the chemical master equation for monomolecular reaction systems analytically. *Journal of Mathematical Biology*, **54**: 1–26.

[60] Anderson, D. F., Craciun, G., Kurtz, T. G., 2010. Product-form stationary distributions for deficiency zero chemical reaction networks. *Bulletin of Mathematical Biology*, **72**(8): 1947–1970.

[61] Gibson, M. A., Bruck, J., 2000. Efficient exact stochastic simulation of chemical systems with many species and many channels. *Journal of Physical Chemistry A*, **105**: 1876–1889.

[62] Gillespie, D. T., 2001. Approximate accelerated stochastic simulation of chemically reaction systems. *Journal of Chemical Physics*, **115**(4): 1716–1733.

[63] Anderson, D. F., 2008. Incorporating postleap checks in tau-leaping. *Journal of Chemical Physics*, **128**(5), 054103.

[64] Keizer, J. *Statistical thermodynamics of nonequilibrium processes*. Springer-Verlag, New York, 1987.

[65] Vellela, M., Qian, H., 2007. A quasistationary analysis of a stochastic chemical reaction: Keizers paradox. *Bulletin of Mathematical Biology*, **69**: 1727–1746.

[66] Childs, P., Keener, J. P., 2012. Slow manifold reduction of a stochastic chemical reaction: Exploring Keizer's paradox. *Discrete and Continuous Dynamical Systems, Series B*, **17**(**6**): 1775–1794.

[67] Anderson, D. F., Enciso, G. A., Johnston, M. D., 2014. Stochastic analysis of biochemical reaction networks with absolute concentration robustness. *Journal of The Royal Society Interface*, **11**(**93**), 20130943.

[68] Hárs, V., Tóth, J., 1981. On the inverse problem of reaction kinetics. *Qualitative Theory of Differential Equations*, eds. Farkas, M., Hatvani, L., 363–379.

[69] Wilhelm, T., Heinrich, R., 1995. Smallest chemical reaction system with Hopf bifurcation. *Journal of Chemical Physics*, **17**: 1–14.

[70] Chellaboina, V., Bhat, S. P., Haddad, W. M., Bernstein, D.S., 2009. Modeling and Analysis of Mass-Action Kinetics. *IEEE Control Systems Magazine*, **29**: 60–78.

[71] Szili, L., Tóth, J, 1997. On the origin of Turing instability. *Journal of Mathematical Chemistry*, **22**: 39–53.

[72] Tóth, J., Hárs, V., 1986. Orthogonal transforms of the Lorenz- and Rössler-equation. *Physica 19D*, 135–144.

[73] Craciun, G., Pantea, C., 2008. Identifiability of chemical reaction networks. *Journal of Mathematical Chemistry*, **44**: 244–259.

[74] Szederkényi, G., 2009. Comment on "identifiability of chemical reaction networks" by G. Craciun and C. Pantea. *Journal of Mathematical Chemistry*, **45**: 1172–1174.

[75] Szederknyi, G., Hangos, K. M., Pni, T., 2011. Maximal and minimal realizations of reaction kinetic systems: computation and properties. *MATCH Communications in Mathematical and in Computer Chemistry*, **65**(**2**): 309–332.

[76] Perko, L. M. *Differential Equations and Dynamical Systems, Third Edition.* Springer-Verlag, New York, 2001.

[77] Wiggins, S. *Introduction to applied nonlinear dynamical systems and chaos, second edition.* Springer-Verlag, New York, 2003.

[78] Escher, C., 1981. Bifurcation and coexistence of several limit cycles in models of open two-variable quadratic mass-action systems. *Chemical Physics*, **63**: 337–348.

[79] Kuznetsov, Y. A. *Elements of Applied Bifurcation Theory, Second Edition.* Springer-Verlag, New York, 2000.

[80] Samardzija, N., Greller, L. D., Wasserman, E., 1989. Nonlinear chemical kinetic schemes derived from mechanical and electrical dynamical systems. *Journal of Chemical Physics*, **90**: 2296–2304.

[81] Hangos, K. M, Szederkényi, G., 2011. Mass action realizations of reaction kinetic system models on various time scales. *Journal of Physics: Conference Series*, **268**.

[82] Pantea, C., Gupta, A., Rawlings, J. B., Craciun, G., 2014. The QSSA in chemical kinetics: as taught and as practiced. *Discrete and Topological Models in Molecular Biology*, pp. 419–442. Springer, Berlin.

[83] Tikhonov, A. N., 1952. Systems of differential equations containing a small parameter multiplying the derivative (in Russian). *Math. Sb.*, **31**: 575–586.

[84] Klonowski, W., 1983. Simplifying principles for chemical and enzyme reaction kinetics. *Biophysical Chemistry*, **18**(**3**): 73–87.

[85] Hangos, K. M, 2010. Engineering model reduction and entropy-based Lyapunov functions in chemical reaction kinetics. *Entropy 12*: 772–797.

[86] Turing, A, 1952. The chemical basis of morphogenesis. *Phil. Trans. Roy. Soc. Lond.*, **237**: 37–72.

[87] Kowalski, K., 1993. Universal formats for nonlinear dynamical systems. *Chemical Physics Letters*, **209**: 167–170.

[88] Kowalsi, K., Steeb, W. H. *Nonlinear Dynamical Systems and Carleman Linearization*. Word Scientific, 1991.

[89] Wilhelm, T., 2000. Chemical systems consisting only of elementary steps - a paradigma for nonlinear behavior. *Journal of Mathematical Chemistry*, **27**: 71–88.

[90] Chicone, C., Jinghuang, T., 1982. On General Properties of Quadratic Systems. *The American Mathematical Monthly*, **89**: 167–178.

[91] Coppel, W., 1966. A Survey of Quadratic Systems. *Journal of Differential Equations*, **2**: 293–304.

[92] Gaiko, V. A. *Global Bifurcation Theory and Hilbert's Sixteenth Problem*. Springer Science, 2003.

[93] Gaiko, V. A., 2009. On the Geometry of Polynomial Dynamical Systems. *Journal of Mathematical Sciences*, **157**(**3**): 400–412.

[94] Perko, L. M., 1984. Limit Cycles of Quadratic Systems in the Plane. *Rocky Mountain Journal of Mathematics*, **14**(**3**): 619–645.

[95] Cherkas, L. A., Artés, J. C., Llibre, J., 2003. Quadratic Systems with Limit Cycles of Normal Size. *Buletinul Academiei de Ştiinţe a Republicii Moldova. Matematica*, **1**(**41**): 31–46.

[96] Artés, J. C., Llibre, J., 1997. Quadratic Vector Fields with a Weak Focus of Third Order. *Publicacions Mathemàtiques*, **41**: 7–39.

[97] Kar, S., Baumann, W. T., Paul, M. R. and Tyson, J. J., 2009. Exploring the roles of noise in the eukaryotic cell cycle. *Proceedings of the National Academy of Sciences of USA*, **106**: 6471–6476.

[98] Vilar, J. M. G., Kueh, H. Y., Barkai, N. and Leibler, S., 2002. Mechanisms of noise-resistance in genetic oscillators. *Proceedings of the National Academy of Sciences of the United States of America*, **99**(**9**): 5988–5992.

[99] Dublanche, Y., Michalodimitrakis, K., Kummerer, N., Foglierini, M. and Serrano, L., 2006. Noise in transcription negative feedback loops: simulation and experimental analysis. *Molecular Systems Biology*, **2**(**41**): E1–E12.

[100] Borisuk, M. T., Tyson, J. J., 1998. Bifurcation Analysis of a Model of Mitotic Control in Frog Eggs. *Journal of Theoretical Biology*, **195**: 69–85.

[101] Escher, C., 1982. Double Hopf-Bifurcation in Plane Quadratic Mass-Action Systems. *Chemical Physics*, **67**: 239–244.

[102] Escher, C., 1979. Models of Chemical Reaction Systems with Exactly Evaluable Limit Cycle Oscillations. *Zeitschrift für Physik B*, **35**: 351–361.

[103] Guidi, G. M., Goldbeter, A., 1997. Bistability without Hysteresis in Chemical Reaction Systems: A Theoretical Analysis of Irreversible Transitions between Multiple Steady States. *Journal of Physical Chemistry*, **101**: 9367–9376.

[104] Guidi, G. M., Goldbeter, A., 1998. Bistability without Hysteresis in Chemical Reaction Systems: The Case of Nonconnected Branches of Coexisting Steady States. *Journal of Physical Chemistry*, **102**: 7813–7820.

[105] Ghomi, M. S., Ciliberto, A., Kar, S., Novak, B., Tyson, J. J., 2008. Antagonism and Bistability in Protein Interaction Networks. *Journal of Theoretical Biology*, **218**: 209–218.

[106] Dickson, R. J., Perko, L. M., 1970. Bounded quadratic systems in the plane. *Journal of Differential Equations*, **7**: 251–273.

[107] Póta, G., 1983. Two-component bimolecular systems cannot have limit cycles: A complete proof. *Journal of Chemical Physics*, **78**(**3**): 1621–1622.

[108] Schlögl, F., 1972. Chemical reaction models for nonequilibrium phase transition. *Z. Physik.*, **253**(**2**): 147–161.

[109] Sandstede, B., 1997. Constructing dynamical systems having homoclinic bifurcation points of codimension two. *Journal of Dynamics and Differential Equations, Vol. 9, No. 2.*, **4**: 296–288.

[110] Lawrence, J. D. *A catalog of special plane curves*. Dover, New York, 1972.

[111] Li, M. Y., and Shu, H., 2011. Multiple Stable Periodic Oscillations in a Mathematical Model of CTL Response to HTLV-I Infection. *Bulletin of Mathematical Biology*, **73**: 1774–1793.

[112] Amiranashvili, A., Schnellbächer, N. D., and Schwarz, U. S., 2016. Stochastic switching between multistable oscillation patterns of the Min-system. *New Journal of Physics*, **18**: 093049.

[113] Perko, L. M., 1975. Rotated vector fields and the global behavior of limit cycles for a class of quadratic systems in the plane. *Journal of differential equations*, **18**: 63–86.

[114] Tung, C-C., 1959. Positions of limit cycles of the system $\mathrm{d}x/\mathrm{d}t = \sum a_{ik}x^i y^k, \mathrm{d}y/\mathrm{d}t = \sum b_{ik}x^i y^k, 0 \leq i+k \leq 2$. *Sci. Sinica*, **8**: 151–171.

[115] Soloveichik, D., Cook, M., Winfree, E., Bruck J., 2008. Computation with finite stochastic chemical reaction networks. *Natural Computing*, **7**(**4**): 615–633.

[116] Plesa, T., Erban, R., Othmer, H. G., 2018. Noise-induced Mixing and Multimodality in Reaction Networks. *European Journal of Applied Mathematics*. Available as https://arxiv.org/abs/1801.09200.

[117] Ohkubo, J., Shnerb, N., Kessler, D. A, 2008. Transition phenomena induced by internal noise and quasi-absorbing state. *Journal of the Physical Society of Japan*, **77**: 044002.

[118] Biancalani, T., Dyson, L., McKane, A. J., 2014. Noise-induced bistable sates and their mean switching time in foraging colonies. *Physical Review Letters*, **112**: 038101.

[119] Saito, N., Kaneko, K., 2015. Theoretical analysis of discreteness-induced transition in autocatalytic reaction dynamics. *Physical Review Letters*, **91**: 022707.

[120] Subramanian, K., Paul, M. R., Tyson, J. J., 2013. Potential role of a bistable histidine kinase switch in the asymmetric division cycle of caulobacter crescentus. *PLOS Computational Biology*, **9**: e1003221.

[121] Süli, E., and Mayers, D. F. *An Introduction to Numerical Analysis*. Cambridge University Press, 2003.

[122] Tyson, J. J, 1973. Some further studies of nonlinear oscillations in chemical systems. *The Journal of Chemical Physics*, **58**, 3919.

[123] Cook, G. B., Gray, P., Knapp, D. G., Scott, S. K., 1989. Blmolecular Routes to Cubic Autocatalysis. *The Journal of Chemical Physics*, **93**: 2749–2755.

[124] Schneider, K. R., and Wilhelm, T., 1998. Model reduction by extended quasi-steady-state approximation. *Weierstraß-Institut für Angewandte Analysis und Stochastik*, Preprint Number 457, Berlin.

[125] Kerner, E. N., 1981. Universal formats for nonlinear ordinary differential systems. *Journal of Mathematical Physics*, **22**: 1366–1371.

[126] Kowalski, K., 1993. Universal formats for nonlinear dynamical systems. *Chem. Phys. Lett.*, **209**: 167–170.

[127] Janssen, J., 1989. The elimination of fast variables in complex chemical reactions. III. Mesoscopic level (reducible case). *Journal of Statistical Physics*, **57**: 171–185.

[128] Gillespie, D. *Markov processes: An introduction for physical scientists*. Academic Press, Inc., Harcourt Brace Jovanowich, 1992.

[129] Thomas, P., Straube, A. V., and Grima, R., 2011. Communication: limitations of the stochastic quasi-steady-state approximation in open biochemical reaction networks. *The Journal of Chemical Physics*, **135**(**18**): 181103.

[130] Kim, J., Josic, K., and Bennett, M., 2014. The validity of quasi-steady-state approximations in discrete stochastic simulations. *Biophysical Journal*, **107**: 783–793.

[131] Agarwal, A., Adams, R., Castellani, G. C., and Shouval, H. Z., 2012. On the precision of quasi steady state assumptions in stochastic dynamics. *The Journal of Chemical Physics*, **137**: 044105.

[132] Mastny, E. A., Hasteltine, E. L., and Rawlings, J. B., 2007. Two classes of quasi-steady-state model reductions for stochastic kinetics. *The Journal of Chemical Physics*, **127**(**9**): 094106.

[133] Rao, C. V., and Arkin, A. P., 2002. Stochastic chemical kinetics and the quasi-steady-state assumption: application to the Gillespie algorithm. *The Journal of Chemical Physics*, **118**: 4999–5010.

[134] Zechner, C., Seelig, G., Rullan, M., and Khammash, M., 2016. Molecular circuits for dynamic noise filtering. *PNAS*, **113**(**17**): 4729–4734.